Sede Amministrativa: Università degli Studi di Padova

Dipartimento di Scienze Chimiche

DOTTORATO DI RICERCA IN SCIENZE MOLECOLARI

INDIRIZZO SCIENZE CHIMICHE

XXV CICLO

Anti-cancer chemotherapeutics in target therapy: from advanced preclinical studies on promising Au(III) peptidomimetics toward the design of new receptor-recognizable metal-based agents

Direttore della Scuola : Ch.mo Prof. Antonino Polimeno

Supervisore: Ch.mo Prof. Dolores Fregona

Dottoranda: Chiara Nardon

A mia nonna Maria...
Con tutto il cuore.

“Your time is limited, so don’t waste it living someone else’s life.
Don’t be trapped by dogma – which is living with the results of other people’s thinking.
Don’t let the noise of other’s opinions drown out your own inner voice.
And most important, have the courage to follow your heart and intuition…”

Steven Paul Jobs
(1955-2011)

CONTENTS

Abstract

At present, though there is no clinically available antineoplastic drug that acts selectively on the tumor tissue, chemotherapy is still the main form of treatment for cancer. To date, platinum-based drugs, whose forerunner is cisplatin, are among the most employed chemotherapeutics in spite of their treatment-related toxicity. Starting from the chemical properties of platinum and the severe toxicological profile of the drug cisplatin, novel Au(III)-dithiocarbamato complexes have been recently designed and biologically studied, showing particularly promising antitumor activity (both *in vitro* and *in vivo*), lack of cross-resistance, and reduced toxic and nephrotoxic side-effects compared to cisplatin, accounting for a different mechanism of action. Following these encouraging results, we aimed to exploit the peculiar features of the tumor microenvironment in order to obtain a targeted delivery of our potential drugs into cancer tissues, resulting in further effectiveness increase and side-effects reduction. Accordingly, for a site-specific delivery strategy, we planned to functionalize the dithiocarbamato ligand moiety by means of biomolecules that are internalized into the pathological cells upon binding to a specific cell membrane transporter or a receptor, upregulated compared to healthy cells.

With respect to human transporters, Au(III)-dithiocarbamato complexes functionalized with di- and tripeptides (our second-generation compounds), designed to exploit the peptide transporters PEPT1 and PEPT2, have been recently synthetized and studied, turning out the filing of an international patent, just extended worldwide. On the other hand, in this work the receptor-mediated strategies have been taken into account as well (third-generation compounds).

Concerning the second-generation complexes, preliminary screening tests on different human tumor cell lines indicated AuD6 and AuD8 as suitable candidates for advanced preclinical studies. We report here on their synthesis, chemical characterization and the biological data collected throughout a 6-month stay as a visiting PhD student at the *Barbara Ann Karmanos Cancer Institute* (Detroit, U.S.A.) in collaboration with Prof. Q. Ping Dou. Several advanced preclinical studies were carried out evaluating the anticancer activity both *in vitro* and *in vivo*, the acute toxicity on animal models and providing insights into the mechanism of action in order to enter phase I clinical trials. The triple-negative breast cancer

cell line MDA-MB-231 was chosen as a model since these cells are highly metastatic and invasive. Notably, AuD6 and AuD8 overcame the *in vitro* resistance of cisplatin against this cell line, displayed outstanding anticancer activity on xenografts (subcutaneous administration) and very negligible acute toxicity in mice upon intravenous and *per os* administrations. In addition to showing a good chemotherapeutic index in terms of toxicity-activity ratio, these two compounds proved strong inhibitors of proteasome – a significant intracellular protein degradation machinery – both *in vitro* and *in vivo*. Therefore, a crystallographic study, aimed at investigating the mechanism of inhibition of 20S proteasome by AuD8 (chosen as a model compound), was performed by means of biotechnological methods.

With respect to the pharmacokinetic profile of the considered compounds, serum albumin was taken into account as it is the most abundant plasma protein and it is a well-known carrier of drugs and endogenous substances such as vitamins and lipids. An investigation of the possible interaction between AuD8 and the serum protein was carried out by circular dichroism and fluorescence spectrophotometry, replacing the human serum albumin with the bovine counterpart since they have an almost identical sequence.

Concerning our third-generation of complexes – designed to work as targeted bullets that could go straight to the cancer cells, bypassing normal ones – we focused on the cholecystokinin (CCK) receptors which belong to the G-protein-coupled receptor superfamily and are overexpressed in many neoplasms. The targeted drug delivery has been achieved by complexation of the metal center with the CCK8 peptide. Thus, the CCK8 peptide was first synthesized, purified and characterized by mass spectrometry, elemental analysis, NMR and FT-IR spectroscopies. The corresponding Au(III) dithiocarbamato derivative was then synthesized and partially characterized by ^{1}H-NMR and UV-Vis spectrophotometry.

Afterwards, we addressed our attention also to the “click chemistry” field, designing and developing a versatile gold(III)-based building block to be functionalized with different targeting peptides. The related overexpressed receptors can specifically recognize and bind the corresponding conjugates, thus intaking them into cytoplasm by mediated internalization. An international patent application is going to be filed about this innovative strategy.

More recently, as a natural extension of our previous studies, we have also taken into account Cu(II), being an endogenous metal characterized by very interesting biochemical properties. Concerning the relationship between copper and cancer, it is worth highlighting

that copper plays a significant role in angiogenesis and therefore is more abundant in cancer cells than in healthy ones, leading to a selectivity of copper-based anticancer agents toward neoplastic tissues. In the present work, two different classes of Cu(II) dithiocarbamato complexes were designed to gain insights into structure-activity relationships and to get the know-how with respect to the chemical behavior of this transition metal in terms of reaction conditions and stability in different solvents.

Their synthesis, wide chemical characterization and preliminary biological data are herein reported. Overall, these findings will be useful for the future development of the more sophisticated copper-based receptor compounds.

Riassunto

Attualmente, sebbene a livello clinico non vi siano farmaci in grado di agire selettivamente sui tessuti tumorali, la chemioterapia rimane la strategia d'elezione nel trattamento del cancro. Ad oggi, i farmaci a base di platino (cisplatino, carboplatino ecc.) sono tra i più utilizzati in ambito terapeutico nonostante la loro elevata tossicità accessoria. Prendendo come *starting point* le proprietà chimiche del platino e il pesante profilo tossicologico del cisplatino, sono stati recentemente progettati e testati biologicamente nuovi complessi ditiocarbammici di Au(III). Quest'ultimi hanno mostrato un'attività antitumorale particolarmente promettente (sia *in vitro* che *in vivo*), mancanza di resistenza crociata con il cisplatino e ridotta tossicità sia sistemica che renale, mettendo in luce un differente meccanismo di azione rispetto al chemioterapico di riferimento. Sulla base di questi risultati incoraggianti, ci siamo proposti di sfruttare le caratteristiche peculiari del microambiente tumorale al fine di ottenere un rilascio mirato dei nostri potenziali farmaci nei tessuti cancerosi con conseguente amplificazione dell'efficacia chemioterapica e ulteriore riduzione degli effetti collaterali. Per ottenere quindi un rilascio sito-specifico, abbiamo progettato di funzionalizzare il legante ditiocarbammico con biomolecole capaci di essere riconosciute e assimilate dalle cellule cancerose in seguito al legame con uno specifico trasportatore o recettore di membrana, sovraespresso rispetto alla cellula sana.

Per quanto concerne i trasportatori presenti nel corpo umano, sono stati recentemente sintetizzati e studiati dei complessi ditiocarbammici di Au(III) funzionalizzati con di- e tripeptidi (d'ora in avanti denominati composti di 2° generazione), progettati per sfruttare i trasportatori peptidici PEPT1 e PEPT2. Il valore dei primi risultati biologici ottenuti ha portato al deposito di un brevetto PCT, esteso recentemente in numerosi Paesi del mondo. Come naturale prosieguo delle ricerche precedenti, in questo lavoro sono state prese in considerazione anche altre strategie mediate dai recettori sovraespressi nei tumori al fine di ottenere i nostri composti di 3° generazione.

Con riferimento ai composti di 2° generazione, test preliminari di *screening*, condotti su svariate linee cellulari tumorali umane, hanno indicato AuD6 e AuD8 quali candidati adatti per ulteriori studi preclinici approfonditi. La loro sintesi e caratterizzazione chimica sono qui riportate insieme ai risultati biologici raccolti personalmente nei laboratori del "Barbara Ann Karmanos Cancer Institute" (Detroit, U.S.A) durante un periodo di ricerca di sei mesi sotto

la supervisione del Prof. Q.Ping Dou. Sono stati condotti numerosi studi avanzati per valutare l'attività antitumorale sia *in vitro* sia *in vivo* e per delucidare un possibile meccanismo di azione nell'ipotesi di accesso alla fase di sperimentazione clinica I; è stata infine testata la tossicità acuta su modelli animali con risultati estremamente interessanti. E' stata scelta come modello, date le sue elevate capacità invasive e metastatiche, la linea cellulare MDA-MB-231 (tumore della mammella triplo-negativo). E' da sottolineare che questa linea cellulare è resistente al cisplatino mentre sia AuD6 che AuD8 hanno mostrato una buona attività antiproliferativa nelle prove in vitro, notevole attività antitumorale su modelli xenografici (somministrazione sottocutanea) e tossicità acuta trascurabile nei topi sia per via endovenosa che orale. Oltre a possedere un buon indice chemioterapico in termini di rapporto tossicità/efficacia, questi due composti sono risultati, sia *in vitro* che *in vivo*, dei potenti inibitori del proteasoma, importante complesso multicatalitico intracellulare deputato all'idrolisi di substrati proteici. Si è di conseguenza condotta un'indagine cristallografica mirata a delucidare il meccanismo di inibizione del proteasoma 20S da parte di AuD8 (composto modello) mediante tecniche biotecnologiche.

Per quanto riguarda il profilo farmacocinetico dei composti in esame, si è preliminarmente considerata l'albumina sierica dato che è la principale proteina plasmatica ed è un noto trasportatore di farmaci e sostanze endogene quali vitamine e lipidi. Si è pertanto condotto uno studio al fine di verificare l'instaurarsi o meno di un'interazione tra AuD8 e la proteina del siero mediante dicroismo circolare e spettrofotometria di fluorescenza. In questi esperimenti si è utilizzato l'albumina bovina dato che condivide un'elevata omologia di sequenza con la controparte umana.

Per quanto concerne i composti di 3° generazione – progettati anch'essi per agire in modo mirato sulle cellule cancerose e quindi capaci di eludere quelle sane – ci siamo concentrati sui recettori delle colecistochinine (CCK), iperespressi in parecchi tumori e appartenenti alla famiglia di recettori accoppiati alle proteine G. Il rilascio mirato del farmaco è possibile mediante complessazione del centro metallico con il peptide CCK8. Tale peptide è stato sintetizzato, purificato e caratterizzato tramite spettrometria di massa, analisi elementare, NMR ed FT-IR. Il corrispondente derivato ditiocarbammico di Au(III) è stato successivamente sintetizzato e caratterizzato parzialmente mediante spettroscopia ^{1}H-NMR e spettrofotometria UV-Vis.

Successivamente abbiamo sfruttato la cosiddetta "click chemistry" nelle fasi di progettazione e sviluppo di un'unità versatile a base di Au(III) da funzionalizzare con diversi

peptidi recettoriali. In seguito al legame con il corrispondente peptide, tali recettori sono solitamente in grado di trasferire nel citoplasma il coniugato metallo-peptide. Una domanda di brevetto internazionale è in fase di deposito per proteggere la proprietà intellettuale del nostro approccio.

Come naturale prosecuzione delle nostre ricerche, più recentemente si è utilizzato il metallo endogeno Cu(II) viste le sue interessanti proprietà biochimiche. La scelta del Cu(II) non è stata casuale ma dettata dal ruolo fondamentale che esso gioca nell'angiogenesi portandolo ad essere presente in concentrazione più elevata nelle cellule cancerose rispetto alle cellule sane. Tale peculiarità è stata sfruttata nella progettazione di agenti antitumorali a base di Cu(II) selettivi verso i tessuti neoplastici. Sono state preparate due diverse classi di complessi ditiocarbammici di Cu(II) al fine di ricavare possibili relazioni struttura-attività e conoscere approfonditamente il comportamento chimico di questo metallo di transizione in termini di condizioni di reazione da adottare e stabilità in diversi solventi. In questa tesi sono riportate le loro sintesi, caratterizzazioni chimiche e i dati biologici preliminari. Nel loro complesso, le informazioni qui raccolte saranno utilizzate per lo sviluppo futuro di composti a base rameica da inserire nel campo delle terapie mirate in oncologia.

Abbreviations and acronyms

2-ME	2-mercaptoethanol
AA	amino acid
AcOH	acetic acid
Aib	α-aminoisobutyric acid (α-methylalanine)
APS	ammonium persulfate
Bis	*N,N'*-methylene- bis-acrylamide
Boc	*tert*-Butyloxycarbonyl
BPB	bromophenol blue
BrAAP	branched chain amino acid-preferring
BSA	bovine serum albumin
CBB	coomassie Brilliant Blue R-250
CD	circular dichroism
***Cis*-DDP**	*cis*-diaminodichloroplatinum(II) (cisplatin)
CP	20S proteasome core particle
CT-like	chymotrypsin-like
DIPEA	*N, N*-Diisopropylethylamine
DMDT	*N,N*-dimethyldithiocarbamate
DMDTM	*S*-methyl-(*N,N*-dimethyldithiocarbamate)
DMSO	dimethylsulfoxide
DSC	differential scanning calorimetry
dtc	dithiocarbamate
dtcM	methylated dithiocarbamate
DTT	dithiothreitol or Cleland's reagent
DUBs	deubiquitylating enzymes
EDTA	ethylenediamine-tetraacetic acid dipotassium salt
EtOH	ethanol
FBS	fetal bovine serum
Fc	crystallizable fragment
FITC	fluorescein isothiocyanate
Fmoc	9-Fluorenylmethoxycarbonyl
FPLC	fast protein liquid chromatography
HeLA	cervix adenocarcinoma cell line
HEPES	4-(2-hydroxyethyl)-1-piperazineethanesulfonic acid
His_6	sequence of six Histidine residues
HMBC	Heteronuclear Multiple Bond Correlation
HOBt	hydroxybenzotrizole
HSA	human serum albumin
IC_{50}	half maximal inhibitory concentration
IgG	immunoglobulin G
IPTG	Isopropil β-D-1-tiogalattopiranoside
LMCT	ligand to metal charge transfer
mAb	monoclonal antibody
MES	morpholinoethanesulfonic acid
MLCT	metal to ligand charge transfer

MPD	(±)-2-methyl-2,4-pentanediol
MTT	(3-(4,5-Dimethylthiazol-2-yl)-2,5-diphenyltetrazolium bromide
MW	molecular weight
MW STD	molecular weight standard
Ni-NTA	Ni-nitrilo-tri-acetic acid agarose affinity column
NMM	*N*-methylmorpholine
NMR	Nuclear Magnetic Resonance
NOESY	Nuclear Overhauser effect spectroscopy
Ntn	*N*-terminal nucleophile
O*t*Bu	O-*tert*-butyl
PBS	phosphate buffered saline
PEPT	peptide transporter
PGPHL	peptidyl-glutamyl-peptide-hydrolizing-like
PI	propidium iodide
PyBop	benzotriazol-1-yl-oxytripyrrolidinophosphonium hexafluorophosphate
PyDT	pyrrolidine dithiocarbamate
PyDTM	1-pyrrolidinecarbodithioato methyl ester
RL	Ringer Lactate®
ROS	reactive oxygen species
RT	room temperature
Sar	sarcosine (*N*-methylglycine)
SDS	sodium dodecyl sulfate
SDS-PAGE	sodium dodecyl sulfate polyacrylamide gel electrophoresis
SEC	size exclusion liquid chromatography
SNAAP	small neutral amino acid-preferring activity
Suc-LLVY-AMC	*N*-Succinyl-Leu-Leu-Val-Tyr-7-amido-4-methylcoumarin
TBST	tris-buffered saline with Tween 20
TEA	triethylamine
TEMED	*N*,*N*,*N'*,*N'*- tetramethylethylenediamine
TEV	tobacco etch virus protease
TEV-ProA	TEV protease-cleavable protein A tag
TG	thermogravimetry
THF	tetrahydrofuran
TL	trypsin-like
TMS	tetramethylsilane
Tris	2-Amino-2-(hydroxymethyl)-1,3-propanediol (or Tris(hydroxymethyl)aminomethane)
UPS	ubiquitin-proteasome system
UV-Vis	ultraviolet-visible spectroscopy
YPD-A	yeast extract, peptone, dextrose and adenine medium
Z-	benzyloxycarbonyl-
Z-ARR-AMC	carboxybenzyl-Ala-Arg-Arg-7-amido-4-methylcoumarin
Z-LLE-AMC	carboxybenzyl-Leu-Leu-Glu-7-amido-4-methylcoumarin
Z-OSu	*N*-(benzyloxycarbonyloxy)succinimide

Introduction

Cancer, an "epidemic" disease

The term cancer (referred to as neoplasia or malignant tumor as well) refers to a heterogeneous group of diseases – that can affect any part of the body – caused by an impairment of the normal functioning of genes, thus leading to a genetic damage. Other terms used are malignant tumors and neoplasms. It is currently believed that cancer is a multi-step process involving the interaction between genes and their environment, and it is caused by a series of genetic mutations, inherited during cell replication, in different genes of a single somatic cell.

Throughout life, the human genome suffers from replication mistakes and is exposed to mutagens, but most damages are usually quickly repaired by the cellular maintenance machinery. However, the mechanisms and multiple dynamic equilibria regulating cell homeostasis are not foolproof. If mutations are involved in two classes of genes, the cancer cycle can start. In fact, some normal genes involved in cell growth, development, and differentiation can be converted into cancer-causing proto-oncogenes by mutation. Other genes that normally prevent the uncontrolled growth of cells, tumor suppressor genes, can also produce cancer if they are knocked out by genetic mutations. Single mutations are generally not sufficient to cause cancer, but they produce changes that may predispose cells to malignant growth. Additional mutations in other genes, caused by environmental damage, favor the malignant transformation of the cells. Acquisition of further somatic mutations, and consequent clonal expansion, result in the evolution of altered cells that may invade surrounding tissues and hence metastasize. This proliferation in an excessive and untimely way, ascribable to metabolic and behavioural modifications of the cells (described in detail below), leads to changes in mechanisms that control cell life-span, relationships with neighboring cells, and capacity to escape the immune system.[(i)]

From the epidemiological point of view, nowadays, cancer is the second leading cause of death worldwide after cardiovascular diseases and accounted for 7.6 million deaths (13% of all deaths) in 2008. Approximately 70% of cancer deaths occur in low- and middle-income countries. According to the last report (2008) of the World Health Organization (WHO), cancer deaths will keep rising to an estimated 9 million people dying from cancer in 2015, and 13 million dying in 2030.

At present, malignancies are the second leading cause of death in Italy as well, and the same situation is estimated to occur in 2030. In Italy in 2005 cancer disease killed approximately 157,000 people, 57,000 of which were younger than 70. [(ii)] In 2005 breast neoplasia was the most frequent cause of cancer death in women, whereas trachea, bronchus, lung cancers were the leading causes of cancer deaths in men. For both sexes, colon and rectum cancers were the second most commonly occurring tumors. [(iii)] Cancer of prostate and the respiratory apparatus ranked third in males and females, respectively.

Through early detection, screening and adequate treatment many cancers can be cured. Traditional cancer treatments are surgery (to remove solid tumors), radiotherapy and chemotherapy, the latter killing the rapidly dividing cancerous cells by radiation or using drugs, respectively. A major drawback of traditional anticancer agents is the onset of serious side-effects (*e.g.*, nausea, weight loss, hair loss and severe fatigue) due to the destruction of healthy cells that normally divide at a fast rate, such as cells in the intestinal mucosa, follicle hair cells, and bone marrow cells.

In the following sections, we will throw some light on the principles of oncology, namely the idiosyncrasies of malignancies and some clinical aspects. Then, currently used chemotherapies will be described in light of the organic or inorganic nature of the involved drugs. Particular attention will be addressed to cisplatin, being the forerunner of metal-based anticancer agents. In our research group, the design of new potential anticancer drugs was based on its chemical properties and toxicological profile. On the basis of these considerations, cisplatin has been considered as a reference drug in the biological experiments reported in this thesis.

Principles of oncology

The traits of cancer

As mentioned above, at present cancer is the most common genetic pathology. It is a complex disease that is very variable in its appearance, development and treatment outcome from one patient to the other. The same changeability and heterogeneity exist at the cellular and molecular levels.

Until recently, cancer was erroneously thought as nothing more than a collection of rather homogeneous non-interconnecting cells. [1] On the contrary, tumors are sophisticated tissues made up of many distinct cell types that participate in heterotypic interactions with one other.

For example, normal cells surrounding the tumor (tumor-associated stroma) may be recruited to be active participants in tumorigenesis, thus contributing to the development and expression of specific cancer traits. In fact, when normal cells evolve to a neoplastic condition, they progressively acquire a series of capabilities such as resisting cell death, sustaining proliferative signaling, evading growth suppressors, inducing angiogenesis, enabling replicative immortality, and activating invasion and metastasis. In other words, being a multi-step process, cancer evolution is due to accumulation of specific genetic modifications that control cell proliferation and lifespan, relationships with neighboring cells, and capacity to escape the immune system. The deep understanding of the role of the "tumor microenvironment" is becoming increasingly important since the involvement of seemingly normal cells plays a major role in the acquisition of the cancer features.

It is likely that most important hallmark of cancerous cells is their capability of sustaining proliferative signaling. Contrary to normal cells, the malignant counterparts lose the control on the production and release of growth-promoting signals, thus entering into and progressing through the cell life cycle in a unregulated way. The unbalanced homeostasis is largely due to the release of mitogenic signals and the conveyance of growth factors to neighboring cells. In the extracellular matrix, growth factors bind to cell-surface receptors, which trigger intracellular signaling pathways involved in cell growth and function. Likewise, these stimuli may be sent to normal cells within the supporting cancer-associated stroma, which reciprocate by supplying the neoplastic cells with several growth factors.[2, 3] Interestingly, some somatic mutations are known to enhance receptor signaling by either up-regulating the receptor proteins at the cancer cell surface or structurally changing the receptor molecule, thus making such cells hyper-responsive to growth factors.[4, 5]

Regarding the feature of circumventing growth suppressors, neoplastic cells are able to evade powerful programs that limit cell growth and proliferation and depend on the actions of tumor suppressor genes. The two prototypical oncosuppressors encode TP53 and the RB (retinoblastoma-associated) proteins. TP53 receives inputs from intracellular abnormalities or stress sensors whereas RB protein integrates predominantly extracellular signals. Being central control nodes, both manage the resolution of cell proliferating or, alternatively, activating senescence and apoptotic programs. A plenty of tumor suppressors have been discovered followed their inactivation in animal or human malignances.[1]

Concerning the cancer capability of resisting cell death, it has been shown by functional studies that programmed cell death by apoptosis is a natural barrier to tumor

development in healthy cells.[6] Albeit only a small part of the signaling circuitry governing the apoptotic program is known, many stress/abnormality sensors have been identified including a DNA-damage sensor which works *via* the TP53 tumor suppressor, described above. Following genetic abnormalities, TP53 induces apoptosis by up-regulating expression of the Noxa and Puma BH3-only proteins.[7] In order to limit or circumvent apoptosis commitment, cancerous cells find out a variety of strategies. In addition to the function loss of the TP53 tumor suppressor (critical damage sensor), tumor may achieve its goal either by down-regulating proapoptotic factors (*e.g.*, Bax, Bim, Puma) or by increasing expression of antiapoptotic regulators (*e.g.*, Bcl-2, Bcl-xL) or of survival signals (Igf1/2).[1]

Intriguingly, some recent studies carried out on mice suggest that induction of autophagy (operating independently of or in concert with apoptosis) may function as a barrier to carcinogenesis. [8] Therefore, in addition to apoptosis, autophagy seems to represent yet another barrier that needs to be circumvented during tumor development.[8] However, other studies are required to elucidate when and how autophagy enables malignant cells to survive or causes them to die. At present, it is known that autophagy normally works at basal levels in cells but can be highly induced under particular stress conditions such as nutrient deficit. The autophagic program enables cells to degrade cellular organelles, such as mitochondria and ribosomes, leading to the resulting catabolites recycle for biosynthesis and energy metabolism. [1]

Another type of cell death is the necrosis and, in contrast to apoptosis and autophagy, releases proinflammatory signals into the surrounding tissue microenvironment. Accordingly, necrotic cells can recruit inflammatory cells of the immune system[9] whose function would be to examine the extent of tissue damage and eliminate associated necrotic debris. However, there is evidence that immune inflammatory cells can be actively tumor promoting, in light of their ability of fostering angiogenesis and cell proliferation by releasing growth-stimulating factors. Moreover, necrotic cells can release bioactive regulatory factors (e.g., IL-1 □) which can directly stimulate the surrounding viable cells to proliferate, thus enabling further neoplastic progression. [9]

Thus, based on the previous considerations, it is preferable to use anticancer agents triggering apoptosis instead of necrosis. In fact, the former is a quick and clean cell death process, which does not damage the neighboring cells and avoids the recruitment of tumor-promoting inflammatory cells.

With respect to the replicative immortality of cancer cells, it is worth noting that normal cells are able to pass through only a defined number of subsequent cell growth-and-division cycles. Thus, repeated cycles of cell division lead first to induction of senescence (a typically irreversible entrance into a nonproliferative but viable state) and then to crisis condition, which results in cell death. Remarkably, it is possible that cells in the crisis phase revert to a proliferating state with an unlimited replicative potential. Such a transition is referred to as immortalization.[1] Literature data point out that telomeres (tandem hexanucleotide repeats protecting the ends of chromosomes) play a key role in this transformation.[10, 11] Contrary to normal (non-immortalized) cells where telomeres progressively shorten, thus ultimately losing the ability to protect the ends of chromosomal DNAs from end-to-end fusions and triggering the entrance into crisis, the neoplastic cells may overcome such "clocking" device. In fact, although premalignant cells are characterized by extensively eroded telomeres, they are able to maintain telomeric DNA long enough to avoid induction of senescence or apoptosis, usually by upregulating the expression of telomerase. [1] Such enzyme is a particular type of DNA polymerase that adds telomere units to the ends of telomeric DNA and is almost absent in non-immortalized cells but overexpressed in cancerous ones. By lengthening telomeric DNA, the tumor cell will not experience the progressive telomere erosion. However, while acquiring higher levels of telomerase in premalignant cells, some tumor-promoting mutations may take place.[12, 13] Thus, after this transient telomerase deficiency, the subsequent action of the newly produced telomerase is able to stabilize the mutant genome, thus conferring an unlimited replication capacity.

Two tightly correlated cancer hallmarks remain to be described: the angiogenesis induction and activation of invasion and metastasis, being the former essential for the latter. The angiogenesis (sprouting of new blood vessels from existing ones) is associated with the tumor need of nutrients and oxygen as well as the need of discharging metabolic wastes and carbon dioxide. Except for wound healing and female reproductive cycle, in the adult, angiogenesis is only transiently activated. In contrast, during malignancy evolution, an "angiogenic switch" is almost always on, resulting in a continuous sprouting of new vessels from the existing vasculature.[14] Tumor neovasculature is characterized by convoluted and excessive vessel branching, irregular blood flow, distorted and enlarged vessels, micro-hemorrhaging, leakiness, and abnormal levels of endothelial cell proliferation and apoptosis.[15] The well-known prototypes of angiogenesis inhibitors and inducers are thrombospondin-1

(TSP-1) and the vascular endothelial growth factor-A (VEGF-A), respectively. VEGF gene expression can by upregulated both by hypoxia and by oncogene signaling.[16, 17] In some tumors, powerful oncogenes, such as Ras and Myc, can upregulate expression of angiogenic factors, whereas in others, such stimuli are yielded indirectly by immune inflammatory cells. In fact, it is now known that macrophages, mast cells, neutrophils, and myeloid progenitors may infiltrate premalignant lesions and advanced tumors and accumulate at the boundaries of such regions. [18, 19] This migration is due to both the leakiness of the tumor vasculature and the presence of chemoattractant substances released by neoplastic cells, able to recruit the inflammatory cells. Interestingly, the peri-tumoral inflammatory cells help to trigger the angiogenic switch in the still quiescent tissues, thus sustaining tumor growth and facilitating local invasion. [1]

The process of invasion and metastasis encompasses a series of discrete cell-biologic changes, starting with local invasion, then intravasation by malignant cells into neighboring blood and lymphatic vessels, transit of neoplastic cells through the lymphatic and circulatory systems, followed by escape of the cells from the lumina of such vessels into the parenchyma of distant tissues (extravasation), the formation of small nodules of cancer cells (micrometastases), and ultimately the growth of micrometastatic lesions to yield macroscopic tumors (colonization). [1]

So far, the hallmarks of cancer have been described as acquired functional capabilities that allow neoplastic cells to survive, proliferate, and disseminate. Notably, two characteristics, namely genomic instability and tumor promoting-inflammation underlie such complex acquisition occurring over-time *via* distinct mechanisms according to the tumor type.

In light of the considerations discussed above, the multistep tumor progression can be depicted as a succession of clonal expansions, each characterized by a distinct enabling mutant genotype. With respect to the amount of mutant genes required to trigger carcinogenesis, cancer cells increasingly favor the rates of mutation due to either a progressive sensitivity to mutagenic agents or the presence of defects in genomic maintenance and repair machinery, or both. [20] Furthermore, compromised surveillance systems, that normally monitor genomic integrity and force genetically damaged cells into either senescence or apoptosis, foster the accumulation of mutations. [21] In this context, the oncosuppressor TP53 plays a critical role, thus accounting for its designation as “guardian of the genome”. [22]

Page's and coworkers recently reported on the immune infiltration in human neoplastic lesions, ranging from subtle infiltrations of immune cells detectable only with cell type-specific antibodies to gross inflammations that are apparent even by standard histochemical staining techniques.[23] As anticipated above, the tumor-associated inflammatory response has the paradoxical effect of fostering tumorigenesis and progression. In fact, immune cells may supply bioactive molecules to the tumor microenvironment, including proangiogenic factors, survival factors that limit cell death, growth factors that promote proliferative signaling, extracellular matrix-modifying enzymes that favor angiogenesis, invasion, and metastasis, and inductive stimuli that trigger the activation of EMT. [9, 18, 24] Moreover, inflammatory cells can release chemicals, such as reactive oxygen species, that are known mutagenic substances for the surrounding cancer cells, thus hastening their genetic evolution toward states of advanced malignancy. [9]

Likewise, highly immunogenic cancer cells may elude immune destruction by inactivating members of the immune system that have been dispatched to eliminate them. For instance, malignant cells may paralyze infiltrating cytotoxic T lymphocytes and natural killer cells, by secreting tumor growth factor-β or other immunosuppressive factors [1] or also by recruiting inflammatory cells that suppress the actions of cytotoxic lymphocytes. [25] However, within the dichotomous nature of the immune system that both antagonizes and enhances tumor development and progression, it is worth highlight that the immune system generally works as an important barrier to tumor formation and progression, at least in some forms of non-virus-induced neoplasia. Cells and tissues are normally overseen by the immune system, which is able to recognize and eliminate the vast majority of incipient malignant cells. The defective immunological monitoring in tumor recognition would seem to be validated by the striking increases of certain cancers in immunocompromised individuals. [26] Likewise, some immunosuppressed organ-transplant recipients have been observed to develop donor-derived tumors, suggesting that the corresponding cancer cells were held in a dormant state in the seemingly tumor-free donors by a fully functional immune system. [27]

In conclusion, another cancer trait needs to be described, namely reprogramming of cellular energy metabolism. Such an adjustment fuels continuous cell growth and division by dramatically changing the energy-generating pathways which normally operate in healthy tissues.

Under aerobic conditions, normal cells convert glucose, first to pyruvate *via* glycolysis in the cytoplasm and thereafter to CO_2 in the mitochondria. Under anaerobic conditions, glycolysis

is favored, resulting in little pyruvate-dispatch to the oxygen-consuming mitochondria. Remarkably, cancer cells can reprogram their glucose metabolism by limiting their energy production mainly to glycolysis even in the presence of oxygen (Warburg effect).[28] Such a metabolic shift seems counterintuitive as it results in a 18-fold lower efficiency of ATP production afforded by glycolysis relative to mitochondrial oxidative phosphorylation. However, neoplastic cells are able to overexpress glucose transporters (*e.g.*, notably GLUT1), thus increasing glucose uptake. [29, 30] Glycolytic pathway has been shown to be associated with activated oncogenes (*e.g.*, MYC and RAS) and mutant tumor suppressors (*e.g.*, TP53) Such dependence on glycolysis can be further accentuated under the hypoxic conditions typically present in malignancies. In addition to upregulating glucose transporters, the hypoxic state upregulates also several enzymes of the glycolytic pathway. [29, 30] Furthermore, this key metabolic switch is also explained in light of the conveyance of the glycolytic intermediates into various biosynthetic pathways, including those generating nucleosides and amino acids, thus fostering in turn the biosynthesis of the organelles and macromolecules needed for assembling new tumor cells.[28]

Clinical oncology and chemotherapy

First of all, tumors can be classified as benign or malignant, the former being localized, generally slow growing and resembling normal cells. In contrast, malignant tumors have an atypical appearance, proliferate more rapidly, may invade and destroy surrounding tissues, leading to death if left untreated. A further categorization relies on where tumor cells arise, distinguishing solid tumors from hematological malignancies. Two types of solid tumors are known, namely carcinomas – tumors of epithelial cells such as lung, colon, breast – and sarcomas – tumors of connective tissue such as bone (*e.g.*, osteosarcoma) or muscle (*e.g.*, leiomyosarcoma). Among the hematological malignancies, there are lymphomas, myelomas and leukemias. The former are tumors of the lympathic system and include Hodgkin and non-Hodgking lymphomas whereas the latter are tumors of blood-forming elements and are classified as acute or chronic, myeloid or lymphoid. [31]

In the context of carcinogenesis, cancers are thought to occur by a multistage mechanism, that involves both genetic and environmental factors. The first step (initiation)

involves the exposure of normal cells to a carcinogen, yielding a genetic damage. Many agents or factors have been recognized in the origin of cancer such as:

- ✓ environmental and occupational exposures, such as ionizing and ultraviolet radiation and exposure to chemicals, including vinyl chloride, benzene, and asbestos;
- ✓ viruses, including epstein-barr virus (ebv), hepatisis B virus (HBV) and human papillomavirus (HPV);
- ✓ genetic factors, including inherited mutations, cancer-causing genes (oncogenes), and defective tumor-suppressor genes;
- ✓ medications, including alkylating agents and immunosuppressants;

lifestyle factors, such as high-fat, low fiber diets and tobacco and ethanol use. [32]

In the stage of promotion, the healthy cells around the neoplastic ones (microenvironment) become altered to allow preferential growth of mutated cells over normal cells, thus yielding the cancerous tissue. At the progression stage, increased proliferation of cancer cells allows for invasion into neighboring healthy tissues and ultimately metastasis.

Upon diagnosis, patients are classified according to the extent of their disease (staging). The stage of the disease is useful in determining prognosis and treatment. Nowadays, two different systems are widely employed for the staging of cancers. In the TNM classification (T stands for the extent of the tumor, N for lymph nodes and M for metastasis), the first number (es. T2) indicates tumor depth and is classified from 0 to 4, with 0 indicating the absence of tumor. The second categorization (N) specifies the presence and extent of regional lymph node spread and is classified from 0 to 3, with 0 indicating no regional lymph node involvement and 3 indicating extensive involvement. The last indication (M) points out the presence of distant metastases and is be classified as 0 (for absence) or 1 (for presence of distant metastases). For example, T2N1M0 designates a moderate-size tumor with limited nodal disease and no distant metastases. [31, 32]

The AJCC system, developed by the American Joint Committee on Cancer, classifies cancers just as stages from 0 to IV. Thus, a defined TNM cancer translates into a stage, with higher numbers indicating deeper tumors with extensive nodal involvement and/or metastasis. According to the AJCC system, there are specific staging criteria for each tumor type. [31]

Following the staging identification, the neoplastic tissue is first reduced by either surgery and/or radiation, followed by chemotherapy/immunotherapy (to attack micrometastases), or a combination of these treatment modalities (notably, chemotherapy alone is exploited when neoplasms are spread and are not amenable to surgery), the goal of

treatment being a cure (i.e., long-term disease-free survival). If it is not possible to achieve a complete response (entire eradication of every neoplastic cell), the ultimate aim is the palliation (*viz.*, no life-threatening toxicity and alleviation of symptoms). The patient hence maintains a "normal" existence along with the cancer, treated as a chronic disease. [32, 33]

When treatment is feasible, it is essential to consider the activity of chemotherapeutic agents with respect to the cell life cycle. Both normal cells and tumor cells go through growth cycles (**Figure 1**). However, normal and neoplastic tissues may differ in the number of cells that are in the various stages of the cycle. Drugs that are effective only against replicating cells (i.e., cycling cells) – are said to be cell-cycle specific whereas the remaining chemotherapeutics are said to be cell-cycle nonspecific. Although the nonspecific drugs, such as cisplatin, generally show higher cytotoxicity against cycling cells, they are also effective against tumors that have a low percentage of replicating cells.

Regarding cell-cycle specificity of drugs, five phases of the cell cycle have been recognized:

1) M phase, or mitosis, is the phase in which the cell divides into two daughter cells;
2) G_1 phase, or postmitotic gap, is when RNA and the proteins required for the specialized functions of the cell are synthesized in preparation for DNA synthesis;
3) S phase is the phase in which DNA synthesis and replication takes place;
4) G_2 phase, or the premitotic or postsynthetic gap, is the phase in which RNA and the enzymes topoisomerase I and II are produced to prepare for duplication of the cell;

G_0 phase, or resting phase, is the phase in which the cell is not committed to division. Cells are reversibly out of phase (e.g., as a result of nutrient deprivation) and may serve as a reserve for repopulation of a tissue. Cells in this phase (nonproliferating cells) are generally not sensitive to chemotherapy but some of these cells may reenter the cycle. Indeed, some chemotherapy regimens are designed to enhance this reentry (recruitment) by killing a large number of actively dividing cells.[31, 32]

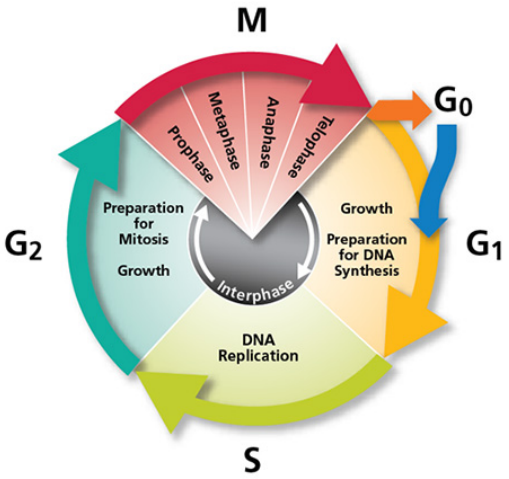

Figure 1. The cell life cycle.

It is worth distinguishing between the cell cycle time and the tumor doubling time. The former is the average time for a cell that has just completed mitosis to grow and divide again, passing through a new mitosis stage.[33] Cell cycle time is specific for each individual tumor (*e.g.*, 28 h and 31 h for the breast cancer cell lines MDA-MB231 and MCF7, respectively[34]). The tumor doubling time (TDT) is the time required for the tumor volume to double in size once. [35] As the tumor enlarges, its TDT gets longer because it contains a smaller proportion of actively dividing or preparing to divide cells (cell growth fraction), owing to restrictions of space, nutrient availability and oxygen supply for replication due to inadequate vascularization.

There is general acceptance that 30–35 tumor doublings are required to achieve a tumor lesion of 5–10 mm diameter (5 mm is more or less the smallest lesion to be diagnosed in the clinic). This corresponds to about 10^9 cells, while a single tumor cell has an approximate volume of 10^{-6} mm^3. [36] Therefore, on the basis of a typical tumor doubling time (a median TDT of at least 100 days[37, 38]) on average about 5-10 years have to pass from tumor initiation in a single malignant cell to the diagnosis of a cancer consisting of approximately 10^9 cells. In fact, such a number of cells is required to produce symptoms and, hence, to be clinically detectable near the plateau phase of the gompertzian (the Gompertz curve was originally derived to estimate human mortality by Benjamin Gompertz in 1832 and then Charles Winsor in 1932 used its expression to describe growth processes) growth curve (**Figure 2**). [31, 32]

As mentioned above, reducing the tumor burden through surgery or radiation favors the recruitment of the remaining cells in G_0 into active proliferation (G_1 phase), thus heightening their susceptibility to chemotherapeutic agents. However, when planning

chemotherapy, several cycles are required as only a certain percentage (depending on the chemotherapy dose) of tumor cells will be killed with each course of therapy. **Figure 3** shows that when cancerous cells are killed, another recruitment occurs, resulting in tumor regrowth. Thus, repeated cycles of chemotherapy are needed to achieve a complete response or remission. It is worth highlighting that the tumor volume never disappears completely because only a percentage of cells are killed with each cycle, including the last one. Accordingly, the immune system may eliminate the remaining cells (less than 10^4).[31-33]

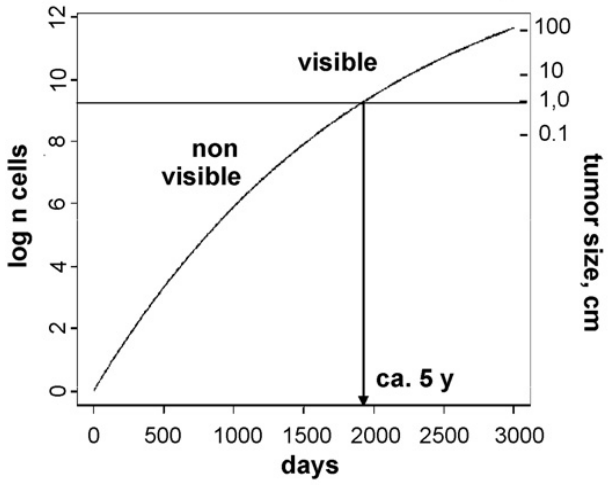

Figure 2. Growth of a tumor modeled by a Gompertzian curve.
The limit of clinical detection is indicated by an arrow.

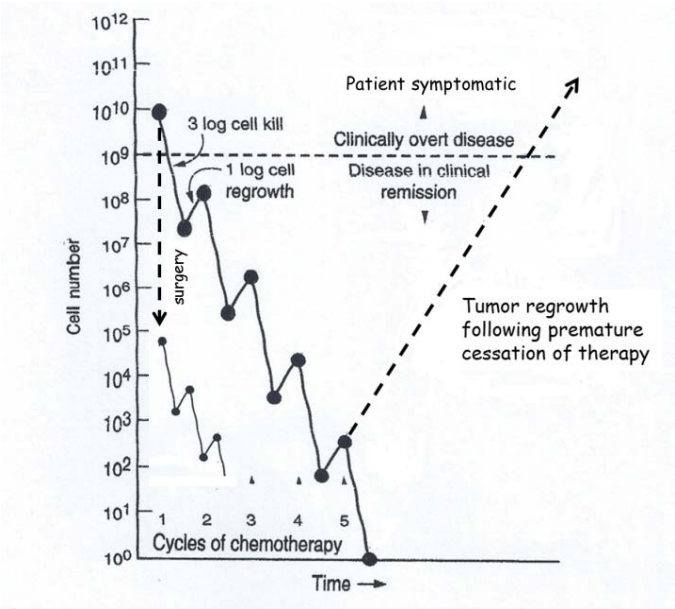

Figure 3. Effects of various treatments on the cancer cell burden in a hypothetical patient. In this example, each cycle of drug adminitration results in 99.9% (3 log) cell kill and 1 log of cell regrowth occurs bewteen cycles. If possible, tumor burden is initially reduced by surgery and/or radiation, followed by chemotherapy cycles.

Regarding the treatment modalities, drugs are usually combined resulting in a more effective therapy compared to single-agent treatments in most of the cancers for which chemotherapy is effective. The advantages for administering combination drugs include enhancement of the effectiveness, cytotoxicity toward a broader range of cells (*e.g.*, both resting and dividing cells), and overcoming or preventing resistance. On the other hand, when combining different agents, some clinical aspects have to be considered such as distinct biomolecular targets and mechanisms of action, no overlapping of the toxicities (otherwise minimal). In addition, scheduling (usually short courses of therapy in cycles) and dosing of combination regimens are significant since they are designed to allow recovery of normal cells. [31]

As stated above, combination-drug chemotherapy should overcome intrinsic resistance or avoid the development of acquired resistance during the treatment (by mutations, particularly after prolonged administration of drugs at low doses). The development of drug resistance is minimized by short-term, sporadic and intensive therapy with combinations of drugs. [31, 33]

A remarkable issue in chemotherapy is the toxicity of the used drugs, which counterbalance their effectiveness due to their usually narrow therapeutic index. In fact, the treatment, aimed at killing rapidly dividing cells, affects normal cells undergoing rapid proliferation as well (*e.g.*, cells of the gastrointestinal and buccal mucosae, the bone marrow, and the hair), resulting in untoward physiological effects such as severe vomiting (controlled by administration of antiemetic drugs), stomatitis, alopecia, myelosuppression, cardiotoxicity and pulmonary fibrosis. The adverse side effects display different durations. For instance, while alopecia is transient, the cardiac, pulmonary, and bladder toxicities are irreversible. However, some toxic reactions may be prevented by different interventions including perfusing the tumor locally or promoting intensive diuresis.[31-33]

Anticancer drugs

When classifying chemotherapeutic agents, several criteria can be used, such as the mechanism of action, the toxicological profile and the chemical features. In this thesis the commonly used drugs will be described according to their mechanism of action but highlighting their organic or inorganic nature. **Table 1** collects four classes of organic anti-cancer agents, namely alkylating agents, antibiotics, antimetabolites and mitotic inhibitors. [31]

Alkylating agents were the first group of antineoplastic drugs, mechlorethamine, or nitrogen mustard, being the archetype. The corresponding cytotoxic effects are caused by their electrophilic character (for instance, due the presence of electron-withdrawing groups such as chloride substituents), thus leading to binding reactions with nucleophilic groups on various cell constituents. The alkylation of DNA is likely the key cytotoxic reaction, which is lethal to the tumor cell. Notably, these drugs are not able to discriminate between resting and cycling cells. Though they are more effective in rapidly dividing cells such as the cancerous ones, all are also mutagenic and hence carcinogenic, causing a possible secondary malignancy. They are used in combination with other agents to treat many lymphatic and solid tumors. [33]

Most of the antitumor antibiotics are obtained from organisms of the *Streptomyces* genus and generally act by intercalation (drug sliding between DNA base pairs triggering DNA or RNA synthesis inhibition). They are cell-cycle specific but phase-nonspecific agents. They can also bind to cell membranes and generate ROS species.

Doxorubicin belongs to this class and is one of the most important and clinically used anticancer drugs. It is used in combination with other agents for treatment of sarcomas and a variety of carcinomas, including breast and lung, as well as for the treatment of acute lymphocytic leukemia and lymphomas. [31]

Tabella 1. Organic anticancer chemotherapeutic agents by mechanism of action and toxicities.

DRUG CATEGORY	Drug	Observed TOX
Alkylating agents	Busulfan	Myelosuppression, pulmonary fibrosis, aplastic anemia, skin hyperpigmentation
	Carmustine	Delayed myelosuppression, nausea and vomiting, hepatotoxicity
	Chlorambucil	Myelosuppression, pulmonary fibrosis, hyperuricemia
	Cyclophosphamide	Myelosuppression, hemorrhagic cystitis, immunosuppression, alopecia, stomatitis, SIADH
	Dacarbazine	Myelosuppression, nausea and vomiting, flulike syndrome, hepatotoxicity, alopecia, flushing
	Ifosfamide	Myelosuppression, hemorrhagic cystitis, somnolence, confusion
	Lomustine	Delayed myelosuppression, nausea and vomiting, hepatotoxicity, neurotoxicity
	Mechlorethamine	Myelosuppression, nausea and vomiting, phlebitis, gonadal dysfunction
	Melphalan	Myelosuppression, anorexia, nausea and vomiting, gonadal dysfunction
	Streptozocin	Renal toxicity, nausea and vomiting, diarrhea, altered glucose metabolism, liver dysfunction
	Temozolomide	Myelosuppression, nausea and vomiting, fatigue, headache, peripheral edema
Antibiotics	Bleomycin	Pneumonitis, pulmonary fibrosis, fever, anaphylaxis, hyperpigmentation, alopecia
	Dactinomycin	Stomatitis, myelosuppression, anorexia, nausea and vomiting, diarrhea, alopecia
	Daunorubicin	Myelosuppression, cardiotoxicity, stomatitis, alopecia, nausea and vomiting
	Doxorubicin	Myelosuppression, cardiotoxicity, stomatitis, alopecia, nausea and vomiting
	Epirubicin	Myelosuppression, nausea and vomiting, cardiotoxicity, alopecia
	Idarubicin	Myelosuppression, nausea and vomiting, stomatitis, alopecia, cardiotoxicity
Antimetabolites	Capecitabine	Diarrhea, stomatitis, nausea and vomiting, hand-foot syndrome, myelosuppression
	Cladribine	Myelosuppression, fever, rash
	Cytarabine	Myelosuppression, nausea and vomiting, diarrhea, stomatitis, hepatotoxicity, fever, conjunctivitis, CNS toxicity
	Fludarabine	Myelosuppression, nausea and vomiting, fever, malaise, pulmonary infiltrates
	5-Fluorouracil	Stomatitis, myelosuppression, diarrhea, nausea and vomiting, cerebellar ataxia
	Gemcitabine	Myelosuppression, fever, flu-like syndrome, rash, mild nausea and vomiting
	6-Mercaptopurine	Myelosuppression, nausea and vomiting, anorexia, diarrhea, cholestasis
	Methotrexate	Mucositis, myelosuppression, pulmonary fibrosis, hepatotoxicity, nephrotoxicity, diarrhea, skin erythema
	6-Thioguanine	Myelosuppression, hepatotoxicity, stomatitis
Mitotic inhibitors	Docetaxel	Myelosuppression, fluid retention, hypersensitivity, paresthesias, rash alopecia
	Paclitaxel	Myelosuppression, peripheral neuropathy, alopecia, mucositis, anaphylaxis, dyspnea
	Vinblastine	Myelosuppression, paralytic ileus, alopecia, nausea, stomatitis
	Vincristine	Peripheral neuropathy, paralytic ileus, SIADH
	Vinorelbine	Peripheral neuropathy, myelosuppression, nausea and vomiting, hepatic dysfunction

Antimetabolites are structural analogs of naturally occurring substrates for biochemical reactions and are cell-cycle specific agents. They generally interfere with the

availability of normal purine or pyrimidine nucleotide precursors by either inhibiting their synthesis or competing with them in DNA/RNA synthesis. Their activity optimum occurs when cells are in the S-phase. The drugs 6-mercaptopurine and 6-thioguanine were the first purine analogs to prove beneficial for treating neoplastic disease such as leukemia.[32]

Mitotic inhibitors affect the microtubule network formation, which is a key component of the mitotic spindle. The mitotic spindle is part of the cytoskeleton that is essential for the movements of various structures, including organelles and vesicles, occurring in the cytoplasm and for the equal partitioning of DNA into two daughter cells during mitosis. Some compounds of vegetal origin belong to this category (*e.g.*, vincristine, vinblastine usually referred to as the vinca alkaloids from the plant *Vinca Rosea*) and they hinder the formation of the mitotic spindle (composed of chromatin and microtubules, in turn made up of the protein tubulin) by binding to tubulin, thus affecting the equilibrium between its polymerized and depolymerized forms. These drugs are both cell-cycle specific and phase-specific as they block mitosis in metaphase. In contrast, the taxanes paclitaxel and docetaxel (active in the G_2/M phase of the cell cycle) strongly promote polymerization of tubulin and overly stabilize the related microtubule polymer, thus leading to chromosome desegregation and cell death. [31, 33]

Another approach used in chemotherapy is the modification of the hormonal equilibria. In particular, tumors that are steroid hormone-sensitive may be either hormone-responsive – the tumor regresses following treatment with a specific hormone – or hormone-dependent – removal of a hormonal stimulus causes tumor regression. Additionally, both situations may take place. Treatment of responsive tumors with steroid hormones is usually only palliative. Removal of hormonal stimuli from hormonal-dependent malignancies can be accomplished by surgery or by drugs. For example, tamoxifen is used for first-line therapy in the treatment of estrogen receptor-positive breast cancer. Being an estrogen antagonist, it binds to the estrogen receptor (by a competitive mechanism) and prevents the growth-promoting effects caused by the natural counterpart. [31]

Another class of anticancer drugs is made up of the topoisomerase inhibitors (*e.g.*, etopoxide, irinotecan), which inhibit the enymes topoisomerases I or II. These enzymes are required for DNA replication and RNA transcription and are G_2 phase-specific agents. [31]
Imatinib was the first approved antitumor drug designed to have targeted enzyme activity. It acts as a signal transduction inhibitor, used specifically to inhibit tumor tyrosine kinase activity which is involved in cell proliferation. Erlotinib and Gefitinib are structurally related

compounds and are selective inhibitors of epidermal growth factor receptor (EGFR) tyrosine kinase. EGFR is a cell surface receptor that is up-regulated in certain solid tumors. The binding of EGFR to its ligand activates tyrosine kinase, which then stimulates growth of the tumor. In those cancers with mutated and overactive EGFR, both drug block the tyrosine kinase cascade and inhibit cancer cell growth. [31, 33]

There are cases (*e.g.*, childhood acute lymphocytic leukemia) wherein enzymes are not the molecular target but the drug, namely the *L*-Asparaginase. Such enzyme catalyzes the deamination of asparagine to aspartic acid and ammonia. Its use (G_1 phase-specific agent) is based on the finding that some cancerous cells have a limited capacity to synthetize asparagine to support growth and function. Upon administration either iv or intramuscularly, *L*-Asparaginase is able to degrade blood asparagine, thus depriving neoplastic cells of this nutrient.[31]

Recently, monoclonal antibodies (mAb) have been further developed to become drugs in cancer chemotherapy. [31, 33]They are obtained from non-antibody-secreting “immortal” myeloma cells (malignant B cells), chosen because they can divide indefinitely, fused with plasma cells (non-cancerous normal B cells), which are short-lived but produce a desired antibody, isolated from the spleen of immunized mice or hamsters. The fusion of a myeloma cell from a line that has lost the capability to secrete immunoglobulin with a B cell known to secrete a particular antibody, results in a remarkable hybrid cell that produces the antibody made by its B-cell component but retains the capability of the corresponding myeloma component to multiply indefinitely. Such hybrid "immortalized" antibody-producing cell is called a “hybridoma” (**Figure 4**). The resulting hybrid cells can be cloned and each clone will yield monoclonal (because they are produced by the identical offspring of a single, cloned antibody producing cell) antibodies able to identify a specific antigen type on the cancer cell surface. Recombinant technology has led to the production of “humanized” antibodies that overcome the immunologic issues previously observed upon administration of mouse antibodies.[(iv)]

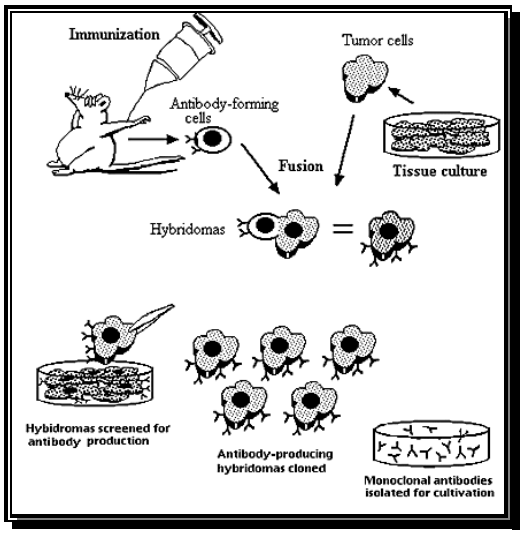

Figure 4. Production of monoclonal antibodies by hybridoma technology. Immunization of animals with a selected antigen stimulates antibody-forming immune cells to produce a range of antibodies with varying specificities and affinities. Collections of immune cells removed from the spleen are fused with tumor (myeloma) cells to produce immortalized hybridoma cells, each with a distinctive reactivity. These hybridoma cells are then screened *in vitro* for those with reactivities against the antigen of interest, and specific clones are isolated by limiting dilution. These cells are grown by clonal expansion, and a single population of mAb, which does not cross react with any other antigen, is harvested.

Rituximab was the first mAb to be approved for the treatment of cancer since its Fab (antigen binding fragment) domain is able to bind to the CD20 antigen, thus allowing the patient's immune system to eliminate those cells (Fc domain-mediated effector functions). Rituximab is commonly used with other drugs such as doxorubicin.[33]

Among the patients with metastatic breast cancer, only 25 to 30% show overexpression of transmembrane human epidermal growth factor-receptor protein 2 (Her2). Trastuzumab specifically targets the estracellular domain of Her2 that has intrinsic tyrosine kinase activity. By competing with the epidermal growth factor, it inhibits the tumor proliferation but the cascade intracellular mechanism has not been elucidated yet. Furthermore, some monoclonal antibodies are conjugated to antitumor agents or radioisotopes to enhance the effectiveness of these drugs due to a targeting effect. In addition to being very expensive, mAb-based strategies require the identification of those patients who express certain antigens on the membrane of neoplastic cells.[31, 33]

Since breast malignancy is the first cause of cancer death in women and in light of the drugs usually employed to treat such neoplasia, in this work we have focused on the breast cancer cell line MDA-MB-231. In fact, these cells are highly metastatic, invasive and resistant to cisplatin.

Moreover, the MDA-MB-231 cell line is a so called “triple-negative” breast cancer which lacks of benefit from both hormonal therapies (based on estrogen and progesterone receptor antagonists such as Tamoxifene) and monoclonal antibody-based therapy targeting the human epidermal growth factor receptor 2 (*i.e.*, Trastuzumab).[39]

The drugs taken into account up till now are organic molecules thereby containing only the elements carbon, hydrogen, oxygen, nitrogen, phosphorus and sulfur. Although they are the greater part of anticancer agents, some therapies involve inorganic compounds. The first inorganic drug to be clinically used was cisplatin, approved by the Us food and Drug Administration in 1978. It has found wide application in the treatment of solid tumors, such as testicular, ovarian and bladder carcinomas.[32] Due to its severe toxicity, in particular nephrotoxicity, other platinum complexes, including carboplatin and oxaliplatin, have been subsequently designed and developed.

Given that the design of our first dithiocarbamato complexes was based on the chemical properties and toxicological profile of cisplatin and the MDA-MB-231 breast cancer cell line – experimentally used in this work – is resistant to such drug, a detailed description of its mechanism of action and the types of observed resistance is reported in a distinct section below. Cisplatin derivatives are briefly described as well, followed by the gold-based antiarthritic drugs.

A successful more recent history in the field of bioinorganic chemistry regards the drug bortezomib (Velcade®), which is a proteasome inhibitor used in patients with multiple myeloma. Proteasomes are multicatalytic enzyme complexes involved in the degradation of proteins which control the cell cycle. In particular, following proteasome inhibition, the inhibitor of the nuclear factor κB (NF-κB) is not digested anymore, so that NF-κB cannot move to the nucleus and transcribe key genes promoting cancer growth.[40] Since in this work two gold-based compounds turned out to be potent proteasome inhibitors both *in vitro* and *in vivo* against MDA-MB-231 cancer cells, we focused our attention on bortezomib mechanism of action at the molecular level, in order to gain further insights into the anticancer activities observed for our complexes. Bortezomib mechanism of action along with its preclinical and clinical histories are described below.

The drug bortezomib (Velcade®)

Drug indication and clinical development

Velcade® (bortezomib) was approved by the United States Food and Drug Administration (FDA) in 2003 experiencing an unprecedented only 8 years program from lead compound discovery to FDA approval owing to a huge clinical need for multiple myeloma (MM) treatment. [41] In addition to MM (a type of plasma-cell neoplasia), Velcade is administered also to patients with mantle cell lymphoma (a cancer of lymph nodes) who have already attempted other treatments. [42]

To date, bortezomib is approved in more than 90 countries and is marketed by Millennium Pharmaceuticals, a biopharmaceutical company based in Cambridge (Mass., USA) and acquired by Takeda Pharmaceutical Company in 2008, thus becoming *Millennium: The Takeda Oncology Company*.(v)

Throughout its development basically two steps proved decisive. Upon National Cancer Institute's 60-cell line screen, bortezomib showed remarkable cytotoxic activity against several cancer types.[43] Besides tumor proliferation inhibition, it induced high apoptosis indexes and overwhelmed drug resistance.[44] Notably, large phase II clinical trials were carried out involving 202 patients with relapsed and refractory MM turning out 35% total response rate (including 4% of complete remission, 6% of almost complete remission, 18% of partial remission, and only 7% of negligible response).[45]

Velcade is administered by an intravenous injection and can cause severe side effects such as neurological (peripheral neuropathy and neuralgia) and cardiovascular disorders, fatigue, gastrointestinal problems (nausea, vomiting, diarrhea, and constipation), neutropenia (low levels of neutrophils) and thrombocytopenia (low levels of platelets).(v)

Mechanism of action

Velcade®, a dipeptidyl boronic acid (**Figure 5**), is the first-in-class proteasome inhibitor. The proteasome is a large multimeric protease complex with a central role in protein degradation in both the cytosol and the nucleus, generating oligopeptides ranging in length from 3 to 15 amino acid residues.[46, 47]

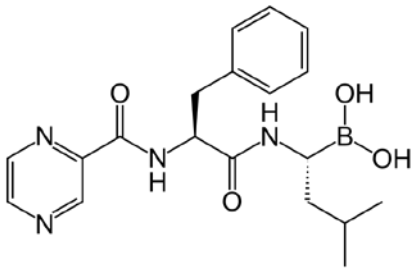

Figure 5. Chemical structure of the drug Velcade®.

The resulting peptide products are subsequently hydrolyzed to amino acids by oligopeptidases and/or amino-carboxyl peptidases. [47, 48] Among the proteasomal enzymes, the most studied is the 26S proteasome whose molecular weight is 2,500 kDa. 26S proteasome is formed by a barrel-shaped multicatalytic complex referred to as the 20S proteasome core particle (CP), capped at each end by a regulatory component termed the 19S complex (**Figure 6**). The role of the 19S particles is to recognize ubiquitinated client proteins, and regulate protein access to the 20S core by playing a key role in their unfolding and translocation into the proteolytic chamber of the CP.[48] The CP (molecular weight of approximately 700 kDa) consists of four heptameric, tightly and axially stacked, rings to form a cylinder-like structure with the two outer rings made up of seven different α-type subunits and two inner rings consisting of seven different β-type subunits, following an $\alpha_{1-7}\ \beta_{1-7}\ \beta_{1-7}\ \alpha_{1-7}$ stoichiometry. [48]The distinguishing multiple peptidase activity of the eukaryotic 20S proteasomes is confined inside the inner cavity at distinct active sites located in the β–subunits. Among them, proteolysis occurs within catalytic pockets of only three β–subunits (β1, β2, and β5), which harbor threonine residues at their *N* termini and show *N*-terminal nucleophile (hereinafter, Ntn) hydrolase activity. Two pairs of these three active sites face the interior of the cylinder since there are two beta rings. [49]

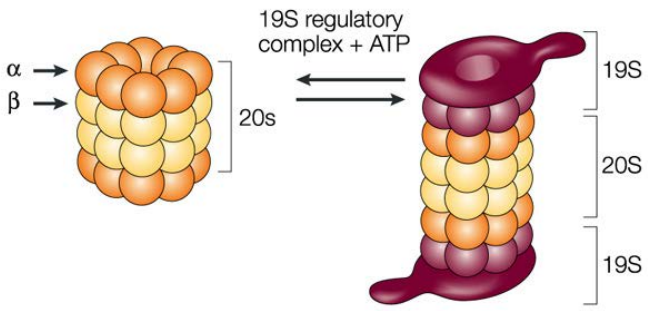

Figure 6. Composition scheme of proteasome 26S.

From the pharmacodynamics point of view, bortezomib antitumor activity occurs by a regioselective and reversible proteasome inhibition and it is maximal 1 h after administration.[50, 51] In order to explain the aforesaid regioselectivity, it is worth noting that the subunits β1, β2, and β5 recognize distinguishing side chains of different peptides, thus resulting in specific activity for each catalytic site, whereas the remaining β-subunits are inactive.[48] Concerning the substrate specificity, *in vitro* assays with chromogenic peptides disclosed that proteasomal activities are restricted to only five distinct cleavage preferences: chymotrypsin-like (CL), trypsin-like (TL), peptidyl-glutamyl-peptide-hydrolizing-like (PGPHL, also called postacidic or caspase-like), branched chain amino acid-preferring (BrAAP), and small neutral amino acid preferring activity (SNAAP). [48, 52] Among these catalytic activities, the first three are the most studied and are assigned to β5, β2, and β1 subunits, respectively. Bortezomib chiefly targets the proteasomal β5 active site (β5> β1>> β2) even though its binding mode to all three subunits is basically identical. [53] Indeed, the oxygen atom on the side chain of the *N*-terminal threonine (Thr1O$^{\gamma}$) of each subunit forms a tetrahedral adduct with the boron atom owing to its Lewis acidity. On the other hand, drug peptide backbone binding mode brings about different affinities to the three proteasomal pockets because of interactions of inhibitor organic moieties with specific functional groups of each enzymatic cleft (topological – morphological and chemical – complementarity). However, in any active site in its bound conformation, bortezomib adopts an antiparallel β–sheet conformation stabilized by direct hydrogen bridges between main chain atoms of the drug and the conserved residues (Gly47N, Thr21N, Thr21O, and Ala49N) of the β-type subunits (**Figure 7**). [54]

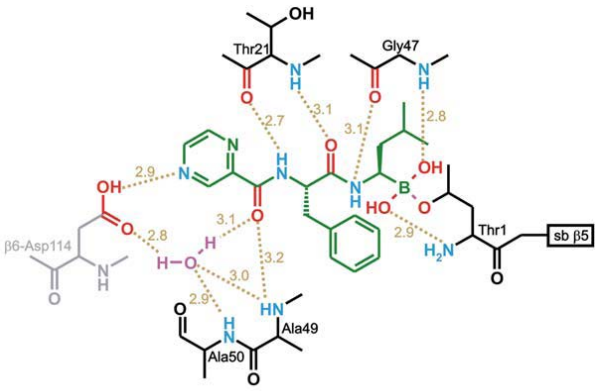

Figure 7. Scheme of boron tetrahedral adduct and intermolecular interactions (11 hydrogen bonds) occurring between bortezomib and the proteasomal β5 pocket.

Figure 8 shows the enzyme-ligand interaction in β5 cleft obtained by means of the software Chimera (PDB code: 2F16).[40, 55]

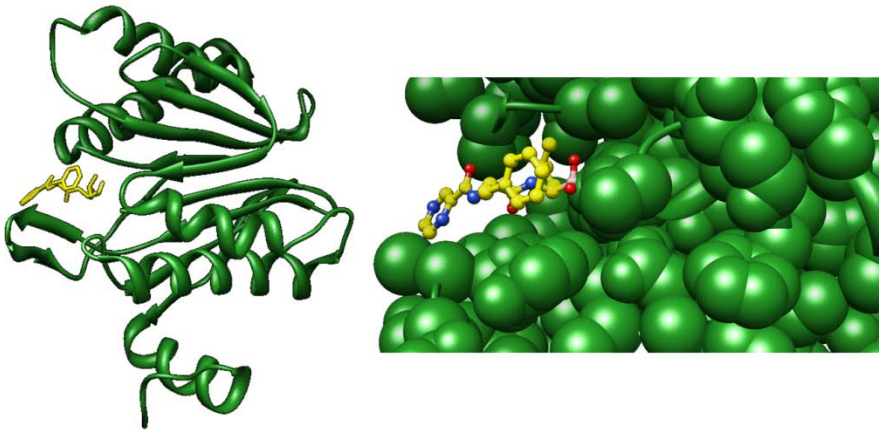

Figure 8. Ribbon backbone representation (left) and molecular surface visualized by space-filling representation (right) of the crystal structure of β5 subunit (green) and bortezomib (yellow) [color code: blue for nitrogen atoms, red for oxygen atoms, yellow for carbon atoms and pink for the boron atom]. [Picture produced using the UCSF Chimera package from the Resource for Biocomputing, Visualization, and Informatics at the University of California, San Francisco].

Interestingly, it has been shown that chymostrypsin-like pocket targeting is associated with apoptosis induction in cancer cells.[56] In addition to the bortezomib high affinity to proteasomal β5 subunit under physiological conditions, Ntn-hydrolases targeting may account for its unmatched antitumor activity for patients with MM. As a matter of fact, Velcade does not show cross-reactivity toward cysteine or serine proteases. Regarding the former hydrolases, according to the Lewis hard-soft acid-base principle, Boron atom preferentially binds to hard oxygen nucleophiles in lieu of soft sulfur donors. In spite of boronic acid derivatives are well-known inhibitors of serine proteases,[57] turning out a serine-boronate tetrahedral adduct,[57, 58] compared to serine proteases, the proteasomal Thr1O^{γ}-bortezomib tetrahedral complex is stabilized by a further tight hydrogen bond between the second acidic boronate hydroxyl moiety (H-donor) and the N-terminal threonine nitrogen atom (H-acceptor).[54]

β-5 subunit inhibition by Velcade triggers various effects in signal transduction pathways that regulate cell cycle and proliferation. For instance, the nuclear factor NF-κB mediates tumor cell survival and proliferation since upon activation it can translocate to the nucleus and elicit transcription of target genes by binding to specific DNA sequences (promoter regions). The involved genes encode for an ever-growing list of species such as

cell adhesion molecules, cytokines, anti-apoptotic factors and enzymes. The inhibitor protein I-κB binds to NF-κB in the cytoplasm, thus inactivating and thereby hampering cell growth as a result of down-regulation of anti-apoptotic target genes. However, I-κB can be phosphorylated, ubiquitinated and therefore degraded by proteasome. On the basis of these considerations, proteasome-bortezomib interaction is followed by an increase in I-κB levels, that leads to tumor growth inhibition.[59, 60] Furthermore, Velcade determines accumulation of proapoptotic proteins, such as NOXA, p53, p27 and BAX, and decreased levels of antiapoptotic proteins, including Bcl-2, MCL-1 and IAP.[44, 61-67] Such altered balance causes mitochondrial membrane potential decrease, subsequent release of cytochrome c in the cytosol and activation of caspases (-9, -7, -3) that ultimately cause DNA cleavage and apoptosis.[65]

From the pharmacokinetic point of view, in preclinical studies Velcade is quickly removed from blood vessels due to its solubility; blood levels drop below the detection threshold within minutes. [52]

Cisplatin: the archetype of metal-based anticancer drugs

Historical survey of a leading anticancer drug

Cisplatin was synthesised for the first time by an Italian researcher, Michele Peyrone, who first graduated as a medical doctor in Turin in 1835, but soon afterwards (1939) abandoned medicine for chemistry and spent several years in different laboratories in France, Germany, Netherlands, Belgium and Great Britain. [(vi)] In the Liebig's laboratory, in Giessen, he synthesised in 1845 a new platinum compound[(vii)] containing two amines and two chlorines, like the already known Reyset's salt, [(viii)] but having different physico-chemical properties. In those times, there was no way to justify the obtainment of two different compounds with the same molecular formula as the tetrahedral geometry was thought typical for tetravalent compounds. 50 years later, Alfred Werner proposed for these compounds a square planar geometry which can accommodate a *cis* and a *trans* isomer, the Peyrone's and Reyset's compounds, respectively (**Figure 9**). [(ix)]

(a) **(b)**

Figure 9. Isomers of diaminodichloroplatinum(II): *cis*-DDP (cisplatin) **(a)** and *trans*-DDP **(b)**.

It was by accident that the biophysicist Barnett Rosenberg, while investigating the effect of an electric field on cell division in *Escherichia coli*, generated electrochemically the Peyrone's compound by reaction of the platinum electrodes with various components present in the cell culture medium.[68-70] In 1968, following further tests against various bacteria, *cis*-diaminodichloroplatinum(II) (hereinafter, cisplatin or *cis*-DDP) was successfully administrated to mice bearing the standard murine transplantable tumour sarcoma-180, causing tumour regression.[71] With confirmatory *in vivo* tests performed at the Chester Beatty Institute in London, cisplatin was taken on by the US National Cancer Institute (NCI) for clinical testing. The first patients were treated in 1971, a remarkably short time, in modern terms, from the original discovery.[72] Approval by the US Food and Drug Administration (FDA) was granted in 1978.[73] Since then, cisplatin has become one of the most used anticancer drugs in the world. It is an effective cure for testicular cancer, one of the most useful against melanoma, bladder and non-small-cell-lung carcinomas, and in combination therapy, it is considerably active against ovarian cancer.[33, 74]

The mechanism of action of cisplatin

Aqueous solution chemistry as a fundamental for the biological activity

Cisplatin is administered to cancer patients intravenously as a sterile saline solution. Once the drug is in the bloodstream and in the extra-cellular fluids, it remains integral due to the relatively high concentration of chloride ions (~100 mM). The neutral compound then enters the cell by either passive diffusion across the lipid bilayer or active uptake mediated by carrier import proteins like organic cation transporters (OCT)[75, 76] or copper transporter 1 (CTR1).[77] Inside the cell, the chloride ion concentration drops from ~100 to ~3-20 mM, and the neutral cisplatin molecule undergoes hydrolysis in which a chloride ligand is replaced by one molecule of water, thus generating a positively charged species (**Figure 10**).[(x)] It is worth highlighting that this hydrolyzed form is able to react with

DNA (see below); in fact, it has been proved that the formation of Pt(II)-DNA adducts and the first cisplatin hydrolysis reaction occur with similar rates, thus suggesting that the mono-aqua species $[(NH_3)PtCl(H_2O)]^+$ is predominant in cytoplasm. (x)

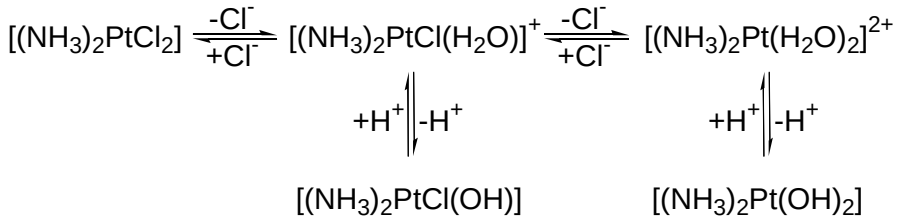

Figure 10. The stepwise hydrolysis reactions of both *cis*- and *trans*- diamminodichloroplatinum(II) (DDP) to form aquo species that can deprotonate at physiological pH.

In particular, although chloride ion is a better *trans*-labilizing ligand than ammonia, it is also a better leaving group. [78,(xi)], thus the first product formed is $[(NH_3)_2PtCl(H_2O)]^+$, rather than $[(NH_3)(H_2O)PtCl_2]$. Notably, the structural features of all the platinum(II)-based drugs showing antitumor activity are interpreted in relationship to the possibility to form platinum(II)-DNA adducts. Strictly, these features (all present in cisplatin itself) are summarized as follows:

1) platinum(II) complexes must contain two labile leaving groups and two inert ligands (that is, chloride ions and ammonia molecules, respectively in cisplatin);
2) both labile and inert ligands must be in reciprocal *cis* position.(xii)

It is generally accepted the DNA is the principal target for cisplatin in cells and that DNA replication and transcription are the major functions impaired by this drug in the tumor cells; in fact, the capability of the adducts cisplatin-DNA to stop the subsequent action of DNA polymerase translates into inhibition of cell division and hence induction of cell death.[79, 80] Notably, cisplatin causes cell death both by apoptosis and non-apoptotic, necrotic-like processes. In general, in tumor and non-tumor cells (both in vitro and in vivo), low concentrations of cisplatin induce apoptosis, whereas higher ones cause necrosis.[81]

As it turns out, formation of any platinated coordination complex with DNA is not sufficient for cytotoxic activity. The corresponding *trans* isomer of cisplatin also forms a coordination complex with DNA but unlike cisplatin, *trans*-DDP is not an effective chemotherapeutic agent. Due to the difference in geometry between *cis*- and *trans*-DDP, the types of coordination complexes formed by the two compounds with DNA are not the same (see below). It appears clear that these differences are of critical importance in determining the efficacy of a particular compound for the treatment of cancer. For this reason, a great

deal of effort has been placed on discovering the specific cellular proteins that recognize cisplatin-DNA complexes and then examining how the interaction of these proteins with the complexes might lead to programmed cell death. [x, xiii]

Once inside the cell, in addition to DNA, cisplatin has a number of other possible targets including RNA, sulfur-containing enzymes (such as metallothionein and glutathione) and mitochondria. Exposure of cells to cisplatin directly causes characteristic mitochondrial alterations leading to the activation of the intrinsic pathway of apoptosis and other signals leading to cell death. [82, 83] As a result, various molecules (*e.g.*, cytochrome c, the apoptosis inducing factor) normally confined to the intermembrane space are secreted into the cytosol, where they initiate specific deadly signaling pathways.[81] However, some evidence suggests that, despite depressing mitochondrial respiration, cisplatin does not target directly the respiratory chain.[84] Interestingly, this drug binds to mitochondrial DNA with higher efficiency with respect to nuclear DNA.[85] This might be due to internal differences in subcellular distribution, but it has been also ascribed to the low efficiency DNA repair in mitochondria.[86] In addition, cisplatin activity has been associated with ROS over-production as well. Treatment with cisplatin inhibits antioxidant enzymes, including superoxide dismutase (SOD), catalase, glutathione peroxidase, glutathione S-transferase[87] and glutathione reductase[88] in kidney tissues, which may explain the depletion of glutathione observed in this tissue. Excessive ROS cause mitochondrial and cellular oxidative stress, including damage to DNA, proteins and lipids, which are associated to cell death.[89] Interestingly, cisplatin also reacts with the plasma membrane. It forms strong bonds with plasmalemmal proteins, and weaker but relevant interactions with negatively charged phospholipids (*e.g.*, phosphatidylserine), in the form of coordination complexes. By reaction with membrane proteins, the drug decreases the activity of some transporters and ion channels such as the Na/K ATPase, the sodium-proton exchanger (NHE1), and the NA/Pi and Na/glucose co-transporters, with still undefined consequences.[81]

Although it is known that DNA is a major target for cisplatin, only about 5% of internalized drug reaches DNA while around 80% binds to nucleophilic sites of intracellular constituents like thiol containing peptides, proteins, replication enzymes, and RNA.[90-93]

The interaction of cisplatin with sulfur-containing enzymes and proteins is believed, in some cases (*e.g.*, glutathione and metallothioneins,), to be involved in promoting drug-resistance and toxicity (see below). The roster of proteins affected by cisplatin include telomerase[94], ubiquitin[95], superoxide dismutase, lysozyme, as well as extracellular proteins such as albumin,

transferrin, and hemoglobin.[96, 97] The effects of cisplatin on RNA and DNA have been studied extensively. Although cisplatin can coordinate to RNA, this interaction is not believed to play an important role in cisplatin physiological mechanism of action. First, a single damaged RNA molecule can be replaced by newly synthesized material and some studies have revealed that cisplatin does not affect RNA synthesis. Second, when cisplatin was administered *in vitro* at its lethal dose to a strain of cancer cells, only a small fraction (1 to 10%) of RNA molecules were damaged. [(x, xiii)] On the contrary, as mentioned above, there is strong evidence that DNA is the most prominent target of the drug. In fact, cisplatin is a well-known DNA-damaging agent and the specific adducts produced in DNA have been well characterized.[(x, xiv)] The reaction between cisplatin and DNA results in the formation of different kinds of adducts, shown in **Figure 11**.

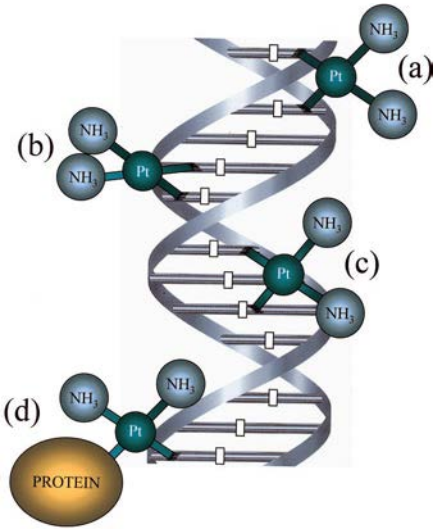

Figure 11. Main adducts formed in the interaction of cisplatin with DNA: (a) interstrand cross-link; (b) 1,2-intrastrand cross-link; (c) 1,3-intrastrand cross-link; (d) protein-DNA cross-link.

Enzymatic studies of DNA platinated by cisplatin[98-100] revealed a strong preference for binding to sequences containing two or more adjacent guanosine nucleosides. The quantification of these and other, less common, adducts was achieved by first degrading DNA platinated *in vitro*[101-103] or *in vivo*[104] to a combination of nucleobases and then separating and identifying the resultant fragments by chromatography and, for the *in vivo* studies, by immunochemical techniques.

The major site of platination in double-stranded DNA (65%) derives from intrastrand cross-links between two neighboring deoxyguanosines, d(GpG). About 20% of the DNA platination derives from intrastrand cross-links at a d(ApG) sequence, but no adducts were detected when these two nucleosides, adenosine and guanosine, are in the opposite order

(*i.e.*, d(GpA)). Another 9% of the platination derives from cross-links between two not adjacent deoxyguanosines (d(GpNpG), where N is any nucleoside). All of these modifications occur through the N(7) position on the purine ring because it does not form hydrogen bonds with any other DNA base; these nitrogen atoms are located in the DNA major groove, so they are more exposed to platination (**Figure 12**). [(xv)]

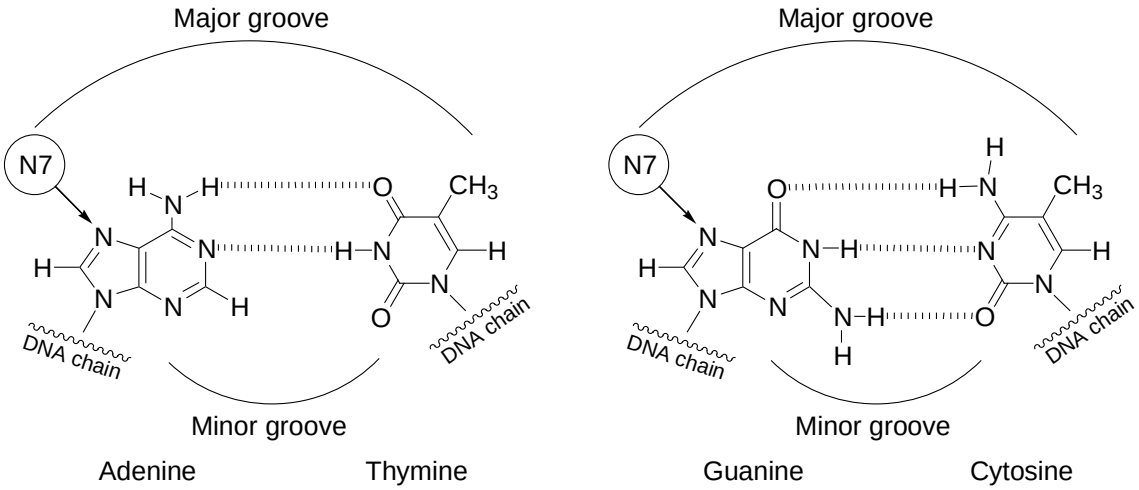

Figure 12. The DNA base pairs; cisplatin coordinates to the N(7) atoms of the guanine and adenine purine rings.

Following DNA platination for few minutes, over 40% of the platinated DNA is in the form of monofunctional modification of deoxyguanosine; however, after a few hours, , these adducts rearrange rapidly to the various bifunctional adducts. [(xvi)] Monofunctional adducts are rapidly produced by both *cis*- and *trans*-diamminodichloroplatinum(II), but this adduct is not believed to show any biological activity, , as it is labile and determines only slight structural modifications on DNA without inhibiting DNA synthesis. [105-107]

DNA interstrand cross-links have been also found to be formed between two deoxyguanosines, but this requires a major contortion of the DNA structure and may occur when an alternate purine is not in close proximity of guanosine on the same strand.[108] This presumably explains why interstrand cross-links occur at less than 1% of the total platination of DNA.

One other adduct that was shown to be formed was a cross-link between deoxyguanosine and a protein or a glutathione molecule; this adduct can be produced when DNA is first platinated for a short time to give monofunctional adducts, and then protein or glutathione is added.[109]

Hence, it has been proved that the formation of the monofunctional platinum(II)-DNA adduct is the first step involved in the platination of DNA, followed by the solvolysis of the

second chloride atom and the subsequent rearrangement to a bifunctional adduct, mainly identified as a d(GpG) intrastrand cross-link. In this second phase, it is determinant the *cis* or *trans* geometry of the platinum(II) complex, as reactions with DNA occur with retention of stereochemistry. [xvii]

Due to its geometry, *trans*-DDP cannot form d(GpG) intrastrand adducts with DNA; since *trans*-DDP is inactive in killing cancer cells, it was supposed that these intrastrand adducts formed between cisplatin and DNA are important for the anticancer activity of cisplatin itself. In fact, when *cis*-DDP binds to DNA forming bifunctional adducts, it promotes super helical unwinding and shortens the double helix; [110, 111] the distortions induced in the DNA double helix by inter- and intrastrand cross-links have been characterized by several techniques. For example, in the interstrand d(GpG) cross-links the platinum residue is positioned in the minor groove, and the axis of the double helix is bent of about 45-47° towards the minor groove, with a large unwinding of about 70-79°. [112] On the other hand, the formation of intrastrand d(GpG) cross-links causes the non-stacking of purines and thereby the bending of the DNA helix (**Figure 13**) of 26-35° toward the major groove and a shorter unwinding of the double helix (~13°). [113]

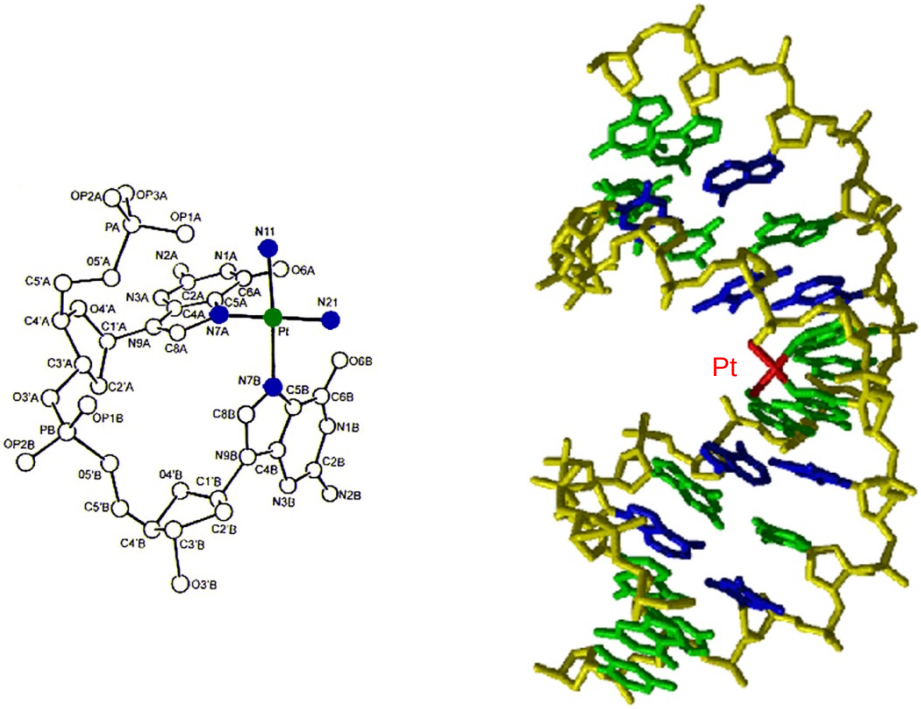

Figure 13. On the left, the structure of cisplatin (with platinum shown in green and nitrogen ligands shown in blue) coordinated to a dinucleotide containing two guanines. Notice the de-stacking of guanine bases, which would normally be parallel to one another. On the right, the structure of cisplatin coordinated to two guanines in a DNA duplex.

The main structural alterations in DNA caused by cisplatin are reported below (**Table 2**).[114]

Table 2. Structural alterations in double-stranded DNA caused by cisplatin.

DNA-cisplatin adduct	DNA	
	unwinding angle [°]	bending angle [°]
d(GpG) intrastrand cross-link	13	26-35
d(ApG) intrastrand cross-link	13	35
d(GpTpG) intrastrand cross-link	23	33
d(GpG) interstrand cross-link	70-79	45-47

From Pt-DNA adducts to apoptosis

Once it has been shown how cisplatin binds DNA, it seemed to be fundamental to explain how the binding of cisplatin to DNA led to programmed cell death (apoptosis). Researchers have found that this binding affects both replication and transcription of DNA, as well as mechanisms of DNA repair (see below). [(xviii)] The effects of both cisplatin and *trans*-DDP on DNA replication were studied both *in vitro* (using cell extracts outside the host organism) and *in vivo* (inside the host organism). *In vitro* studies on both prokaryotic (bacterial) and eukaryotic (mammalian) cells revealed that DNA adducts of both *cis*-DDP and *trans*-DDP blocked the action of DNA polymerase, an enzyme necessary for replication. In particular, 1,2-intrastrand adducts of cisplatin with DNA stopped all polymerase functions. Likewise, further studies showed that cisplatin and the *trans*-analogue inhibited replication equally well. Since other studies have shown that cisplatin is an effective antitumor agent but *trans*-DDP is not, these results suggested that DNA replication is not the only factor important for the clinical activity of cisplatin in destroying cancer cells. [(xiii)] The effects of *cis*-DDP and *trans*-DDP on DNA transcription are harder to interpret than the effects on replication. However, cisplatin does not appear to inhibit transcription, possibly leading to programmed cell death. [(xiii)] Thus, the cytotoxic activity of cisplatin may arise from the cell inability to repair DNA damage elicited by the drug. In fact, there are several known cellular defense mechanisms (see below), which interact with or respond to damaged DNA, and may be able to remove lesions from DNA and correct any unwanted changes. The unusual conformations of platinated DNA might act as recognition sites for proteins that

process damaged DNA. Several types of assays can differentiate between platinated DNA that is bound to a protein and free one. Investigators used these assays to isolate several proteins that bind to cisplatin-DNA adducts. These proteins all contain a common portion (that is, similar or even identical sequences of amino acids) called high mobility group (HMG); proteins in this class are called HMG-domain proteins. [(xviii)]

The HMG-domain proteins constitute the largest and most extensively characterized group of non-histone chromosomal proteins; they can bind to specific structures in DNA or in chromatin with little or no specificity for the target DNA sequence.[115] Two families of HMG proteins have been reported. The first consists of proteins containing two or more HMG domains; it includes HMG1 and HMG2 proteins, the nucleolar RNA polymerase I transcription factor UBF (upstream binding factor) and the mitochondrial transcription factor mtTF. In the second family there are proteins containing single HMG domain, such as tissue-specific transcription factors. Several types of HMG proteins, including HMG1, HMG2 and UBF bind to DNA-cisplatin adducts with high affinity and specificity. [116, 117] These proteins recognize 1,2-intrastrand cross-links including the majority of adducts formed by cisplatin *in vivo*. Domain A of the structure-specific HMG protein HMG1 was reported to bind to the widened minor groove of a 16-base-pair DNA duplex containing a site-specific *cis*-$(NH_3)_2$Pt-d(GpG) adduct.[118] DNA is strongly kinked where the DNA-platinum cross-link is present and the protein binding was shown to take place at the 3' side of the platinated strand (**Figure 14**).

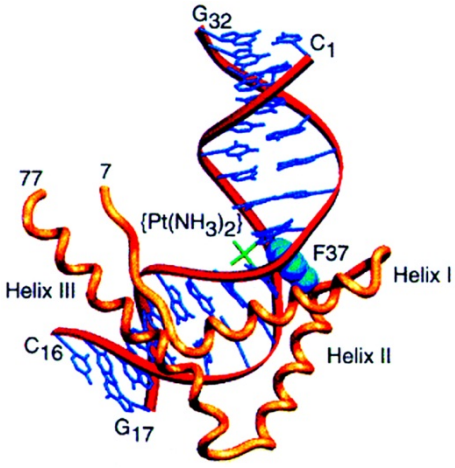

Figure 14. Structure of the complex between the non-sequence-specific domain A of HMG1 and cisplatin-modified DNA

Two theories explain the possible role of HMG-domain proteins in cisplatin's cytotoxic activity. Many HMG-domain proteins are transcription factors, required for the synthesis of RNA.The firsttheory asserts that if HMG-domain-containing transcription factors bind preferentially to the cisplatin-DNA adducts, they could wreak havoc with the transcriptional machinery, resulting in "cisplatin-mediated transcription factor hijacking" which reduces rRNA synthesis in growing cells,[119] possibly leading to cell death. The second theory suggests that when HMG-domain proteins bind to the cisplatin-DNA adducts, the adducts would not be recognized by the repair machinery. DNA repair thereby results slower than normal, as shown in **Figure 15**. This could interfere with the normal functions of the cell (among them, replication and transcription) and possibly trigger cell death.[120]

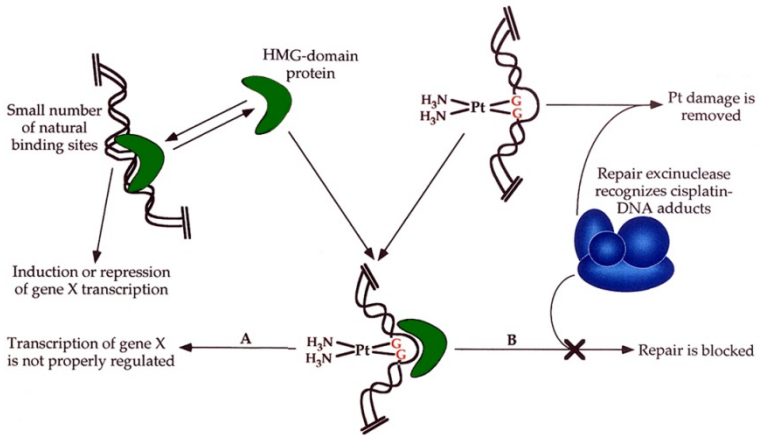

Figure 15. Models for HMG involvement in the cisplatin mechanism of action. **A**) When a cell is exposed to a lethal dose of cisplatin, 10^4-10^5 DNA adducts are formed. If HMG-domain proteins bind with similar affinity to these lesions and to their natural binding sites, the proteins could be titrated away from their transcriptional regulatory function. **B**) The HMG-domain proteins could block access of the excision repair complex and shield the adducts from repair.

Onset of resistance to cisplatin

Even though cisplatin has proved to be an highly effective chemotherapeutic agent for treating various types of cancers, it can encounter the same fate as many other drugs used in cancer chemotherapy, namely "drug resistance". Resistance occurs when cells, after the first cycle of treatment with a drug, no longer respond to treatment with that drug. Drug resistance is a major complication in cancer chemotherapy and accounts for the failure of chemotherapy to cure the majority of cancer patients. Indeed, drug resistance has significant clinical implications. When cells become resistant to cisplatin, the doses must be increased; a large dose escalation can lead to severe multiorgan toxicities (such as failures

of kidneys and bone marrow), intractable vomiting and deafness.[121] Drug resistance exists in two forms: "acquired resistance", in which a drug is initially beneficial but becomes ineffective over time and "intrinsic resistance", in which the drug is ineffective from the outset.

Galluzzi and coworkers has recently provided a systematic classification of the mechanisms involved in cisplatin resistance, including the steps (i) preceding the binding of cisplatin to DNA (pre-target resistance), (ii) directly related to DNA–cisplatin adducts (on-target resistance), (iii) concerning the lethal signaling pathway(s) elicited by cisplatin-mediated DNA damage (post-target resistance) and (iv) affecting molecular circuitries that do not present obvious links with cisplatin-triggered signals (off-target resistance).[122]

Within the pre-target resistance, there are at least two mechanisms by which malignant cells evade the cytotoxic potential of cisplatin before it binds to cytoplasmic targets and DNA: (1) a reduced intracellular accumulation of cisplatin and (2) an increased sequestration of cisplatin by inactivating sulfur-containing molecules such as GSH, metallothioneins and other cytoplasmic 'scavengers' with nucleophilic properties.[123] With respect to the first case, cisplatin is able to use copper transporting proteins to reach intracellular compartments. In particular, the high affinity copper transporter (CTR) 1 is the main influx transporter in multiple cell types.[124] It is a key protein in the regulation of intracellular copper level for homeostasis maintenance.[125] Studies carried out by Ishida *et al.* showed that specific mutations or deletions in the CTR1 gene confer strong resistance to cisplatin[77]. CTR1 gene mutations are also associated with reduced intracellular levels of platinum in yeast and mammalian cells.[126] In agreement, deletion of CTR1 is present in cells resistant to cisplatin, both in *in vitro* and *in vivo* systems[124]. Conversely, intracellular accumulation of cisplatin is enhanced when the human CTR1 gene is overexpressed as for example in human ovarian cancer cells.[127] Another CTR, namely CTR2, has recently called attention with regard to cisplatin handling. CTR2 is normally expressed in late endosomes and lysosomes, and maybe also in the cell membrane in mammalian cells.[128] CTR2 reduces cisplatin accumulation through the inhibition of endocytosis, which is mediated by activation of Rac1 (Ras-related C3 botulinum toxin substrate 1) and cdc42 (cell division control protein 42).[129]

On the whole, cisplatin-resistant cells, in addition to downregulate CTR1 levels[126], thus reducing drug uptake, may increase its efflux. Interestingly, the intracellular copper P-type adenosine triphosphate transporters (ATP7A and ATP7B), which localize to the trans-Golgi network, have shown to be involved in the sequestration and efflux of copper and platinum

compounds toward the plasma membrane.[130] These metal-extruding proteins are upregulated in cisplatin-resistant cancer cell lines[131] and their transfection-enforced overexpression has been shown to drive the acquisition of the cisplatin-resistant phenotype[130].

Once inside the cell, cisplatin can interact with a variety of other molecules besides DNA including two sulfur-containing macromolecules, metallothionein and glutathione, that sequester cisplatin and remove it from the cell. Metallothionein (MT) are low molecular mass cysteine-rich proteins and are believed to be involved with detoxification of metal ions in the cell. Production of MT is triggered by the presence of heavy metal ions, glucocorticoids (which are steroid hormones that promote the formation of both glucose from non-carbohydrate sources and glycogen, enhance the degradation of fats and proteins, and enable animals to respond to stress), interferon (which is a signaling molecule in the immune system that greatly enhances antiviral responses) and stress. Cisplatin administration leads to the induction of MT in, *e.g.*, the liver and may bind and inactivate platinum ion. Reactions between MT and cisplatin lead to displacement of the amino ligands and give rise to $[PtS_4]$ clusters containing 7-10 platinum atoms per mole.[132] MT may contribute to cisplatin resistance, but the results are inconclusive. In some cases, the levels of MT are higher in cisplatin-resistant cells, but in other cases, the MT levels are unaffected.[121] *Trans*-DDP reacts with MT faster than cisplatin and this may be one of the possible causes of its inactivity. (xix)

Like metallothionein, glutathione (GSH, **Figure 16.a**) is also involved in detoxification.[133] GSH reacts with hydrogen peroxide and organic peroxides, the harmful bioproducts of aerobic life; GSH is also essential for maintaining the normal structure of red blood cells. (xx) The binding of platinum(II) to *S*-thiolates tends to be irreversible, in contrast to *S*-thioethers. Reaction between cisplatin and GSH forms a 2:1 (GSH:Pt) complex which may therefore inactivate the drug and be a part of cellular resistance mechanism.[107] Moreover, there is an over-expression of the pump for glutathione conjugates in cisplatin resistant cells, suggesting that Pt-GSH complexes are pumped out of the cell.[134] Again, like MT, levels of GSH are increased in some, but not all, cisplatin-resistant cells, suggesting that there are other mechanisms of cellular resistance.[121]

For cisplatin, binding to methionine (Met, **Figure 16.b**) is normally considered as an inactivating step. The metabolite $[Pt(Met)_2]$ has been detected in the urine of patients treated with cisplatin and it is a relatively unreactive complex, existing in solution as a mixture of three diastereoisomers of each of the two geometrical isomers.[135]

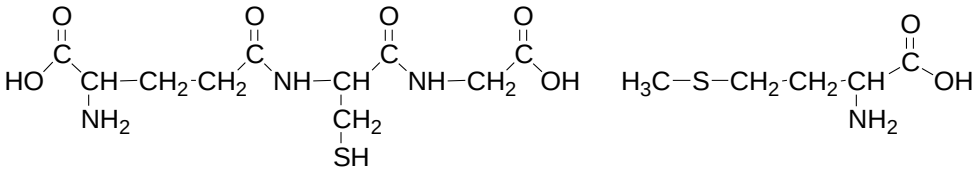

(**a**) (**b**)

Figure 16. Chemical drawing of glutathione (**a**) and methionine (**b**).

Regarding the on-target resistance, the recognition of inter- and intra-strand DNA adducts and the consequent generation of an apoptotic signal is often lessened in cisplatin-resistant cancer cells because of a variety of defects. Alternatively, cisplatin-resistant cells quickly acquire the ability to repair platinated DNA by enzymes[(xxi)], or become able to tolerate unrepaired DNA lesions, thanks to a particular class of DNA polymerases that mediate the so-called translesion synthesis.[122]

As shown in **Figure 17**, several types of proteins can interact with cisplatin-damaged DNA: NER (nucleotide excision repair), TFs (transcription factors), MMR (mismatch repair), p53 tumor suppressor gene (nuclear protein that exerts its effects through transcriptional regulation maintaining the genomic stability) and HMG (high mobility group, see above) proteins. [(xviii)]

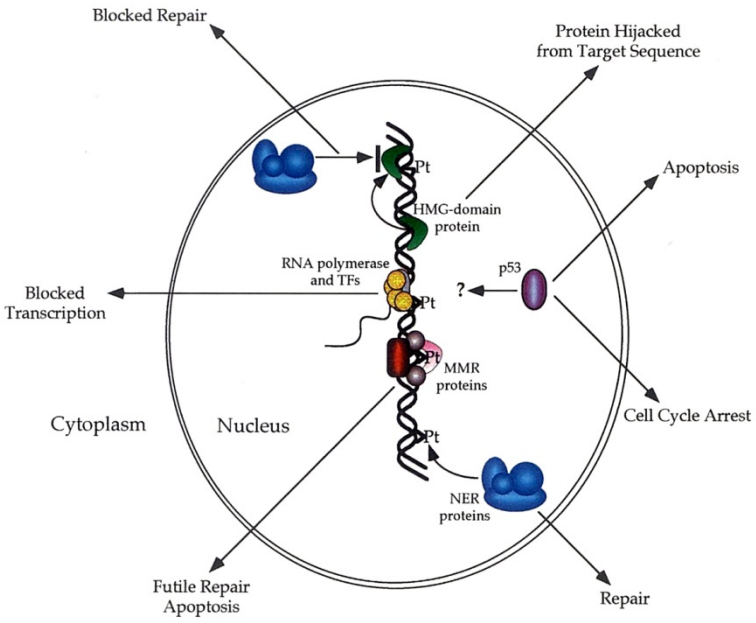

Figure 17. Effects of cisplatin-DNA adducts on some of the proteins in the nucleus that interact with the lesions.

The repair of cisplatin adducts occurs primarily by the NER system;[136] in this pathway, the DNA lesion is excised as a small, single-strand oligonucleoside fragment, and new DNA is

synthesized to fill the resulting gap.[137] The more distorting 1,3-intrastrand d(GpTpG)-cisplatin cross-link is repaired about 15-20-fold more effectively by human whole cell extract than the less distorting 1,2-intrastrand d(GpG)-cisplatin cross-link.[138] The poorer repair of 1,2-intrastrand cross-link in comparison with 1,3-intrastrand cross-link is a consequence of different structural alterations of the DNA helix and a repair-shielding mechanism mediated by some proteins attached to cisplatin-DNA adducts.[114]

Regarding the MMR system, defects in the component MLH1 are associated with increased DNA synthesis which is not blocked but proceeds beyond cisplatin adducts (phenomenon called translesion synthesis).[139] Such translesion synthesis, also known as replicative bypass, is mediated by the concerted activity of a specific group of DNA polymerases including POLH, POLI, POLK, REV1, REV3 and REV7.[140]

Enhanced proficiency has been detected in the machinery for homologous recombination (HR) in which nucleotide sequences are exchanged between two similar or identical molecules of DNA.[141] Cisplatin-induced inter-strand cross-links can lead to the so-called double-strand breaks, that are DNA lesions that are normally repaired in the S phase of the cell cycle (or shortly after) by this HR apparatus. Two pivotal components of the HR system are encoded by the two genes BRCA1 and BRCA2 that are frequently mutated in familial breast and ovarian cancers.[142]

With respect to post-target cisplatin resistance, acquired issues may result from a plethora of alterations including defects in the signal transduction pathways that normally elicit apoptosis in response to DNA damage as well as problems with the cell death executioner machinery itself.[122] One of the most prominent mechanisms of post-target resistance involves the inactivation of TP53,[143] which occurs in approximately half of all human malignancies.[144] This has been proved *in vitro*, by comparing the sensitivity to cisplatin of a wide panel of TP53-proficient and -deficient tumor cell lines[145], and also *in vivo*, in the clinical setting.[146] Thus, patients with ovarian cancer harboring wild-type TP53 show a higher probability to benefit from cisplatin-based chemotherapy than patients with TP53 mutations.[147] In particular, p53 (the protein espression of the gene TP53) is considered the “guardian of the genome” and normally facilitates DNA repair before replication. When damage is not repaired, p53 activates transcription of pro-apoptotic mediators (*e.g.*, Bax and Bak) and suppresses that of anti-apoptotic proteins including Bcl-2, to induce cell apoptosis and prevent undesirable mutations to be consolidated within the genome.[81]

Concerning the off-target resistance, increasing evidence suggests that the cisplatin-resistant phenotype can also be fostered by changes in signaling pathways that are not directly associated with cisplatin, thus blocking drug-elicited lethal signals.[122] An example of stress response is the autophagy, an evolutionary-conserved catabolic pathway associated with lysosomal degradation of organelles and other structure present in the cytosol.[148] Both ovarian and NSCLC cells have been displayed to progressively acquire cisplatin resistance while overexpressing components of the autophagic pathway. Consequently, if autophagy is inhibited, a little of cisplatin sensitivity may be restored, at least *in vitro.*[149]

A very recent investigation discovered a new mechanism by which the oncoprotein c-Myc enables cancer cells to acquire cisplatin resistance by suppressing BIN1 (bridging integrator 1), thereby releasing the DNA repair protein poly(ADP-ribose)polymerase (PARP) 1. In fact, BIN1 was identified as a nucleocytoplasmic adaptor protein that can serve as a tumor suppressor by directly interacting with the c-Myc oncoprotein.[151] Complete or partial losses of BIN1 were documented in 60% of breast cancer tissues analyzed by immunohistochemistry or RT-PCR. Conversely, reintroduction of BIN1 into human breast cancer and melanoma cell lines that lack its endogenous expression leads to loss of proliferation capacity and cellular death mediated by both caspase- and p53-independent pathways.[152] Furthermore, the activation of nuclear factor kappa B (NF-κB) also contributes to drug resistance in pancreatic carcinoma and it was demonstrated that pretreatment of pancreatic carcinoma cells with genistein, one of several known isoflavones, down-regulates NF-κB activity, thus enhancing the apoptosis-inducing effect of cisplatin, and leading to higher antitumor activity *in vivo.*[153]

Cisplatin toxicity

Since cancer is a disease in which tumor cells divide quickly, many chemotherapeutic agents used to treat cancer target also healthy rapidly dividing cells. Such cells can be found in the gastrointestinal tract, in hair follicles and in bone marrow. For this reason, some of the common adverse side effects of drugs used in cancer chemotherapy are nausea, alopecia (hair loss) and myelosuppression (reduction of activity in the bone marrow, in particular toxicity to the blood forming elements). Indeed, nearly all people who are treated with cisplatin experience gastrointestinal problems, specifically intense nausea and vomiting. Nausea and vomiting usually begin within 1 to 4 hours after treatment and can last

up to 24 hours. [xxii] However, in the case of cisplatin, it is believed that the nausea and vomiting result from an effect on the central nervous system rather than from gastrointestinal damage. [xxiii] Some people who are given cisplatin treatments also experience alopecia. Furthermore, myelosuppression occurs in 25 to 30 percent of people who undergo treatments with cisplatin. The levels of platelets and white blood cells (leukocytes), associated with myelosuppression, are generally lowest about 3 weeks after treatment and return to normal levels a little more than 2 weeks after the reduction. The loss of platelets (called thrombocytopenia) and the loss of leukocytes (called leucopenia) are more pronounced when higher doses of cisplatin are given. In addition to a loss of platelets and white blood cells, the use of cisplatin can also cause a decrease in the number of red blood cells (anemia). Anemia occurs with the same frequency and with the same timing as thrombocytopenia and leucopenia. [xxiv] Some people receiving cisplatin treatments also experience hearing difficulties (ototoxicity). Ototoxicity has been observed in up to a third of the people treated with cisplatin and can be manifested in the form of tinnitus (a buzzing, ringing or whistling in the ears) or hearing loss in the high frequency range, and, in a few cases, total deafness. This hearing loss results from damage to the sound detecting hair cells in the inner ear. [xxiii, xxv] Overall, there is a need for otoprotective agents that could be administered without compromising cancer treatment.[154]

Several other negative side effects are sometimes associated with the use of cisplatin: serum electrolytes disturbances, particularly those involving low levels of magnesium, calcium, sodium, potassium and phosphates, have been reported and are probably related to renal tubular damage.[155] Hyperuricemia (an increase in uric acid) has also been stated. In addition, neurotoxicity (abnormalities with the nervous system) can be a complication; symptoms include muscle cramps, seizures and a loss of taste. Cases of ocular toxicity, including inflammation of the optic nerve and cerebral blindness, have been reported in rare cases even when cisplatin is administered in the recommended doses. Anaphylactic-like reactions have occasionally been described in conjunction with the use of cisplatin and can be controlled by injection of epinephrine with corticosteroids and/or antihistamines. Finally,also hepatotoxicity, in which liver enzymes are elevated, is often a medical complication. [xxiv]

Recently, cardiotoxicity has also been associated to cisplatin treatment, resulting in alterations of the electrocardiogram including a prolongation of QT-interval and emesis of different grades.[156]

In addition to the innumerable adverse side effects listed above, the use of cisplatin has been linked with nephrotoxicity (that is, kidney toxicity); in fact, renal insufficiency is the major and most severe form of toxicity associated with the use of cisplatin as chemotherapeutic agent. Renal toxicity can result both from doses that are higher than recommended and from an accumulation of cisplatin in the body[(xxiv)] , but the mechanistic basis for such toxicity is not well explained yet. It has been hypothesized that cisplatin nephrotoxicity may be a consequence of platinum binding and inactivation of thiol-containing enzymes.[157] On the basis of these considerations, a large number of thiol-based or sulfur-containing nucleophiles have been tested as chemoprotectants to modulate cisplatin nephrotoxicity[(xxvi)] (see below § State of the art of our researches).

Cisplatinum derivatives

Once a successful drug has been discovered for the treatment of a particular disease or condition, researchers will often try to improve on that drug synthesizing and studying related compounds, referred to as analogs or second-generation drugs. There are several reasons for making such analogs. First, the analogs may be able to improve on the efficacy of the original drug, meaning that lower doses are able to produce the same beneficial effects. Second, the toxicity profile of the analogs may be better than that of the original drug; in other words, the analogs may have fewer toxic effects than the original drug. Third, the analogs may be able to be used to treat cases that have become resistant to the original drug. Finally, if the original drug can only be administered intravenously, the analogs may be able to be taken orally. After the efficacy and toxicity profiles of second-generation analogs are obtained, more analogs can be synthesized and studied; these analogs are called third-generation drugs.

As explained above, the usefulness of cisplatin is limited by (1) the spectrum of its anticancer activity (not active enough against several types of cancer), (2) the development of resistance after continued treatment and (3) its high toxicity to some normal cells. Platinum(II) complexes are among the most widely used drugs for the treatment of cancer. In addition to cisplatin, three injectable dia(m)mino platinum(II) compounds have been approved for clinical use: carboplatin (**Figure 18.a**), nedaplatin (**Figure 18.b**) and oxaliplatin (**Figure**

18.c). Like cisplatin, all of them are tetracoordinate in a square-planar geometry with two amino ligands in *cis* position.[158]

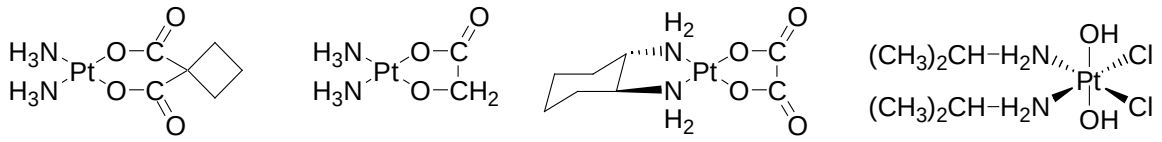

Figure 18. Anticancer platinum(II) drugs in clinical use: carboplatin (**a**), nedaplatin (**b**), oxaliplatin (**c**) and iproplatin (**d**).

Carboplatin (*cis*-diammino(1,1-cyclobutane-dicarboxylato)platinum(II)) entered clinical trials on 1981 and showed a very similar activity profile to that of cisplatin, with good response in ovarian, small cell lung, head and neck, and testicular cancers. It was approved by the *Food and Drug Administration* for the treatment of ovarian cancers in 1989 and is commonly referred to as the organic version of cisplatin but with reduced toxicity and potency [(xxvii)]. Unlike its parent compound, carboplatin causes myelosuppression which is its dose-limiting factor. The drug is most toxic toward the platelet precursors and neuropenia and anemia are indeed frequently observed. The other toxicities of carboplatin are generally milder and better tolerated than those of cisplatin. Nausea and vomiting are less severe, shorter in duration, and more easily controlled at standard doses than with cisplatin. At effective doses, carboplatin produced substantially reduced nephrotoxicity, ototoxicity, neurotoxicity, and alopecia. The lack of nephrotoxicity at standard doses means that extensive hydration is not required and, in fact, the drug may be administered in under outpatient conditions.[159] The mechanism of action of carboplatin is very similar to that of cisplatin, forming preferential cross-links with guanine in DNA, thus eventually causing cell death. It may also interact with nuclear proteins, and is phase-non-specific; unfortunately, this explains why it is cross-resistant with the parent drug, and shows similar survival durations [(xxviii)]. Tumors resistant to carboplatin are becoming more common, and like that of cisplatin, the cause of drug resistance is not completely elucidated. Like the majority of second-generation platinum-based drugs, carboplatin has a lower activity to that of cisplatin. A study has shown that with equimolar doses of carboplatin and cisplatin, the former was less effective than the latter with respect to ovarian cancer. Comparative studies have also shown that carboplatin takes longer to bind to the nucleophilic sites of DNA than cisplatin; in fact, it would take three weeks for

carboplatin to reach the same level of reaction that cisplatin reached in five days.[160] This difference in rate indicates that for carboplatin to have the same efficacy as cisplatin, a larger dose must be given for a longer period of time. Anyway, carboplatin is nevertheless still used as an effective anticancer drug because of its reduced toxicity and greater ease of administration. It is slowly replacing the use of cisplatin for certain cancers and situations where toxicity is a crucial factor.

Nedaplatin (*cis*-diammino-glycolate)platinum(II)), is a cytotoxic drug developed in Japan; it has been shown to be active in several solid tumors without renal toxicity. The reported dose limiting toxicity is myelosuppression, especially thrombocytopenia. (xxvii)

The third most widely available platinum-based drug, is oxaliplatin (*trans*-l-diaminecyclohexane-oxalate)platinum(II)). This compound is administered intravenously; the dose-limiting factor is sensory neuropathy, which is different to cisplatin, and it is minimized by a split-dose schedule. Oxaliplatin is generally less toxic, with reduced myelosuppression, nephrotoxicity and ototoxicity; however, nausea and vomiting remain acute, but respond well to antiemetics. The activity of oxaliplatin has been shown to have a more powerful pharmacological effect than cisplatin, that is due to its different mechanism of action. Studies point out that it binds to proteins which are essential for DNA transcription, thus preventing cell division and ultimately causing cell death.[161]

In addition to carboplatin and other second-generation cisplatin analogs, several third-generation drugs have been synthesized and tested. This broad class of potential drugs is represented by the orally-active platinum(IV) complex JM216 called iproplatin (*cis*-dichloro-*trans*-dihydroxy-*cis*-bis(isopropylamine)platinum(IV), **Figure 18.d**), that is on clinical trials.[162] This complex is stable enough to survive the passage down the digestive tract; then it is transported across the gastrointestinal mucosa into the bloodstream. After absorption into the bloodstream, iproplatin is metabolized to form a tetracoordinate platinum(II) cisplatin analog, which is assumed to be the active form of the drug. (xxvii) It is less toxic than cisplatin with respect to alopecia, the degree and duration of nausea and vomiting, renal toxicity, neurotoxicity and anemia. Moreover, like carboplatin, this complex is also toxic toward certain cancer cisplatin-resistant cell.[163]. However, it causes the same cumulative toxicity on hemoglobin, leukocyte count and platelet count, provoking thrombocytopenia, diarrhea and leucopenia. Anyway, researchers believe that this third-generation drug is more effective than cisplatin because it is taken up into the cell in greater concentrations than cisplatin.[164]

Gold in medicine: antiarthritic drugs

The phenomenon of gold in medicine dates back to antiquity with both Arabic and Chinese physicians using gold preparations to treat a variety of ailments. The application of gold-based drugs has assumed an impressive title to distinguish it from all other forms of chemotherapy. In fact, chrysotherapy (from the Greek *chrysos* = gold) is referred to the clinical use of gold compounds, usually gold thiolates, which are able not only to alleviate the symptoms associated with rheumatoid arthritis, but especially to have therapeutic action at hyaline cartilage level.[165]

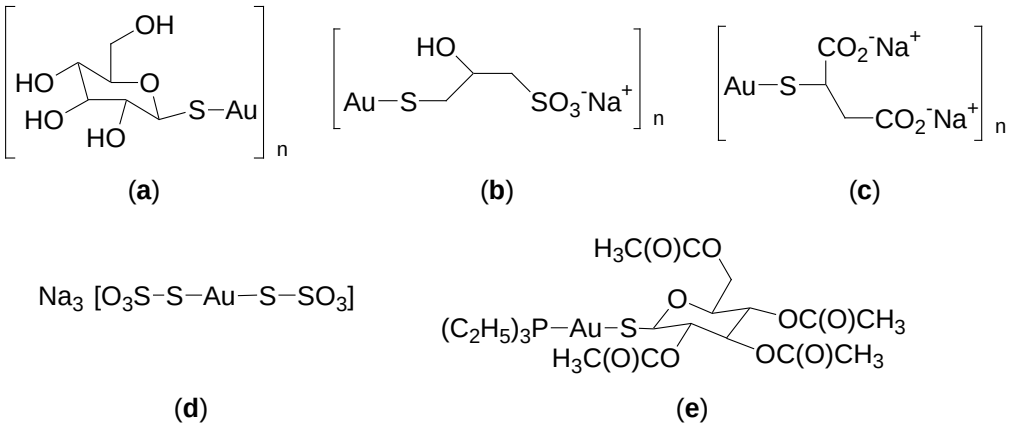

Figure 19. Chemical drawing of some gold(I) thiolates used in the treatment of rheumatoid arthritis: solganol (**a**), allocrysin (**b**), myocrysin (**c**), sanocrysin (**d**) and auranofin (**e**).

In the early part of the 20th century, it was believed that there was a relationship between tuberculosis and rheumatoid arthritis, and the same drugs were tried for the treatment of both diseases. The beginning of chrysotherapy is usually ascribed to Landé who, in 1922, reported on the use of aurothioglucose (solganol, **Figure 19.a**) to treat various diseases, including rheumatic fever. (xxix) Two years later Forestier widened the range of compounds, although his major report did not appear until 1935.(xxx) He used, among others, the aurothiopropanol sulfonate (allocrysin, **Figure 19.b**), aurothiomalate (myocrysin, **Figure 19.c**) and aurothiosulfate (sanocrysin, **Figure 19.d**). All these compounds are gold(I) derivatives characterized by linear -S-Au-S- geometries, and the first three compounds appear to be polymeric. Despite the importance of these compounds, crystallographic evidence for their structures is largely lacking, owing to the difficulty of obtaining suitable crystals for X-ray analysis; only EXAFS[166] and WAXS[167] studies have recently elucidated their polymeric

structure. A full trial was planned in 1938 but was delayed by World War II and did not start until 1957. The reports in 1960 and 1961 showed that myocrysin was undoubtedly effective against rheumatoid arthritis. [(xxxi)] It is now fully accepted that chrysotherapy can be highly beneficial.[168] However, it has some adverse effects, such as skin rashes, diarrhea and kidney inflammation, and patients widely differ in their tolerance. Likely for this reason, its use is usually postponed until alternative methods have failed. This is somewhat unfortunate, since it is one of the few treatments which appears able to produce remission of the disease, rather than simply arresting its development. [(xxxii)] It has been claimed that it was the organic part of the drugs which was beneficial; however, recent data point out that the therapeutic agent in these substances is indeed the gold center and that the organic ligands represent a suitable delivery system and prevent the gold ion from reduction in storage.[169] These gold(I) thiolates have good solubility in water, thus making administration easy, usually by intramuscular injection, and allowing good control of dosage. Unfortunately, when given by mouth, these materials are immediately cleared from the body. [(xxxiii)]

More recently, a lot of endeavors have been made to find a gold-containing drug which could be administered orally. The most effective appears to be 2,3,4,6-tetra-*O*-acetyl-1-thio-β-D-glucopyranosato-*S*-triethylphosphine gold(I) (auranofin, **Figure 19.e**), that may be regarded as a second-generation drug.[170] It is a monomeric neutral gold(I) species and may be administered orally. Contrary to simple gold(I) phosphine compounds, such as [(Et_3P)AuCl], which give severe irritation of stomach and bowel, auranofin is well absorbed from the gastrointestinal tract.[(xxxiv)] It has been claimed that auranofin leads to lower levels of gold retained in the kidney and, therefore, to fewer problems.[171]

The principal difference between auranofin and the earlier gold(I) drugs is the presence of the phosphine molecule bound to the gold atom; this is a good example of a compound that would be expected to be toxic but, in practice, even though the phosphine becomes free in the body, it is rapidly made harmless by oxidation. [(xxxv)]

Regardless of the form of administration, it is likely that gold-based drugs quickly undergo substitution reactions with sulfur-containing biomolecules, such as albumin and glutathione. Thus, it may be concluded that the gold compounds act as pro-drugs, providing a mean of gold delivery to sites of inflammation. [(xxxvi)]

Au(III)-based anticancer compounds

The wide clinical success of cisplatin and subsequent analogues has prompted a great deal of interest in other platinum and non-platinum metallodrugs that should display higher or comparable cytotoxic properties, hopefully associated with a different pattern of antitumor specificities and a more favorable toxicological profile. In this context, it should be underlined that the attention has been directed toward gold compounds owing to their antiarthritic activity. In fact, the investigation of the efficacy of some anticancer drugs (*e.g.,* the *6*-mercaptopurine and cyclophosphamide) in the treatment of rheumatoid arthritis arose from their well-known immune-suppressive and anti-inflammatory actions.[172] Thus, such work established a connection, at least in principle, between the two therapies. However, this reason is not the only one that account for the investigation of gold compounds as anticancer agents. Indeed, gold in the +3 oxidation state is isoelectronic with platinum(II) and forms similar square-planar complexes. On the other hand, compounds containing gold(III) may be expected to be reduced *in vivo* to gold(I) or metallic gold due to the generally reducing human physiological environment. Nevertheless, the proper selection of the ligand types can enhance the stabilization of the gold(III) metal center. The first gold(III) complexes were reported by Parish *et al*. in the 1990s.[173, 174] The acceptable solution stability of these compounds enabled wide pharmacological testing, both *in vitro* and *in vivo*, with encouraging results. Subsequently, various classes of cytotoxic gold(III) compounds were developed in a few laboratories worldwide and were found to exhibit very attractive biological profiles.[175-180] Except for chloride ligands, the coordination sphere present in these complexes is composed of *N*-, *O*- and *P*-donor ligands, the first representing the most common cases (*i.e.*, complexes with aldiminate derivatives, porphyrins, aliphatic amines and heteroaromatic rings).

In light of the wide structural variety of the investigated ligands, an unique mode of action or a single pharmacological profile are unlikely to exist, and several intracellular targets, other than DNA, have to be considered to elucidate the biology of gold-based metallodrugs. Although gold(III) complexes show chemical features very close to those of clinically established platinum(II) complexes (preference for square-planar coordination and typical d^8 electronic configuration), a few (compared to platinum compounds) studies exist on their anticancer activity. The paucity of biological data probably derives from their high redox potential and relatively poor stability, thus making their use rather problematic under

physiological conditions. Furthermore, most data regarding cytotoxic effects have been collected under heterogeneous experimental conditions and using a limited panel of different human tumor cell lines or even a single human tumor cell line. Thus, recently, a group of thirteen structurally different gold(III) complexes, including our dithiocarbamato complex AUL12 (*see the subsequent section*), has been tested *in vitro* at the German Biotech Company Oncotest GmbH according to a specific comparative strategy for the development of new anticancer agents.[181] Among all, AUL12 turned out to be the second best performer with IC_{50} values in the low micromolar range on all the screened 36 human tumor cell lines, in particular against ovary and brain cancers, and showed an excellent degree of selectivity (17%). Intriguingly, from a comparative analysis by 110 reference substances with known modes of action, AUL12 proved to be the only gold(III) complex whose mechanism of action did not resemble that of any other reference compound.[181]

The first compound ranking in this systematic investigation is a dinuclear species with the formula $[Au_2(bipy^{Me,Me})_2(\mu\text{-}O)_2](PF_6)_2$ where $bipy^{Me,Me}$ stands for 6,6'-dimethyl-2,2'-bipyridine (hereinafter E5). In this screening, an evident relationship has emerged between reactivity (*e.g.*, redox properties, stability in aqueous solution) and cytotoxicity. This type of correlation is plain with both AUL12 and E5, being the most reactive and also most potent cytotoxic agents.

The additional reason for developing new gold complexes is generally valid for all metal-based compounds. In fact, in most cases, the metal center is the pivotal moiety, the organic part (ligand) playing functional roles such as enhancing water solubility, stabilizing the oxidation state and reducing systemic toxicity. Thus, recently, coordination compounds have received considerable attention due to their peculiar properties compared to organic molecules. The choice of the metal center, its oxidation state and the types of ligand (*O*-, *N*-, *S*-donors, monodentate or chelating ones etc.) determines the traits, including the coordination geometry and stereochemistry, of the final compound, resulting in distinguishing kinetic and thermodynamic properties. For instance, modification of the oxidation state of the metal center radically changes the structural and chemical properties and the resulting biological activity of a complex.[40,182, 183] Accordingly, the distinctive chemistry of metal-based drugs may lead to unexpected pharmacological profiles due to novel mechanisms of action at the cellular level.

State of the art of our researches

Au(III)-based dithiocarbamato complexes

As previously mentioned, nephrotoxicity (*i.e.*, kidney toxicity) limits the use of cisplatin and related platinum-based therapeutics. It may result from either too high administered doses or accumulation of platinum in the body. The effects of cisplatin on renal functions are not fully understood, but some studies have provided new insights in the mechanism of cisplatin-induced nephrotoxicity, especially on the signaling pathways leading to tubular cells death and inflammation. It has been hypothesized that renal failure may be induced by platinum binding to and, consequently, inactivation of thiol-containing renal enzymes.[184] Overall, sulfur-containing biomolecules, such as cysteine, methionine, glutathione, metallothionein and albumin, play a major role in platinum toxicity and anticancer activity owing to their high affinity to Pt(II) ion. Thus, likewise to glutathione (**Figure 20.a**)[185], it has been hypothesized that they all act as endogenous defense systems toward such electrophile by coordination to the metal center through the sulfur-based moiety to yield a non-toxic thioether.[185, 186] These conjugated species can be further metabolized and excreted in the urine or bile. Although few of such conjugated species have been isolated, it is presumed that this direct mechanism may explain most of the activity of the thiol-based endogenous modulators, even if there are some evidences that other mechanisms, such as growth factor stimulation, may also be operative. (xxvi)

At a more general level, strong and irreversible binding of cisplatin to intracellular thiol-containing biomolecules is considered as a major inactivation step, and reactions with sulfur donors in peptides and proteins are believed to alter their conformations, resulting in changes in their biological activity (*e.g.*, enzymatic processes) and onset of drug resistance and detoxification mechanisms.[187]

Since sulfur is involved in the entire metabolic process of platinum drugs, a number of sulfur-containing nucleophiles have been tested as chemoprotectants to modulate cisplatin nephrotoxicity. (xxvi)

Two main issues have to be taken into account for the development of chemoprotectants: (i) the selective protection of non-tumor normal cells, and (ii) the addition of little, if any, toxicity. Many sulfur-based chemoprotectants have been designed and tested (**Figure 20**), and some showed promising for clinical use. However, a selective protection of normal tissues without inhibition of the anticancer activity proved challenging.[188-192]

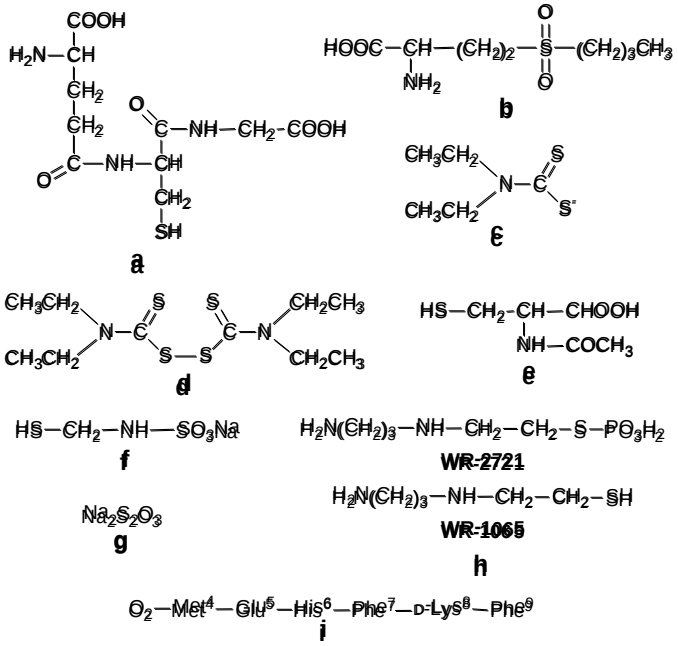

Figure 20. Cisplatin modulatory sulfydryls and peptide derivatives: glutathione (GSH, **a**), the GSH-depleting antimetabolite L-buthionine sulfoximine (L-BSO, **b**), the sulfydryl metabolite of disulfiram diethyldithiocarbamate (DEDT, **c**), the parent disulfide disulfiram (antabuse, **d**), *N*-acetyl- L-cysteine (L-NAC, **e**), *S*-mercaptoethane sulfonate sodium salt (mesna, **f**), sodium thiosulfate (**g**), the phosphothiol-amifostine (**WR-2721**) and its active metabolite actifostine (**WR-1065**) formed by alkaline phosphatase activity (**h**), and the melanocortin-derived peptide ORG-2766 (**i**).

In this context, positive outcomes were achieved with sodium diethyldithiocarbamate (DEDTNa, **Figure 20.c**). In fact, it was shown to provide protection against renal, gastrointestinal and bone marrow toxicity induced by cisplatin without decreasing its antitumor activity. (xxxvii)

The chemoprotective effect results from the capability to remove platinum from the thiol groups of proteins without reversal of platinum-DNA adducts, responsible for its antitumor activity. Platinum-DNA adducts (1,2-intrastrand cross-links) were shown to decrease by *ca.* 50% upon treatment with DEDTNa soon after cisplatin administration, causing a loss of therapeutic effect, whereas no change in anticancer activity was observed when DEDTNa was administered 3 h after the drug. This behavior is ascribable

to DEDTNa-cisplatin reaction, resulting in the inactivation of the drug, when diethyldithiocarbamate is administered soon after cisplatin. In particular, this reaction is 40,000-fold faster than that with water (hydrolysis), leading to the direct chloride substitution rather than a rate-limiting hydrolysis. Conversely, when DEDTNa is administered 3 h later, the drug has already reached and bound DNA. Thus, the dithiocarbamate is not able to cleave platinum-DNA adducts, wherein chlorides have been replaced by guanine residues, but it can remove platinum centers from a variety of other sulfur-containing molecules, making further drug available for other interactions with DNA[112]. Thus, the accurate use and dosing of DEDTNa as chemoprotectant reduces nephrotoxicity of cisplatin chemotherapy without decreasing its antitumor properties. [(xxvi)] Nevertheless, the overall nephroprotective benefits of DEDTNa are somewhat limited by the acute inherent toxicity of dithiocarbamates themselves. In fact, potential health hazards associated with free (*i.e.* not coordinated) dithiocarbamates is still being investigated, including genotoxicity.[193] Furthermore, DEDT does not give the possibility to treat patients with a dose-intensive program and there is a little evidence that it is able to significantly reduce also non-renal toxicities, particularly the cumulative neuropathies, associated with cisplatin treatment[(xxvi)].

However, nowadays chemoprotectants are not clinically used anymore and it is preferred to exploit aggressive hydration and diuresis, and antiemetic prophylaxis during the cisplatin treatment. In the meantime, a continuous effort is still being made by researchers in order to reduce cisplatin-induced toxicity.

On the basis of these considerations, the research group, wherein this work has been performed, has been designing a number of metal-dithiocarbamato complexes potentially able to combine the cytotoxic activity of the related metal centers (*e.g.* Pt(II), Pd(II), Au(III), Ru(III), Ru(II), Zn(II), Cu(II)) with the lack of nephrotoxicity due to the inherent chemoprotective action of the ligand.[182, 194] The rationale of our strategy is based on the chemical features of the dithiocarbamato moiety (–$NCSS^-$). Dithiocarbamates are bidentate chelating ligands and, upon coordination to a metal ion, the resulting complexes are expected to be quite stable due to the so-called “chelate effect”, so the possible decomposition with subsequent loss of the dithiocarbamato ligand is unlikely to occur. Moreover, the solubility properties of the metal-dithiocarbamato derivatives may be, at least in theory, modulated by modifying the organic chain of the dithiocarbamato ligand.

Regarding square-planar complexes, the presence of a chelating dithiocarbamate should make the coordination of additional *S*-donor ligands (*e.g.*, methionine and cysteine residues) – in *trans* position with respect to the –NCSS moiety – less favorable due to the rather strong *trans* effect of the dithiocarbamato sulfur atoms, thus potentially avoiding the interaction of the metal center with thiol-containing renal enzymes and, accordingly, reducing nephrotoxic side-effects.

Up to now, our toxicological and anticancer activity results point out that the design of our compounds proved very successful in both stabilizing the heavy metal center and in avoiding the non-specific reactivity of the compound occurring in healthy tissues that could give rise to systemic toxicity. The most promising results were obtained with gold(III)-dithiocarbamato derivatives of the type $[Au^{III}X_2(dtc)]$ (X = Cl, Br; dtc = various dithiocarbamato ligands) (**Figure 21**), that have been designed so to reproduce very closely the main features of cisplatin. All the compounds have been fully characterized by means of several techniques, confirming that coordination of the dithiocarbamato ligand takes place in a near square-planar geometry through the sulfur-donating atoms, the –NCSS moiety coordinating the metal center in a bidentate symmetrical fashion and lying in the same plane, as reported in the literature for analogous complexes. The remaining coordination positions are occupied by two *cis*-halogen atoms which may undergo hydrolysis. When X-ray structures were not available, density functional calculations were performed, confirming the structural conclusions deduced by other characterization techniques.[195]

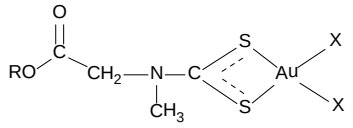

R = CH_3, X = Cl, $[Au^{III}Cl_2(MSDT)]$
R = CH_3, X = Br, $[Au^{III}Br_2(MSDT)]$
R = CH_3CH_2, X = Cl, $[Au^{III}Cl_2(ESDT)]$ (AUL13)
R = CH_3CH_2, X = Br, $[Au^{III}Br_2(ESDT)]$ (AUL12)

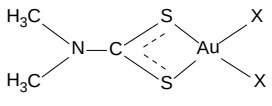

X = Cl, $[Au^{III}Cl_2(DMDT)]$ (AUL10)
X = Br, $[Au^{III}Br_2(DMDT)]$ (AUL14)

Figure 21. Selected Au(III)-dithiocarbamato derivatives: X = Cl, Br;
DMDT = *N*,*N*-dimethyldithiocarbamate ($(CH_3)_2CSS^-$);
MSDT = methylsarcosinedithiocarbamate ($CH_3O(O)CCH_2N(CH_3)CSS^-$);
ESDT = ethylsarcosinedithiocarbamate ($CH_3CH_2O(O)CCH_2N(CH_3)CSS^-$).

Since the physiological environment is generally reducing, gold(III) complexes, often characterized by high redox potentials, are likely to undergo reduction to the corresponding

less active gold(I) species, a major drawback for their pharmacological development. Thus, the inherent electrochemical properties of our gold(III) compounds have been studied in a physiological-like solution by cyclic voltammetry, showing that both DMDT (AUL10 and AUL14) and ESDT (AUL12 and AUL13) derivatives undergo irreversible stepwise reduction processes, leading to the corresponding dinuclear gold(I) species $[Au^{I}(DMDT)]_2$ and $[Au^{I}(ESDT)]_2$, at *ca.* -300 mV and -180 mV (*vs.* saturated calomel electrode, SCE), respectively. Remarkably, these reduction reactions occur at potentials considerably lower than the typical vales for the Au(III)/Au(I) couple known for the corresponding $K[AuX_4]$ (X = Cl, Br) precursors (*ca.* +1.29 V).[196] Therefore, coordination by dithiocarbamates induces a large stabilization of the metal ion in the +3 oxidation state, owing to the electron-donating capability and the stabilizing chelate effect of the dithiocarbamato moiety.

Concerning their solution properties, these gold(III) complexes hydrolyze in a physiological-like environment delivering two moles of halide per mole of starting complex, leading to the corresponding Au(III)-diaquo counter-parts within 30-40 min. Intriguingly, the hydrolyzed species were proved to be reasonably stable in physiological solution, reduction to gold(I) occurring after 12-24 h.

From comparative *in vitro* cytotoxicity studies on our Pt(II)-, Pd(II)-, and Au(III)-MSDT derivatives on human squamous cervical adenocarcinoma (HeLa) cells and human leukemic promyelocytes (HL60), gold(III) complexes resulted to be significantly more active (IC_{50} *ca.* 1 μM) than both cisplatin (IC_{50} *ca.* 2 μM) and Pt(II) and Pd(II) counter-parts (IC_{50} >15 and 5 μM, respectively) under the same experimental conditions, inducing apoptosis especially in HL60 cells.[197] $[Au^{III}X_2(MSDT)]$-type compounds were also tested on a panel of acute myelogenous leukemia cell lines, representing different French-American-British subtypes, and toward the Philadelphia-positive (K562) cells.[198] Compared to the corresponding palladium(II) analogues, they showed to inhibit cell growth in all the tested myeloid cell lines with IC_{50} values *ca.* ten-fold lower than the reference drug.[199] Moreover, after short exposure (18 h), they induced strong and rapid apoptosis by down-regulating the antiapoptotic molecule Bcl-2 and up-regulating the proapoptotic molecule Bax, whereas cisplatin did not. Finally, after long exposure (72 h), they were proved to induce only modest cell cycle perturbations but high DNA fragmentation, whereas classical platinum(II) complexes are known to promote characteristic cell cycle alterations resulting in increased G_2M cell fraction. [(xxxviii)] Therefore, $[Au^{III}X_2(MSDT)]$-type complexes are able

to promote early apoptosis and membrane damage to a much greater extent than cisplatin, suggesting a different mechanism of action.

Regarding the derivatives [$Au^{III}Cl_2$(DMDT)], [$Au^{III}Br_2$(DMDT)], [$Au^{III}Cl_2$(ESDT)] and [$Au^{III}Br_2$(ESDT)] (hereinafter referred to as AUL10, AUL14, AUL13 and AUL12, respectively) turned out to be much more cytotoxic *in vitro* than cisplatin even toward human tumor cell lines intrinsically resistant to cisplatin itself, such as Daudi, MeWo, LoVo and A549 cells. Moreover, they appeared to be extremely more active also on cisplatin-resistant cell lines, with activity levels comparable to those recorded on the corresponding cisplatin-sensitive parent cell lines, ruling out the occurrence of cross-resistance phenomena (**Table 3**).[200] Overall, our complexes proved to be much more potent than cisplatin even at nanomolar concentration, with IC_{50} values up to five orders of magnitude lower than the reference drug.

Table 3. *In vitro* cytotoxic activity of Au(III)-dithiocarbamato derivatives [$Au^{III}Cl_2$(DMDT)] (AUL10), [$Au^{III}Br_2$(DMDT)] (AUL14), [$Au^{III}Cl_2$(ESDT)] (AUL13) and [$Au^{III}Br_2$(ESDT)] (AUL12), and the reference drug cisplatin tested under the same experimental conditions toward established human tumor cell lines: human squamous cervical adenocarcinoma (HeLa), human leukemic promyelocytes (HL60), human Burkitt's lymphoma (Daudi), human malignant melanoma (MeWo), human colon adenocarcinoma (LoVo), human non small lung adenocarcinoma (A549), human ovarian carcinoma cisplatin-sensitive (2008) and cisplatin-resistant (C13*), human squamous cervix carcinoma cisplatin-sensitive (A431) and cisplatin-resistant (A431-R), human osteosarcoma cisplatin-sensitive (U2OS) and cisplatin-resistant (U2OS-R) cells. Data are expressed in terms of IC_{50} ± S.D. (standard deviation) values (μM).

Cell line	Compound				
	AUL10	AUL14	AUL13	AUL12	cisplatin
HeLa	2.10 ± 0.01	3.50 ± 0.01	8.2 ± 0.2	7.6 ±0.2	15.6 ± 0.4
HL60	$(0.80 \pm 0.01)\cdot10^{-2}$	$(0.70 \pm 0.01)\cdot10^{-2}$	0.43 ± 0.09	0.14 ± 0.02	25.6 ±0.3
Daudi	$(0.10 \pm 0.01)\cdot10^{-2}$	$(0.10 \pm 0.01)\cdot10^{-2}$	4.65 ± 0.09	5.8 ± 0.2	95 ± 1
MeWo	2.0 ± 0.3	$(0.10 \pm 0.01)\cdot10^{-2}$	12.5 ± 0.9	10.0 ± 0.9	48 ± 2
LoVo	$(2.40 \pm 0.04)\cdot10^{-2}$	3.8 ± 0.1	7.6 ± 0.2	7.9 ± 0.1	56 ± 2
A549	$(0.35 \pm 0.01)\cdot10^{-2}$	0.41 ± 0.03	4.73 ± 0.04	9.6 ± 0.2	35 ± 1
2008	$(0.20 \pm 0.01)\cdot10^{-2}$	30.0 ± 0.1	49.3 ± 0.1	16.5 ± 0.4	43.2 ± 0.4
C13*	$(0.10 \pm 0.01)\cdot10^{-2}$	21.8 ± 0.2	23.8 ± 0.1	$(0.10 \pm 0.01)\cdot10^{-2}$	556 ± 3
A431	$(1.20 \pm 0.01)\cdot10^{-2}$	1.8 ± 0.1	0.29 ± 0.01	$(1.50 \pm 0.01)\cdot10^{-2}$	77.4 ± 0.4
A431-R	$(0.20 \pm 0.01)\cdot10^{-2}$	2.8 ± 0.2	0.43 ± 0.03	$(0.10 \pm 0.01)\cdot10^{-2}$	382 ± 3
U2OS	4.8 ± 0.3	18 ± 1	5.8 ± 0.4	0.49 ± 0.09	35 ± 2
U2OS-R	6.4 ± 0.1	13 ± 1	5.2 ± 0.2	0.24 ± 0.09	84 ± 3

It is worth highlighting that usually *in vitro* anticancer activity of gold compounds is not confirmed by subsequent *in vivo* studies.[201] Instead, the in vivo antitumor activity of our gold(III)-dithiocarbamato derivatives, evaluated against human tumors implanted on immunodepressed nude mice (xenografts), was fully consistent with *in vitro* data. For example, treatment of MDA-MB-231 breast tumor-bearing nude mice with AUL14 resulted in significant inhibition of tumor growth (*ca.* 50% inhibition after daily treatment at 1 mg kg^{-1} body weight s.c. compared to control). Interestingly, during the

29-day treatment, no toxicity was observed, and mice did not display signs of weight loss, decreased activity or anorexia.[202] Analogously, administration of 1 mg kg^{-1} s.c. every second day of AUL10 caused an overall 85% reduction of PC3 human prostate tumor implanted in nude mice after a 19-day treatment (compared to control untreated mice). Again, chemotherapy was well tolerated by treated mice which suffered from minimal systemic toxicity only, and histology showed no detectable damage to main animals' organs.[203] Among all the Au(III)-dithiocarbamato derivatives, AUL12 has been selected, due to its overall favorable solubility, stability and antitumor properties, for additional *in vivo* studies. Thus, *in vivo* nephrotoxicity studies were also carried out with AUL12 by measuring some specific biomarkers in both urines (total urinary proteins (TUP), *N*-acetyl-β-d-glucosaminidase (NAG) and glutamine synthetase (GS)) and renal tissues (*p*-aminohippuric acid (PAH) and glutamine synthetase (GS)) of the treated rats.[204] In this investigation, cisplatin administration induced a significant increase of all the urinary biomarkers and a significant inhibition of GS activity in renal cortical slices, whereas the gold(III)-dithiocarbamato derivative caused negligible changes compared to untreated control rats (mainly observable at the higher dose, 20 mg kg^{-1} body weight), accounting for a substantial lack of nephrotoxic side-effects. The favorable toxicity profile was also confirmed by the LD_{50} value of 30 mg kg^{-1} recorded for AUL12 that is, as far as we know, among the higher ever reported for gold-based therapeutics (cisplatin LD_{50} = 11.4 mg kg^{-1}). Subsequent histopathological investigations showed that no significant histologically detectable toxicity involving treated animals' organs was observed, and SEM evaluation of the surface of all tissues examined were considered compatible with normal conditions when compared to control animals. Surprisingly, no gold was detected in the investigated tissues, thus ruling out the accumulation of the metal in any of the organs taken into account (*i.e.*, heart, liver, spleen, kidneys, testicles, pancreas, lungs and brain). Accumulation around the injection site (*i.e.*, peritoneal area) was also excluded, and these results are in full agreement with the fact that gold seems to be quickly cleared from the body (within 48 h), the large majority being excreted through the feces (>89%) and only about 10% *via* the urinary system[204]. This result is extremely positive when compared with the data reported in literature showing the renal toxicity induced by gold derivatives. For instance, it is well known that the anti-arthritic drugs, auranofin and myochrysine, induce proteinuria and kidney disfunctions, and gold nanoparticles are able to penetrate renal cells causing nephrotoxicity.[205]

In light of these very encouraging results, a new class of gold(III) compounds, namely dithiocarbamato derivatives of oligopeptides, has been recently synthetized and characterized by means of several techniques.[206] These compounds were designed as carrier-mediated delivery systems exploiting the human peptide transporters PEPT1 and PEPT2 (plasma membrane integral proteins), which are able to mediate the cellular uptake of di- and tripeptides, and peptide-like drugs. Their peculiar feature is that they can transport inside the cell all possible di- and tripeptides containing *L*-enantiomers, regardless of sequence, size, charge and hydrophobicity.[207] Moreover, these transporters are up-regulated in some types of malignancies and it is hence possible to exploit them to specifically deliver the cytotoxic moiety (*i.e.*, the transition metal) within a targeted chemotherapy.

Based on preliminary cell-line screenings[206, 208], we selected for further investigation the complexes AuD6 and AuD8 ([$Au^{III}Br_2$(dtc-Sar-AA-O(*t*-Bu))] with AA = Gly or Aib, respectively) whose ligands are di-peptide derivatives differing only in the substituents at the α-carbon atom at the *C*-terminus (**Figure 1.1**). **Table 4** collects the biological data obtained for these two compounds on a panel of human tumor cell lines in comparison with cisplatin.

Table 4. Growth inhibition of human prostate cancer (PC3 and DU145), ovarian adenocarcinoma cisplatin-sensitive (2008) and -resistant (C13), and Hodgkin's lymphoma (L540) cells by two gold(III)−dipeptidodithiocarbamato derivatives in comparison with that by the reference drug cisplatin (over 72 h).

Linea cellulare	IC_{50} [μM]		
	AuD6	**AuD8**	***cis*-platino**
PC3	1.3 ± 0.1	0.8 ± 0.1	3.3 ± 0.3
DU145	4.5 ± 0.9	1.4 ± 0.1	4.5 ± 0.1
2008	18 ± 2	4.5 ± 0.2	19 ± 1
C13	12 ± 1	3.7 ± 0.3	117 ± 9
L540	2.1 ± 0.2	1.5 ± 0.2	2.5 ± 0.1

During this PhD work the crystal structure of AuD8 has been solved (*Chapter 1*) and several advanced biological studies have been carried out (*Chapters 2-5*) on both complexes in order to gain insights into their mechanism of action, anticancer activity and toxicity on animal models.

Cu(II)-based dithiocarbamato complexes

In this thesis we have focused also on the endogenous transition metal Cu(II) owing to its prominent biochemical properties. Interestingly, copper homeostasis is significantly altered in serum and in neoplastic tissues.[209-212] In fact, copper accumulation in tumors has been related to angiogenesis (formation of new blood vessels).[213] The increase of copper levels has been shown to foster cell proliferation and the integrin-mediated migration of endothelial cells as well.[214] Additionally, Fox *et al.* reported that copper is an essential cofactor in the extracellular matrix degradation and in the cytokine production.[215] Based on these findings, many copper chelators have been studied and shown to *in situ* react with the pro-angiogenic copper, thus converting the tumor tissue copper to a selective anti-cancer weapon.[182]

Instead of using organic molecules as prodrugs able to remove copper ions by coordination to the metal center, we decided to exploit another strategy, namely studying novel copper(II)-dithiocarbamato compounds exploiting enhanced copper uptake in malignant cells. Complexes involving different types of ligands, such as *N,N*-dimethyl dithiocarbamate (DMDT), pyrrolidine dithiocarbamate (PyDT) and ester derivatives of sarcosinedithiocarbamate (*tert*-butyl (TSDT), ethyl (ESDT) and methyl (MSDT)) have been synthesized and characterized.[216] In all compounds, the metal-ligand stoichiometry is 1:2 with symmetrical bidentate (chelate) coordination of the ligands. The complexes were tested as chemotherapeutics on human ovarian and cervix carcinoma cell lines (2008 and A431) and the corresponding cisplatin-resistant subclones (C13 and A431Pt). Consequently, cisplatin was used as a reference drug. All the investigated compounds inhibited tumor cell growth in a dose-dependent manner both in wild-type and in cisplatin-resistant cells. As expected, cisplatin was more potent in wild-type cancer cells than in resistant subclones. Remarkably, regarding the latter subclones, all the copper complexes showed lower IC_{50} values than cisplatin, some of them reported at least one order of magnitude lower values, thus ruling out the occurrence of cross-resistance with cisplatin. In wild-type cancer cells [$Cu(DMDT)_2$], [$Cu(MSDT)_2$] and [$Cu(ESDT)_2$] proved the most potent compounds with IC_{50} values comparable or lower than the reference drug. Among all, [$Cu(ESDT)_2$] was the most promising with IC_{50} values about three- to twenty-fold lower than cisplatin in 2008 and A431 cell lines, respectively. Its higher stability and solubility in physiologic-like media may account for the observed greater cytotoxic activity toward the investigated cell lines[216]. Moreover, [$Cu(PyDT)_2$] was further investigated since the ligand PyDT alone has been

reported to inhibit the activation of the nuclear factor κB. [217] Such compound was tested on the androgen receptor-independent human prostate cancer cells PC-3, two estrogen receptor α-positive human breast cancer cell lines (MCF-7 and MCF10dcis.com) and the triple negative highly metastatic MDA-MB-231 breast cancer cells, thus inducing 90%, 85%, 95% and more than 80% growth inhibition, respectively.[218]

Based on these promising results, we designed two different classes of new Cu(II) dithiocarbamato complexes and their synthesis, characterization and preliminary biological studies are reported in the *Section 2*.

Introduction references

(i) International Agency for Research on Cancer (IARC) and World Health Organization (WHO), *Word Cancer Report 2008*, edited by Peter Boyle and Bernard Levin, IARC press.

(ii) C. Mathers, D. Loncar, *Projections of global mortality and burden of disease from 2002 to 2030 PLoS Medicine*, (2006), **3**, 442.

(iii) Data from "Associazione Italiana dei registri tumori (AIRTUM) and from the web-site www.who.int.

(iv) D.Voet, J.G. Voet, C.W. Pratt, *Fondamenti di Biochimica*, Ed. Ital. Zanichelli 2001.

(v) www.millennium.com

(vi) Soldi S., *Chim. Ind.*, **1995**, *77*, 989.

(vii) Peyrone M., *Ann. Chem. Pharm.*, **1845**, *51*, 1.

(viii) Reyset J., *Compt. Rend.*, **1844**, *18*, 1103.

(ix) Werner A., *Z. Anorg. Chem.*, **1893**, *3*, 267.

(x) M. C. Lim, R. B. Martin, *J. Inorg. Nucl. Chem.*, 1976, **38**, 1911.

(xi) M. A. Tucker, C. B. Calvin, D. S. Martin Jr., *Inorg. Chem.*, 1964, **3**, 1373.

(xii) M. E. Howe Grant, S. J. Lippard, *Met. Ions. Biol. Syst.*, 1980, **11**, 63.

(xiii) P. Pil, S. J. Lippard, in: J. R. Bertino (Ed.), *Encyclopedia of Cancer*, Vol. 1, Academic Press, San Diego, 1997, p. 392.

(xiv) P. Frit, P. Calsou, Y. Conitrat, C. Muller, B. Salles, *Anticancer Drugs*, 1996, **7**, 101.

(xv) A. L. Pinto, S. J. Lippard, in: T. G. Spiro (Ed.), *Metal Ions in Biology 1*, John Wiley & Sons, 1980, p. 31.

(xvi) A. Eastman, in: B. Lippert (Ed.), *Cisplatin: Chemistry and Biochemistry of a Leading Anticancer Drug*, Wiley-VCH, Zurich, 1999, p. 111.

(xvii) S. J. Lippard, *Pure Appl. Chem.*, 1987, **59**, 731.

(xviii) D. B. Zamble, S. J. Lippard, in: B. Lippert (Ed.), *Cisplatin: Chemistry and Biochemistry of a Leading Anticancer Drug*, Wiley-VCH, Zurich, 1999, p. 73.

(xix) B. L. Zhang, W. X. Tong, *J. Inorg. Biochem.*, 1994, **56**, 143.

(xx) L. Stryer, *Biochemistry*, 4th ed., W. H. Freeman & Co., New York, 1995.

(xxi) A. Eastman, N. Schulte, *Biochem.*, 1988, **27**, 4730.

(xxii) R. Arky, *Physician's Desk Reference*, 50th ed., Medical Economics Company, Montvale, 1996.

(xxiii) B. Rosenberg, L. V. Camp, T. Krigas, *Nature*, 1965, **205**, 698.

(xxiv) W. R. Wood, *Cancer Res.*, 1987, **47**, 6549

(xxv) K. J. Barnham, Z. Guo, P. J. Sadler, *J. Chem. Soc., Dalton Trans.*, 1996, 2867.

(xxvi) R. T. Dorr, in: H. M. Pinedo, J. H. Schornagel (Eds.), *Platinum and Other Metal Coordination Compounds in Cancer Chemotherapy 2*, Plenum Press, New York, 1996, p. 131.

(xxvii) N. Farrell, *Transition Metal Complexes as Drugs and Chemotherapeutic Agents*; Kluwer Academic Publishers, Boston, 1989.

(xxviii) D. S. Alberts, *Semin. Oncol.*, 1995, **22**, 88.

(xxix) K. Landé, *Münch. Med. Wachenschr.*, 1927, **74**, 1132.

(xxx) N. Forestier, *J. Lab. Clin. Med.*, 1935, **20**, 827.

(xxxi) Empire Rheumatism Council, *Ann. Rheum. Dis.*, 1960, **19**, 95 and 1961, **20**, 315.

(xxxii) B. M. Sutton, R. G. Franz, *Bioinorganic Chemistry of Gold Coordination Compounds*, Smith, Kline and French, Philadelphia, 1983.

(xxxiii) R. V. Parish, *Int. Sci. Rev.*, 1992, **17**, 221.

(xxxiv) A. J. Lewis, D. T. Waltz, *Prog. Med. Chem.*, 1982, **19**, 1.

(xxxv) W. E. Smith, J. Reglinski, *Met.-Based Drugs*, 1994, **1**, 497.

(xxxvi) C. F. Shaw III, *Chem. Rev.*, 1999, **99**, 2589.

(xxxvii) R. F. Borch, P. C. Dedon, A. Gringeri and T. J. Montine, in *Platinum and OtherMetal Coordination Compounds in Cancer Chemotherapy*, ed. M. Nicolini, Martinus Nijoff Publishing, Boston, 1988, pp. 216–281.

(xxxviii) A. Eastman, in Cisplatin. Chemistry and Biochemistry of a Leading Anticancer Drug, ed. B. Lippert,Wiley-VCH,Weinheim, 1999, pp. 111– 134

(1) Hanahan, D.; Weinberg, R. A. Hallmarks of Cancer: The Next Generation. *Cell* **2011**, *144*, 646-674.

(2) Cheng, N.; Chytil, A.; Shyr, Y.; Joly, A.; Moses, H. L. Transforming Growth Factor-B Signaling-Deficient Fibroblasts Enhance Hepatocyte Growth Factor Signaling in Mammary Carcinoma Cells to Promote Scattering and Invasion. *Molecular Cancer Research* **2008**, *6*, 1521-1533.

(3) Bhowmick, N. A.; Neilson, E. G.; Moses, H. L. Stromal Fibroblasts in Cancer Initiation and Progression. *Nature* **2004**, *432*, 332-337.

(4) Davies, M. A.; Samuels, Y. Analysis of the Genome to Personalize Therapy for Melanoma. *Oncogene* **2010**, *29*, 5545-5555.

(5) Yuan, T. L.; Cantley, L. C. PI3K Pathway Alterations in Cancer: Variations on a Theme. *Oncogene* **2008**, *27*, 5497-5510.

(6) Adams, J. M.; Cory, S. The Bcl-2 Apoptotic Switch in Cancer Development and Therapy. *Oncogene* **2007**, *26*, 1324-1337.

(7) Junttila, M. R.; Evan, G. I. P53 a Jack of all Trades but Master of None. *Nature Reviews Cancer* **2009**, *9*, 821-829.

(8) White, E.; DiPaola, R. S. The Double-Edged Sword of Autophagy Modulation in Cancer. *Clinical Cancer Research* **2009**, *15*, 5308-5316.

(9) Grivennikov, S. I.; Greten, F. R.; Karin, M. Immunity, Inflammation, and Cancer. *Cell* **2010**, *140*, 883-899.

(10) Shay, J. W.; Wright, W. E. Hayflick, His Limit, and Cellular Ageing. *Nature Reviews Molecular Cell Biology* **2000**, *1*, 72-76.

(11) Blasco, M. A. Telomeres and Human Disease: Ageing, Cancer and Beyond. *Nature Reviews Genetics* **2005**, *6*, 611-622.

(12) Chin, K., et al In Situ Analyses of Genome Instability in Breast Cancer. *Nat. Genet.* **2004**, *36*, 984-988.

(13) Raynaud, C. M.; Hernandez, J.; Llorca, F. P.; Nuciforo, P.; Mathieu, M. -.; Commo, F.; Delaloge, S.; Sabatier, L.; André, F.; Soria, J. -. DNA Damage Repair and Telomere Length in Normal Breast, Preneoplastic Lesions, and Invasive Cancer. *American Journal of Clinical Oncology: Cancer Clinical Trials* **2010**, *33*, 341-345.

(14) Hanahan, D.; Folkman, J. Patterns and Emerging Mechanisms of the Angiogenic Switch during Tumorigenesis. *Cell* **1996**, *86*, 353-364.

(15) Baluk, P.; Hashizume, H.; McDonald, D. M. Cellular Abnormalities of Blood Vessels as Targets in Cancer. *Current Opinion in Genetics and Development* **2005**, *15*, 102-111.

(16) Gabhann, F. M.; Popel, A. S. Systems Biology of Vascular Endothelial Growth Factors. *Microcirculation* **2008**, *15*, 715-738.

(17) Carmeliet, P. VEGF as a Key Mediator of Angiogenesis in Cancer. *Oncology* **2005**, *69*, 4-10.

(18) Qian, B. -.; Pollard, J. W. Macrophage Diversity Enhances Tumor Progression and Metastasis. *Cell* **2010**, *141*, 39-51.

(19) Murdoch, C.; Muthana, M.; Coffelt, S. B.; Lewis, C. E. The Role of Myeloid Cells in the Promotion of Tumour Angiogenesis. *Nature Reviews Cancer* **2008**, *8*, 618-631.

(20) Negrini, S.; Gorgoulis, V. G.; Halazonetis, T. D. Genomic Instability an Evolving Hallmark of Cancer. *Nature Reviews Molecular Cell Biology* **2010**, *11*, 220-228.

(21) Jackson, S. P.; Bartek, J. The DNA-Damage Response in Human Biology and Disease. *Nature* **2009**, *461*, 1071-1078.

(22) Lane, D. P. p53, Guardian of the Genome. *Nature* **1992**, *358*, 15-16.

(23) Pagès, F.; Galon, J.; Dieu-Nosjean, M. -.; Tartour, E.; Sautès-Fridman, C.; Fridman, W. -. Immune Infiltration in Human Tumors: A Prognostic Factor that should Not be Ignored. *Oncogene* **2010**, *29*, 1093-1102.

(24) DeNardo, D. G.; Andreu, P.; Coussens, L. M. Interactions between Lymphocytes and Myeloid Cells Regulate Pro-Versus Anti-Tumor Immunity. *Cancer Metastasis Rev.* **2010**, *29*, 309-316.

(25) Mougiakakos, D.; Choudhury, A.; Lladser, A.; Kiessling, R.; Johansson, C. C. Regulatory T Cells in Cancer. *Adv. Cancer Res.* **2010**, *107*, 57-117.

(26) Vajdic, C. M.; Van Leeuwen, M. T. Cancer Incidence and Risk Factors After Solid Organ Transplantation. *International Journal of Cancer* **2009**, *125*, 1747-1754.

(27) Strauss, D. C.; Thomas, J. M. Transmission of Donor Melanoma by Organ Transplantation. *The Lancet Oncology* **2010**, *11*, 790-796.

(28) Heiden, M. G. V.; Cantley, L. C.; Thompson, C. B. Understanding the Warburg Effect: The Metabolic Requirements of Cell Proliferation. *Science* **2009**, *324*, 1029-1033.

(29) Jones, R. G.; Thompson, C. B. Tumor Suppressors and Cell Metabolism: A Recipe for Cancer Growth. *Genes and Development* **2009**, *23*, 537-548.

(30) DeBerardinis, R. J.; Lum, J. J.; Hatzivassiliou, G.; Thompson, C. B. The Biology of Cancer: Metabolic Reprogramming Fuels Cell Growth and Proliferation. *Cell Metabolism* **2008**, *7*, 11-20.

(31) L. Shargel, A.H. Mutnik, P.F. Sauney, L.N. Swanson, *Comprehensive Pharmacy Review*, 6th Ed. Lippincott Williams&Linkins.

(32) B.G. Katzung, S.B. Masters, A.J. Trevor, Farmacologia Generale e Clinica, 8° Ed. Italiana, Ed. Piccin, 2011.

(33) R.D. Howland, M.J.Mycek,*Pharmacology* 3rd Ed. Lippincott Williams&Linkins, 2006.

(34) Saeed, M.; Kohen, A. Novel Positron Emission Tomography Tracer Distinguishes Normal from Cancerous Cells. *J. Biol. Chem.* **2011**, *286*, 33872-33878.

(35) Spratt, J. S.; Meyer, J. S.; Spratt, J. A. Rates of Growth of Human Solid Neoplasms: Part I. *J. Surg. Oncol.* **1995**, *60*, 137-146.

(36) Spratt, J. S.; Spratt, J. A. What is Breast Cancer Doing before we can Detect it? *J. Surg. Oncol.* **1985**, *30*, 156-160. 36b. Gompertz, B. On the Nature of the Function Expressive of the Law of Human Mortality, and on a New Mode of Determining the Value of Life Contingencies. *Phil. Trans. Roy. Soc. London*, **1832,** *123*, 513-585.

(37) Fournier, D. V.; Weber, E.; Hoeffken, W. Growth Rate of 147 Mammary Carcinomas. *Cancer* **1980**, *45*, 2198-2207.

(38) Arnerlov, C.; Emdin, S. O.; Lundgren, B.; Roos, G.; Soderstrom, J.; Bjersing, L.; Norberg, C.; Angquist, K. A. Breast Carcinoma Growth Rate Described by Mammographic Doubling Time and S-Phase Fraction: Correlations to Clinical and Histopathologic Factors in a Screened Population. *Cancer* **1992**, *70*, 1928-1934.

(39) Yang, L.; Wu, X.; Wang, Y.; Zhang, K.; Wu, J.; Yuan, Y. -.; Deng, X.; Chen, L.; Kim, C. C. H.; Lau, S.; Somlo, G.; Yen, Y. FZD7 has a Critical Role in Cell Proliferation in Triple Negative Breast Cancer. *Oncogene* **2011**, *30*, 4437-4446.

(40) Dalla Via, L.; Nardon, C.; Fregona, D. Targeting the Ubiquitin-Proteasome Pathway with Inorganic Compounds to Fight Cancer: A Challenge for the Future. *Future Medicinal Chemistry* **2012**, *4*, 525-543.

(41) Bross, P. F., et al Approval Summary for Bortezomib for Injection in the Treatment of Multiple Myeloma. *Clin. Cancer Res.* **2004**, *10*, 3954-3964.

(42) Pérez-Galán, P.; Roue, G.; Villamor, N.; Montserrat, E.; Campo, E.; Colomer, D. The Proteasome Inhibitor Bortezomib Induces Apoptosis in Mantle-Cell Lymphoma through Generation of ROS and Noxa Activation Independent of p53 Status. *Blood* **2006**, *107*, 257-264.

(43) Adams, J.; Palombella, V. J.; Sausville, E. A.; Johnson, J.; Destree, A.; Lazarus, D. D.; Maas, J.; Pien, C. S.; Prakash, S.; Elliott, P. J. Proteasome Inhibitors: A Novel Class of Potent and Effective Antitumor Agents. *Cancer Res.* **1999**, *59*, 2615-2622.

(44) Hideshima, T.; Richardson, P.; Chauhan, D.; Palombella, V. J.; Elliott, P. J.; Adams, J.; Anderson, K. C. The Proteasome Inhibitor PS-341 Inhibits Growth, Induces Apoptosis, and Overcomes Drug Resistance in Human Multiple Myeloma Cells. *Cancer Res.* **2001**, *61*, 3071-3076.

(45) Richardson, P. G., et al A Phase 2 Study of Bortezomib in Relapsed, Refractory Myeloma. *New Engl. J. Med.* **2003**, *348*, 2609-2617.

(46) Jackson, G.; Einsele, H.; Moreau, P.; San Miguel, J. Bortezomib, a Novel Proteasome Inhibitor, in the Treatment of Hematologic Malignancies. *Cancer Treat. Rev.* **2005**, *31*, 591-602.

(47) Tanaka, K. The Proteasome: Overview of Structure and Functions. *Proc. Jpn. Acad. Ser. B Phys. Biol. Sci.* **2009**, *85*, 12-36.

(48) Groll, M.; Huber, R. Inhibitors of the Eukaryotic 20S Proteasome Core Particle: A Structural Approach. *Biochim. Biophys. Acta Mol. Cell Res.* **2004**, *1695*, 33-44.

(49) Groll, M.; Ditzel, L.; Löwe, J.; Stock, D.; Bochtler, M.; Bartunik, H. D.; Huber, R. Structure of 20S Proteasome from Yeast at 2.4 Å Resolution. *Nature* **1997**, *386*, 463-471.

(50) Bochtler, M.; Ditzel, L.; Groll, M.; Hartmann, C.; Huber, R. The Proteasome. *Annu. Rev. Biophys. Biomol. Struct.* **1999**, *28*, 295-317.

(51) Orlowski, R. Z., et al Phase I Trial of the Proteasome Inhibitor PS-341 in Patients with Refractory Hematologic Malignancies. *Journal of Clinical Oncology* **2002**, *20*, 4420-4427.

(52) Papandreou, C. N., et al Phase I Trial of the Proteasome Inhibitor Bortezomib in Patients with Advanced Solid Tumors with Observations in Androgen-Independent Prostate Cancer. *Journal of Clinical Oncology* **2004**, *22*, 2108-2121.

(53) Groll, M.; Heinemeyer, W.; Jäger, S.; Ullrich, T.; Bochtler, M.; Wolf, D. H.; Huber, R. The Catalytic Sites of 20S Proteasomes and their Role in Subunit Maturation: A Mutational and Crystallographic Study. *Proc. Natl. Acad. Sci. U. S. A.* **1999**, *96*, 10976-10983.

(54) Groll, M.; Berkers, C. R.; Ploegh, H. L.; Ovaa, H. Crystal Structure of the Boronic Acid-Based Proteasome Inhibitor Bortezomib in Complex with the Yeast 20S Proteasome. *Structure* **2006**, *14*, 451-456.

(55) Pettersen, E. F.; Goddard, T. D.; Huang, C. C.; Couch, G. S.; Greenblatt, D. M.; Meng, E. C.; Ferrin, T. E. UCSF Chimera - A Visualization System for Exploratory Research and Analysis. *Journal of Computational Chemistry* **2004**, *25*, 1605-1612.

(56) An, B.; Goldfarb, R. H.; Siman, R.; Dou, Q. P. Novel Dipeptidyl Proteasome Inhibitors Overcome Bcl-2 Protective Function and Selectively Accumulate the Cyclin-Dependent Kinase Inhibitor p27 and Induce Apoptosis in Transformed, but Not Normal, Human Fibroblasts. *Cell Death Differ.* **1998**, *5*, 1062-1075.

(57) Walker, B.; Lynas, J. F. Strategies for the Inhibition of Serine Proteases. *Cellular and Molecular Life Sciences* **2001**, *58*, 596-624.

(58) London, R. E.; Gabel, S. A. Development and Evaluation of a Boronate Inhibitor of Γ-Glutamyl Transpeptidase. *Arch. Biochem. Biophys.* **2001**, *385*, 250-258.

(59) Jackson, G.; Einsele, H.; Moreau, P.; San Miguel, J. Bortezomib, a Novel Proteasome Inhibitor, in the Treatment of Hematologic Malignancies. *Cancer Treat. Rev.* **2005**, *31*, 591-602.

(60) Transue, T. R.; Krahn, J. M.; Gabel, S. A.; DeRose, E. F.; London, R. E. X-Ray and NMR Characterization of Covalent Complexes of Trypsin, Borate, and Alcohols. *Biochemistry* **2004**, *43*, 2829-2839.

(61) Iijima, M.; Momose, I.; Ikeda, D. TP-110, a New Proteasome Inhibitor, Down-Regulates IAPs in Human Multiple Myeloma Cells. *Anticancer Res.* **2009**, *29*, 977-986.

(62) Gomez-Bougie, P.; Wuillème-Toumi, S.; Ménoret, E.; Trichet, V.; Robillard, N.; Philippe, M.; Bataille, R.; Amiot, M. Noxa Up-Regulation and Mcl-1 Cleavage are Associated to Apoptosis Induction by Bortezomib in Multiple Myeloma. *Cancer Res.* **2007**, *67*, 5418-5424.

(63) Podar, K.; Gouill, S. L.; Zhang, J.; Opferman, J. T.; Zorn, E.; Tai, Y. -.; Hideshima, T.; Amiot, M.; Chauhan, D.; Harousseau, J. -.; Anderson, K. C. A Pivotal Role for Mcl-1 in Bortezomib-Induced Apoptosis. *Oncogene* **2008**, *27*, 721-731.

(64) Mulligan, G., et al Gene Expression Profiling and Correlation with Outcome in Clinical Trials of the Proteasome Inhibitor Bortezomib. *Blood* **2007**, *109*, 3177-3188.

(65) Li, B.; Dou, Q. P. Bax Degradation by the Ubiquitin Proteasome-Dependent Pathway: Involvement in Tumor Survival and Progression. *Proc. Natl. Acad. Sci. U. S. A.* **2000**, *97*, 3850-3855.

(66) Qin, J. -.; Ziffra, J.; Stennett, L.; Bodner, B.; Bonish, B. K.; Chaturvedi, V.; Bennett, F.; Pollock, P. M.; Trent, J. M.; Hendrix, M. J. C.; Rizzo, P.; Miele, L.; Nickoloff, B. J. Proteasome Inhibitors Trigger NOXA-Mediated Apoptosis in Melanoma and Myeloma Cells. *Cancer Res.* **2005**, *65*, 6282-6293.

(67) Sánchez-Serrano, I. Success in Translational Research: Lessons from the Development of Bortezomib. *Nat. Rev. Drug Discov.* **2006**, *5*, 107-114.

(68) Rosenberg, B.; Van Camp, L.; Krigas, T. Inhibition of Cell Division in Escherichia Coli by Electrolysis Products from a Platinum Electrode [17]. *Nature* **1965**, *205*, 698-699.

(69) Rosenberg, B.; Renshaw, E.; Vancamp, L.; Hartwick, J.; Drobnik, J. Platinum-Induced Filamentous Growth in Escherichia Coli. *J. Bacteriol.* **1967**, *93*, 716-721.

(70) Rosenberg, B.; Van Camp, L.; Grimley, E. B.; Thomson, A. J. The Inhibition of Growth Or Cell Division in Escherichia Coli by Different Ionic Species of Platinum(IV) Complexes. *J. Biol. Chem.* **1967**, *242*, 1347-1352.

(71) Rosenberg, B.; VanCamp, L.; Trosko, J. E.; Mansour, V. H. Platinum Compounds: A New Class of Potent Antitumour Agents [24]. *Nature* **1969**, *222*, 385-386.

(72) Higby, D. J.; Wallace Jr, H. J.; Albert, D. J.; Holland, J. F. Diaminodichloroplatinum: A Phase I Study Showing Responses in Testicular and Other Tumors. *Cancer* **1974**, *33*, 1219-1225.

(73) Hambley, T. W. Developing New Metal-Based Therapeutics: Challenges and Opportunities. *Dalton Transactions* **2007**, 4929-4937.

(74) Kelland, L. The Resurgence of Platinum-Based Cancer Chemotherapy. *Nature Reviews Cancer* **2007**, *7*, 573-584.

(75) Zhang, S.; Lovejoy, K. S.; Shima, J. E.; Lagpacan, L. L.; Shu, Y.; Lapuk, A.; Chen, Y.; Komori, T.; Gray, J. W.; Chen, X.; Lippard, S. J.; Giacomini, K. M. Organic Cation Transporters are Determinants of Oxaliplatin Cytotoxicity. *Cancer Res.* **2006**, *66*, 8847-8857.

(76) Lovejoy, K. S.; Todd, R. C.; Zhang, S.; McCormick, M. S.; D'Aquino, J. A.; Reardon, J. T.; Sancar, A.; Giacomini, K. M.; Lippard, S. J. Cis-Diammine(Pyridine)Chloroplatinum(II), a Monofunctional Platinum(II) Antitumor Agent: Uptake, Structure, Function, and Prospects. *Proc. Natl. Acad. Sci. U. S. A.* **2008**, *105*, 8902-8907.

(77) Ishida, S.; Lee, J.; Thiele, D. J.; Herskowitz, I. Uptake of the Anticancer Drug Cisplatin Mediated by the Copper Transporter Ctr1 in Yeast and Mammals. *Proc. Natl. Acad. Sci. U. S. A.* **2002**, *99*, 14298-14302.

(78) Tucker, M. A.; Colvin, C. B.; Martin Jr., D. S. Substitution Reactions of Trichloroammineplatinate(II) Ion and the Trans Effect. *Inorg. Chem.* **1964**, *3*, 1373-1383.

(79) Lippard, S. J. CHEMISTRY AND MOLECULAR BIOLOGY OF PLATINUM ANTICANCER DRUGS. *Pure and Applied Chemistry* **1987**, *59*, 731-742.

(80) Florea, A. -.; Büsselberg, D. Cisplatin as an Anti-Tumor Drug: Cellular Mechanisms of Activity, Drug Resistance and Induced Side Effects. *Cancers* **2011**, *3*, 1351-1371.

(81) Sancho-Martínez, S. M.; Prieto-García, L.; Prieto, M.; López-Novoa, J. M.; López-Hernández, F. J. Subcellular Targets of Cisplatin Cytotoxicity: An Integrated View. *Pharmacology and Therapeutics* **2012**, *136*, 35-55.

(82) Cullen, K. J.; Yang, Z.; Schumaker, L.; Guo, Z. Mitochondria as a Critical Target of the Chemotheraputic Agent Cisplatin in Head and Neck Cancer. *J. Bioenerg. Biomembr.* **2007**, *39*, 43-50.

(83) Servais, H.; Ortiz, A.; Devuyst, O.; Denamur, S.; Tulkens, P. M.; Mingeot-Leclercq, M. -. Renal Cell Apoptosis Induced by Nephrotoxic Drugs: Cellular and Molecular Mechanisms and Potential Approaches to Modulation. *Apoptosis* **2008**, *13*, 11-32.

(84) Custódio, J. B. A.; Cardoso, C. M. P.; Santos, M. S.; Almeida, L. M.; Vicente, J. A. F.; Fernandes, M. A. S. Cisplatin Impairs Rat Liver Mitochondrial Functions by Inducing Changes on Membrane Ion Permeability: Prevention by Thiol Group Protecting Agents. *Toxicology* **2009**, *259*, 18-24.

(85) Murata, T.; Hibasami, H.; Maekawa, S.; Tagawa, T.; Nakashima, K. Preferential Binding of Cisplatin to Mitochondrial DNA and Suppression of ATP Generation in Human Malignant Melanoma Cells. *Biochem. Int.* **1990**, *20*, 949-955.

(86) Preston, T. J.; Abadi, A.; Wilson, L.; Singh, G. Mitochondrial Contributions to Cancer Cell Physiology: Potential for Drug Development. *Adv. Drug Deliv. Rev.* **2001**, *49*, 45-61.

(87) Greggi Antunes, L. M.; D'arc C. Darin, J.; Bianchi, M. D. L. P. Protective Effects of Vitamin C Against Cisplatin-Induced Nephrotoxicity and Lipid Peroxidation in Adult Rats: A Dose-Dependent Study. *Pharmacological Research* **2000**, *41*, 405-411.

(88) Kadikoylu, G.; Bolaman, Z.; Demir, S.; Balkaya, M.; Akalin, N.; Enli, Y. The Effects of Desferrioxamine on Cisplatin-Induced Lipid Peroxidation and the Activities of Antioxidant Enzymes in Rat Kidneys. *Human and Experimental Toxicology* **2004**, *23*, 29-34.

(89) Masgras, I.; Carrera, S.; De Verdier, P. J.; Brennan, P.; Majid, A.; Makhtar, W.; Tulchinsky, E.; Jones, G. D. D.; Roninson, I. B.; Macip, S. Reactive Oxygen Species and Mitochondrial Sensitivity to Oxidative Stress Determine Induction of Cancer Cell Death by p21. *J. Biol. Chem.* **2012**, *287*, 9845-9854.

(90) Kelland, L. R. New Platinum Antitumor Complexes. *Crit. Rev. Oncol.* **1993**, *15*, 191-219.

(91) Volckova, E.; Evanics, F.; Yang, W. W.; Bose, R. N. Unwinding of DNA Polymerases by the Antitumor Drug, Cis-Diamminedichloroplatinum(II). *Chemical Communications* **2003**, *9*, 1128-1129.

(92) Fuertes, M. A.; Alonso, C.; Pérez, J. M. Biochemical Modulation of Cisplatin Mechanisms of Action: Enhancement of Antitumor Activity and Circumvention of Drug Resistance. *Chem. Rev.* **2003**, *103*, 645-662.

(93) Ahmad, S. Platinum-DNA Interactions and Subsequent Cellular Processes Controlling Sensitivity to Anticancer Platinum Complexes. *Chemistry and Biodiversity* **2010**, *7*, 543-566.

(94) Söti, C.; Rácz, A.; Csermely, P. A Nucleotide-Dependent Molecular Switch Controls ATP Binding at the C-Terminal Domain of Hsp90. N-Terminal Nucleotide Binding Unmasks a C-Terminal Binding Pocket. *J. Biol. Chem.* **2002**, *277*, 7066-7075.

(95) Peleg-Shulman, T.; Gibson, D. Cisplatin-Protein Adducts are Efficiently Removed by Glutathione but Not by 5′-Guanosine Monophosphate. *J. Am. Chem. Soc.* **2001**, *123*, 3171-3172.

(96) Arnesano, F.; Natile, G. "Platinum on the Road": Interactions of Antitumoral Cisplatin with Proteins. *Pure and Applied Chemistry* **2008**, *80*, 2715-2725.

(97) Gómez-Ruiz, S.; Maksimović-Ivanić, D.; Mijatović, S.; Kaluderović, G. N. On the Discovery, Biological Effects, and use of Cisplatin and Metallocenes in Anticancer Chemotherapy. *Bioinorganic Chemistry and Applications* **2012**, *2012*.

(98) Royer-Pokora, B.; Gordon, L. K.; Haseltine, W. A. Use of Exonuclease III to Determine the Site of Stable Lesions in Defined Sequences of DNA: The Cyclobutane Pyrimidine Dimer and Cis and Trans Dichlorodiammine Platinum II Examples. *Nucleic Acids Res.* **1981**, *9*, 4595-4609.

(99) Tullius, T. D.; Lippard, S. J. Cis-Diamminedichloroplatinum(II) Binds in a Unique Manner to Oligo(dG)·oligo(dC) Sequences in DNA - A New Assay using Exonuclease III. *J. Am. Chem. Soc.* **1981**, *103*, 4620-4622.

(100) Cohen, G. L.; Ledner, J. A.; Bauer, W. R.; Ushay, H. M.; Caravana, C.; Lippard, S. J. Sequence Dependent Binding of Cis-Dichlorodiammineplatinum(II) to DNA [24]. *J. Am. Chem. Soc.* **1980**, *102*, 2487-2488.

(101) Fichtinger-Schepman, A. M. J.; Lohman, P. H. M.; Reedijk, J. Detection and Quantification of Adducts Formed upon Interaction of Diamminedichloroplatinum (II) with DNA, by Anion-Exchange Chromatography After Enzymatic Degradation. *Nucleic Acids Res.* **1982**, *10*, 5345-5356.

(102) Fichtinger-Schepman, A. M. J.; Van Der Veer, J. L.; Den Hartog, J. H. J.; Lohman, P. H. M.; Reedijk, J. Adducts of the Antitumor Drug Cis-Diamminedichloroplatinum(II) with DNA: Formation, Identification, and Quantitation. *Biochemistry* **1985**, *24*, 707-713.

(103) Eastman, A. Reevaluation of Interaction of Cis-Dichloro(Ethylenediamine)Platinum(II) with DNA. *Biochemistry* **1986**, *25*, 3912-3915.

(104) Plooy, A. C. M.; Fichtinger-Schepman, A. M. J.; Schutte, H. H.; van Dijk, M.; Lohman, P. H. The Quantitative Detection of various Pt-DNA-Adducts in Chinese Hamster Ovary Cells Treated with Cisplatin: Application of Immunochemical Techniques. *Carcinogenesis* **1985**, *6*, 561-566.

(105) Reeder, F.; Guo, Z.; Murdoch, P. D. S.; Corazza, A.; Hambley, T. W.; Berners-Price, S. J.; Chottard, J. -.; Sadler, P. J. Platination of a GG Site on Single-Stranded and Double-Stranded Forms of a 14-Base Oligonucleotide with Diaqua Cisplatin Followed by NMR and HPLC. Influence of the Platinum Ligands and Base Sequence on 5'-G Versus 3'-G Platination Selectivity. *European Journal of Biochemistry* **1997**, *249*, 370-382.

(106) Reeder, R.; Gonnet, F.; Kozelka, J.; Chottard, J. -. Reactions of the Double-Stranded Oligonucleotide D(TTGGCCAA)2 with Cis- [Pt(NH3)2(H2O2]2+ and [Pt(NH3)3(H2O)]2+. *Angewandte Chemie - International Edition in English* **1996**, *35*, 1068-1076.

(107) Berners-Price, S. J.; Kuchel, P. W. Reaction of Cis- and Trans-[PtCl2(NH3)2] with Reduced Glutathione Inside Human Red Blood Cells, Studied by 1H and 15N-{1H} Dept NMR. *J. Inorg. Biochem.* **1990**, *38*, 327-345.

(108) Eastman, A. Interstrand Cross-Links and Sequence Specificity in the Reaction of Cis-Dichloro(Ethylenediamine)Platinum(II) with DNA. *Biochemistry* **1985**, *24*, 5027-5032.

(109) Eastman, A. Cross-Linking of Glutathione to DNA by Cancer Chemotherapeutic Platinum Coordination Complexes. *Chem. Biol. Interact.* **1987**, *61*, 241-248.

(110) Macquet, J. P.; Butour, J. L. Modifications of the DNA Secondary Structure upon Platinum Binding: A Proposed Model. *Biochimie* **1978**, *60*, 901-914.

(111) Cohen, G. L.; Bauer, W. R.; Barton, J. K.; Lippard, S. J. Binding of Cis- and Trans-Dichlorodiammineplatinum(II) to DNA: Evidence for Unwinding and Shortening of the Double Helix. *Science* **1979**, *203*, 1014-1016.

(112) Huang, H.; Zhu, L.; Reid, B. R.; Drobny, G. P.; Hopkins, P. B. Solution Structure of a Cisplatin-Induced DNA Interstrand Cross-Link. *Science* **1995**, *270*, 1842-1845.

(113) Marzilli, L. G.; Saad, J. S.; Kuklenyik, Z.; Keating, K. A.; Xu, Y. Relationship of Solution and Protein-Bound Structures of DNA Duplexes with the Major Intrastrand Cross-Link Lesions Formed on Cisplatin Binding to DNA. *J. Am. Chem. Soc.* **2001**, *123*, 2764-2770.

(114) Woźniak, K.; Błasiak, J. Recognition and Repair of DNA-Cisplatin Adducts. *Acta Biochim. Pol.* **2002**, *49*, 583-596.

(115) Bustin, M.; Reeves, R. High-Mobility-Group Chromosomal Proteins: Architectural Components that Facilitate Chromatin Function. *Prog. Nucleic Acid Res. Mol. Biol.* **1996**, *54*, 35-100.

(116) Turchi, J. J.; Henkels, K. M.; Hermanson, I. L.; Patrick, S. M. Interactions of Mammalian Proteins with Cisplatin-Damaged DNA. *J. Inorg. Biochem.* **1999**, *77*, 83-87.

(117) Kartalou, M.; Essigmann, J. M. Recognition of Cisplatin Adducts by Cellular Proteins. *Mutation Research - Fundamental and Molecular Mechanisms of Mutagenesis* **2001**, *478*, 1-21.

(118) Ohndorf, U. -.; Rould, M. A.; He, Q.; Pabo, C. O.; Lippard, S. J. Basis for Recognition of Cisplatin-Modified DNA by High-Mobility-Group Proteins. *Nature* **1999**, *399*, 708-712.

(119) Treiber, D. K.; Zhai, X.; Jantzen, H. -.; Essigmann, J. M. Cisplatin-DNA Adducts are Molecular Decoys for the Ribosomal RNA Transcription Factor hUBF (Human Upstream Binding Factor). *Proc. Natl. Acad. Sci. U. S. A.* **1994**, *91*, 5672-5676.

(120) McA'Nulty, M. M.; Lippard, S. J. The HMG-Domain Protein Ixr1 Blocks Excision Repair of Cisplatin-DNA Adducts in Yeast. *Mutation Research - DNA Repair* **1996**, *362*, 75-86.

(121) Chu, G. Cellular Responses to Cisplatin. the Roles of DNA-Binding Proteins and DNA Repair. *J. Biol. Chem.* **1994**, *269*, 787-790.

(122) Galluzzi, L.; Senovilla, L.; Vitale, I.; Michels, J.; Martins, I.; Kepp, O.; Castedo, M.; Kroemer, G. Molecular Mechanisms of Cisplatin Resistance. *Oncogene* **2012**, *31*, 1869-1883.

(123) Meijer, C.; Mulder, N. H.; Hospers, G. A. P.; Uges, D. R. A.; De Vries, E. G. E. The Role of Glutathione in Resistance to Cisplatin in a Human Small Cell Lung Cancer Cell Line. *Br. J. Cancer* **1990**, *62*, 72-77.

(124) Howell, S. B.; Safaei, R.; Larson, C. A.; Sailor, M. J. Copper Transporters and the Cellular Pharmacology of the Platinum-Containing Cancer Drugs. *Mol. Pharmacol.* **2010**, *77*, 887-894.

(125) Safaei, R. Role of Copper Transporters in the Uptake and Efflux of Platinum Containing Drugs. *Cancer Lett.* **2006**, *234*, 34-39.

(126) Holzer, A. K.; Howell, S. B. The Internalization and Degradation of Human Copper Transporter 1 Following Cisplatin Exposure. *Cancer Res.* **2006**, *66*, 10944-10952.

(127) Holzer, A. K.; Samimi, G.; Katano, K.; Naerdemann, W.; Lin, X.; Safaei, R.; Howell, S. B. The Copper Influx Transporter Human Copper Transport Protein 1 Regulates the Uptake of Cisplatin in Human Ovarian Carcinoma Cells. *Mol. Pharmacol.* **2004**, *66*, 817-823.

(128) Bertinato, J.; Swist, E.; Plouffe, L. J.; Brooks, S. P. J.; L'Abbé, M. R. Ctr2 is Partially Localized to the Plasma Membrane and Stimulates Copper Uptake in COS-7 Cells. *Biochem. J.* **2008**, *409*, 731-740.

(129) Blair, B. G.; Larson, C. A.; Adams, P. L.; Abada, P. B.; Pesce, C. E.; Safaei, R.; Howell, S. B. Copper Transporter 2 Regulates Endocytosis and Controls Tumor Growth and Sensitivity to Cisplatin in Vivo. *Mol. Pharmacol.* **2011**, *79*, 157-166.

(130) Samimi, G.; Katano, K.; Holzer, A. K.; Safaei, R.; Howell, S. B. Modulation of the Cellular Pharmacology of Cisplatin and its Analogs by the Copper Exporters ATP7A and ATP7B. *Mol. Pharmacol.* **2004**, *66*, 25-32.

(131) Safaei, R.; Holzer, A. K.; Katano, K.; Samimi, G.; Howell, S. B. The Role of Copper Transporters in the Development of Resistance to Pt Drugs. *J. Inorg. Biochem.* **2004**, *98*, 1607-1613.

(132) Lemkuil, D. C.; Nettesheim, D.; Shaw III, C. F.; Petering, D. H. Reaction of Cd7-Metallothionein with Cis-Dichlorodiammine Platinum (II). *J. Biol. Chem.* **1994**, *269*, 24792-24797.

(133) Kuo, M. T.; Chen, H. H. W. Role of Glutathione in the Regulation of Cisplatin Resistance in Cancer Chemotherapy. *Metal-Based Drugs* **2010**, *2010*.

(134) Ishikawa, T.; Wright, C. D.; Ishizuka, H. GS-X Pump is Functionally Overexpressed in Cis-Diamminedichloroplatinum(II)-Resistant Human Leukemia HL-60 Cells and Down- Regulated by Cell Differentiation. *J. Biol. Chem.* **1994**, *269*, 29085-29093.

(135) Del Socorro Murdoch, P.; Ranford, J. D.; Sadler, P. J.; Berners-Price, S. J. Cis-Trans Isomerization of [Pt(L-Methionine)2]: Metabolite of the Anticancer Drug Cisplatin. *Inorg. Chem.* **1993**, *32*, 2249-2255.

(136) Zamble, D. B.; Mu, D.; Reardon, J. T.; Sancar, A.; Lippard, S. J. Repair of Cisplatin-DNA Adducts by the Mammalian Excision Nuclease. *Biochemistry* **1996**, *35*, 10004-10013.

(137) Wood, R. D. Nucleotide Excision Repair in Mammalian Cells. *J. Biol. Chem.* **1997**, *272*, 23465-23468.

(138) Moggs, J. G.; Szymkowski, D. E.; Yamada, M.; Karran, P.; Wood, R. D. Differential Human Nucleotide Excision Repair of Paired and Mispaired Cisplatin-DNA Adducts. *Nucleic Acids Res.* **1997**, *25*, 480-490.

(139) Bassett, E.; Vaisman, A.; Tropea, K. A.; McCall, C. M.; Masutani, C.; Hanaoka, F.; Chaney, S. G. Frameshifts and Deletions during in Vitro Translesion Synthesis Past Pt-DNA Adducts by DNA Polymerases B and H. *DNA Repair* **2002**, *1*, 1003-1016.

(140) Shachar, S.; Ziv, O.; Avkin, S.; Adar, S.; Wittschieben, J.; Reißner, T.; Chaney, S.; Friedberg, E. C.; Wang, Z.; Carell, T.; Geacintov, N.; Livneh, Z. Two-Polymerase Mechanisms Dictate Error-Free and Error-Prone Translesion DNA Synthesis in Mammals. *EMBO J.* **2009**, *28*, 383-393.

(141) Smith, J.; Mun Tho, L.; Xu, N.; A. Gillespie, D. The ATM-Chk2 and ATR-Chk1 Pathways in DNA Damage Signaling and Cancer. *Advances in Cancer Research* **2010**, *108*, 73-112.

(142) Narod, S. A.; Foulkes, W. D. BRCA1 and BRCA2: 1994 and Beyond. *Nature Reviews Cancer* **2004**, *4*, 665-676.

(143) Vousden, K. H.; Lane, D. P. p53 in Health and Disease. *Nature Reviews Molecular Cell Biology* **2007**, *8*, 275-283.

(144) Kirsch, D. G.; Kastan, M. B. Tumor-Suppressor p53: Implications for Tumor Development and Prognosis. *Journal of Clinical Oncology* **1998**, *16*, 3158-3168.

(145) O'Connor, P. M.; Jackman, J.; Bae, I.; Myers, T. G.; Fan, S.; Mutoh, M.; Scudiero, D. A.; Monks, A.; Sausville, E. A.; Weinstein, J. N.; Friend, S.; Fornace Jr., A. J.; Kohn, K. W. Characterization of the p53 Tumor Suppressor Pathway in Cell Lines of the National Cancer Institute Anticancer Drug Screen and Correlations with the Growth-Inhibitory Potency of 123 Anticancer Agents. *Cancer Res.* **1997**, *57*, 4285-4300.

(146) Hengstler, J. G.; Pilch, H.; Schmidt, M.; Dahlenburg, H.; Sagemüller, J.; Schiffer, I.; Oesch, F.; Knapstein, P. G.; Kaina, B.; Tanner, B. Metallothionein Expression in Ovarian Cancer in Relation to Histopathological Parameters and Molecular Markers of Prognosis. *International Journal of Cancer* **2001**, *95*, 121-127.

(147) Feldman, D. R.; Bosl, G. J.; Sheinfeld, J.; Motzer, R. J. Medical Treatment of Advanced Testicular Cancer. *JAMA - Journal of the American Medical Association* **2008**, *299*, 672-684.

(148) Kroemer, G.; Mariño, G.; Levine, B. Autophagy and the Integrated Stress Response. *Mol. Cell* **2010**, *40*, 280-293.

(149) Ren, J. -.; He, W. -.; Nong, L.; Zhu, Q. -.; Hu, K.; Zhang, R. -.; Huang, L. -.; Zhu, F.; Wu, G. Acquired Cisplatin Resistance in Human Lung Adenocarcinoma Cells is Associated with Enhanced Autophagy. *Cancer Biotherapy and Radiopharmaceuticals* **2010**, *25*, 75-80.

(150) Yu, H.; Su, J.; Xu, Y.; Kang, J.; Li, H.; Zhang, L.; Yi, H.; Xiang, X.; Liu, F.; Sun, L. P62/SQSTM1 Involved in Cisplatin Resistance in Human Ovarian Cancer Cells by Clearing Ubiquitinated Proteins. *Eur. J. Cancer* **2011**, *47*, 1585-1594.

(151) Tanida, S.; Mizoshita, T.; Ozeki, K.; Tsukamoto, H.; Kamiya, T.; Kataoka, H.; Sakamuro, D.; Joh, T. Mechanisms of Cisplatin-Induced Apoptosis and of Cisplatin Sensitivity: Potential of BIN1 to Act as a Potent Predictor of Cisplatin Sensitivity in Gastric Cancer Treatment. *International Journal of Surgical Oncology* **2012**, *2012*.

(152) Ge, K.; Duhadaway, J.; Sakamuro, D.; Wechsler-Reya, R.; Reynolds, C.; Prendergast, G. C. Losses of the Tumor Suppressor BIN1 in Breast Carcinoma are Frequent and Reflect Deficits in Programmed Cell Death Capacity. *International Journal of Cancer* **2000**, *85*, 376-383.

(153) Mohammad, R. M.; Banerjee, S.; Li, Y.; Aboukameel, A.; Kucuk, O.; Sarkar, F. H. Cisplatin-Induced Antitumor Activity is Potentiated by the Soy Isoflavone Genistein in BxPC-3 Pancreatic Tumor Xenografts. *Cancer* **2006**, *106*, 1260-1268.

(154) Drottar, M.; Liberman, M. C.; Ratan, R. R.; Roberson, D. W. The Histone Deacetylase Inhibitor Sodium Butyrate Protects Against Cisplatin-Induced Hearing Loss in Guinea Pigs. *Laryngoscope* **2006**, *116*, 292-296.

(155) Splettstoesser, F.; Florea, A. -.; Büsselberg, D. IP 3 Receptor Antagonist, 2-APB, Attenuates Cisplatin Induced Ca 2+-Influx in HeLa-S3 Cells and Prevents Activation of Calpain and Induction of Apoptosis. *Br. J. Pharmacol.* **2007**, *151*, 1176-1186.

(156) Keller, G. A.; Ponte, M. L.; Di Girolamo, G. Other Drugs Acting on Nervous System Associated with QT-Interval Prolongation. *Current Drug Safety* **2010**, *5*, 105-111.

(157) Borch, R. F.; Pleasants, M. E. Inhibition of Cis-Platinum Nephrotoxicity by Diethyldithiocarbamate Rescue in a Rat Model. *Proc. Natl. Acad. Sci. U. S. A.* **1979**, *76*, 6611-6614.

(158) Sadler, P. J.; Guo, Z. Metal Complexes in Medicine: Design and Mechanism of Action. *Pure and Applied Chemistry* **1998**, *70*, 863-871.

(159) Alberts, D. S. Carboplatin Versus Cisplatin in Ovarian Cancer. *Semin. Oncol.* **1995**, *22*, 88-90.

(160) Markman, M.; Reichman, B.; Hakes, T.; Rubin, S.; Lewis Jr., J. L.; Jones, W.; Barakat, R.; Curtin, J.; Almadrones, L.; Hoskins, W. Evidence Supporting the Superiority of Intraperitoneal Cisplatin Compared to Intraperitoneal Carboplatin for Salvage Therapy of Small-Volume Residual Ovarian Cancer. *Gynecol. Oncol.* **1993**, *50*, 100-104.

(161) Legallicier, B.; Leclere, C.; Monteil, C.; Elkaz, V.; Morin, J. P.; Fillastre, J. P. The Cellular Toxicity of Two Antitumoural Agents Derived from Platinum, Cisplatinum Versus Oxaliplatinum, on Cultures of Tubular Proximal Cells. *Drugs Exp. Clin. Res.* **1996**, *22*, 41-50.

(162) Farrell, N. P. Platinum Formulations as Anticancer Drugs Clinical and Pre-Clinical Studies. *Current Topics in Medicinal Chemistry* **2011**, *11*, 2623-2631.

(163) Anderson, H.; Wagstaff, J.; Crowther, D.; Swindell, R.; Lind, M. J.; McGregor, J.; Timms, M. S.; Brown, D.; Palmer, P. Comparative Toxicity of Cisplatin, Carboplatin (CBDCA) and Iproplatin (CHIP) in Combination with Cyclophosphamide in Patients with Advanced Epithelial Ovarian Cancer. *European Journal of Cancer and Clinical Oncology* **1988**, *24*, 1471-1479.

(164) Kelland, L. R.; Murrer, B. A.; Abel, G.; Giandomenico, C. M.; Mistry, P.; Harrap, K. R. Ammine/Amine Platinum(IV) Dicarboxylates: A Novel Class of Platinum Complex Exhibiting Selective Cytotoxicity to Intrinsically Cisplatin- Resistant Human Ovarian Carcinoma Cell Lines. *Cancer Res.* **1992**, *52*, 822-828.

(165) Kean, W. F.; Forestier, F.; Kassam, Y.; Buchanan, W. W.; Rooney, P. J. The History of Gold Therapy in Rheumatoid Disease. *Semin. Arthritis Rheum.* **1985**, *14*, 180-186.

(166) Mazid, M. A.; Razi, M. T.; Sadler, P. J.; Greaves, G. N.; Gurman, S. J.; Koch, M. H. J.; Phillips, J. C. An EXAFS Study of Gold Co-Ordination in the Anti-Arthritic Drugs Myocrisin and Solganol. *Journal of the Chemical Society, Chemical Communications* **1980**, 1261-1263.

(167) Elder, R. C.; Ludwig, K.; Cooper, J. N.; Eidsness, M. K. EXAFS and WAXS Structure Determination for an Antiarthritic Drug, Sodium Gold(I) Thiomalate. *J. Am. Chem. Soc.* **1985**, *107*, 5024-5025.

(168) Best, S. L.; Sadler, P. J. Gold Drugs: Mechanism of Action and Toxicity. *Gold Bulletin* **1996**, *29*, 87-93.

(169) Cottrill, S. M.; Sharma, H. L.; Dyson, D. B.; Parish, R. V.; McAuliffe, C. A. The Role of the Ligand in Chrysotherapy: A Kinetic Study of 199Au- and 35S-Labelled Myocrisin and Auranofin. *Journal of the Chemical Society, Perkin Transactions 2* **1989**, 53-58.

(170) Tiekink, E. R. T. Gold Derivatives for the Treatment of Cancer. *Crit. Rev. Oncol.* **2002**, *42*, 225-248.

(171) Mirabelli, C. K.; Johnson, R. K.; Sung, C. M.; Faucette, L.; Muirhead, K.; Crooke, S. T. Evaluation of the in Vivo Antitumor Activity and in Vitro Cytotoxic Properties of Auranofin, a Coordinated Gold Compound, in Murine Tumor Models. *Cancer Res.* **1985**, *45*, 32-39.

(172) Ward, J. R. Role of Disease-Modifying Antirheumatic Drugs Versus Cytotoxic Agents in the Therapy of Rheumatoid Arthritis. *Am. J. Med.* **1988**, *85*, 39-44.

(173) Parish, R. V.; Mack, J.; Hargreaves, L.; Wright, J. P.; Buckley, R. G.; Elsome, A. M.; Fricker, S. P.; Theobald, B. R. C. Chemical and Biological Reactions of Diacetato[2-(Dimethylaminoniethyl)-Phenyl]Gold(III), [Au(O 2CMe) 2(Dmamp)]. *Journal of the Chemical Society - Dalton Transactions* **1996**, 69-74.

(174) Parish, R. V.; Howe, B. P.; Wright, J. P.; Mack, J.; Pritchard, R. G.; Buckley, R. G.; Elsome, A. M.; Fricker, S. P. Chemical and Biological Studies of Dichloro(2-((Dimethylamino)Methyl)Phenyl)Gold(III). *Inorg. Chem.* **1996**, *35*, 1659-1666.

(175) Che, C. -.; Sun, R. W. -.; Yu, W. -.; Ko, C. -.; Zhu, N.; Sun, H. Gold(III) Porphyrins as a New Class of Anticancer Drugs: Cytotoxicity, DNA Binding and Induction of Apoptosis in Human Cervix Epitheloid Cancer Cells. *Chemical Communications* **2003**, *9*, 1718-1719.

(176) Messori, L.; Abbate, F.; Marcon, G.; Orioli, P.; Fontani, M.; Mini, E.; Mazzei, T.; Carotti, S.; O'Connell, T.; Zanello, P. Gold(III) Complexes as Potential Antitumor Agents: Solution Chemistry and Cytotoxic Properties of some Selected Gold(III) Compounds. *J. Med. Chem.* **2000**, *43*, 3541-3548.

(177) Marcon, G.; Carotti, S.; Coronnello, M.; Messori, L.; Mini, E.; Orioli, P.; Mazzei, T.; Cinellu, M. A.; Minghetti, G. Gold(III) Complexes with Bipyridyl Ligands: Solution Chemistry, Cytotoxicity, and DNA Binding Properties. *J. Med. Chem.* **2002**, *45*, 1672-1677.

(178) Abbate, F.; Orioli, P.; Bruni, B.; Marcon, G.; Messori, L. Crystal Structure and Solution Chemistry of the Cytotoxic Complex 1,2-Dichloro(O-Phenanthroline)Gold(III) Chloride. *Inorg. Chim. Acta* **2000**, *311*, 1-5.

(179) Coronnello, M.; Mini, E.; Caciagli, B.; Cinellu, M. A.; Bindoli, A.; Gabbiani, C.; Messori, L. Mechanisms of Cytotoxicity of Selected Organogold(III) Compounds. *J. Med. Chem.* **2005**, *48*, 6761-6765.

(180) Casini, A.; Cinellu, M. A.; Minghetti, G.; Gabbiani, C.; Coronnello, M.; Mini, E.; Messori, L. Structural and Solution Chemistry, Antiproliferative Effects, and DNA and Protein Binding Properties of a Series of Dinuclear Gold(III) Compounds with Bipyridyl Ligands. *J. Med. Chem.* **2006**, *49*, 5524-5531.

(181) Casini, A.; Kelter, G.; Gabbiani, C.; Cinellu, M. A.; Minghetti, G.; Fregona, D.; Fiebig, H. -.; Messori, L. Chemistry, Antiproliferative Properties, Tumor Selectivity, and Molecular Mechanisms of Novel Gold(III) Compounds for Cancer Treatment: A Systematic Study. *Journal of Biological Inorganic Chemistry* **2009**, *14*, 1139-1149.

(182) Márta, E.; Ronconi, L.; Nardon, C.; Fregona, D. Noble Metal-Dithiocarbamates Precious Allies in the Fight Against Cancer. *Mini-Reviews in Medicinal Chemistry* **2012**, *12*, 1216-1229.

(183) Nagy, E. M.; Nardon, C.; Giovagnini, L.; Marchiò, L.; Trevisan, A.; Fregona, D. Promising Anticancer Mono- and Dinuclear Ruthenium(Iii) Dithiocarbamato Complexes: Systematic Solution Studies. *Dalton Transactions* **2011**, *40*, 11885-11895.

(184) Pabla, N.; Dong, Z. Cisplatin Nephrotoxicity: Mechanisms and Renoprotective Strategies. *Kidney Int.* **2008**, *73*, 994-1007.

(185) Appleton, T. G.; Connor, J. W.; Hall, J. R.; Prenzler, P. D. NMR Study of the Reactions of the Cis-Diamminediaquaplatinum(II) Cation with Glutathione and Amino Acids Containing a Thiol Group. *Inorg. Chem.* **1989**, *28*, 2030-2037.

(186) Andrews, P. A.; Howell, S. B. Cellular Pharmacology of Cisplatin: Perspectives on Mechanisms of Acquired Resistance. *Cancer Cells* **1990**, *2*, 35-43.

(187) Wang, X.; Guo, Z. Towards the Rational Design of Platinum(II) and Gold(III) Complexes as Antitumour Agents. *Dalton Transactions* **2008**, 1521-1532.

(188) Dorr, R. T.; Lagel, K. Interaction between Cisplatin and Mesna in Mice. *J. Cancer Res. Clin. Oncol.* **1989**, *115*, 604-605.

(189) Goel, R.; Cleary, S. M.; Horton, C.; Kirmani, S.; Abramson, I.; Kelly, C.; Howell, S. B. Effect of Sodium Thiosulfate on the Pharmacokinetics and Toxicity of Cisplatin. *J. Natl. Cancer Inst.* **1989**, *81*, 1552-1560.

(190) Lerza, R.; Bogliolo, G.; Muzzulini, C.; Pannacciulli, I. Failure of N-Acetylcysteine to Protect Against Cis-Dichlorodiammineplatinum(II)-Induced Hematopoietic Toxicity in Mice. *Life Sci.* **1986**, *38*, 1795-1800.

(191) Hamers, F. P. T.; Brakkee, J. H.; Cavalletti, E.; Tedeschi, M.; Marmonti, L.; Pezzoni, G.; Neijt, J. P.; Gispen, W. H. Reduced Glutathione Protects Against Cisplatin-Induced Neurotoxicity in Rats. *Cancer Res.* **1993**, *53*, 544-549.

(192) Stewart, D. J.; Verma, S.; Maroun, J. A. Phase I Study of the Combination of Disulfiram with Cisplatin. *American Journal of Clinical Oncology: Cancer Clinical Trials* **1987**, *10*, 517-519.

(193) Segovia, N.; Crovetto, G.; Lardelli, P.; Espigares, M. In Vitro Toxicity of several Dithiocarbamates and Structure - Activity Relationships. *Journal of Applied Toxicology* **2002**, *22*, 353-357.

(194) Ronconi, L.; Fregona, D. The Midas Touch in Cancer Chemotherapy: From Platinum- to Gold-Dithiocarbamato Complexes. *Dalton Transactions* **2009**, 10670-10680.

(195) Ronconi, L.; MacCato, C.; Barreca, D.; Saini, R.; Zancato, M.; Fregona, D. Gold(III) Dithiocarbamate Derivatives of N-Methylglycine: An Experimental and Theoretical Investigation. *Polyhedron* **2005**, *24*, 521-531.

(196) Koelle, U.; Laguna, A. Electrochemistry of Au-Complexes. *Inorg. Chim. Acta* **1999**, *290*, 44-50.

(197) Giovagnini, L.; Ronconi, L.; Aldinucci, D.; Lorenzon, D.; Sitran, S.; Fregona, D. Synthesis, Characterization, and Comparative in Vitro Cytotoxicity Studies of Platinum(II), Palladium(II), and Gold(III) Methylsarcosinedithiocarbamate Complexes. *J. Med. Chem.* **2005**, *48*, 1588-1595.

(198) Aldinucci, D.; Lorenzon, D.; Stefani, L.; Giovagnini, L.; Colombatti, A.; Fregona, D. Antiproliferative and Apoptotic Effects of Two New Gold(III) Methylsarcosinedithiocarbamate Derivatives on Human Acute Myeloid Leukemia Cells in Vitro. *Anticancer Drugs* **2007**, *18*, 323-332.

(199) Aldinucci, D.; Cattaruzza, L.; Lorenzon, D.; Giovagnini, L.; Fregona, D.; Colombatti, A. Antiproliferative and Apoptotic Effects of Two New Pd(II) Methylsarcosinedithiocarbamate Derivatives on Human Acute Myeloid Leukemia Cells in Vitro. *Oncol. Res.* **2008**, *17*, 103-113.

(200) Ronconi, L.; Giovagnini, L.; Marzano, C.; Bettìo, F.; Graziani, R.; Pilloni, G.; Fregona, D. Gold Dithiocarbamate Derivatives as Potential Antineoplastic Agents: Design, Spectroscopic Properties, and in Vitro Antitumor Activity. *Inorg. Chem.* **2005**, *44*, 1867-1881.

(201) Kostova, I. Gold Coordination Complexes as Anticancer Agents. *Anti-Cancer Agents in Medicinal Chemistry* **2006**, *6*, 19-32.

(202) Milacic, V.; Chen, D.; Ronconi, L.; Landis-Piwowar, K. R.; Fregona, D.; Dou, Q. P. A Novel Anticancer Gold(III) Dithiocarbamate Compound Inhibits the Activity of a Purified 20S Proteasome and 26S Proteasome in Human Breast Cancer Cell Cultures and Xenografts. *Cancer Res.* **2006**, *66*, 10478-10486.

(203) Cattaruzza, L.; Fregona, D.; Mongiat, M.; Ronconi, L.; Fassina, A.; Colombatti, A.; Aldinucci, D. Antitumor Activity of Gold(III)-Dithiocarbamato Derivatives on Prostate Cancer Cells and Xenografts. *International Journal of Cancer* **2011**, *128*, 206-215.

(204) Marzano, C.; Ronconi, L.; Chiara, F.; Giron, M. C.; Faustinelli, I.; Cristofori, P.; Trevisan, A.; Fregona, D. Gold(III)-Dithiocarbamato Anticancer Agents: Activity, Toxicology and Histopathological Studies in Rodents. *Int. J. Cancer* **2011**, *129*, 487-496.

(205) Sereemaspun, A.; Rojanathanes, R.; Wiwanitkit, V. Effect of Gold Nanoparticle on Renal Cell: An Implication for Exposure Risk. *Ren. Fail.* **2008**, *30*, 323-325.

(206) Negom Kouodom, M.; Ronconi, L.; Celegato, M.; Nardon, C.; Marchiò, L.; Dou, Q. P.; Aldinucci, D.; Formaggio, F.; Fregona, D. Toward the Selective Delivery of Chemotherapeutics into Tumor Cells by Targeting Peptide Transporters: Tailored Gold-Based Anticancer Peptidomimetics. *J. Med. Chem.* **2012**, *55*, 2212-2226.

(207) Brandsch, M. Transport of Drugs by Proton-Coupled Peptide Transporters: Pearls and Pitfalls. *Expert Opin. Drug Metab. Toxicol.* **2009**, *5*, 887-905.

(208) Kouodom, M. N.; Boscutti, G.; Celegato, M.; Crisma, M.; Sitran, S.; Aldinucci, D.; Formaggio, F.; Ronconi, L.; Fregona, D. Rational Design of Gold(III)-Dithiocarbamato Peptidomimetics for the Targeted Anticancer Chemotherapy. *J. Inorg. Biochem.* **2012**.

(209) Gregoriadis, G. C.; Apostolidis, N. S.; Romanos, A. N.; Paradellis, T. P. A Comparative Study of Trace Elements in Normal and Cancerous Colorectal Tissues. *Cancer* **1983**, *52*, 508-519.

(210) Coates, R. J.; Weiss, N. S.; Daling, J. R.; Rettmer, R. L.; Warnick, G. R. Cancer Risk in Relation to Serum Copper Levels. *Cancer Res.* **1989**, *49*, 4353-4356.

(211) Apelgot, S.; Coppey, J.; Fromentin, A.; Guille, E.; Poupon, M. F.; Roussel, A. Altered Distribution of Copper (64Cu) in Tumor-Bearing Mice and Rats. *Anticancer Res.* **1986**, *6*, 159-164.

(212) Gupta, S. K.; Shukla, V. K.; Vaidya, M. P.; Roy, S. K.; Gupta, S. Serum Trace Elements and Cu/Zn Ratio in Breast Cancer Patients. *J. Surg. Oncol.* **1991**, *46*, 178-181.

(213) Lowndes, S. A.; Harris, A. L. Copper Chelation as an Antiangiogenic Therapy. *Oncol. Res.* **2004**, *14*, 529-539.

(214) Hu, G. -. Copper Stimulates Proliferation of Human Endothelial Cells Under Culture. *J. Cell. Biochem.* **1998**, *69*, 326-335.

(215) Fox, S. B.; Gasparini, G.; Harris, A. L. Angiogenesis: Pathological, Prognostic, and Growth-Factor Pathways and their Link to Trial Design and Anticancer Drugs. *Lancet Oncology* **2001**, *2*, 278-289.

(216) Giovagnini, L.; Sitran, S.; Montopoli, M.; Caparrotta, L.; Corsini, M.; Rosani, C.; Zanello, P.; Dou, Q. P.; Fregona, D. Chemical and Biological Profiles of Novel Copper(II) Complexes Containing S-Donor Ligands for the Treatment of Cancer. *Inorg. Chem.* **2008**, *47*, 6336-6343.

(217) Parodi, F. E.; Mao, D.; Ennis, T. L.; Bartoli, M. A.; Thompson, R. W. Suppression of Experimental Abdominal Aortic Aneurysms in Mice by Treatment with Pyrrolidine Dithiocarbamate, an Antioxidant Inhibitor of Nuclear Factor-κB. *Journal of Vascular Surgery* **2005**, *41*, 479-489.

Aim of the work

The dream of delivering drugs in a highly selective way to the tumor only, is still not a reality, but we are getting closer with new systems of drug targeting.

Adapted from J. Cassidy

Cancer represents a tremendous burden for patients, families and the whole society in terms of both human and financial costs. New potent selective therapies are required to prevent damage to normal cells and hence reduce the occurrence of severe side effects. As previously discussed, cancerous cells overexpress some membrane proteins, such as transporters and receptors, that can be specifically targeted by cytotoxic agents.

In order to obtain targeted anticancer drugs, we have functionalized some biological ligands – recognized by human up-regulated transporters or receptors – with sulfur donor atoms, yielding bidentate chelating moieties (i.e., dithiocarbamato functional group) able to coordinate a metal center. Dithiocarbamates make the corresponding metal complexes reasonably stable under physiological conditions and in addition, play a chemoprotecting function toward normal cells, thus preventing adverse side effects such as nephrotoxicity.[1] Therefore, combining the targeting and chemoprotecting action of a properly functionalized bio-ligand with the anticancer activity of a metal center allows to selectively transport a cytotoxic cargo (in our case a transition metal), acting as a smart bullet, into the tumor site.

In the present work, many dithiocarbamato complexes have been studied involving two transition metals and different biological ligands. For clarity purposes, this PhD thesis has been divided in two distinct sections relevant to the metals used in the present work, namely gold (*Section 1*) and copper (*Section 2*). The first section has been split in turn into three parts on the basis of the ligand type present in the various Au(III) dithiocarbamato derivatives.

Part I reports on advanced preclinical studies aimed at evaluating the pharmacodynamic, toxicological and pharmacokinetic profiles of two Au(III) peptidomimetics of the type [$Au^{III}Br_2$(dtc-Sar-AA-O(*t*-Bu))] with AA = Gly (AuD6) or Aib (AuD8). These dipeptido derivatives were designed as carrier-mediated delivery systems exploiting the peptide transporters PEPT1 and PEPT2, which are able to mediate the cellular

uptake of di- and tripeptides. [2] Their peculiar feature is that they can transport inside the cell all possible di- and tripeptides containing *L*-enantiomers, regardless of their amino acidic sequence, size, hydrophobicity and charge. These transporters seem to be up-regulated in some cancer types such as bladder, prostate, gastric, bile duct, pancreas, intestinal and renal cancers, osteosarcoma and fibrosarcoma.[3-7] AuD6 and AuD8 were first synthesized (in a stepwise process) and characterized in a previous PhD work.[8] Subsequently, the yields of some syntheses and purification steps have been increased, and AuD8 crystal structure has been solved.[8] For clarity reasons, the synthesis conditions and characterization of both dipeptido compounds are herein briefly reported along with the solved crystal structure (***Chapter 1***).

Overall, the biological studies were planned considering those required for entering phase I clinical trials and were performed (during a 6-month stay as a visiting PhD student) at the *Barbara Ann Karmanos Cancer Institute*, Department of Oncology, School of Medicine, Wayne State University, Detroit, U.S.A. in collaboration with Prof. Q. Ping Dou. In detail, we report here on anticancer activity (both *in vitro* and *in vivo*) of the compounds AuD6 and AuD8 on the triple-negative human breast cancer cell line MDA-MB-231. These cells were chosen as are highly metastatic, invasive and resistant to the antineoplastic drug cisplatin. Concerning mechanism of action, the proteasome has been identified as a major target both *in vitro* and *in vivo* (***Chapter 2***). The proteasome is an ATP-dependent protease and plays a key role in nuclear and cytoplasmic homeostasis by degrading different proteins such as abnormal and misfolded proteins, transcriptional factors and cyclins.[9, 10] Proteasome inhibition is a recent, very promising strategy to treat cancers and, in 2003, the first proteasome inhibitor, bortezomib (Velcade®), was approved for clinical use.[11] Encouragingly, our compounds exhibited potent proteasome-inhibitory activity, associated with induction of cell death *via* apoptosis both *in vitro* and *in vivo*. In order to gain insight, at the atomic level, into the proteasome mechanism of inhibition by our gold(III) derivatives, we addressed our attention on crystallizable cytoplasmic proteasomes. This part of the work was performed in collaboration with the Structural Biology research group directed by Prof. Giuseppe Zanotti (Dept. of Biomedical Sciences, University of Padova). Since human and *Saccharomyces Cerevisiae* 20S proteasomes are characterized by the same phylogenetic origin and therefore by similar amino acid sequences and structures, we have exploited yeast cultures to obtain the pure target protein. From the biotechnological point of view, the eukaryotic cells of baker's yeast are easily obtainable in huge amounts, from which it is

possible to yield active 20S proteasome by properly performed extraction and subsequent purification. Moreover, *Saccharomyces Cerevisiae* is an organism suitable for the production of *ad-hoc* strains able to yield specific tagged forms of 20S proteasome by means of combined biochemical and genetic approaches. With respect to the gold(III) complexes, AuD8 was chosen as a model compound for the crystallization attempts trying several inhibition conditions. Furthermore, the crystallization trials were carried out by both crystal soaking (diffusion of the inhibitor through the crystal) and co-crystallization approach. Plenty of crystallization tests were performed but all turned out to be unfruitful so far, thus the mechanism of inhibition of the enzyme has not been elucidated yet (***Chapter 3***).

Afterwards, we addressed our attention on the pharmacokinetic profile, investigating if an interaction may begin between AuD8 and serum albumin as the latter is the most abundant plasma protein and it is a well-known carrier of drugs and endogenous substances such as vitamins and lipids. In these studies, carried out by circular dichroism and fluorescence spectrophotometry, the human serum albumin was substituted with the bovine analogue since they have a wide sequence homology and therefore a very similar structure (***Chapter 4***).

It is worth highlighting that the mice bearing human breast cancer MDA-MB-231 xenografts appeared healthy and very active throughout the AuD6/AuD8 treatment at 1.0 mg kg^{-1} d^{-1} s.c. and did not display signs of fatigue, weight loss or anorexia, thus ruling out the onset of systemic toxicity (*§ Chapter 2*). To further confirm the good chemotherapeutic index of our compounds, due to both a very negligible toxicity and a promising antiproliferative activity, we performed an investigation of acute toxicity of the model compound AuD8 in healthy mice in compliance with the Good Laboratory Practice (GLP) regulations, upon intravenous and *per os* administrations of a single dose to female and male mice at three different dosages for each administration way. The corresponding administration vehicles were defined following stability studies of AuD8 in different media, carried out by various analytical techniques such as UV-Vis spectrophotometry (***Chapter 5***).

Part II is relevant to receptor-mediated strategies and focuses on the cholecystokinin (CCK) receptors which belong to the G-protein-coupled receptor superfamily and are overexpressed in many neoplasms. We discuss here the peptide CCK8 – a receptor-recognized biological ligand whose cell uptake is higher in some cancers – and its functionalization with the metal center Au(III). The related design, stepwise synthesis and characterization have been reported along with some stability studies of a model compound

under acidic and basic conditions.

In the ***Part III*** of this thesis we describe the "click chemistry" strategy and, in particular, the Huisgen 1,3-dipolar cycloaddition reaction of azides and alkynes, yielding 1,2,3-triazoles as linking moieties. We designed a versatile gold(III) building block, namely Au(III) dithiocarbamato complex of 11-Azido-3,6,9-trioxaundecan-1-amine (AuCAD), which can be bioconjugated ideally to any peptide recognizable by up-regulated receptors in the malignant tissues. We report here on the synthesis and characterization of AuCAD, and the "click" reaction of such fragment with a tetrapeptide, used as a model, functionalized with an alkyne group. An international patent application will be shortly filed with respect to this innovative strategy.

The encouraging chemical and biological results so far obtained with the gold-based complexes, involving ligands recognized by overexpressed transporters or receptors, prompted us to move one step forward. Therefore, we have taken into account an endogenous transition metal, *viz.* Cu(II), due to its interesting biochemical properties. It is worth highlighting that copper plays a significant role in angiogenesis (i.e., the formation of new blood vessels from pre-existing ones) and, hence, is more abundant in cancer cells than in healthy ones, leading to a selectivity of copper-based anticancer agents toward neoplastic tissues. In the present work, two different classes of Cu(II) dithiocarbamato complexes were designed to gain insights into structure-activity relationship**s** and to get the know-how with respect to the chemical behavior of this metal in terms of reaction conditions and stability in different solvents. The first group of complexes comprises compounds with a 1:2 metal to ligand stoichiometry whereas the second category (which closely resemble the chemical features of cisplatin and its analogues) was obtained employing methylated dithiocarbamates, leading to a final 1:1 metal to ligand ratio. Their synthesis, wide chemical characterization and preliminary biological data are herein reported (***Section 2***). Overall, these findings will be useful for the development of copper-based receptor compounds, which are more difficult to obtain due to the borderline Lewis acid character of Cu(II) (according to Pearson's hard soft acid base – HSAB – principle).

---

(1) Ronconi, L.; Fregona, D. The Midas Touch in Cancer Chemotherapy: From Platinum- to Gold-Dithiocarbamato Complexes. *Dalton Transactions* **2009**, 10670-10680.

(2) Brandsch, M. Transport of Drugs by Proton-Coupled Peptide Transporters: Pearls and Pitfalls. *Expert Opin. Drug Metab. Toxicol.* **2009**, *5*, 887-905.

(3) Mitsuoka, K.; Miyoshi, S.; Kato, Y.; Murakami, Y.; Utsumi, R.; Kubo, Y.; Noda, A.; Nakamura, Y.; Nishimura, S.; Tsuji, A. Cancer Detection using a PET Tracer, 11C-Glycylsarcosine, Targeted to H +/Peptide Transporter. *Journal of Nuclear Medicine* **2008**, *49*, 615-622.

(4) Inoue, M.; Terada, T.; Okuda, M.; Inui, K. -. Regulation of Human Peptide Transporter 1 (PEPT1) in Gastric Cancer Cells by Anticancer Drugs. *Cancer Lett.* **2005**, *230*, 72-80.

(5) Knütter, I.; Rubio-Aliaga, I.; Boll, M.; Hause, G.; Daniel, H.; Neubert, K.; Brandsch, M. H+-Peptide Cotransport in the Human Bile Duct Epithelium Cell Line SK-ChA-1. *American Journal of Physiology - Gastrointestinal and Liver Physiology* **2002**, *283*, G222-G229.

(6) Gonzalez, D. E.; Covitz, K. -. Y.; Sadée, W.; Mrsny, R. J. An Oligopeptide Transporter is Expressed at High Levels in the Pancreatic Carcinoma Cell Lines AsPc-1 and Capan-2. *Cancer Res.* **1998**, *58*, 519-525.

(7) Nakanishi, T.; Tamai, I.; Takaki, A.; Tsuji, A. Cancer Cell-Targeted Drug Delivery Utilizing Oligopeptide Transport Activity. *International Journal of Cancer* **2000**, *88*, 274-280.

(8) Negom Kouodom, M.; Ronconi, L.; Celegato, M.; Nardon, C.; Marchiò, L.; Dou, Q. P.; Aldinucci, D.; Formaggio, F.; Fregona, D. Toward the Selective Delivery of Chemotherapeutics into Tumor Cells by Targeting Peptide Transporters: Tailored Gold-Based Anticancer Peptidomimetics. *J. Med. Chem.* **2012**, *55*, 2212-2226.

(9) Tanaka, K. The Proteasome: Overview of Structure and Functions. *Proc. Jpn. Acad. Ser. B Phys. Biol. Sci.* **2009**, *85*, 12-36.

(10) Groll, M.; Ditzel, L.; Löwe, J.; Stock, D.; Bochtler, M.; Bartunik, H. D.; Huber, R. Structure of 20S Proteasome from Yeast at 2.4 Å Resolution. *Nature* **1997**, *386*, 463-471.

(11) Dalla Via, L.; Nardon, C.; Fregona, D. Targeting the Ubiquitin-Proteasome Pathway with Inorganic Compounds to Fight Cancer: A Challenge for the Future. *Future Medicinal Chemistry* **2012**, *4*, 525-543.

Materials and methods

Chemicals and solvents used

Acetic acid, 1-butanol, chloroform, dichloromethane, diethyl ether, ethanol, ethyl acetate, hydrochloric acid (37% aqueous solution), methanol, petroleum ether (boiling range 40-60°C), sodium hydrogenocarbonate, potassium hydrogenosulphate, sodium hydroxyde, sodium sulphate anhydrous, sulphuric acid (98% aqueous solution), methyl iodide, toluene, triethylamine (*Carlo Erba*), isobutyl chloroformate (*Lancaster*), *iso*butene (*Siad*), *N*-benzyloxycarbonyl-oxysuccinimide (*Iris Biotech*), Ringer Lactate (*Eurospital*), potassium tetrabromoaurate(III) dihydrate (*Alfa Aesar*), phosphoric anhydride (*Acros-Janssen*), DMSO, DMSO-d_6, acetone-d_6, carbon disulfide, methylethanolamine, diethanolamine,sodium *N*,*N*-dimethyldithiocarbamate, ammonium pyrrolidine dithiocarbamate, trifluoroacetic acid, copper(II) acetate dihydrate, *n*-pentane, acetone, piperidine (*Aldrich*), palladium catalyst (10% on activated charcoal), tetrahydrofurane, acetonitrile, ethanol, *N*-methylmorpholine and sarcosine, Phosphate Buffer Saline (PBS), Bovine Serum Albumin (BSA) (*Fluka*, Switzerland), Fmoc-protected amino acid derivatives, coupling reagents, and Rink amide *p*-methylbenzhydrylamine (MBHA) resin were purchased from Calbiochem-Novabiochem (*Laufelfingen*) and copper(II) chloride dihydrate (*J.T. Baker chemicals*) were of high purity and were used as supplied without any further purification.

N^{α}-Benzyloxycarbonylglycyltert-butyl ester (Z-Gly-OtBu) and N^{α}-benzyloxycarbonyl-α-aminoisobutyric acid were available in the laboratory. All chiral amino acids have configuration *L*.

In reactions occurring in aqueous medium, departmental deionized water has been employed.

Instrumentation

Elemental analysis

Elemental analyses were carried out at the microanalysis lab. (Chemistry Dept., University of Padova) by a Carlo Erba 1108 CHNS-O microanalyzer.

FT-IR spectroscopy

Infrared spectra have been recorded at room temperature in N_2 atmosphere, in solid KBr by a spectrophotometer *Nicolet Nexus 5SXC* (32 scansions, 2 cm^{-1} resolution) in the range 4000-400 cm^{-1}, and in nujol between two polyethylene tablets on a spectrophotometer *Nicolet Nexus 870* (200 scansions, 4 cm^{-1} resolution) in the range 600-50 cm^{-1}. Data processing was carried out using OMNIC version 5.1 (Nicolet Instrument Corporation).

UV-Vis spectroscopy

Electronic spectra were acquired at 25°C and 37°C in different ranges (usually 190 ÷ 600 nm) with an Agilent Cary 100 UV-Vis double been spectrophotometer (1 cm optical path, quartz cuvettes), using fresh solutions of the samples in the appropriate solvent.
When performing kinetic studies, the complete dissolution of the complex was considering as initial time (time 0). Regarding the studies carried out in water, RL, saline solution and PBS, the measurements were corrected for the absorption of organic solvent using the aqueous solution as a blank with the exact added amount of DMSO for each sample.

Circular Dichroism

Circular Dichroism measurements were recorded on a spectropolarimeter J-715 at room temperature employing a 0.1 mm optical path cell for the range 193 ÷ 260 nm while a 1 mm optical path cell for the range 240 ÷ 350 nm. The measurements were corrected for the absorption of organic solvent using the phosphate buffered saline as a blank with the exact added amount of dimethyl sulfoxide for each sample.

Fluorescence

Emission spectra were acquired at room temperature by a Perkin Elmer LS50B Luminescence Spectrometer (1 cm optical path, quartz cuvettes) with λ_{exc}= 288 nm and $\Delta\lambda_{emi}$= 300 ÷ 400 nm.

NMR spectroscopy

All ^{1}H-NMR and ^{13}C-NMR monodimensional spectra were acquired in the proper deuterated solvent at 298 K on a Bruker Avance DRX300 spectrophotometer equipped with a BBI [^{1}H, X] probe-head, an Hewlett Packard Vecta. Bidimensional NMR spectra were registered in DMSO-d6 at 298 K (unless otherwise stated) on a Bruker Avance DRX400 spectrophotometer equipped with with a BBI-5 mm z-field gradient probe-head, and a Silicon Graphics O2 workstation, operating in Fourier transform.

Typical acquisition parameters for 1D ^{1}H NMR spectra (^{1}H: 300.13 MHz): 32 transients, spectral width 12 kHz, using 32 k data points and a delay time of 5.0 s. Typical acquisition parameters for 2D [^{1}H,^{13}C] HMBC NMR spectra (^{1}H: 300.13/^{13}C: 75.48 MHz): 512 transients of 32 scans/block, spectral width 7.5/18.8 kHz, 2k/2k data points and a delay time of 2.0 s. Sequences were optimized for $^{1}J(^{13}C,^{1}H)$ = 145 Hz/$^{n}J(^{13}C,^{1}H)$ = 5 Hz with no ^{1}H decoupling. Spectra were processed by using sine-square weighting with a resolution of 1.0/3.0 Hz and a line-broadening threshold of 0.3/1.0 Hz. Data processing was carried out by means of MestReNova version 6.2.0 (Mestrelab Research S.L.). Chemical shifts were referenced to external tetramethylsilane (TMS). Peak multiplicity is described as follows: s (singlet), br s (broad singlet), d (doublet), t (triplet), m (multiplet).

ESI-MS analysis

ESI-MS spectra were recorded on a Mariner Perspective Biosystem instrument, setting a 5kV ionization potential and a 20 μL/min flow rate. A mixture of coumarin and 6-methyl-triptophan was used as a standard. Samples were dissolved in methanol, while methanol with 1% formic acid was used as eluent. ESI-MS spectra have been processed by the software *Data Explorer*.

LC-MS analysis

Purity and identity were assessed using a Finnigan Surveyor MSQ single quadrupole electrospray ionization (Finnigan/Thermo Electron Corpo-ration San Jose, CA) equipped with a C18 Phenomenex column.

HPLC purification

The crude products were purified by RP-HPLC on a LC8 Shimadzu HPLC system (Shimadzu Corporation, Kyoto, Japan) equipped with a UV lambda-Max Model 481 detector using a Phenomenex (Torrance, CA) C18 (300 Å, 250x 21.20 mm, 5 μ) column.

Thermogravimetric analysis

Thermogravimetric (TG) and differential scanning calorimetry (DSC) curves were recorded with a TA Instruments thermobalance equipped with a DSC 2929 calorimeter. Measurements were carried out in the range 25-1000°C in alumina crucibles under air (flux rate 30 cm^3 min^{-1}) at a heating rate of 5°C min^{-1}, using alumina as reference.

X-Ray diffraction

Single crystal data were collected with a Bruker Smart APEXII area detector diffractometer, Mo Kα: λ = 0.71073 Å. The unit cell parameters were obtained using 60 ω-frames of 0.5° width and scanned from three different zone of reciprocal lattice. The intensity data were integrated from several series of exposures frames (0.3° width) covering the sphere of reciprocal space. An absorption correction was applied using the program SADAB. The structures were solved by direct methods (SIR2004) and refined on F2 with full-matrix least squares (SHELXL-97), using the Wingx software package. Non hydrogen atoms were refined anisotropically for all compounds and the hydrogen atoms were placed at their calculated positions. Graphical material was prepared with the ORTEP3 for Windows.
One of the hydroxyl groups of complex CuC5 was statically disordered in two positions that were refined with site occupancy factors of 0.5 each.

Biological evaluation of Copper complexes

Materials

PBS (Phosphate buffered saline): NaCl 0.1 M (*Merk*), KCl 0.002 M (*Sigma*), $Na_2HPO_4 \cdot 2H_2O$ 0.008 M (*Sigma*), KH_2PO_4 0.0015 M (*Panreac*) at pH 7.0;
Trypan Blue: 1% w/v in PBS buffer;
Trypsin-EDTA: Trypsin 10mM (*Sigma*), EDTA 0.3 mM (*Sigma*) in PBS buffer.

Physiological solution: NaCl 0.9% w/v (Merck) in H_2O milliQ.

Cell culture

Antiproliferative activity studies were carried out on human cervix adenocarcinoma cells (HeLa cell line) grown in monolayer in the presence of sterilized Nutrient Mixture F-12 [HAM] (N6760, *Sigma*) supplemented with 10% heat-inactivated fetal bovine serum (*Seromed*). Penicillin, streptomycin and amphotericin B (A5955, *Sigma*) were added to the medium to reach the final concentration of 100 U/mL, 100 µg/mL and 0.25 µg/mL, respectively. The cells were cultured at 37°C in a moist atmosphere of 5% carbon dioxide in air. Laminar flow hood ICN faster (Ultrafase 48) was used for culture manipulation.

Section 1
Au(III) dithiocarbamato derivatives

Part I
Gold(III) peptidomimetics

Chapter 1. Design, synthesis and characterization of gold(III) peptidomimetics

1.1.Chemistry of Gold

Gold is not particularly difficult to recover from minerals. Panning is among the oldest and simplest techniques in the history of recovering metals from natural deposits, and gold is easy to purify.[1] The physical characteristics of the metal, such as its crystal structure (cubic close packed) and the ductility associated with it, its melting point (1064°C) or its density (specific gravity 19.32 $g \cdot cm^{-3}$), are not really unusual, nor is its conduction of heat and electricity, which is easily matched by, for example, silver. The yellow color of gold is perhaps more of an exception given the bright silvery appearance of many other metals, but there are several with even deeper color (such as copper), and this is even more true if alloys, for example common brass, are included.

It thus appears that it is the chemistry of gold that makes this element an extreme case.[2, 3] The "noble" character of gold means that it does not combine or mix with other elements even after long exposure to extremely aggressive conditions, or at least only very reluctantly.

Most applications of gold and its compounds until the early 1980s[3b] made use of the inertness of gold metal to give lasting protection of materials against degradation by chemicals or light (for example, astronauts' gold mirrored visors or non-corrodible electrical conductors at very small dimensions). The durability and ductility of the metal allowed the production of extremely thin films (gold foil, gold leaf) and wires for such purposes by simple mechanical procedures, but deposition techniques from gaseous precursors (including gold vapors) or from solutions of gold chemicals (by electrolysis, electroplating or electro-less methods) are also available.[3c]

Chemical compounds of gold have then played a minor role compared with the omnipresent gold metal. Initially, these compounds functioned as intermediates in the recovery of gold from ores (in which gold is present in metallic form). The most important

species are the gold cyanide complexes formed in the cyanide leaching and extraction processes, in which finely crushed ores are treated with sodium cyanide in the presence of oxygen.

Typically, the resulting sodium gold cyanides are then adsorbed on high affinity carbon-in-pulp coal and, after re-extraction, depleted of gold by various reductive processes to yield gold metal.[4] For further conversion, gold metal can again be taken up in cyanide or in *aqua regia*, the classical mixture of nitric and hydrochloric acids that is the only effective acid medium able to dissolve metallic gold. In this process, one of the very few thermodynamically stable gold compounds, tetrachloroauric acid, is formed; this acid and its salts are used for the preparation of other gold chemicals, the overwhelming majority of which is thermodynamically labile and is proved to decompose into metallic gold and side products.

Therefore, it is not surprising that the chemistry of gold, which is clearly dominated by the metallic state, remained undeveloped for so long. It was merely regarded as an art to recover and convert gold metal into possible forms for decorative, monetary, anticorrosive or electrical usages.

While established areas of research have been continuously expanded, since the early 1980s gold chemistry has, above all, been characterized by innovative approaches and by unprecedented diversification of research interests.[5] New ways of reclaiming the metal are being explored, which are of particular relevance in view of the environmental hazard posed by the traditional amalgam and cyanide processes. The use of non-toxic and biologically degradable thiourea for the recovery of gold from electronic scrap is an example in point.[6] Biomass, prepared from algal cells, has been shown to be an efficient binding medium for gold salts in aqueous solution, and this bio-absorption process may provide a lucrative alternative for the recovery of gold from mining effluents.[7]

The most active aspects of the coordination chemistry of gold, besides the organometallic chemistry,[8, 9] appear to be the studies of gold compounds in unusual oxidation states and stereochemistry,[10-12] the bioinorganic chemistry of gold with especial reference to the treatment of rheumatoid arthritis (chrysotherapy) and cancer,[13] and the synthesis and properties of gold clusters and other complexes with gold-metal bonds.[14] Recently, a lot of attention was focused on gold nanoparticles (np) in different fields. However, regarding the diagnostic and therapeutic applications, it should be highlighted that gold np are able to penetrate renal cells causing nephrotoxicity.[15]

The complexes of gold are most readily classified according to their oxidation state. Gold(I) and gold(III) are the most common oxidation states in coordination complexes.

Gold(I) has the electron configuration [Xe]$4f^{14}5d^{10}$ and it can form linear, trigonal-planar or tetrahedral complexes, in which the hybridization at gold center may be considered to be *sp*, sp^2 and sp^3 respectively, using the 6*s* and one or more of the 6*p* orbitals of gold in bonding. However, this picture is oversimplified since 5*d* orbitals of gold are involved in bonding to some extent. In fact, the involvement of 5*d* orbitals is nowadays considered as the major cause of the high tendency of gold(I) to form linear complexes. Gold(I) is a very "soft" metal ion and the stability constants (determined in acetonitrile solution, where disproponation of gold(I) does not cause major problems) follow the following series [15b]:

1. anionic complexes $[AuX_2]^-$: $CNO^- < CNS^- \sim Cl^- < Br^- < I^- << CN^-$;
2. cationic complexes $[AuL_2]^+$: $Ph_3PO < Me_2S < Py < Ph_3As < NH_3 << Ph_3P \sim ArNC < MeNC < Ph_2PMe < PhPMe_2$;
3. neutral complexes [AuXL]: $Me_2O << Me_2S < Me_2Se < Ph_3Sb < ArNC \sim Ph_3As < Me_2Te < MeNC \sim Ph_3P < Ph_2PMe < PhPMe_2$.

In complexes with potentially bidentate ligands, gold(I) almost invariably bonds to the softer end of the ligand; for example, the ligands NCO^-, $S_2O_3^{2-}$ and SO_3^{2-} are bound through *N* or *S* rather than *O* atom[15c]. Similarly, SCN^- is normally bound through *S* rather than *N* atom, although the equilibrium between *N*- and *S*-bonded species in [AuL(SCN)] complexes depends on the nature of the ligand *L*.[16] An example of a trigonal-planar complex is $[Au(SCN)(PPh_3)_2]$ with *S*-bonded thiocyanate[16b].

The electron configuration of gold(III) is [Xe]$4f^{14}5d^8$ and all known gold(III) complexes are diamagnetic with a low-spin configuration. The vast majority of these complexes are square-planar, but complexes with coordination number five or six, in distorted square-pyramidal and tetragonally distorted octahedral structures respectively, are known.[16c] Gold(III) is a "soft" metal ion; although it forms many more complexes with "hard" ligands, such as oxygen donors, than gold(I) does, it has been argued that gold(III) displays the higher selectivity for "soft" ligands. [16d] The "noble" character of gold is a consequence of its high reduction potential.[1] The value of its standard electrochemical potential (E_0) is the highest of any other metal:

$$Au^{3+} \xrightarrow{1.29\,V} Au^{+} \xrightarrow{1.68\,V} Au$$

$$Au^{3+} \xrightarrow{1.42\,V} Au$$

This means that gold in any cationic form will accept electrons from virtually any source (reducing agent) to form neutral gold atoms which can aggregate to form gold metal in bulk. As a rule, the reduction potentials of gold may be reduced by complex formation.[12]

1.2. Design of gold-based peptidomimetics

Therapeutic effectiveness of drug candidates is limited by their abilities to traverse the plasma membrane. In order to overcome this outstanding problem, several carrier-mediated delivery strategies have been studied. Among them, much attention has been lately given to peptide-based delivery systems. Peptide transporters are integral plasma membrane proteins that regulate the cellular uptake of di- and tripeptides and peptide-like molecules (*i.e.* peptidomimetics). To date, two peptide transporters (i.e., PEPT1 and PEPT2) have been discovered in mammals. They are localized chiefly in epithelial cells of the mammary glands, lungs, bile ducts, small intestine, kidneys and choroid plexus[17, 18], but are also present in other tissues (pancreas, liver, gastrointestinal tract)[19] and, interestingly, seem to be up-regulated in some cancer types such as osteosarcoma, bladder, prostate, gastric, bile duct, pancreatic, fibrosarcoma, intestinal and renal. [20-25].

These transporters are stereoselective toward peptides containing L-enantiomers of amino acids and are able to deliver into the cytoplasm most di- and tripeptides into the cell regardless of sequence, size, charge and hydrophobicity.[26] Such a trait relies on their substrate binding site that can accommodate a wide range of molecules such as some peptidomimetic/non-peptidic drugs and prodrugs, angiotensin converting enzyme inhibitors and β-lactam antibiotics due to their likeness to di- or tripeptides.[27] Thus, in order to obtain high bioavailability and tumor specificity, we synthesized and widely characterized novel gold(III)-dithiocarbamato complexes with oligopeptides as ligands. Based on preliminary cell-line screenings[28, 29], we selected for further investigation the complexes AuD6 and AuD8 ([$Au^{III}Br_2$(dtc-Sar-AA-O(*t*-Bu))] with AA = Gly or Aib, respectively) whose ligands are di-peptide derivatives differing only in the substituents at the α–carbon atom at the *C*-terminus (**Figure 1.1**).

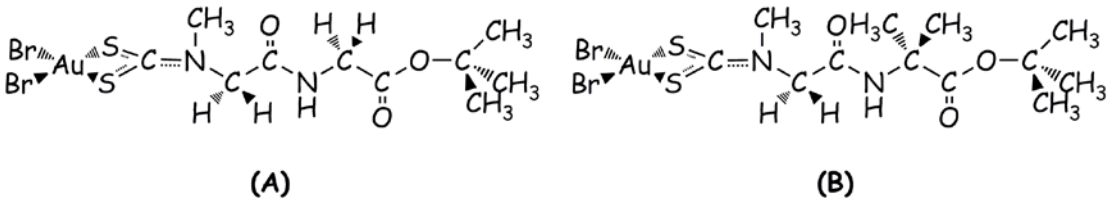

Figure 1.1. Chemical structures of investigated gold(III)-based compounds AuD6 **(A)** and AuD8 **(B)**.

We maintained the sarcosinedithiocarbamato moiety to resemble our first generation gold(III) analogues[30] and selected the *C*-terminal amino acids to evaluate the effect of flexibility (Gly) and rigidity (α-aminoisobutyric acid, Aib) on the cytotoxic activity of the corresponding complexes. The choice of Aib, a natural non-coded amino acid, was not accidental. Aib shows peculiar conformational preferences[31], highly affecting the backbone structure of the final peptide, which is usually folded into either α helix or 3_{10} helical arrangement. Therefore, rigid Aib-containing molecules have the capability to alter cell membrane permeability and they exhibit antibiotic, antiviral and anticancer activities.[32, 33]. Additionally, C^{α}-tetrasubstituted amino acids are able to overcome resistance to enzymatic degradation. *C*-terminal esterification of our complexes was required as previous analogues containing a free carboxylic group proved inactive.[34] In order to provide stability to the final compounds, bulky *t*-butyl groups were chosen, thus decreasing the possibility of hydrolysis. Lastly, peptide transport studies often involve the sarcosine-containing dipeptide Gly-Sar as a reference substrate as it shows good affinity toward both PEPT1 and PEPT2.[35]

With reference to **Figure 1.2.A**, the *t*-butyl-esterified dipeptides were again prepared as hydrochlorides [HCl·H-Sar-AA-O(*t*-Bu), AA = Gly (**P1**), Aib (**P2**)][29] by classical solution coupling strategies[36, 37] with the aim of increasing both the yields and the pureness of the products of the different steps. The synthesis of the Au(III)-dithiocarbamato derivatives starting from the corresponding dipeptide ligands is shown in the panel B.

The syntheses of dipeptides are first reported, followed by syntheses of the corresponding complexes. All the compounds were characterized by means of elemental and thermogravimetric analyses, FT-IR and mono- and multidimensional NMR spectroscopy. Moreover, in this work we were able to obtain the crystal structure of the compound AuD8.[29]

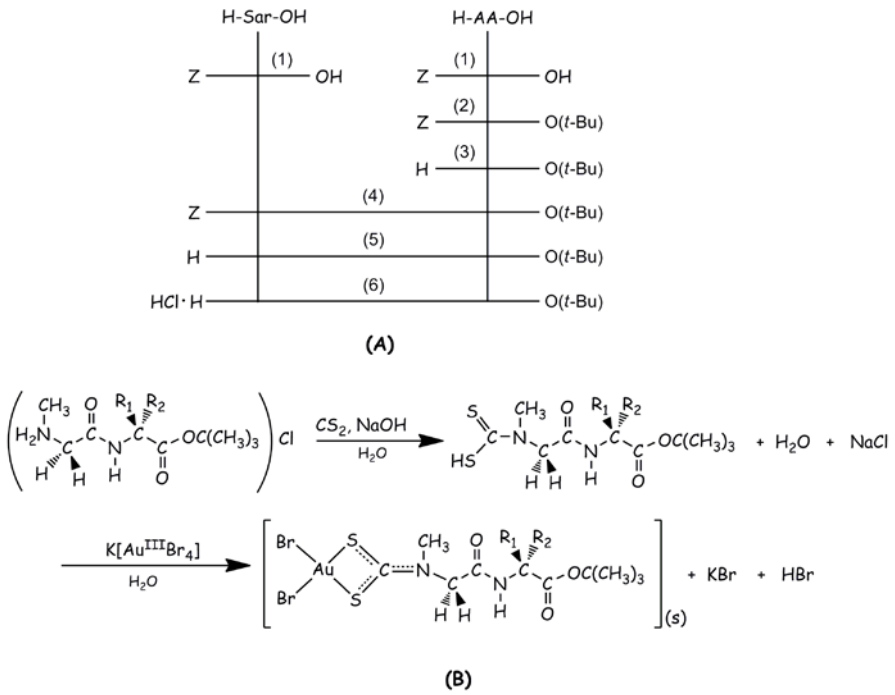

Figure 1.2. Synthetic scheme **(A)** for the preparation of dipeptides HCl•H-Sar-AA-O(t-Bu) (AA = Gly (AuD6), Aib (AuD8)): (1) ZOSu, TEA, CH_3CN/H_2O, r.t., 4 d; (2) isobutene, H_2SO_4 (cat.), CH_2Cl_2, -70°C/r.t., 7 d; (3) 30% Pd-C, H_2, CH_2Cl_2; (4) NMM, isobutylchloroformiate, $THF/CHCl_3$, -15°C/r.t., o.n.; (5) 10% Pd-C, H_2, MeOH; (6) HCl/Et_2O. Template reaction **(B)** exploited for the preparation of the complexes $[Au^{III}Br_2$(dtc-Sar-AA-O(*t*-Bu))] with AA = Gly (AuD6) or Aib (AuD8).

1.3. Experimental

1.3.1. Synthesis and characterization of AuD6 and AuD8

1.3.1.1. Synthesis of dipeptides functionalized with tert-butyl ester group

With reference to **Figure 1.2.A**, the first step was the *t*-butyl esterification of the Z-protected amino acid (Z-AA-OH) through the acid-catalyzed reaction with isobutene, followed by the removal of the Z-protecting group by catalytic hydrogenation with Pd on charcoal. The dipeptides H-Sar-AA-O(*t*-Bu) were then obtained by condensation of Z-Sar-OH with H-AA-O(*t*-Bu) using isobutyl chloroformate for activation of Z-Sar-OH and NMM as a base, and subsequent catalytic hydrogenation. The resulting purified products were finally isolated as hydrochlorides by slow addition of 1 eq of dilute HCl in diethyl ether. This procedure allowed to avoid the hydrolysis of the *t*-butyl ester and, consequently, to increase yields as well as to reduce the occurrence of side products.

Z-Sar-OH [36, 37]

A solution of Z-OSu (0.19 mol) in CH_3CN was added to a solution of H-Sar-OH (0.19 mol) in water and TEA (27 mL, 0.19 mol). After adjusting the pH to 8 by addition of TEA, the mixture was stirred at room temperature for 4 days. CH_3CN was evaporated under reduced pressure. The solution was diluted with 5% $NaHCO_3$ and the unreacted Z-OSu was extracted with diethyl ether (Et_2O). The aqueous layer was acidified to pH 2 with $KHSO_4$ and extracted with AcOEt. Such an organic layer was washed several times with water, dried over Na_2SO_4, and concentrated.

Yield: 60%.

IR (KBr): 1706, 1692 cm^{-1}.

^1H NMR ($CDCl_3$, 300 MHz), δ/ppm: 7.34 [m, 5H, Z phenyl CH] , 5.12 [m, 2H, Z CH_2], 4.08 [s, 2H, Sar CH_2], 3.02 [s, 3H, NCH_3].

MS, $[M]^+$ calculated (found): 224.23 (224.08).

Z-Gly-O*t*Bu

Already available in the lab.

Z-Aib-O*t*Bu [37]

Z-Aib-OH was already available, therefore the ester derivative was prepared dissolving Z-Aib-OH (0.04 mol) in CH_2Cl_2 (126 mL) in a pression-proof container and cooled to -70 °C in an acetone-dry ice bath. *Iso*butene (48 mL, 0.51 mol) was bubbled, and concentrated H_2SO_4 (0.42 mL) was dropwise added. The container was plugged and left for 7 days at room temperature.

Yield: 82 %.

IR (KBr): 3370, 1712, 1519 cm^{-1}.

^1H NMR ($CDCl_3$, 200 MHz), δ/ppm: 7.33 [5H, Z phenyl], 5.45 [s, 1H, NH], 5.08 [s, 2H, Z CH_2], 1.51 [s, 6H, β-CH_3], 1.43 [s, 9H, $C(CH_3)_3$].

Z-Sar-Gly-O*t*Bu

To a solution of Z-Sar-OH (6.37 mmol) and NMM (0.70 mL, 6.37 mmol) in THF (20 mL), cooled to -15 °C, isobutylchloroformiate (0.87 g, 6.37 mmol) was added.[38] After 10 min, a cooled suspension of H-Gly-O*t*Bu (9.56 mmol, obtained by catalytic hydrogenation in CH_2Cl_2 of the corresponding Z-protected derivative) and NMM (1.05 mL, 9.56 mmol) in $CHCl_3$ (12 mL) was added. The pH was adjusted and kept to 8 by addition of NMM. After

stirring at room temperature overnight, the reaction mixture was concentrated under reduced pressure. The residue was taken up with AcOEt, washed with 10% $KHSO_4$, H_2O, 5% $NaHCO_3$, H_2O, and dried over Na_2SO_4. The organic layer was concentrated to dryness. The product was purified by "flash chromatography" (silica gel column), using a petroleum ether-AcOEt 1:1 mixture as eluent.

Yield: 68 %.

IR (KBr): 3324, 1743, 1706, 1536 cm^{-1}.

^1H NMR (DMSO, 400 MHz), δ/ppm: 8.28 [m, 1H, NH], 7.37, 7.31 [2m, 5H, phenyl CH isomers], 5.05 [2s, 2H, Z CH_2 isomers], 3.91 [d, 2H, Gly α-CH_2], 3.73 [2s, 2H, Sar α-CH_2 isomers], 2.88, 2.86 [s, 3H, NCH_3 isomers], 1.39 [s, 9H, $C(CH_3)_3$].

MS, $[M+H]^+$ calculated (found): 337.41 (337.16).

HCl·H-Sar-Gly-O*t*Bu (P1)

To a solution of H-Sar-Gly-O*t*Bu (3.63 mmol, obtained by catalytic hydrogenation in MeOH of the corresponding Z-protected derivative) in Et_2O, a 2.3 M solution of HCl (1.58 mL) in Et_2O was dropwise added under stirring. The solvent was evaporated to dryness, the residue taken up with Et_2O and filtered.

Yield: 79 %.

IR (KBr): 3416, 3307, 1745, 1729, 1669, 1576, 1538 cm^{-1}.

^1H NMR (DMSO, 300.13 MHz), δ/ppm: 8.99 [m, 1H, NH_2Cl], 8.91 [t, 1H, Gly NH], 3.82 [d, 2H, Gly α-CH_2], 3.72 [m, 2H, Sar α-CH_2], 2.53 [s, 3H, NCH_3], 1.41 [s, 9H, $C(CH_3)_3$].

^{13}C NMR (DMSO, 75.48 MHz), δ/ppm: 168.42 [Gly carbonylic C], 165.61 [Sar carbonylic C], 80.75 [OtBu quaternary C], 48.59 [Sar secondary C], 41.13 [Gly secondary C], 39.51 [NCH_3 C], 27.46 [$(CH_3)_3$ C].

$C_9H_{19}ClN_2O_3$ (MW. 238.72) Elemental analysis %: (calculated) found, C(45.28) 45.27, H (8.02) 8.18, N (11.74) 11.52.

Z-Sar-Aib-O*t*Bu

To a solution of Z-Sar-OH (7.73 mmol) and NMM (0.85 mL, 7.73 mmol) in THF (20 mL), cooled to -15 °C, isobutylchloroformiate (7.73 mmol) was added.[38] After 10 min, a cooled suspension of H-Aib-O*t*Bu (11.6 mmol, obtained by catalytic hydrogenation in CH_2Cl_2 of the corresponding Z-protected derivative) and NMM (1.3 mL, 11.6 mmol) in $CHCl_3$ (15 mL) was added. The pH was adjusted and kept to 8 by addition of NMM. After stirring at room

temperature overnight, the reaction mixture was concentrated under reduced pressure. The residue was taken up with AcOEt, washed with 10% $KHSO_4$, H_2O, 10% $NaHCO_3$, H_2O, and dried over Na_2SO_4. The organic layer was concentrated until a yellow oil was isolated. This oil was converted to the solid form by grinding at 0 °C. Following two washes with petroleum ether, the product was spinned-off and dried *under vacuo* until constant weight.

Yield: 91 %.

IR (KBr): 3370, 1712, 1519 cm^{-1}.

^1H NMR ($CDCl_3$, 200 MHz), δ/ppm: 8.15 [d, 1H, NH], 7.33 [m, 5H, Z phenyl], 5.05 [d, 2H, Z CH_2 isomers], 3.83 [s, 2H, Sar α-CH_2], 2.83 [d, 3H, NCH_3 isomers], 1.33 [d, 9H, $C(CH_3)_3$ isomers], 1.29 [d, 6H, β-CH_3 isomers].

MS, $[M+H]^+$ calculated (found): 365.46 (335.21).

HCl·H-Sar-Aib-O*t*Bu (P2)

To a solution of H-Sar-Aib-O*t*Bu (4.94 mmol, obtained by catalytic hydrogenation in MeOH of the corresponding Z-protected derivative) in Et_2O, a solution of HCl 2.3 M (2.15 mL) in Et_2O was dropwise added under stirring. The solvent was evaporated to dryness, the residue taken up with Et_2O and filtered.

Yield: 87 %.

IR (KBr): 3442, 3215, 1735, 1726, 1676, 1557 cm^{-1}.

^1H NMR (DMSO, 300.13 MHz), δ/ppm: 9.05 [m, 1H, NH_2Cl], 8.84 [s, 1H, Aib NH], 3.64 [m, 2H, Sar α-CH_2], 2.52 [s, 3H, NCH_3], 1.37 [s, 9H, $C(CH_3)_3$], 1.35 [s, 6H, β-CH_3].

^{13}C NMR (DMSO, 75.48 MHz), δ/ppm: 172.23 [Aib carbonylic C], 164.24 [Sar carbonylic C], 79.91 [OtBu quaternary C], 55.80 [Aib quaternary C], 48.61 [Sar secondary C], 32.41 [NCH_3 C], 27.32 [$(CH_3)_3$ C], 25.36 [Aib $(CH_3)_2$ C].

$C_{11}H_{23}ClN_2O_3$ (PM. 266.78) Elemental analysis %: (calculated) found, C (49.53) 49.53, H (8.69) 8.47, N (10.50) 10.37.

MS, $[M]^+$ calculated (found): 231.33 (231.16).

1.3.1.2. Synthesis of gold(III)-peptidodithiocarbamato derivatives

[$Au^{III}Br_2$(dtc-Sar-Gly-O*t*Bu)] (AuD_6)

An aqueous solution (1.5 mL) of NaOH (0.27 mmol) was added to a water solution (3 mL) of HCl·Sar-Gly-O*t*Bu (0.27 mmol). Then, such a mixture was dropwise treated under continuous stirring with CS_2 (0.27 mmol). When the pH turned from 9 to 6 after about 1 hour, the solution was slowly added under stirring to an aqueous solution (2 mL) of dihydrate $K[AuBr_4]$ (0.27 mmol), leading to the immediate precipitation of a solid that was filtered off, washed with water and lastly, dried *in vacuo* over P_4O_{10}, the final yield being 78%.

Color: dark orange

IR (KBr): 3352, 1736, 1673, 1568, 1228, 1161, 1006, 556, 387, 252, 227 cm^{-1}.

^1H NMR (acetone-D_6, 300.13 MHz), δ/ppm: 7.96 [m, 1H, Gly NH] , 4.75, 4.71 [2s, 2H, Sar α-CH_2 isomers], 3.96, 3.95 [2d, 2H, Gly α-CH_2 isomers], 3.57, 3.53 [2s, 3H, NCH_3 isomers], 1.41 [s, 9H, $C(CH_3)_3$].

^{13}C NMR (acetone-D_6, 75.48 MHz), δ/ppm: 200.48, 196.74 [CSS C], 169.93 [Gly carbonylic C], 165.35, 165.06 [Sar carbonylic C], 82.59 [O*t*Bu quaternary C], 58.98, 55.12 [Sar secondary C], 43.09 [Gly secondary C], 41.12, 40.13 [NCH_3 C], 28.66 [$(CH_3)_3$ C].

$C_{10}H_{17}AuBr_2N_2O_3S_2$ (MW. 634.16) Elemental analysis %: (calculated) found C (18.94) 19.20, H (2.70) 2.88, N (4.42) 4.42, S (10.11) 10.45.

[$Au^{III}Br_2$(dtc-Sar-Aib-O*t*Bu)] (AuD_8)

The synthesis procedure is very similar to the previous one. Dihydrate $K[AuBr_4]$ (0.34 mmol) reacted with a solution of HCl·Sar-Aib-O*t*Bu (0.34 mmol), CS_2 (15 μL, 0.34 mmol) and NaOH (0.34 mmol), the final yield being 80%.

Color: yellow earth

IR (KBr): 3362, 1734, 1690, 1560, 1531, 1215, 1144, 996, 545, 383, 253, 223 cm^{-1}.

^1H NMR (acetone-D_6, 300.13 MHz), δ/ppm: 7.90 [s, 1H, Aib NH], 4.66, 4.62 [2s, 2H, Sar α-CH_2 isomers], 3.54, 3.51 [m, 3H, NCH_3 isomers], 1.46, 1.45 [2s, 6H, β-CH_3 isomers], 1.44 [s, 9H, $C(CH_3)_3$].

^{13}C NMR (acetone-D_6, 75.48 MHz), δ/ppm: 200.26, 196.57 [CSS C], 173.73 [Aib C carbonylic], 164.00 [Sar carbonylic C], 81.91 [O*t*Bu quaternary C], 58.35 [Aib quaternary

C], 56.15, 55.26 [Sar secondary C], 41.20, 40.21 [NCH_3 C], 28.60 [$(CH_3)_3$ C], 25.61 [Aib $(CH_3)_2$ C].

$C_{12}H_{21}AuBr_2N_2O_3S_2$ (MW. 662.21) Elemental analysis %: (calculated) found C (21.76) 22.03, H (3.20) 3.33, N (4.23) 4.34, S (9.68) 8.58.

1.4. Results and discussion

Two *t*-butyl-esterified dipeptides were prepared as hydrochlorides and used to synthesize the corresponding gold(III)-dithiocarbamato derivatives.

Both the starting dipeptides and the corresponding gold(III)-dithiocarbamato derivatives have been characterized by means of several techniques in order to check the expected stoichiometry as well as to investigate their structural features. With regard to the thermogravimetric analyses, **Table 1.1** points out a good correlation between calculated and found weight loss values to metallic gold.

Table 1.1. TG and DSC data for the gold(III)-dithiocarbamato derivatives AuD6 and AuD8.

Compound	Weight loss to Au(0) [%]		Peak temperature [°C] (process)[a]
	Calculated	Found	
AuD6	-68.9	-68.6	153 (endo),481 (exo), 1079 (endo)
AuD8	-70.3	-70.2	166 (endo), 472 (exo), 1065 (endo)

[a]endo/exo = endothermic/exothermic.

The interpretation of FT-IR spectra of dithiocarbamato derivatives of transition metals is a diagnostic tool to determine the coordination mode and the nature of bonds in the complexes. Furthermore, FT-IR spectroscopy provided insights into the structural features of complexes AuD6 and AuD8 as well. **Table 1.2** highlights the disappearance of the broad band at 2680-2780 cm^{-1} ($\nu_{a/s}(NH_2^+)$) and the appearance of two new bands at *ca.* 1560 and 1000 cm^{-1} (assigned to the ν(N–CSS) and ν_a(S–C–S), respectively) on passing from the starting dipeptide ester hydrochlorides P1 and P2 to the corresponding gold derivatives AuD6 and AuD8[47]. This behavior is consistent with chelating dithiocarbamato ligands coordinated to a gold(III) metal center, in agreement with data previously reported.[30] The detection of a single band at *ca.* 1000 cm^{-1} in both gold(III) complexes indicates that the –NCSS moiety chelates the metal center in a symmetrical bidentate mode, as based on the

Bonati-Ugo criterion.[39]The presence of two new bands, absent in the IR spectra of the free dipeptides, in the range 380-420 cm^{-1} assigned to gold(III)-sulfur stretching vibrations may further account for such coordination geometry.[40] he two remaining coordination sites are taken up by *cis*-bromides as two new bands are visible at 215-255 cm^{-1} and can be ascribed to the $\nu_{a/s}$(Br–Au–Br).[41, 42]

Table 1.2. Selected FT-IR frequencies of the starting dipeptides P1-P2 and the corresponding gold(III)-dithiocarbamato derivatives AuD6 and AuD8.

Compound	Vibrational mode [cm^{-1}]									
	ν NH	**$\nu_{a/s}$ NH_2^+**	**ν C=O**	**Amide I**	**ν N–CSS**	**Amide II**	**Amide III**	**$\nu_{a/s}$ SCS**	**$\nu_{a/s}$ SAuS**	**$\nu_{a/s}$ BrAuBr**
P1	3307	2777/2709	1732	1669	-	1576	1258	-	-	-
AuD6	3352	-	1736	1673	1568[a]		1252	1006/557	418/387	252/217
P2	3292	2744/2683	1736	1689	-	1563	1259	-	-	-
AuD8	3362	-	1734	1690	1560	1531	1259	996/545	411/383	252/223

[a]Overlapped.

Intriguingly, the dithiocarbamate formation and the subsequent metal coordination does not affect to a great extent the other main frequencies deriving from the organic backbone of the molecule, except for a significant increase of the ν(N–H) along with a shift of the Amide II band toward lower wavenumbers. The vibrational modes referred to as Amide I and Amide II give rise to quite strong infrared absorptions and are very sensitive to the formation of hydrogen bonds.[43] The Amide I mode is mostly ascribed to the in-plane peptide carbonyl stretching, and is generally observed in the range 1660-1710 cm^{-1} for "free" C=O groups or at lower frequencies (1620-1660 cm^{-1}) for H-bonded carbonyls.[48] The wavenumbers of Amide I bands are consistent with non-hydrogen-bonded peptide carbonyl groups for both the starting dipeptides P1-P2 and the corresponding gold(III)-dithiocarbamato derivatives. The Amide II band, associated with the in-plane N–H bending, is observed in the range 1540-1570 cm^{-1} when the N–H groups are involved in hydrogen bonds (1500-1520 cm^{-1} would be consistent with "free" N–H groups).[44]

In all cases the amide N–H groups seem to form hydrogen bonds, even if their strength decreases on passing from free dipeptides to the gold(III) counterparts (as confirmed by the shift of the Amide II band of the gold-based compounds toward lower frequencies). Furthermore, the broad band at *ca.* 3300 cm^{-1}, assigned to the stretching of *trans* peptide N–H groups, shifts toward slightly higher wavenumbers in the complexes if compared to the

corresponding free dipeptides, accounting for less strong hydrogen bonds.[49] In addition, the amide III mode, composed of 30% C-N stretching and 40% N-H bending[45], is basically unaffected by the coordination to the metal center.

As above anticipated, bands related to the remaining functional groups of each dipeptide are negligibly affected by the gold(III) coordination as they are located farther from the metal center.

The structural hypothesis based on FT-IR data was confirmed by the X-ray crystal structure of the complex [$Au^{III}Br_2$(dtc-Sar-Aib-O(*t*-Bu))] (AuD8), shown in **Figure 1.3**.[29] In fact, the gold(III) complex adopts a distorted square-planar geometry with two *cis*-bromides, and some hydrogen bonds involving the peptide amide group are established. The distortion from the ideal geometry relies on the small bite angle of the bidentate dithiocarbamato ligand (*ca.* 75°). A list of selected bond lengths and angles and the crystallographic data are reported in **Tables 1.3** and **1.4**, respectively. It is worth highlighting that the Au–S distances are approximately 0.1 Å shorter than Au–Br ones.

Table 1.3. Selected bond lengths (Å) and angles (°) for [$Au^{III}Br_2$(dtc-Sar-Aib-O(*t*-Bu))] (AuD8).

Au–S(1)	2.316(2)
Au–S(2)	2.313(3)
Au–Br(1)	2.439(2)
Au–Br(2)	2.440(1)
C(1)–S(1)	1.745(9)
C(1)–S(2)	1.721(9)
C(1)–N(1)	1.280(1)
S(1)–Au–S(2)	75.46(9)
S(1)–Au–Br(1)	95.68(7)
S(2)–Au–Br(2)	96.38(7)
Br(1)–Au–Br(2)	92.48(5)
C(1)–S1–Au	87.10(3)
C(1)–S2–Au	87.80(3)
S(1)–C1–S(2)	109.60(5)

Table 1.4. Crystallographic data and refinement details for [$Au^{III}Br_2$(dtc-Sar-Aib-O(*t*-Bu))] (AuD8).

Empirical formula	$C_{12}H_{21}AuBr_2N_2O_3S_2$
Molecular weight	662.21

Color, habit	Yellow, plate
Temperature [K]	293(2)
λ [Å]	0.71073
Crystal system	Monoclinic
Space group	$P2_1/n$
a [Å]	6.475(1)
b [Å]	40.922(3)
c [Å]	7.509(1)
α [°]	90
β [°]	99.370(1)
γ [°]	90
V [Å^3]	1963(2)
Z	4
ρ (calc) [mg m^{-3}]	2.241
μ [mm^{-1}]	11.788
θ range [°]	2.79 to 25.99
No. of rflcn/unique	22749/3828
GoF	1.030
*R*1[a]	0.0444
*wR*2[b]	0.1091

[a]$R1 = \Sigma||Fo|-|Fc||/\Sigma|Fo|$. [b]$wR2 = [\Sigma[w(Fo^2-Fc^2)^2]/\Sigma[w(Fo^2)^2]]^{½}$, $w = 1/[\sigma^2(Fo^2) + (aP)^2 + bP]$, where $P = [\max(Fo^2,0) + 2Fc^2]/3$.

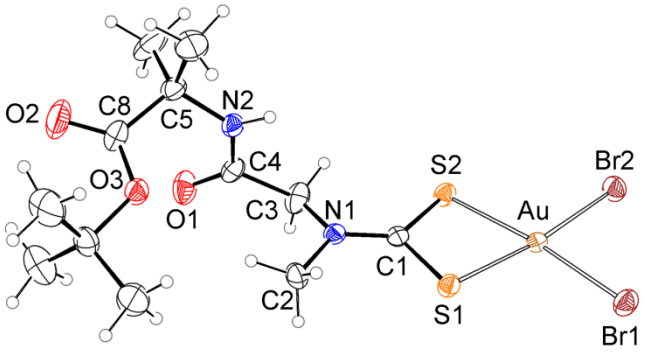

Figure 1.3. X-ray crystal structure with atom numbering scheme for [Au^{III}Br$_2$(dtc-Sar-Aib-O(*t*-Bu))], with thermal ellipsoids drawn at 30% probability.

The dithiocarbamato nitrogen atom is functionalized with two distinct moieties, that is, the *N*-methyl group (C(2)) and the dipeptide chain (comprising an amide and a *t*-butyl ester functions). The conformation adopted by the latter is such that the planar amide and the ester groups form an angle of approximately 74°, and the *t*-butyl group is spatially close to the sarcosine *N*-methyl moiety. The projection of the crystal packing along the *c* crystallographic axis (**Figure 1.4.A**) reveals the presence of two distinct zones defined by two types of weak interactions, one characterized by the antiparallel superimposition of the coordination planes whereas the second is associated with the hydrophobic interaction between the peripheral *t*-butyl substituents. In addition, couples of symmetry-related molecules form two weak hydrogen bonds between the amide group (N(2)) and one gold(III)-bound bromide belonging to an adjacent molecule (Br(2)') (**Figure 1.4.B**).

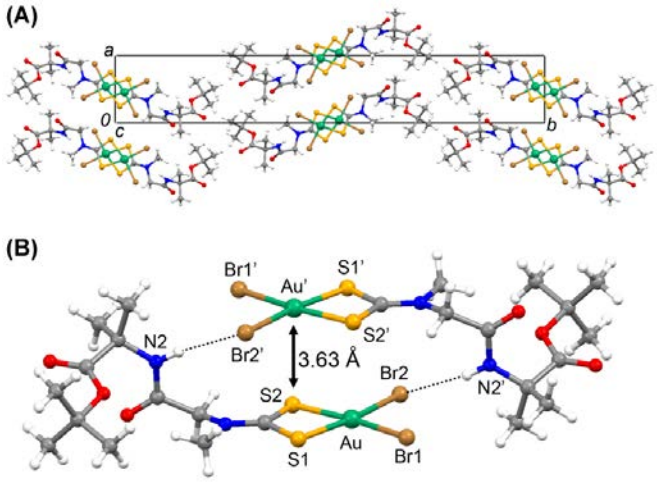

Figure 1.4. (A) Crystal packing of [$Au^{III}Br_2$(dtc-Sar-Aib-O(*t*-Bu))] projected along the *c* crystallographic axis. **(B)** Depiction of the hydrogen bonds formed between two symmetry-related molecules (N(2)H–Br(2)' = 3.791(8) Å).

With respect to NMR characterization, mono- (^{1}H, **Table 1.5**) and bidimensional ([^{1}H,^{13}C] HMBC, **Table 1.6**) spectra were recorded. The disappearance of the $-NH_2^+$ proton signal, along with the detection of a new ^{13}C signal at about 200 ppm (assigned to the dithiocarbamato carbon atom) for both complexes,[34] confirms the formation of the gold(III)-peptido derivatives. A general shift of all proton signals toward higher δ values was observed for the dipeptide backbone upon formation of the corresponding gold(III)-dithiocarbamato counterparts, the larger change (*ca.* 1 ppm) involving the sarcosine methyl and the methylene groups. On moving away from the –NCSS moiety, the δ variation decreases until being

negligible for the *t*-butyl ester group. Such a behavior is in agreement with data recorded for the first generation compounds and is observed for ^{13}C signals as well.[30] An upfield shift (*ca.* 1 ppm) was detected only for the amide proton peaks. Intriguingly, likewise to the previously studied compounds,[30, 46] in each case the sarcosine residue gives rise to two sets of signals (both in ^{1}H and ^{13}C spectra), suggesting the coexistence of two distinct forms in solution. For instance, upon dissolution of AuD6 in acetone-d_6, two ^{1}H signals at 3.53/3.57 and 4.71/4.75 ppm are recorded for sarcosine -NCH_3 and -NCH_2 groups, respectively, with a *ca* 1:1 intensity ratio. Notably, a species interconverts into the other one over time as shown in **Figure 1.5**.

Table 1.5. ^{1}H NMR spectral data [ppm] of HCl·Sar-Gly-O*t*Bu (P1), HCl·Sar-Aib-O*t*Bu (P2) and their corresponding gold(III)-dithiocarbamato complexes.

Compound	NH_2^+ Sar	NH	αCH_2 Sar	N-CH_3 Sar
P1[(a)]	8.99	8.91	3.72	2.53
AuD$_6$[(b)]	-	7.96	4.71/4.75[(c)]	3.53/3.57[(c)]
P2[(a)]	9.05	8.84	3.64	2.52
AuD$_8$[(b)]	-	7.90	4.62/4.66	3.51/3.54[(c)]

[(a)] performed in $(CD_3)_2SO$, [(b)] performed in $(CD_3)_2CO$, [(c)] isomers.

Table 1.6. ^{13}C NMR spectral data [ppm] of HCl·Sar-Gly-O*t*Bu (P1), HCl·Sar-Aib-O*t*Bu (P2) and their corresponding gold(III)-dithiocarbamato complexes.

Compound	CSS	αCH_2 Sar	N-CH_3 Sar
P1[(a)]	-	48.59	32.38
AuD$_6$[(b)]	196.74/200.48	55.12/58.98	40.13/41.12
P2[(a)]	-	48.61	32.41
AuD$_8$[(b)]	196.57/200.26	55.26/56.15	40.21/41.20

[(a)] performed in $(CD_3)_2SO$, [(b)] performed in $(CD_3)_2CO$.

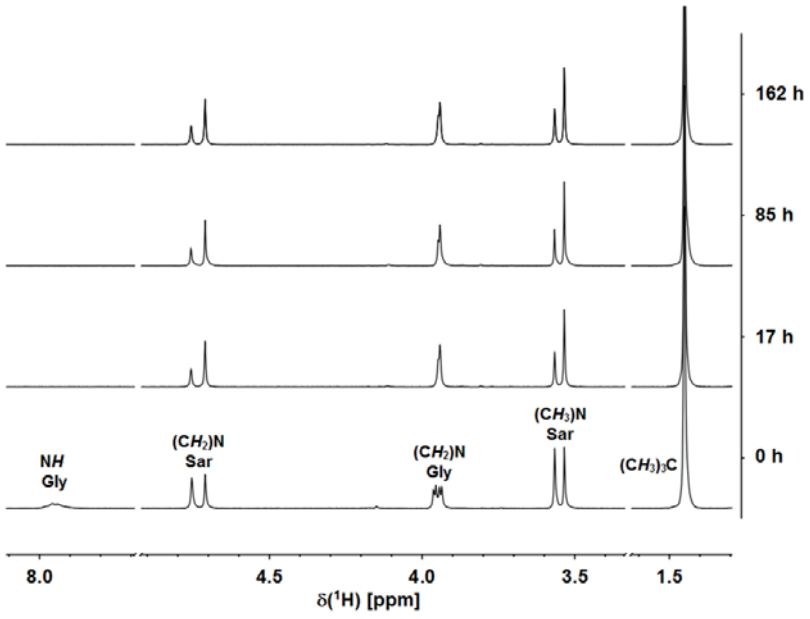

Figure 1.5. ^{1}H NMR spectra of complex AuD6 in acetone-d_6 over time.

For both complexes the downfield peaks gradually decrease in intensity while their highfield counterparts increase over time, reaching a stationary condition within 85 h (the final ratio being *ca.* 1:3). The coexistence of two different species of each compound was confirmed by the detection of two signals for the –NCSS carbon atom in the [^{1}H,^{13}C] HMBC spectrum as well (**Figure 1.6**), each coupling with one set of *N*-methyl and *N*-methylene sarcosine groups. The solvent affects to a great extent the rate of the conversion between the two forms. As a matter of fact, conversion takes place in acetone and in trifluoroacetic acid (data not shown) but not in DMSO, as shown in **Figure 1.7**.

Given that same results were obtained for AuD8, it is likely that the chemical structures described above are related to the major species in solution.

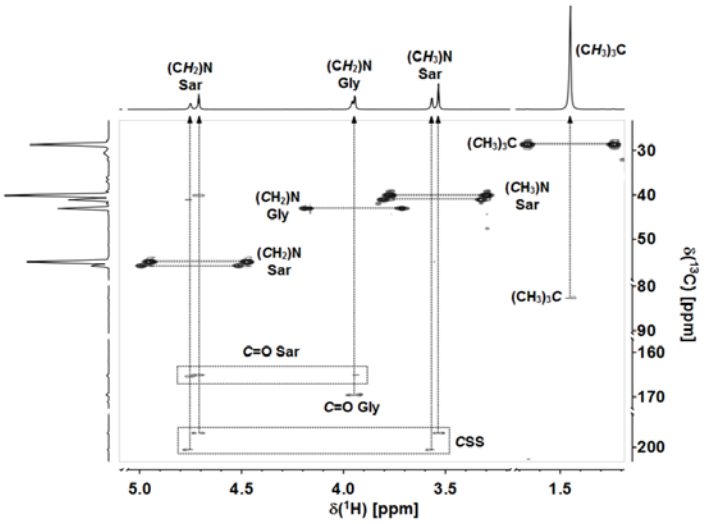

Figure 1.6. [^{1}H,^{13}C] HMBC spectrum of complex AuD6 in acetone-d_6.

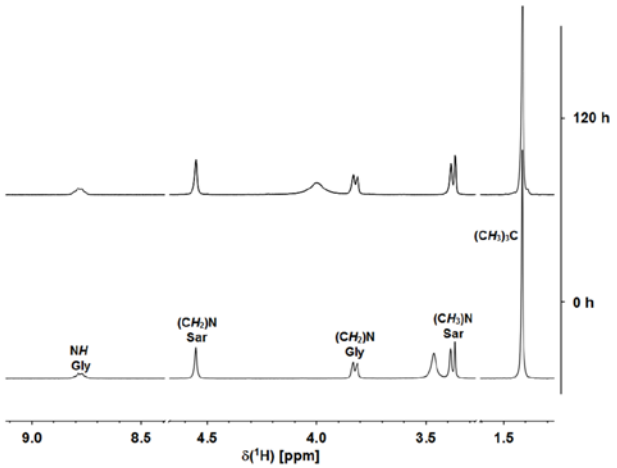

Figure 1.7. ^{1}H NMR spectra of complex AuD6 in DMSO-d_6 over time.

Recently, we were able to isolate the predominant species present in solution (following the synthesis by a protracted work-up in an acetone/water mixture) and its NMR and FT-IR spectra are reported in **Figure 1.8** and **1.9**, respectively.

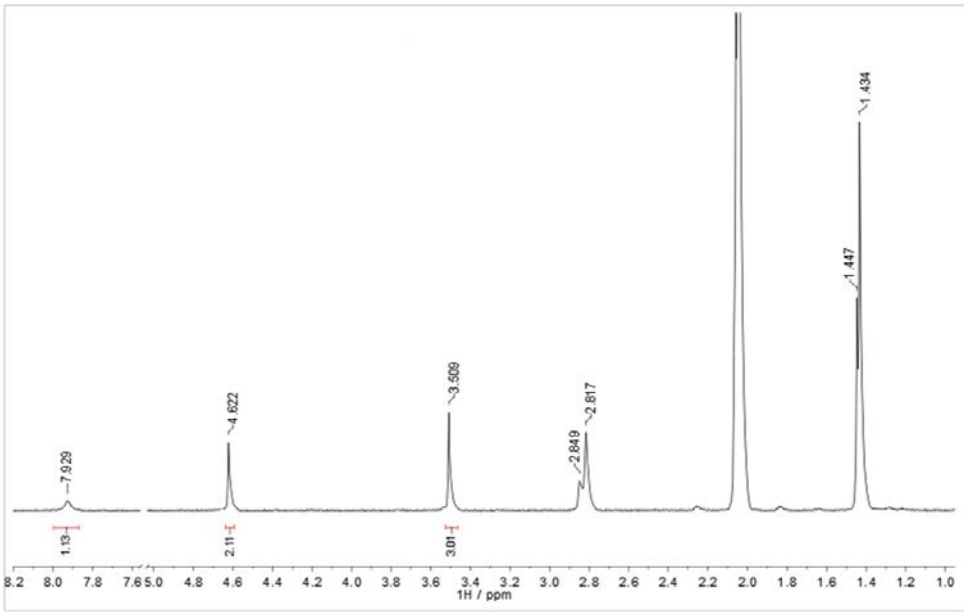

Figure 1.8. NMR spectrum recorded for the isolated predominant species of AuD8.

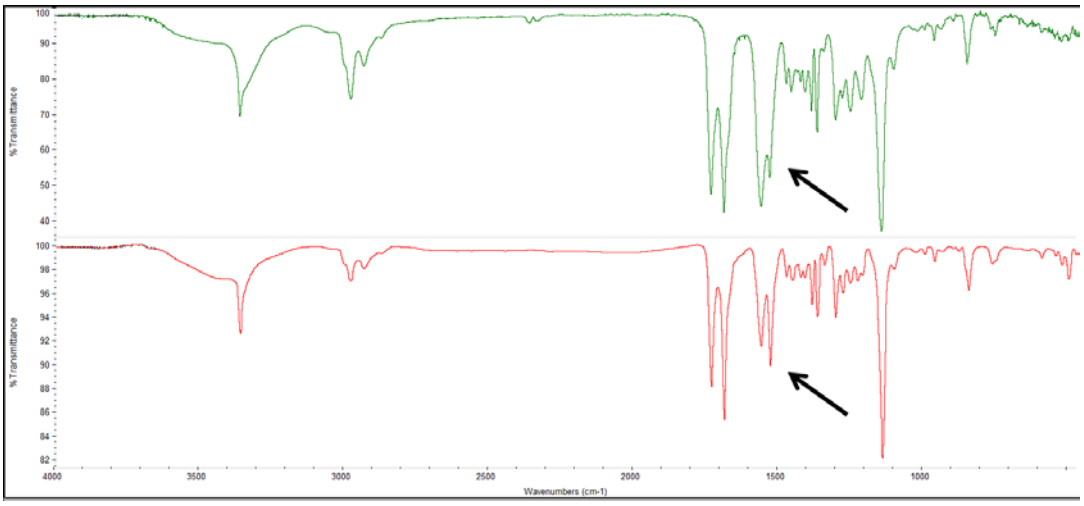

Figure 1.9. FT-IR spectra recorded for the usually obtained AuD8 mixture of two species (green) and the predominant isomer (red).

At present, the unique difference among the two species is visible in the IR spectrum (arrows in Figure 1.9), namely the band related to stretching of the N–CSS moiety and the amide II band (associated with the N–H bending) occurring at about 1560 and 1530 cm^{-1}, respectively, show an intensity pattern opposite to that usually observed for the mixture of the two species (upper panel). Other characterizations are required to ultimately define the nature of this species and, accordingly, that of the minority one.

It is worth highlighting that after 17 h the ^{1}H signal of the amide proton is not detectable anymore in acetone-d_6 (Figure 1.5), leading to the subsequent simplification of the multiplicity of the vicinal glycine α-methylene protons. Such an unexpected experimental evidence is likely to be due to the possible hydrogen/deuterium exchange with solvent. Peptide amides are well-known to easily undergo hydrogen exchange reactions with protic deuterated solvents (*e.g.* D_2O and methanol-d_4)[50] whereas, as far as we know, it is not reported for aprotic deuterated solvents. On the other hand, it is plain that such exchange reaction occurs for the compound AuD6 in acetone-d_6 (Figure 1.5) and that it is solvent-dependent since it does not take place in DMSO-d_6 (Figure 1.7). It is likely that acetone tautomeric processes, involving also water molecules, may occur and thereby account for this phenomenon.

Chapter 1 references

(1) N. N. Greenwood, A. N. Earnshaw (Eds.), *The Chemistry of the Elements*, Pergamon Press, Oxford, 1986.

(2) R. J. Puddephat, in: G. Wilkinson, R. D. Gillard, J. A. McCleverty (Eds.), *Comprehensive Coordination Chemistry. The Synthesis, Reactions, Properties and Applications of Coordination Compounds*, Vol. 5, Pergamon Press, Oxford, 1987, p. 861.

(3) A. Grahmann, H. Schmidbaur, in: E. W. Abel, F. G. A. Stone, G. Wilkinson (Eds.), *Comprehensive Organometallic Chemistry 2. A Review of the Literature 1982-1994*, Vol. 3, Pergamon Press, Oxford, 1995, p. 1.; 3b. W. S. Rapson, T. Groenewold (Eds.), *Gold Usage*, Academic Press, London, 1978; 3c. D. M. Jacobson, G. Humpston, *Interdisc. Sci. Rev.*, 1992, 17, 244.

(4) Schmidbaur, H. Is Gold Chemistry Important?. *Angew. Chem.* **1976**, *88*, 830-843.

(5) Rapson, W. S. The Science and Technology of Gold. A Twenty-Year Perspective. *Gold Bull.* **1988**, *21*, 10-16.

(6) Mehringer, G.; Simon, J. The Hydrometallurgical Recycling of Gold by Biological Degradable Thiourea Instead of Cyanide Leaching. *Metall (Berlin)* **1989**, *43*, 624-627.

(7) Watkins II, J. W.; Elder, R. C.; Greene, B.; Darnall, D. W. Determination of Gold Binding in an Algal Biomass using EXAFS and XANES Spectroscopies. *Inorg. Chem.* **1987**, *26*, 1147-1151.

(8) Li, D.; Che, C. -.; Kwong, H. -.; Yam, V. W. -. Photoinduced C-C Bond Formation from Alkyl Halides Catalysed by Luminescent Dinuclear Gold(I) and Copper(I) Complexes. *Journal of the Chemical Society, Dalton Transactions* **1992**, 3325-3329.

(9) King, C.; Khan, M. N. I.; Staples, R. J.; Fackler Jr., J. P. Luminescent Mononuclear Gold(I) Phosphines. *Inorg. Chem.* **1992**, *31*, 3236-3238.

(10) Jones, P. G. X-RAY STRUCTURAL INVESTIGATIONS OF GOLD COMPOUNDS. *Gold bulletin* **1983**, *16*, 114-124.

(11) Jiang, Y.; Alvarez, S.; Hoffmann, R. Binuclear and Polymeric Gold(I) Complexes. *Inorg. Chem.* **1985**, *24*, 749-757.

(12) Antonova, L. V.; Busygina, T. E.; Polovnyak, V. K.; Usachev, A. E. Stability of Gold(II) Complexes. *Russian Journal of General Chemistry* **1997**, *67*, 491-494.

(13) Tiekink, E. R. T. Gold Derivatives for the Treatment of Cancer. *Crit. Rev. Oncol.* **2002**, *42*, 225-248.

(14) Zeller, E.; Beruda, H.; Kolb, A.; Bissinger, P.; Riede, J.; Schmidbaur, H. Change of Coordination from Tetrahedral Gold-Ammonium to Square-Pyramidal Gold-Arsonium Cations. *Nature* **1991**, *352*, 141-143.

(15) Sereemaspun, A.; Rojanathanes, R.; Wiwanitkit, V. Effect of Gold Nanoparticle on Renal Cell: An Implication for Exposure Risk. *Ren. Fail.* **2008**, *30*, 323-325; 15b. R. Roulet, A. Zolkin, M. O. Faltens, D. H. Templeton, *Inorg. Chem.*, 1974, **13**, 1836; 15c. P. C. Hydes, H. Middleton, *Gold Bull.*, 1979, **12**, 90.

(16) Melpolder, J. B.; Burmeister, J. L. Antisymbiosis and the Trans-Influence in Gold(I) Thiocyanate Complexes. *Inorg. Chim. Acta* **1981**, *49*, 115-120; 16b. J. A. Muir, M. M. Muir, S. Arias, *Acta Crystallogr., Sect. B*, 1982, **38**, 1318, 16c. R. J. Puddephat (Ed.), *The Chemistry of Gold*, Elsevier, Amsterdam, 1978; 16d. L. H. Skibsted, J. Bjerrum, *Acta Chem. Scand., Ser. A*, 1977, **31**, 155.

(17) Rubio-Aliaga, I.; Daniel, H. Peptide Transporters and their Roles in Physiological Processes and Drug Disposition. *Xenobiotica* **2008**, *38*, 1022-1042.

(18) Biegel, A.; Knütter, I.; Hartrodt, B.; Gebauer, S.; Theis, S.; Luckner, P.; Kottra, G.; Rastetter, M.; Zebisch, K.; Thondorf, I.; Daniel, H.; Neubert, K.; Brandsch, M. The Renal Type H+/Peptide Symporter PEPT2: Structure-Affinity Relationships. *Amino Acids* **2006**, *31*, 137-156.

(19) Terada, T.; Shimada, Y.; Pan, X.; Kishimoto, K.; Sakurai, T.; Doi, R.; Onodera, H.; Katsura, T.; Imamura, M.; Inui, K. -. Expression Profiles of various Transporters for Oligopeptides, Amino Acids and Organic Ions Along the Human Digestive Tract. *Biochem. Pharmacol.* **2005**, *70*, 1756-1763.

(20) Inoue, M.; Terada, T.; Okuda, M.; Inui, K. -. Regulation of Human Peptide Transporter 1 (PEPT1) in Gastric Cancer Cells by Anticancer Drugs. *Cancer Lett.* **2005**, *230*, 72-80.

(21) Knütter, I.; Rubio-Aliaga, I.; Boll, M.; Hause, G.; Daniel, H.; Neubert, K.; Brandsch, M. H+-Peptide Cotransport in the Human Bile Duct Epithelium Cell Line SK-ChA-1. *American Journal of Physiology - Gastrointestinal and Liver Physiology* **2002**, *283*, G222-G229.

(22) Mitsuoka, K.; Miyoshi, S.; Kato, Y.; Murakami, Y.; Utsumi, R.; Kubo, Y.; Noda, A.; Nakamura, Y.; Nishimura, S.; Tsuji, A. Cancer Detection using a PET Tracer, 11C-Glycylsarcosine, Targeted to H +/Peptide Transporter. *Journal of Nuclear Medicine* **2008**, *49*, 615-622.

(23) Nakanishi, T.; Tamai, I.; Takaki, A.; Tsuji, A. Cancer Cell-Targeted Drug Delivery Utilizing Oligopeptide Transport Activity. *International Journal of Cancer* **2000**, *88*, 274-280.

(24) Gonzalez, D. E.; Covitz, K. -. Y.; Sadée, W.; Mrsny, R. J. An Oligopeptide Transporter is Expressed at High Levels in the Pancreatic Carcinoma Cell Lines AsPc-1 and Capan-2. *Cancer Res.* **1998**, *58*, 519-525.

(25) Nakanishi, T.; Tamai, I.; Sai, Y.; Sasaki, T.; Tsuji, A. Carrier-Mediated Transport of Oligopeptides in the Human Fibrosarcoma Cell Line HT1080. *Cancer Res.* **1997**, *57*, 4118-4122.

(26) Brandsch, M. Transport of Drugs by Proton-Coupled Peptide Transporters: Pearls and Pitfalls. *Expert Opin. Drug Metab. Toxicol.* **2009**, *5*, 887-905.

(27) Brandsch, M.; Knütter, I.; Bosse-Doenecke, E. Pharmaceutical and Pharmacological Importance of Peptide Transporters. *J. Pharm. Pharmacol.* **2008**, *60*, 543-585.

(28) Kouodom, M. N.; Boscutti, G.; Celegato, M.; Crisma, M.; Sitran, S.; Aldinucci, D.; Formaggio, F.; Ronconi, L.; Fregona, D. Rational Design of Gold(III)-Dithiocarbamato Peptidomimetics for the Targeted Anticancer Chemotherapy. *J. Inorg. Biochem.* **2012**.

(29) Negom Kouodom, M.; Ronconi, L.; Celegato, M.; Nardon, C.; Marchiò, L.; Dou, Q. P.; Aldinucci, D.; Formaggio, F.; Fregona, D. Toward the Selective Delivery of Chemotherapeutics into Tumor Cells by Targeting Peptide Transporters: Tailored Gold-Based Anticancer Peptidomimetics. *J. Med. Chem.* **2012**, *55*, 2212-2226.

(30) Ronconi, L.; Giovagnini, L.; Marzano, C.; Bettìo, F.; Graziani, R.; Pilloni, G.; Fregona, D. Gold Dithiocarbamate Derivatives as Potential Antineoplastic Agents: Design, Spectroscopic Properties, and in Vitro Antitumor Activity. *Inorg. Chem.* **2005**, *44*, 1867-1881.

(31) Paterson, Y.; Rumsey, S. M.; Benedetti, E.; Némethy, G.; Scheraga, H. A. Sensitivity of Polypeptide Conformation to Geometry. Theoretical Conformational Analysis of Oligomers of A-Aminoisobutyric Acid. *J. Am. Chem. Soc.* **1981**, *103*, 2947-2955.

(32) Brown, K. L.; Hancock, R. E. W. Cationic Host Defense (Antimicrobial) Peptides. *Curr. Opin. Immunol.* **2006**, *18*, 24-30.

(33) Johnstone, S. A.; Gelmon, K.; Mayer, L. D.; Hancock, R. E.; Bally, M. B. In Vitro Characterization of the Anticancer Activity of Membrane-Active Cationic Peptides. 1. Peptide-Mediated Cytotoxicity and Peptide-Enhanced Cytotoxic Activity of Doxorubicin Against Wild-Type and P-Glycoprotein Over-Expressing Tumor Cell Lines. *Anticancer Drug Des.* **2000**, *15*, 151-160.

(34) Ronconi, L.; MacCato, C.; Barreca, D.; Saini, R.; Zancato, M.; Fregona, D. Gold(III) Dithiocarbamate Derivatives of N-Methylglycine: An Experimental and Theoretical Investigation. *Polyhedron* **2005**, *24*, 521-531.

(35) Geissler, S.; Zwarg, M.; Knütter, I.; Markwardt, F.; Brandsch, M. The Bioactive Dipeptide Anserine is Transported by Human Proton-Coupled Peptide Transporters. *FEBS J.* **2010**, *277*, 790-795.

(36) Valle, G.; Formaggio, F.; Crisma, M.; Bonora, G. M.; Toniolo, C.; Bavoso, A.; Benedetti, E.; Di Blasio, B.; Pavone, V.; Pedone, C. Linear Oligopeptides. Part 147. Chemical and Crystallographic Study of the Reaction between Benzyloxycarbonyl Chloride and A-Aminoisobutyric Acid. *Journal of the Chemical Society, Perkin Transactions 2* **1986**, 1371-1376.

(37) McGahren, W. J.; Goodman, M. Synthesis of Peptide Oxazolones and Related Compounds. *Tetrahedron* **1967**, *23*, 2017-2030.

(38) Vaughan Jr., J. R.; Osato, R. L. Preparation of Peptides using Mixed Carboxylic Acid Anhydrides. *J. Am. Chem. Soc.* **1951**, *73*, 5553-5555.

(39) Bonati, F.; Ugo, R. Organotin(IV) N,N-Disubstituted Dithiocarbamates. *J. Organomet. Chem.* **1967**, *10*, 257-268.

(40) Forghieri, F.; Preti, C.; Tassi, L.; Tosi, G. Preparation, Properties and Reactivity of Gold Complexes with some Heterocyclic Dithiocarbamates as Ligands. *Polyhedron* **1988**, *7*, 1231-1237.

(41) Beurskens, P. T.; Blaauw, H. J. A.; Cras, J. A.; Steggerda, J. J. Preparation, Structure, and Properties of Bis(N,N-Di-N-Butyldithiocarbamato)Gold(III) Dihaloaurate(I). *Inorg. Chem.* **1968**, *7*, 805-810.

(42) Coates, G. E.; Parkin, C. Tertiary Phosphine Complexes of Trimethylgold: Infrared Spectra of Complexes of Gold and some Other Metals. *Journal of the Chemical Society (Resumed)* **1963**, 421-429.

(43) Picquart, M.; Abedinzadeh, Z.; Grajcar, L.; Baron, M. H. Spectroscopic Study of N-Acetylcysteine and N-Acetylcystine/Hydrogen Peroxide Complexation. *Chem. Phys.* **1998**, *228*, 279-291.

(44) Fillaux, F.; de Lozé, C. Structure of Matrix Isolated N-Methylacetamide. *Chem. Phys. Lett.* **1976**, *39*, 547-551.

(45) Susi, H.; Byler, D. M. Fourier Transform Infrared Study of Proteins with Parallel B-Chains. *Arch. Biochem. Biophys.* **1987**, *258*, 465-469.

(46) Giovagnini, L.; Ronconi, L.; Aldinucci, D.; Lorenzon, D.; Sitran, S.; Fregona, D. Synthesis, Characterization, and Comparative in Vitro Cytotoxicity Studies of Platinum(II), Palladium(II), and Gold(III) Methylsarcosinedithiocarbamate Complexes. *J. Med. Chem.* **2005**, *48*, 1588-1595.

(47) Colthup, N. B.; Daly, L. H.; Wiberley, S. E. Introduction to Infrared and Raman Spectroscopy; Academic Press: New York, 1990.

(48) Fillaux, F.; De Lozé, C. Spectroscopic Study of Monosubstituted Amides. II. Rotation Isomers in Amides Substituted by Aliphatic Side-Chain Models. *Biopolymers* **1972**, *11*, 2063-2077.

(49) Lin-Vien, D.; Colthup, N. B.; Fateley, W. G.; Grasselli, J. G. Infrared and Raman Characteristic Frequencies of Organic Molecules; Academic Press: London, 1991; pp 144-145.

(50) Dempsey, C. E. Hydrogen Exchange in Peptides and Proteins Using NMR Spectroscopy. *Prog. Nucl. Magn. Reson. Spectrosc.* **2001**,*39*, 135−170.

Chapter 2.
Antitumor activity against human MDA-MB-231 breast cancer cell cultures and xenografts and insights into the mechanism of action

In the previous chapter, we reported on the design, synthesis and characterization of two gold(III)-peptidodithiocarbamato complexes, namely AuD6 and AuD8 (**Figure 1.1**). In fact, based on preliminary cell-line screenings, briefly discussed in the *Introduction Section* of this thesis[1, 2], we selected them for further biological investigation. During a 6-month overseas stay, in collaboration with Prof. Q. Ping Dou's research group (Barbara Ann Karmanos Cancer Institute, Departments of Oncology, School of Medicine, Wayne State University, Detroit, U.S.A.) some studies were carried out both *in vitro* and *in vivo* in order to provide insights into their mechanism of action, and evaluate their anticancer activity and toxicity (§ *Chapter 5*) on animal models.

The triple-negative human breast cancer cell line MDA-MB-231 was used as a model since these cells are highly metastatic, invasive and resistant to cisplatin. We first tested the effects of AuD6 and AuD8 on cell proliferation, evaluating the IC50 values (*i.e.*, concentration needed to inhibit half of the control – not treated sample – cell proliferation). We also checked whether ROS species are intracellularly produced using the ROS scavenger TROLOX.

Since first generation compounds were able to inhibit the chymotrypsin-like active site of the proteasome (an ATP-dependent protease with a key role in both nuclear and cytoplasmic homeostasis)[3, 4],we hypothesized that also novel complexes could target the tumor proteasome. To test this hypothesis, we investigated the effects of both compounds on the proteasomal chymotrypsin (CT)-like, trypsin (T)-like and peptidyl-glutamyl-peptide-hydrolizing (PGPH)-like activities of MDA-MB-231 cell extracts and purified human 20S proteasome. In order to elucidate to what extent cellular proteasome is inhibited by our compounds, we treated breast cancer cells with both complexes at different concentrations for 24 h, followed by measurement of proteasomal activities.

Furthermore, to provide insights into the mechanism of action, we carried out dose- and time-dependent *in vitro* studies. In the first investigation, MDA-MB-231 cells were treated with both complexes AuD6 and AuD8 for 24 h at different concentrations whereas in the second they were treated with both compounds at 20 μM for 4, 8, 16 and 24 h. Since these studies highlighted that cell death occurs *via* apoptosis, we carried out an Annexin V/PI assay to further confirm the data.

Finally, we studied the cytotoxic activity *in vivo* on female athymic nude mice bearing human breast cancer MDA-MB-231 cells.

In this investigation, we identified the proteasome as a major target both *in vitro* and *in vivo*. The proteasome is an ATP-dependent protease and plays a key role in nuclear and cytoplasmic homeostasis by degrading a large range of proteins marked with poly-ubiquitin chains. Among the proteasomal enzymes, the most studied is the 26S proteasome whose molecular weight is 2,500 kDa. 26S proteasome is formed by a barrel-shaped multicatalytic complex referred to as the 20S proteasome core particle (CP), capped at each end by a regulatory component termed the 19S complex.[5] The role of the 19S particles is to recognize ubiquitinated client proteins and mediate their entry to the 20S core regulating their unfolding and translocation into the proteolytic chamber. The CP (MW~750 kDa) consists of 28 subunits, which are arranged in four axially stacked seven-membered rings, yielding a cylinder-like complex with a $\alpha_{1-7}\beta_{1-7}\beta_{1-7}\alpha_{1-7}$ stoichiometry. Eukaryotic 20S proteasomes contain only three proteolytically active β subunits per β ring (subunits β1, β2 and β5), whereas the remaining β subunits and α subunits are inactive. The β1, β2 and β5 subunits are responsible for three different catalytic activities: peptidyl glutamyl peptide hydrolyzing-like, trypsin-like and chymotrypsin-like (hydrolysis at the *C*-terminal side of acidic, basic and hydrophobic amino acid residues, respectively). In addition to chymotrypsin-like activity, BrAAP (branched chain amino acid-preferring) and SNAAP (small neutral amino acid-preferring activity) activities are ascribed to the β5 subunit as well.[6, 7] Proteasome inhibition is a recent, very promising strategy to treat cancers and, in 2003, the first proteasome inhibitor, bortezomib (Velcade®)[8], was approved for clinical use. Encouragingly, our compounds exhibit potent proteasome-inhibitory activity, associated with induction of cell death *via* apoptosis.

2.1. Experimental

2.1.1. Materials

Fluorogenic peptide substrates Suc-LLVY-AMC, Z-ARR-AMC, and Z-LLE-AMC (for the proteasomal chymotrypsin-like, trypsin-like and PGPH-like activities, respectively) and Ac-DEVD-AMC (for caspase-3 like activity) were purchased from Calbiochem (San Diego, CA). Purified human 20S proteasome was from Boston Biochem (Boston, MA). EZ-RUN Pre-stained Rec protein ladder was purchased from Fisher Scientific (Pittsburgh, PA), 40% bis-acrylamide 29:1 solution and TEMED for electrophoresis were from Bio-Rad (Hercules, CA). DMEM/F12 cell growth medium, sodium pyruvate, HEPES, penicillin, and streptomycin were purchased from Invitrogen (Carlsbad, CA) while standard fetal bovine serum was from Aleken Biologicals (Nash, TX). Rabbit monoclonal antibody against cleaved caspase-3 (active form, 5A1, Asp175) was purchased from Cell Signaling Technology (Danvers, MA). Mouse monoclonal antibodies against ubiquitin (P4D1), p27 (F-8), Bax (B-9), IκB-α (H-4), GAPDH (9B3), rabbit polyclonal antibody against caspase-3 (H-277), and secondary antibodies were from Santa Cruz Biotechnology, Inc. (Santa Cruz, CA). Rabbit polyclonal antibody against human proteasomal β5 subunit and human poly(ADP-ribose) polymerase (PARP) were purchased from Enzo Life Sciences (Farmingdale, NY). FITC Annexin V apoptosis detection kit I was purchased from BD Biosciences (San Jose, CA). Sodium azide, NaCl, Tris base, sterile DMSO, 3-(4,5-Dimethyl-2-thiazolyl)-2,5-diphenyl-2H-tetrazolium bromide (MTT), *cis*-diammineplatinum(II) dichloride (hereinafter, cisplatin), Tween-20, cremophor, ethanol, and other chemicals) were from Sigma-Aldrich (St. Louis, MO).

All chemicals were of high grade pureness and used as purchased without any further purification.

2.1.2. Methods

Cell cultures and cell proliferation assay. Human breast cancer MDA-MB-231 cells were obtained from American Type Culture Collection (Manassas, VA) and grown in DMEM/F12 supplemented with 10% fetal bovine serum, 1 mM sodium pyruvate, 10 mM HEPES, 100 U/mL penicillin and 100 μg/mL streptomycin. Cells were grown in a humidified incubator with 5% CO_2 at 37 °C. Cells were seeded in octuplicate in 96-well plates and grown to 70% - 80% confluence, followed by treatment with DMSO (control) or each compound (dissolved in DMSO) in fresh medium at the indicated concentrations. After 24 or 72 hours incubation

at 37 °C, inhibition of cell proliferation was measured by MTT assay, as elsewhere described.[9] The cytotoxicity of the compounds was quantified as the percentage of cells surviving relative to untreated cells. Four MTT tests for each compound were performed in order to evaluate the corresponding IC_{50} values.

For comparison purposes, cells were plated in quadruplicate in 96-well plates and grown to 70% - 80% confluence, followed by treatment with cisplatin (dissolved in 0.9% $NaCl_{(aq)}$) in fresh medium at 3 different concentrations.

In order to investigate whether cell death is affected by free radicals produced *in situ* by our compounds, cells were seeded in quadruplicate and treated with both complexes and Trolox. We first pretreated cells for 1 h with Trolox at 100 μM and after changing medium, treated cells with compounds and incubated for an additional 24 h. Alternatively, we co-treated cells for 24 h with both compounds and Trolox (100 μM), followed by MTT assay.

Proteasome activity assay in purified 20S proteasome and MDA-MB-231 whole-cell extract. Purified human 20S proteasome (0.5 nM) was incubated in triplicate with three different proteasomal fluorogenic substrates (20 μM) and each compound (dissolved in DMSO) at various concentrations ranging from 0.1 to 10 μM (or an equivalent volume of solvent DMSO as a control) in 100 μL of assay buffer [20 mM Tris-HCl (pH 7.5)]. After 1 hour and 2 hours incubation at 37°C, inhibition of each proteasomal activity was measured[10], recording the fluorescence of hydrolyzed AMC groups using a Wallac Victor^3 1420 multilabel plate reader (PerkinElmer, Waltham, MA) with an excitation wavelength of 355 nm, an emission wavelength of 460 nm, and measurement time of 0.1 s.

Likewise, MDA-MB-231 whole-cell extract (10 μg/well) was incubated in quadruplicate with each complex and each fluorogenic substrate in 100 μL of assay buffer [20 mM Tris-HCl (pH 7.5)]. Fluorescence data were acquired after 1 hour and 2 hours incubation at 37°C. The whole-cell extract was prepared as described elsewhere.[5]

Proteasome activity assay in intact breast cancer MDA-MB-231 cells. MDA-MB-231 breast cancer cells were plated in quadruplicate and grown to around 75% confluence, followed by treatment with both complexes at different concentrations for 24 h at 37 °C (DMSO as a control). The exhausted medium was then removed and fresh medium and

proteasomal fluorogenic substrates (20 μM) were added to each well. Plates were incubated for 24 h at 37 °C prior to recording fluorescence at 460 nm.

Only two proteasomal activities (chymotrypsin-like and PGPH-like) were measured since our complexes showed some selectivity in studies on the purified enzyme. Besides, the arginine-rich fluorogenic substrate (positively charged) for the trypsin-like activity was not used owing to its poor capability in cell-membrane crossing.

Cellular morphology and Western blot analyses. A Zeiss (Thornwood, NY) Axiovert 25 microscope was used for cellular morphology microscopic imaging with phase contrast.

MDA-MB-231 cells were grown to around 75% confluence, treated with gold-based complexes or solvent as a control, harvested, and lysed. Cell lysates (30 μg/lane) were separated by SDS-PAGE and transferred to a nitrocellulose membrane. After blocking of non-specific binding (5% non-fat dry milk in Tris-Buffered Saline with Tween 20-TBST), membranes were incubated overnight at 4 °C with primary antibodies, followed by washing with TBST and incubation for 2 h with secondary antibodies. Bands of interest were visualized using HyGLO Chemiluminescent HRP Antibody detection reagent, HyBlot Chemiluminescence films (Denville Scientific Inc.; Metuchen, NJ) and a HOPE Micro-MAX film processor.

Apoptosis assay. Apoptosis indexes were measured using the Annexin-V fluorescein isothiocyanate (FITC) apoptosis detection kit I from by BD Pharmingen. MDA-MB-231 cells were grown to around 75% confluence, treated with gold-based complexes (20 μM) or solvent as a control for 16 or 24 h, harvested by means of a scraper and centrifugation. Cell pellets were washed twice with ice cold PBS and cells were then resuspended in 1X binding buffer at a concentration of $1 \cdot 10^6$ cells/mL. 100 μL of the suspension was then transferred to a 5 mL flow cytometry tube and 5 μL FITC Annexin V and 5 μL PI for double stained samples (either 5 μL of FITC Annexin V or 5 μL of PI for controls) were added. Mixtures were gently vortexed and incubated for 15 min at RT in the dark followed by addition of 400 μL 1X binding buffer to each tube. Then, analysis by flow cytometry occurred within 1 h at the Microscopy, Imaging and Cytometry Resources (MICR) Core at the Karmanos Cancer Institute, Wayne State University. Data (**Figure 2.5**) are presented as density plots of Annexin-V (x-axis) and propidium iodide (PI, y-axis) stainings. Unstained cells, cells stained with either PI or FITC Annexin-V only and untreated cells stained with both PI and Annexin-

V, were used to set up compensation and quadrants. The excitation wavelength was 488 nm and the detection wavelengths were 530 ± 15 and 620 ± 21 nm for Annexin V and PI, respectively. Cells staining negative for both markers were considered viable since Annexin V and PI are both cell membrane impermeable while cells staining positive for both markers were considered in late apoptosis. Cells staining positive for Annexin only were considered in early apoptosis whereas cells staining positive for PI only were considered dead by a necrotic pathway. Percentages of viable, apoptotic, and necrotic cells are reported in the corner of each quadrant (**Figure 2.5**).

Human breast tumor xenograft experiments. Seven-week-old female athymic nude mice were purchased from Harlan Laboratories (Indianapolis, USA) and housed in accordance with protocols approved by the Institutional Laboratory Animal Care and Use Committee of Wayne State University. Human breast cancer MDA-MB-231 cells suspended in 0.1 mL of serum-free DMEM/F12 cell growth medium were inoculated subcutaneously (s.c.) into the right flank of each mouse. When tumors reached a volume of around 115 mm^3, the mice were randomly allocated into three groups (seven mice per group) and treated five days a week by s.c. injection of either vehicle [1:1:1 v/v PBS, DMSO, Cremophore/ethanol (1:4)] or medium containing 1.0 mg/kg of AuD6 or AuD8. Tumor length (L) and width (W) were measured every other day using a caliper, and tumor volumes were evaluated according to the standard formula $(\pi \cdot L \cdot W^2)/6$. Mouse weights were monitored twice a week. Mice were sacrificed after 27 days of treatment, or when tumors reached ~ 1,800 mm^3. The tumors were collected and weighed. Tumor tissues were used to measure proteasome inhibition and caspase-3 activation by enzymatic activity assays and by Western blot analysis.

Immunohistochemistry. IHC was performed using a previously reported protocol.[11] Briefly, tumor samples were paraffin-embedded by the Pathology Core at Karmanos Cancer Institute (Detroit, MI, USA). Samples were then cut and stained for p27 or TUNEL by the BioBank at William Beaumont Hospital (Royal Oak, MI, USA). Anti-p27 (VP-P951) was from Vector Laboratories (Burlingame, CA, USA) and was used at a 1:30 dilution followed by detection by DAKO instrument. Samples were counterstained with DAB/Hematoxylin. TUNEL staining was performed using anti-digoxigenin and peroxidase substrate, followed by counterstaining with methyl green. In both cases, brown colored cells were considered positive.

2.1.3. Results

Inhibition of MDA-MB-231 cell proliferation by AuD6 and AuD8 in comparison with cisplatin. MTT assay was used to assess the *in vitro* cytotoxicity of AuD6 and AuD8 against MDA-MB-231 cells after 24 or 72 h treatment. Although both complexes inhibited tumor cell growth in a dose-dependent manner, AuD8 proved more potent than AuD6, with IC_{50} values ± SD of 6.5 ± 0.6 and 17 ± 1 μM, respectively. After 72 h treatment, the IC_{50} of AuD6 decreased to 13 ± 1 μM. Notably, MDA-MB-231 cells were resistant to cisplatin under the same experimental conditions. In fact, after 24 h treatment the IC_{50} value was not reached using concentrations ranging from 25 to 100 μM in agreement with literature data.[12, 13] At 100 μM cisplatin exhibited a growth-inhibitory effect of around 40% after 24 h treatment whereas after 72 h around 23% cell viability was observed in agreement with the known slower activity kinetics presented by the reference drug.[14]

Influence of the ROS scavenger Trolox on the anticancer activity of gold(III) complexes. In order to elucidate if ROS species are produced intracellularly by our gold-based compounds, we co-treated MDA-MB-231 cells with both complexes and the hydrophilic form of vitamin E (Trolox), which is able to react with free radicals.[15] We carried out two independent experiments (**Figure 2.1**), and observed different results. First, we pretreated cells for 1 h with Trolox at 100 μM, followed by 24 h treatment with the compounds. We observed no changes in IC_{50} values for either compound, suggesting that cell growth inhibition is independent of ROS generation. In the second experiment, we co-treated cells with each of the two compounds and Trolox (100 μM) for 24 h. As expected, we observed higher antiproliferative activity in the presence of Trolox. In fact, Trolox alone can inhibit tumor cell growth by approximately 25% after 24 h treatment. Interestingly, AuD6 showed a greater synergistic effect than AuD8.

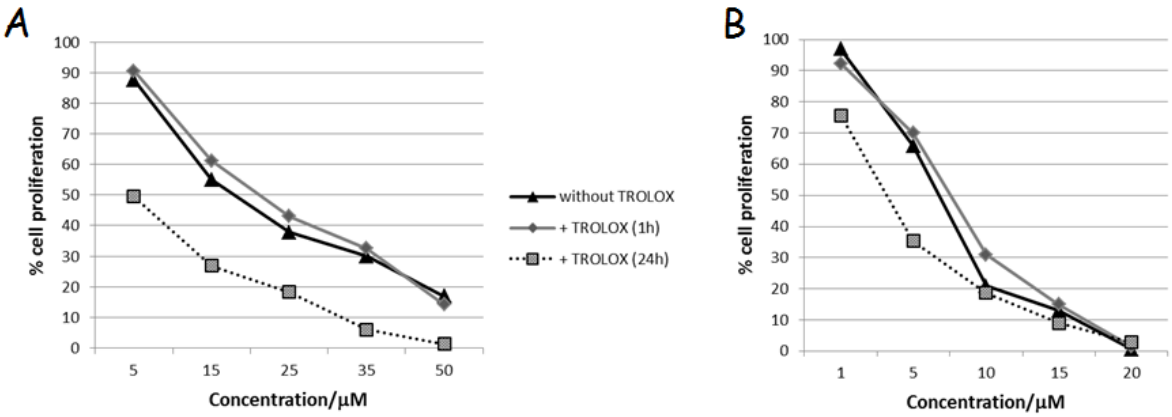

Figure. 2.1. Growth inhibition curves obtained after treatment of MDA-MB-231 tumor cells for 24 h at different concentrations of AuD6 **(A)** or AuD8 **(B)** either in the absence or in the presence (1h pretreatment or 24 h co-treatment) of the ROS scavenger TROLOX .

***In vitro* inhibition of proteasomal activities by AuD6 and AuD8 on purified 20S and cell extracts.** Since first generation compounds were able to inhibit the chymotrypsin-like active site of the proteasome,[16, 17] we hypothesized that these second generation complexes could target the tumor proteasome as well. To test this hypothesis, we investigated the effects of both compounds on the proteasomal chymotrypsin (CT)-like, trypsin (T)-like and peptidyl-glutamyl-peptide-hydrolizing (PGPH)-like activities of MDA-MB-231 cell extracts. Both complexes were able to inhibit all the three proteasomal enzymatic activities (**Table 2.1**) in a concentration-dependent manner. However, AuD8 showed some selectivity for CT-like activity mediated by the β5 subunit.[7, 18]

To provide direct evidence for this selectivity, we incubated purified human 20S proteasome with each compound at different concentrations and the fluorogenic substrates specific for each activity, using DMSO as a control. We observed that AuD8 preferentially inhibited the CT-like activity of the purified 20S proteasome as well (**Table 2.1**). Remarkably, in terms of proteasome inhibition, both complexes proved to be about an order of magnitude more potent than the first generation compounds.[16, 17] Velcade® (bortezomib) was used as a positive control (IC_{50} = 2.2 ± 0.6 nM for the CT-like pocket) (*see Discussion*).

Table 2.1. IC_{50} values (μM ± SD) obtained for the three proteasomal activities on the purified 20S proteasome and on MDA-MB-231 cell extract after 2 h incubation.

	Proteasomal activity	AuD6	AuD8
Purified 20S	*Chymotrypsin-like*	0.42 ± 0.03	0.29 ± 0.07
	Trypsin-like	0.51 ± 0.07	0.61 ± 0.02
	PGPH-like	0.49 ± 0.09	0.54 ± 0.08
Cell extract	*Chymotrypsin-like*	3.3 ± 0.4	2.9 ± 0.6
	Trypsin-like	3.0 ± 0.9	5.7 ± 0.1
	PGPH-like	2.3 ± 0.8	4.5 ± 0.9

Treatment of breast cancer cells with AuD6 and AuD8 triggers proteasome inhibition and apoptosis. In order to elucidate to what extent cellular proteasome is inhibited by our compounds we treated breast cancer cells with both complexes at different concentrations for 24 h, followed by measurement of proteasomal activities. AuD8 showed a greater degree of selectivity for the CT-like pocket than AuD6 in these cells. Notably, both compounds were also able to inhibit proteasomal PGPH-like activity (**Figure 2.2**).

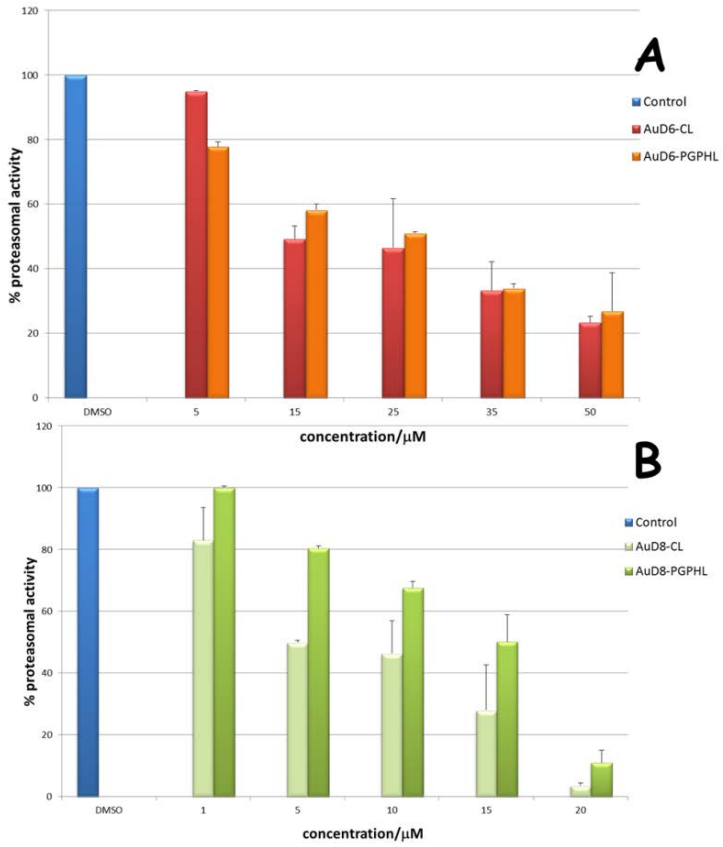

Figure 2.2. Inhibition of the proteasomal CT-like and PGPH-like activities in MDA-MB-231 cells after 24 h treatment with AuD6 **(A)** and AuD8 **(B)**.

To gain insight into the mechanism of action of our compounds, we performed dose- and time-dependent *in vitro* studies. MDA-MB-231 cells were treated with either (i) AuD6 or AuD8 for 24 h at different concentrations (5, 10, 15 and 20 μM) (**Figure 2.3.A-B**) or (ii) each compound at 20 μM for 4, 8, 16 or 24 h (**Figure 2.4.A**). Overall, we observed accumulation of ubiquitinated proteins, p27 and IκBα, caspase-3 activation, PARP cleavage and, interestingly, changes in levels of the proteasomal β5 subunit after treatment with AuD8. Treatment with AuD8 also resulted in enhanced levels of p36/Bax and consequent decrease or complete disappearance of p21/Bax and p18/Bax fragments. In fact, it has been reported that Bax protein (p21/Bax) could be hydrolyzed by calpain, thus yielding a p18/Bax fragment. This cleavage is associated with cell death commitment and leads to formation of the p36/Bax homodimer. Gao *et al*. reported that p18 and p36/Bax are more potent in disrupting mitochondrial integrity than full-length Bax.[19] Importantly, progressive decrease in full-length caspase-3 in **Figure 2.4.A** is in agreement with the increase in levels of cleaved caspase-3 (active form) in **Figure 2.3.A**. Additionally, **Figures 2.3** and **2.4** highlight the affinity of AuD8 for the proteasomal β5 subunit, as at higher concentrations and longer times

the band intensity decreases, indicating that upon treatment with AuD8, some modifications occur in this protein subunit. Accordingly, such an interaction may account for the accumulation of ubiquitinated proteins, the proteasomal target proapoptotic proteins p27 and IκB-α that leads to tumor growth inhibition/apoptosis.

The complex AuD6 was less potent than AuD8 in agreement with its higher IC_{50} value, reported above. Indeed, we observed bands as intense as the control for some proteins while weaker effects were observed on the apoptotic phenomena (i.e., PARP cleavage and caspase-3 activation) following treatment with higher concentrations or for longer time periods.

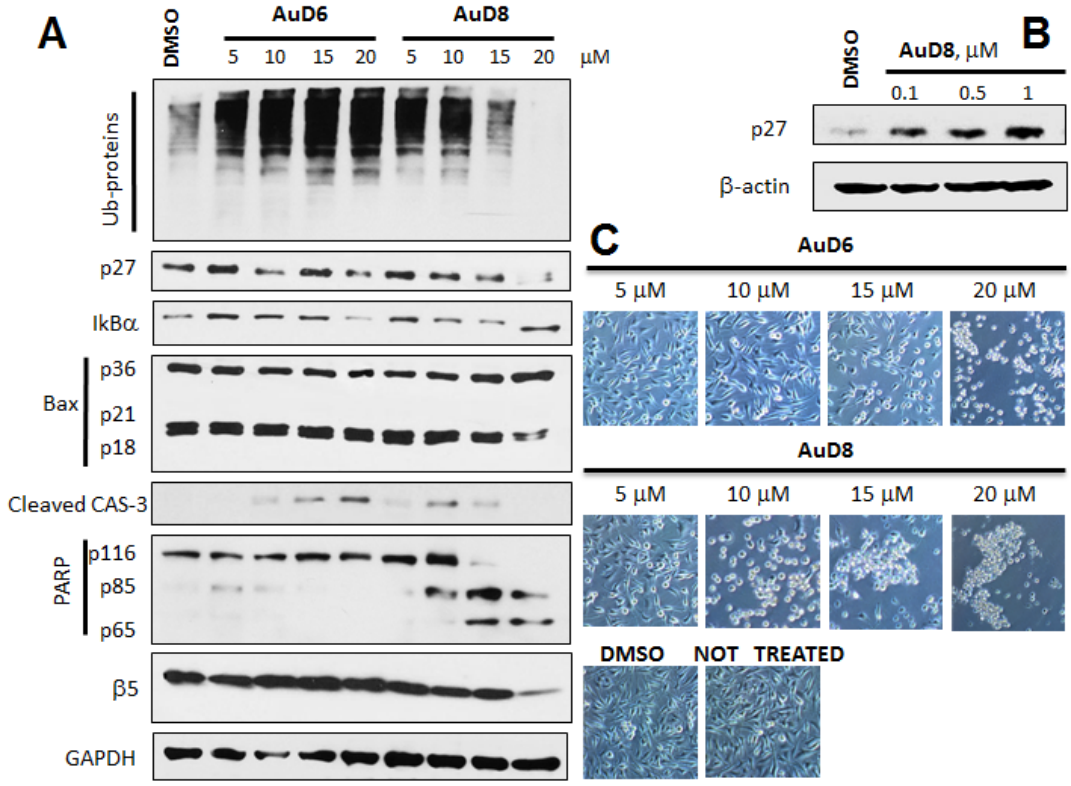

Figure 2.3. **A**, Western blot analysis of breast cancer MDA-MB-231 cell extracts. Cells were treated with the complexes AuD6 and AuD8 at the indicated concentrations for 24 h. **B**, Western blot analysis of the p27 protein amount in MDA-MB-231 cell extract after treatment with the compound AuD8 at the indicated concentrations for 24 h. The solvent DMSO was used as a control while GAPDH as a loading control. **C**, Apoptotic morphological changes of MDA-MB-231 cells after treatment with AuD6 and AuD8 at the indicated concentrations for 24 h (phase contrast imaging, 100X magnification).

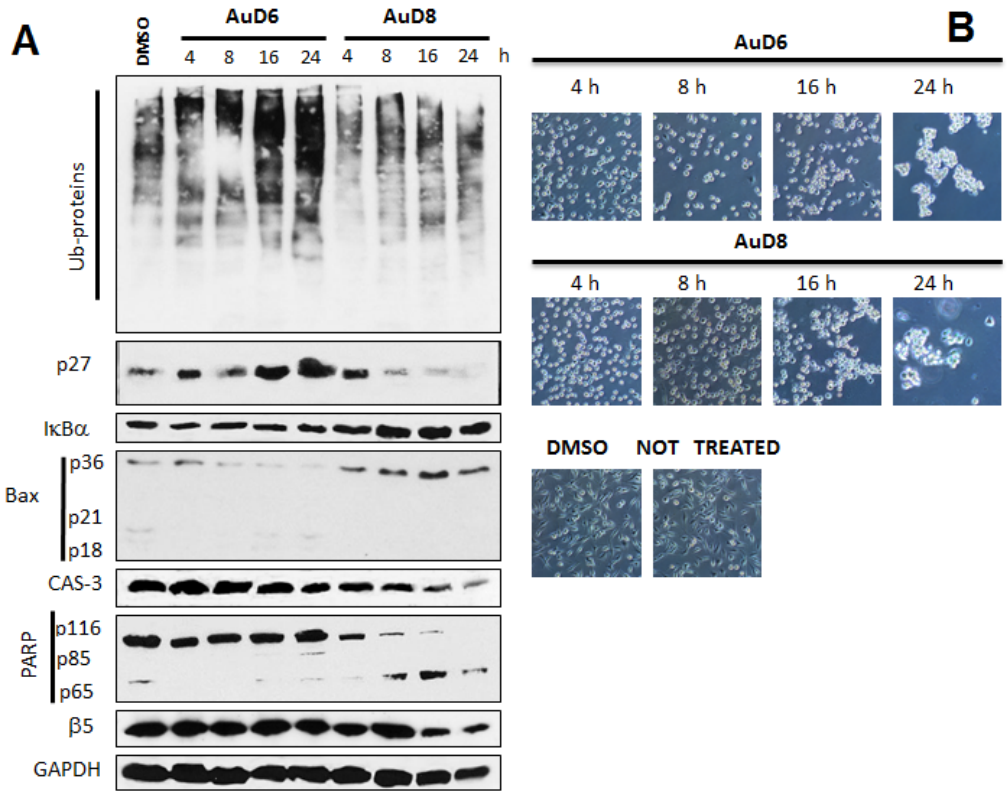

Figure 2.4. A, Western blot analysis of breast cancer MDA-MB-231 cell extracts. Cells were treated with the complexes AuD6 and AuD8 (20 μM) over the indicated times. The solvent DMSO was used as a control while GAPDH as a loading control. **B**, Apoptotic morphological changes of MDA-MB-231 cells after treatment with AuD6 and AuD8 at 20 μM for the indicated times (phase contrast imaging, 100X magnification).

To further confirm that cell death takes place *via* apoptosis, we carried out an Annexin V/Propidium Iodide (PI) assay. MDA-MB-231 cells were treated with AuD6 or AuD8 for 16 or 24 h at 20 μM. Cells were then harvested and stained with Annexin-V FITC and PI prior to flow cytometry. Remarkably, the amount of cells undergoing non-apoptotic cell death was comparable to the solvent control (**Figure 2.5**). After 16 h treatment with AuD8 the majority of cell death (62.9%) occurred by apoptosis (late stage) and this percentage further increased after 24 h (74.1%). Although both compounds showed similar percentages of cells in early stage apoptosis (around 7-9%), AuD6 proved less potent than AuD8 as it induced late stage apoptosis in only 49% of cells after 24 h.

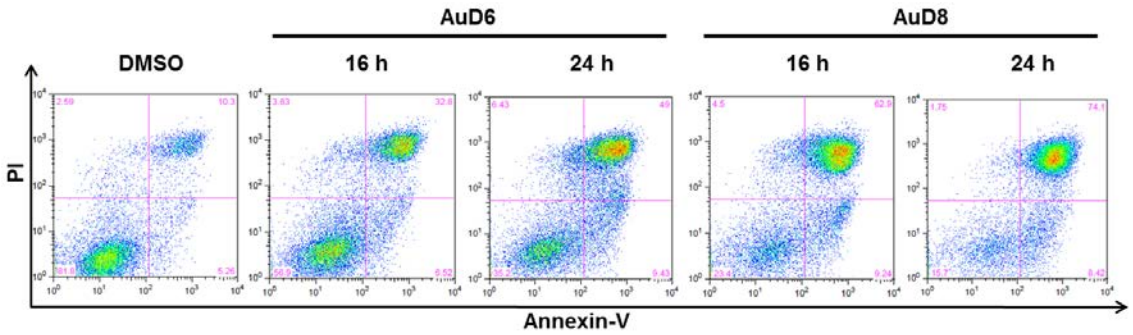

Figure 2.5. MDA-MB-231 cells were treated with the complexes AuD6 and AuD8 (20 μM) for 16 and 24 h. Then, cells were labeled with Annexin–V FITC and PI and analyzed by flow cytometry in order to evaluate the percentage of apoptotic cells. Apoptotic cells at early stage occur in the lower right quadrant while apoptotic cells at late stage set in the up-right part. The percentage in the lower left quadrant is due to viable cells whereas the upper left part to non-apoptotic cell death.

***In vivo* experiments.** We investigated the anticancer activity of both compounds *in vivo* in female athymic nude mice bearing human breast cancer MDA-MB-231 xenografts. During treatment mice did not display signs of fatigue, weight loss or anorexia and were sacrificed after 27 days of treatment (1.0 mg kg^{-1} d^{-1}), when control tumors reached approximately 1,800 mm^3. AuD8 showed slightly higher anticancer activity than AuD6 (**Figure 2.6.A**); AuD8-treated tumors grew to 849 ± 79 mm^3, corresponding to 53% inhibition of tumor growth compared to control. However, if only the most responsive mice are taken into account (40%), 85% inhibition was observed after 13 days (**Figure 2.6.B**), with some mice exhibiting tumor shrinkage. Tumors were collected and weighed, followed by immunohistochemical staining, Western blot analysis and proteasome and caspase-3 activity assays.

The immunohistochemical data in mouse xenografts indicate that AuD8 treatment resulted in a significant (~95%) increase in levels of p27 expression compared to control (**Figure 2.6.C**). A moderate increase (~20%) in p27 was observed following AuD6 treatment. These results are similar to those seen *in vitro*, with AuD8 being a more potent proteasome inhibitor than AuD6. Western blot analysis confirmed the proteasome-inhibitory activity of these gold-based compounds. AuD8 is slightly more potent toward IκB-α and Bax accumulation than AuD6 (**Figure 2.7.A-B**). Additionally, AuD8 was a more potent proteasome inhibitor than AuD6, resulting in 33% and 14% inhibition of the CT-like pocket, respectively (**Figure 2.7.D**).

Proteasome inhibition *in vivo* was accompanied by apoptosis induction in tumors treated with these gold compounds. AuD6 treatment resulted in a higher level of TUNEL positivity

compared to AuD8 treatment (~75% vs. ~30%; **Figure 2.6.C**). Consistently, AuD6 was a more potent activator of caspase-3 than AuD8 (**Figure 2.7.C**). These data could suggest that proteasome inhibition may not be the only major mechanism responsible for apoptotic cell death mediated by these gold compounds. In summary, these gold-based compounds showed potent proteasome-inhibitory and apoptosis-inducing activities *in vivo*.

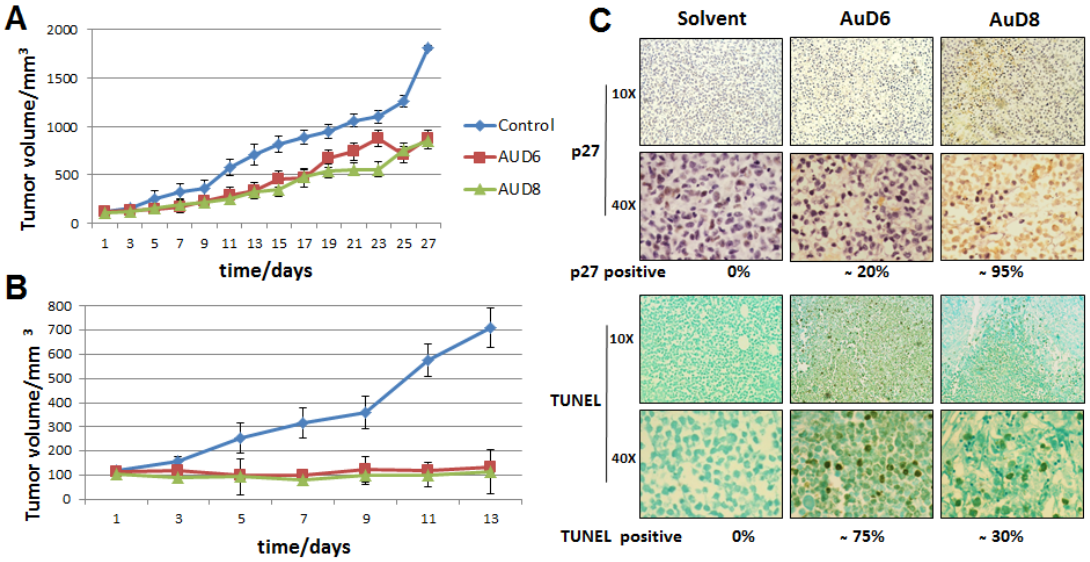

Figure 2.6. Female nude mice bearing MDA-MB-231 tumors were treated with either vehicle (control) or the compounds AuD6 and AuD8 at 1 mg kg^{-1} d^{-1}. Inhibition of tumor growth by both complexes (**A**). Tumor volumes were measured every other day using a caliper. Points represent the mean ± SD (bars) of seven mice per group. If only the most responsive mice are considered, the xenograft growth inhibition is greater (**B**). Immunohistochemical p27 and TUNEL staining of tumor samples indicates proteasome inhibition and apoptosis as a result of both compounds. Stronger p27 staining is observed following AuD8 treatment, and more TUNEL positive cells are observed following AuD6 treatment. Brown colored cells are considered positive (**C**).

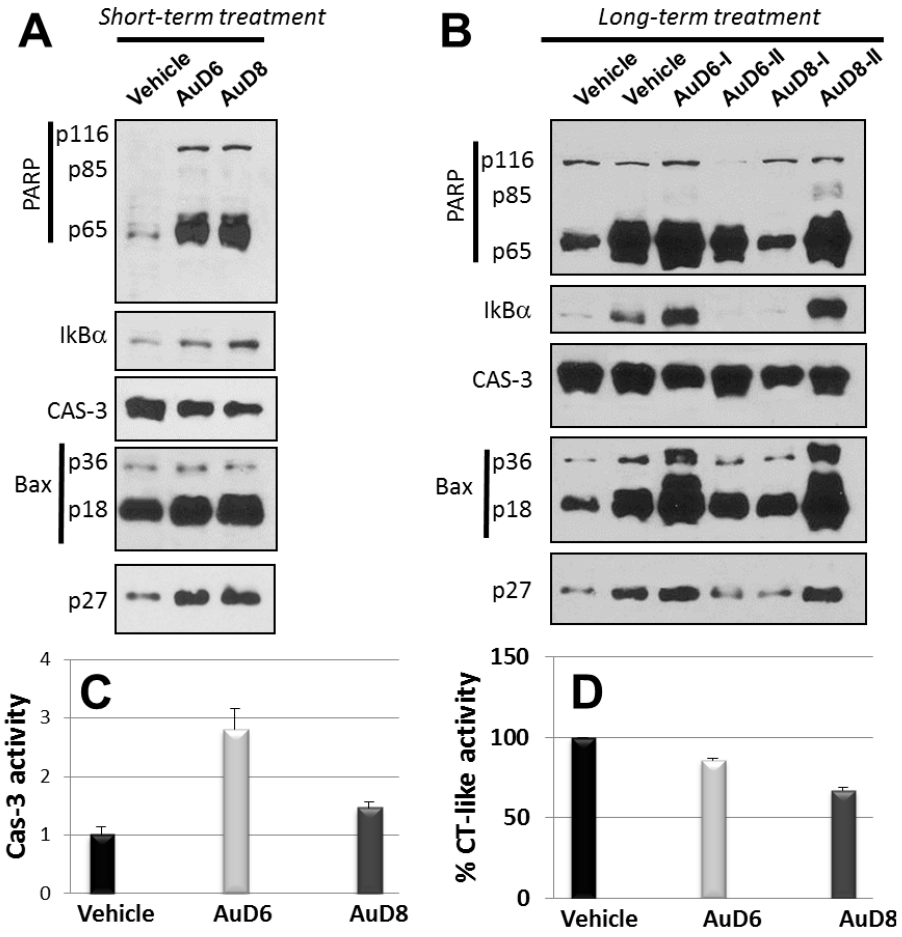

Figure 2.7. Female nude mice bearing MDA-MB-231 tumors were treated with either vehicle (control) or the compounds AuD6 and AuD8 at 1 mg kg^{-1} d^{-1}. Tumors were collected and the corresponding tissues prepared for Western blot analysis after either 13-day treatment (**A**) or 27-day treatment (**B**) [I and II denote distinct experiments]. Tissues were also prepared for the assays of caspase-3 activity (**C**) and of proteasomal CT-like activity (**D**) after 27 days of treatment.

2.2. Discussion of the experimental data

In this preclinical investigation, we have found that the gold(III) dithiocarbamato-peptide derivatives AuD6 and AuD8 were able to inhibit MDA-MB-231 tumor growth both *in vitro* (IC_{50} = 6.5 ± 0.6 and 17 ± 1 μM, respectively) and *in vivo* at a low dose of 1.0 mg kg^{-1} per day. The MDA-MB-231 cell line is a triple-negative breast cancer (TNBC), usually associated with poor prognosis and lack of benefit from both hormonal therapies (based on estrogen and progesterone receptor antagonists) and monoclonal antibody therapy targeting the human epidermal growth factor receptor 2.[20] Thus, MDA-MB-231 tumors develop aggressively and frequently lead to early gastrointestinal metastases.[21] Notably, 53% inhibition of human breast cancer xenograft growth compared to control treatment was

observed after 27 days (**Figure 2.6.A**). Six mice (three for each compound) showed 85% inhibition and, in some cases, tumor shrinkage after 13 days of treatment (**Figure 2.6.B**). Remarkably, mice appeared healthy and very active throughout the treatment; in fact, they showed neither signs of fatigue nor weight loss, indicating little to no systemic toxicity. Unexpectedly, our gold compounds showed comparable anticancer activity toward the xenografts. In fact, contrary to the results observed *in vitro* after 24 h treatment, AuD6 was as active as AuD8 in both the short- and long-term treatments, highlighting the significance of animal models due to the varied physiology of tumor tissues. Overall, the toxicological and anticancer activity results point out that the design of our compounds proved very successful in both stabilizing the heavy metal center and in avoiding the aspecific reactivity of the compound occurring in healthy tissues that could give rise to systemic toxicity.[22]

Being coordination compounds of a redox-active noble metal, we have investigated whether ROS species are generated in the cellular milieu after treatment. If MDA-MB-231 cells are pretreated with 100 μM Trolox for 1 h, no change in the cytotoxic profile of the complexes is observed after 24 h (**Figure 2.1**). On the contrary, when tumor cells are co-treated with either of our compounds and the ROS scavenger for 24 h an enhancement of the anticancer activity is detected, showing a synergistic effect in agreement with literature data.[23] Therefore, cell death commitment is triggered by apoptotic mechanisms independent of free radicals formed *in situ* (*see below*).

Interestingly, it is known that cancerous cells are more sensitive than normal ones to apoptosis-inducing signals. In this regard, in spite of initial skepticism, proteasome inhibition has proven a winning strategy to treat malignancies. The ubiquitin-proteasome system (UPS) plays a major role in several intracellular processes such as cell cycle progression, apoptosis, DNA damage and repair, endocytosis, drug resistance, angiogenesis and cell differentiation,[4, 8] In tumor cells protein homeostasis is unbalanced, rendering cancer cells more sensitive to inhibitors of the UPS than normal cells.[24] Bortezomib (Velcade®), a dipeptidyl boronic acid, is the first-in-class proteasome inhibitor, approved by the FDA in 2003 for the treatment of some hematologic malignancies including multiple myeloma.[25] In addition, it is also the first boron-containing inorganic pharmaceutical. As described in the introduction of this thesis, Bortezomib forms a reversible covalent complex with the proteasomal β5 subunit, thus blocking proteolysis and therefore leading to cell death.[26] The drug mainly targets the proteasomal β5 active site (β5> β1>> β2) but its binding to the three subunits essentially occurs in the same way.[27] Indeed, due to its Lewis acidity, boron binds to the oxygen atom

on the side chain of the *N*-terminal threonine (Thr1O$^{\gamma}$) of each subunit, thus yielding a proteasomal Thr1O$^{\gamma}$-drug tetrahedral complex. Our gold compounds are also potent proteasome inhibitors and although AuD6 and AuD8 closely resemble cisplatin (i.e., square planar geometry with a d^8 electronic configuration), the latter is not a proteasome inhibitor, possibly explaining the resistance of MDA-MB-231 cells to cisplatin (IC_{50} > 100 μM after 24 h) *in vitro*. Like bortezomib, our compounds are electrophilic species. Being coordination compounds[8], both types of inhibitors consist of an electrophilic trap, the semimetal element boron for the former and the metal center Au(III) for the latter. In its compounds, boron may form an extra reversible bond in order to complete the octet whereas the transition metal gold(III) forms four covalent bonds in a square-planar geometry *via* an associative mechanism. Similar to boron in bortezomib, the metal center Au(III) could bind to the proteasomal active sites, likely irreversibly, but, differently from boron, it may also be involved in a redox process that would lead to the formation of gold(I)-containing species or metallic gold by oxidation of some residue of the multicatalytic protease such as the nucleophilic threonine.

In vitro AuD8 showed a degree of selectivity toward the β5 subunit (CT-like). As mentioned above, in addition to chymotrypsin-like activity, BrAAP and SNAAP activities are ascribed to the β5 subunit as well.[18] Overall, these properties could account for the selectivity observed for AuD8 toward the β5 subunit in the cell-free system. In fact, considering the peptide portion of our inhibitors, AuD8 is slightly more hydrophobic and more branched than AuD6. AuD6 showed no selectivity toward a specific proteolytic subunit as comparable IC_{50} values were observed for all three activities in both the purified proteasome and MDA-MB-231 cell extracts (**Table 2.1**). Importantly, it has been shown that targeting the chymotrypsin-like activity is associated with apoptosis induction in cancer cells.[5] However, recently, co-targeting the PGPH-like and/or trypsin-like sites has been suggested as a new strategy in treating malignancies because it increases the cytotoxicity of proteasome inhibitors.[28,29] Based on this finding, Goldberg *et al*. reported that when one proteolytic activity is inhibited, the two others are increasingly important in protein breakdown and the subsequent inactivation of either of the remaining catalytic sites has a greater effect on decreasing proteolysis than when one site alone is inhibited. Thus, the complete or near complete inhibition of all three sites seems to be required to induce cell death.[28] Accordingly, we hypothesize that a cascade effect on the different proteasomal subunits may take place after interaction of the multicatalytic protease with our metal complexes.

In this work, we observed morphological changes such as shrinkage and characteristic apoptotic blebbing with increasing compound concentration or over time (**Figures 2.3.C** and **2.4.B**). In kinetic experiments, cells treated with both compounds detached and rounded up after only 4 h and these apoptotic features were significantly enhanced after 24 h. In dose-dependent studies, cells treated with AuD6 only appeared detached and clustered at 20 μM whereas several shrunken cells were observed upon treatment with AuD8 at 10 μM in good agreement with the calculated IC_{50} values. Notably, Annexin V-FITC staining confirmed that cell death takes place *via* apoptosis rather than necrosis. In fact, high percentages of cells undergoing apoptosis were observed after 16 h and 24 h treatments, with higher values recorded for AuD8 (**Figure 2.5**). Similarly, after treatment, Bax (fragments p36 or p18) and IκB-α levels increased with generally less intense bands observed for AuD6 (**Figures 2.3.A, 2.4.A, 2.7.A-B**). Interestingly, p21/Bax fragment hydrolysis is usually followed by release of mitochondrial cytochrome c, activation of caspase-3 and cleavage of poly(ADP-ribose) polymerase (PARP), leading to apoptotic cell death. Upon activation, caspase-3 is able to hydrolyze PARP, explaining the disappearance of intact PARP (116 kDa) and the appearance of the characteristic fragments p65 and p85. The accumulation of ubiquitinated proteins and the proteasomal target protein p27 suggests that the observed apoptotic death is related to proteasome inhibition both *in vitro* (**Figures 2.3.A, 2.4.A**) and *in vivo* (**Figure 2.7.A-B-D**). Notably, AuD8 was able to induce p27 accumulation at treatment concentrations below 1 μM (**Figure 2.3.B**). Additionally, to validate the proteasome-inhibitory and apoptosis-inducing activities *in vivo*, we performed tests using tumor xenografts. IHC staining shows increased p27 staining in both AuD6 and AuD8 treated tumors, demonstrating proteasome inhibition *in vivo* (**Figure 2.6.C**). Furthermore, increased TUNEL positivity was detected in xenografts treated with both compounds, indicating apoptotic cell death *in vivo* (**Figures 2.6.C-2.7.C**). However, apoptosis induction may not be solely due to the proteasome-inhibitory abilities of these gold compounds, because while AuD8 treatment resulted in greater p27 staining than AuD6, AuD6 treatment caused stronger TUNEL staining. Thus, multiple targets may be responsible for cancer cell death triggered by these gold compounds.

In conclusion, since the proteasome has been identified as a major *in vivo* and *in vitro* target of our compounds, we aimed to elucidate the mechanism of inhibition of this important multicatalytic protease by AuD8 (used as a model compound) at the atomic level (§ *Chapter 3*). In addition, another biomolecule has been taken into account in this work and its

interaction with AuD8 has been studied by circular dichroism and fluorescence (§ *Chapter 4*).

Chapter 2 references

(1) Negom Kouodom, M.; Ronconi, L.; Celegato, M.; Nardon, C.; Marchiò, L.; Dou, Q. P.; Aldinucci, D.; Formaggio, F.; Fregona, D. Toward the Selective Delivery of Chemotherapeutics into Tumor Cells by Targeting Peptide Transporters: Tailored Gold-Based Anticancer Peptidomimetics. *J. Med. Chem.* **2012**, *55*, 2212-2226.

(2) Kouodom, M. N.; Boscutti, G.; Celegato, M.; Crisma, M.; Sitran, S.; Aldinucci, D.; Formaggio, F.; Ronconi, L.; Fregona, D. Rational Design of Gold(III)-Dithiocarbamato Peptidomimetics for the Targeted Anticancer Chemotherapy. *J. Inorg. Biochem.* **2012**.

(3) Tanaka, K. The Proteasome: Overview of Structure and Functions. *Proc. Jpn. Acad. Ser. B Phys. Biol. Sci.* **2009**, *85*, 12-36.

(4) Groll, M.; Ditzel, L.; Löwe, J.; Stock, D.; Bochtler, M.; Bartunik, H. D.; Huber, R. Structure of 20S Proteasome from Yeast at 2.4 Å Resolution. *Nature* **1997**, *386*, 463-471.

(5) An, B.; Goldfarb, R. H.; Siman, R.; Ping Dou, Q. Novel Dipeptidyl Proteasome Inhibitors Overcome Bcl-2 Protective Function and Selectively Accumulate the Cyclin-Dependent Kinase Inhibitor p27 and Induce Apoptosis in Transformed, but Not Normal, Human Fibroblasts. *Cell Death Differ.* **1998**, *5*, 1062-1075.

(6) Groll, M.; Heinemeyer, W.; Jäger, S.; Ullrich, T.; Bochtler, M.; Wolf, D. H.; Huber, R. The Catalytic Sites of 20S Proteasomes and their Role in Subunit Maturation: A Mutational and Crystallographic Study. *Proc. Natl. Acad. Sci. U. S. A.* **1999**, *96*, 10976-10983.

(7) Groll, M.; Huber, R. Inhibitors of the Eukaryotic 20S Proteasome Core Particle: A Structural Approach. *Biochim. Biophys. Acta Mol. Cell Res.* **2004**, *1695*, 33-44.

(8) Dalla Via, L.; Nardon, C.; Fregona, D. Targeting the Ubiquitin-Proteasome Pathway with Inorganic Compounds to Fight Cancer: A Challenge for the Future. *Future Medicinal Chemistry* **2012**, *4*, 525-543.

(9) Daniel, K. G.; Chen, D.; Orlu, S.; Cui, Q. C.; Miller, F. R.; Dou, Q. P. Clioquinol and Pyrrolidine Dithiocarbamate Complex with Copper to Form Proteasome Inhibitors and Apoptosis Inducers in Human Breast Cancer Cells. *Breast Cancer Res.* **2005**, *7*, R897-R908.

(10) Chen, D.; Daniel, K. G.; Chen, M. S.; Kuhn, D. J.; Landis-Piwowar, K. R.; Dou, Q. P. Dietary Flavonoids as Proteasome Inhibitors and Apoptosis Inducers in Human Leukemia Cells. *Biochem. Pharmacol.* **2005**, *69*, 1421-1432.

(11) Yang, H.; Chen, D.; Qiuzhi, C. C.; Yuan, X.; Dou, Q. P. Celastrol, a Triterpene Extracted from the Chinese "Thunder of God Vine," is a Potent Proteasome Inhibitor and Suppresses Human Prostate Cancer Growth in Nude Mice. *Cancer Res.* **2006**, *66*, 4758-4765.

(12) Provencher-Mandeville, J.; Debnath, C.; Mandal, S. K.; Leblanc, V.; Parent, S.; Asselin, E.; Bérubé, G. Design, Synthesis and Biological Evaluation of Estradiol-PEG-Linked Platinum(II) Hybrid Molecules: Comparative Molecular Modeling Study of Three Distinct Families of Hybrids. *Steroids* **2011**, *76*, 94-103.

(13) Hong, Y.; Yang, J.; Wu, W.; Wang, W.; Kong, X.; Wang, Y.; Yun, X.; Zong, H.; wei, Y.; Zhang, S.; Gu, J. Knockdown of BCL2L12 Leads to Cisplatin Resistance in MDA-MB-231 Breast Cancer Cells. *Biochim. Biophys. Acta Mol. Basis Dis.* **2008**, *1782*, 649-657.

(14) Ronconi, L.; Marzano, C.; Zanello, P.; Corsini, M.; Miolo, G.; Maccà, C.; Trevisan, A.; Fregona, D. Gold(III) Dithiocarbamate Derivatives for the Treatment of Cancer: Solution Chemistry, DNA Binding, and Hemolytic Properties. *J. Med. Chem.* **2006**, *49*, 1648-1657.

(15) Arellano, J. B.; Li, H.; González-Pérez, S.; Gutiérrez, J.; Melø, T. B.; Vacha, F.; Naqvi, K. R. Trolox, a Water-Soluble Analogue of A-Tocopherol, Photoprotects the Surface-Exposed Regions of the Photosystem II Reaction Center in Vitro. is this Physiologically Relevant? *Biochemistry (N. Y.)* **2011**, *50*, 8291-8301.

(16) Milacic, V.; Chen, D.; Ronconi, L.; Landis-Piwowar, K. R.; Fregona, D.; Dou, Q. P. A Novel Anticancer Gold(III) Dithiocarbamate Compound Inhibits the Activity of a Purified 20S Proteasome and 26S Proteasome in Human Breast Cancer Cell Cultures and Xenografts. *Cancer Res.* **2006**, *66*, 10478-10486.

(17) Zhang, X.; Frezza, M.; Milacic, V.; Ronconi, L.; Fan, Y.; Bi, C.; Fregona, D.; Dou, Q. P. Inhibition of Tumor Proteasome Activity by Gold-Dithiocarbamato Complexes Via both Redox-Dependent and -Independent Processes. *J. Cell. Biochem.* **2010**, *109*, 162-172.

(18) Groll, M.; Heinemeyer, W.; Jäger, S.; Ullrich, T.; Bochtler, M.; Wolf, D. H.; Huber, R. The Catalytic Sites of 20S Proteasomes and their Role in Subunit Maturation: A Mutational and Crystallographic Study. *Proc. Natl. Acad. Sci. U. S. A.* **1999**, *96*, 10976-10983.

(19) Gao, G.; Dou, Q. P. N-Terminal Cleavage of Bax by Calpain Generates a Potent Proapoptotic 18-kDa Fragment that Promotes Bcl-2-Independent Cytochrome C Release and Apoptotic Cell Death. *J. Cell. Biochem.* **2000**, *80*, 53-72.

(20) Yang, L.; Wu, X.; Wang, Y.; Zhang, K.; Wu, J.; Yuan, Y. -.; Deng, X.; Chen, L.; Kim, C. C. H.; Lau, S.; Somlo, G.; Yen, Y. FZD7 has a Critical Role in Cell Proliferation in Triple Negative Breast Cancer. *Oncogene* **2011**, *30*, 4437-4446.

(21) Kassam, F.; Enright, K.; Dent, R.; Dranitsaris, G.; Myers, J.; Flynn, C.; Fralick, M.; Kumar, R.; Clemons, M. Survival Outcomes for Patients with Metastatic Triple-Negative Breast Cancer: Implications for Clinical Practice and Trial Design. *Clinical Breast Cancer* **2009**, *9*, 29-33.

(22) Ronconi, L.; Fregona, D. The Midas Touch in Cancer Chemotherapy: From Platinum- to Gold-Dithiocarbamato Complexes. *Dalton Transactions* **2009**, 10670-10680.

(23) Zheng, J.; Payne, K.; Taggart, J. E.; Jiang, H.; Lind, S. E.; Ding, W. -. Trolox Enhances Curcumin's Cytotoxicity through Induction of Oxidative Stress. *Cellular Physiology and Biochemistry* **2012**, *29*, 353-360.

(24) Adams, J. Potential for Proteasome Inhibition in the Treatment of Cancer. *Drug Discov. Today* **2003**, *8*, 307-315.

(25) Bross, P. F., et al Approval Summary for Bortezomib for Injection in the Treatment of Multiple Myeloma. *Clin. Cancer Res.* **2004**, *10*, 3954-3964.

(26) Groll, M.; Berkers, C. R.; Ploegh, H. L.; Ovaa, H. Crystal Structure of the Boronic Acid-Based Proteasome Inhibitor Bortezomib in Complex with the Yeast 20S Proteasome. *Structure* **2006**, *14*, 451-456.

(27) Berkers, C. R.; Verdoes, M.; Lichtman, E.; Fiebiger, E.; Kessler, B. M.; Anderson, K. C.; Ploegh, H. L.; Ovaa, H.; Galardy, P. J. Activity Probe for in Vivo Profiling of the Specificity of Proteasome Inhibitor Bortezomib. *Nature Methods* **2005**, *2*, 357-362.

(28) Kisselev, A.F.; Callard, A.; Goldberg, A.L., Importance of the different proteolytic sites of the proteasome and the efficacy of inhibitors varies with the protein substrate. *J Biol Chem*,**2006**, *281*, 8582-8590.

(29) Kisselev, A.F., Van Der Linden, W.A. & Overkleeft, H.S., Proteasome inhibitors: An expanding army attacking a unique target. *Chemistry and Biology* , 2012, *19*, 99-115.

Chapter 3. Crystallographic investigation of the inhibition mechanism of 20S proteasome by gold(III)-based peptidomimetics

Since the prominent intracellular enzyme proteasome has been recognized as a major target for our compounds (*Chapter 2*), we directed our efforts to elucidate how it is inhibited by AuD8, chosen as a model compound, at the atomic level.

At the best of our knowledge, 20S proteasome co-crystallized with a metal-based inhibitor has not been reported yet. However, recently structures of some covalent and not-covalent 20S proteasome – small organic molecule complexes have been solved. [1, 2] Based on the the same phylogenetic origin (similar amino acid sequence) shared by human 20S proteasome and the *Saccharomyces Cerevisiae* counterpart[3], thus yielding related structures, we have exploited yeast cultures to obtain huge amounts of the enzyme. From the biotechnological point of view, *Saccharomyces Cerevisiae* (also referred to as baker's yeast) is an organism suitable for the production of *ad-hoc* strains able to generate specific tagged forms of 20S proteasome by means of combined biochemical and genetic approaches.

Regarding the 20S proteasome extraction from the eukaryotic cells of baker's yeast and subsequent purification, a protocol has been progressively set up, leading to the successful crystallization of the purified enzyme. Afterwards, the interaction between the biomolecule and AuD8 has been performed under several favorable conditions including incubation with sodium dodecyl sulfate at 0.04% (w/v) and heating. Plenty of crystallization tests were carried out but all turned out to be unfruitful so far, thus the mechanism of inhibition of the enzyme has not been elucidated yet. In addition, the crystallization trials were carried out by both crystal soaking (*diffusion of the inhibitor through the crystal)* and co-crystallization approach.

This part of the work was performed in collaboration with the Structural Biology research group directed by Prof. Giuseppe Zanotti (Dept. of Biomedical Sciences, University of Padova).

3.1. The ubiquitin-proteasome pathway

Intracellular proteolysis is an outstanding process for the turnover of many critical proteins involved in a huge number of metabolic pathways.[4] In eukaryotes the non-lysosomal protein degradation is carried out by the strictly controlled complex enzymatic machinery of the ubiquitin-proteasome pathway. The ubiquitin-proteasome system (UPS) is essential to maintain normal cellular homeostasis and it is involved in almost all basic cellular processes, including the removal of abnormal, misfolded or improperly assembled proteins, stress response (by processing or degrading transcriptional regulators), cell-cycle progression (by degradation of cyclins), cell differentiation and metabolic adaption (by destruction of transcription factors, metabolic enzymes or short-lived regulatory species), proliferation, apoptosis, inflammation, and the cellular immune response (by generating antigenic peptides presented by major histocompatibility complex (MHC) class I molecules).[5, 6]

The mechanism of degradation is constituted by strictly successive steps: protein substrates selected for destruction are bioconjugated to poly-ubiquitin chains, thus being recognized and digested by the 30S proteasome enzyme, a 2,500 kDa multicatalytic molecular machine (*for more details about its structure and functions see 1.3 section*). Ubiquitin is a highly conserved 76-amino acid protein whose omopolymerized chains and covalently linked to the target proteins act as degradation signal, thus determining their shuttle to the proteasome.[5] The covalent attachment of a chain consisting of at least four ubiquitin molecules occurs through the concerted actions of a network of proteins, including the E1 (ubiquitin-activating), E2 (ubiquitin-conjugating) and E3 (ubiquitin-ligating) enzymes (**Figure 3**).[5] For accurate selection of the proteins to be degraded, numerous enzymes are involved in this cascade process. Furthermore, it is worth highlighting that ubiquitylation is a reversible reaction due to the intracellular presence of many **de**-**ub**iquitylating cysteine-protease and metalloprotease enzymes (DUBs). Interestingly, the human genome encodes approximately 95 putative DUBs.[5]

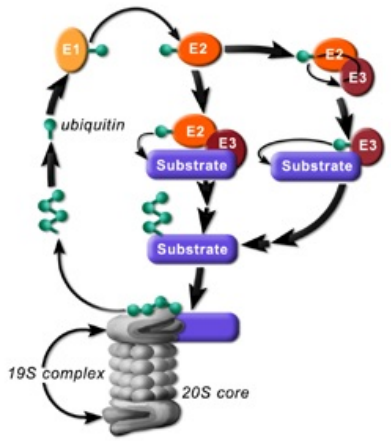

Figure 3.1. The ubiquitin-proteasome pathway. A three-stepped highly regulated enzymatic process involving an Ub-activating (E1), Ub-conjugating (E2), and Ub-ligating (E3) enzymes is able to covalently modify a target protein. Once multiple ubiquitin molecules are attached to the target protein, it is escorted to the proteasome, recognized by the 19S cap, de-ubiquinated and then degraded by the catalytic 20S core into oligopeptides. The ubiquitin molecules are released and recycled.

In addition, certain DUBs are responsible for the maturation of ubiquitin from its precursor proteins and product of genes that encode polyubiquitin or ubiquitin fused with ribosomal proteins. Other DUBs function at the initial stage during the breakdown of ubiquitin-tagged proteins to allow ubiquitins to be recycled.

With few exceptions, only proteins containing polyubiquitin chains on sequential lysine residues are recognized and degraded by the proteasome. The best-known ubiquitin-independent proteasome substrate is the ornithine decarboxylase enzyme. Although subject to ubiquitin-dependent degradation, cell-cycle regulators p53 and p21 are also degraded via ubiquitin-independent mechanisms.[7] Finally, under conditions of cellular stress, many structurally aberrant, misfolded, or highly oxidized proteins could also be degraded by the ubiquitin-independent proteosomal degradation.[7]

3.2. An overview of yeast proteasome structure and functions

As aforementioned, the proteasome is a large multimeric protease complex with a central role in protein degradation in both the cytosol and the nucleus, generating oligopeptides ranging in length from 3 to 15 amino-acid residues.[4, 5] The resulting peptide products are subsequently hydrolyzed to amino acids by oligopeptidases and/or amino-carboxyl peptidases.[4, 5] Among the proteasomal enzymes, the most studied is the 30S proteasome whose molecular weight is 2,500 kDa; sometimes 30S proteasome is improperly called 26S proteasome. 30S proteasome is formed by a barrel-shaped multicatalytic complex referred to as the 20S proteasome core particle (CP), capped at each end by a regulatory component termed the 19S complex (regulatory particle, RP or PA700) (**Figure 3.2**).[4] The

role of the 19S particles is to recognize ubiquitinated client proteins, and regulate protein entry to the 20S core by playing a key role in their unfolding and translocation into the proteolytic chamber of the CP. The size difference between the 26S and 30S proteasomes is due to the attachment of one or two (located on each side of the catalytic core) 19S RPs to the 20S proteasome, respectively. The elongated 30S macromolecule is likely the functional unit in the cell.[6]

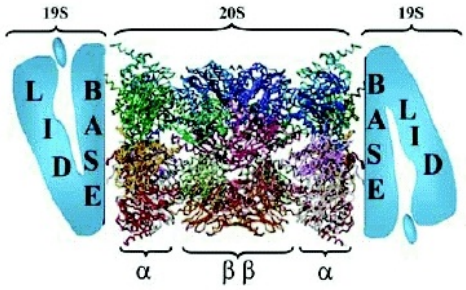

Figure 3.2. Composition scheme of 30S proteasome.

The CP (molecular weight of approximately 750 kDa) consists of four heptameric, tightly and axially stacked, rings to form a cylinder-like structure with the two outer rings composed of seven different α-type subunits and two inner rings consisting of seven different β-type subunits, following an $\alpha_{1-7}\beta_{1-7}\beta_{1-7}\alpha_{1-7}$ stoichiometry (**Figure 3.3**).[4] These subunits, listed in **Table 3.1**, are placed within the complex with C2 simmetry, and the α- and β- nomenclature reflects their location in the 20S proteasome. Starting with the α-subunit Prs2 and the β-subunit Pre3, which touch the diad axis, the α- and β-subunits have been numbered according to their position on the ring, proceeding in counterclockwise orientation as seen in head-on views of the multicatalytic complex.[4, 8] (**Figure 3.3**).

Table 3.1. Nomenclature and features of 20S proteasome subunits.
The exchangeable subunits in the "immuno" proteasome are marked with an "i".

New systematic name	Traditional name *S. Cerevisiae*	Traditional name *Homo sapiens*	Molecular weight/kDa human (yeast)	amino acids human (yeast)
α1_sc	SCL1/YC7/Prs2	PROS-27 (Iota)	27.4 (34.6)	246 (252)
α2_sc	Y7/Pre8	HC3	25.9 (27)	234 (250)
α3_sc	Y13/Pre9	HC9	29.5 (28.6)	261 (258)
α4_sc	Pre6	HC6/XAPC7	27.9 (28.3)	248 (254)
α5_sc	Pup2/DOA5	Zeta	26.4 (28.6)	241 (260)
α6_sc	Pre5	HC2	29.6 (25.6)	263 (234)
α7_sc	YC1/Prs1/Pre10	HC8	28.4 (31.4)	255 (288)
β1_sc	Pre3	Y/delta	25.3 (16.2)	239 (215)
β1i_hs		Lmp2	23.2	219
β2_sc	Pup1	Z	30.0 (25)	277 (261)
β2i_hs		Mecl1	28.9	273
β3_sc	Pup3	C10	22.9 (22.6)	205 (205)
β4_sc	C11/Pre1	HC7	22.8 (22.5)	201 (198)
β5_sc	Pre2/DOA3	X/MB1/epsilon	22.9 (23.3)	263 (287)
β5i_hs		Lmp7	30.4	276
β6_sc	C5/Prs3/Pre7	HC5	26.5 (24.8)	241 (241)
β7_sc	Pre4	HN3/beta	29.2 (25.9)	264 (266)

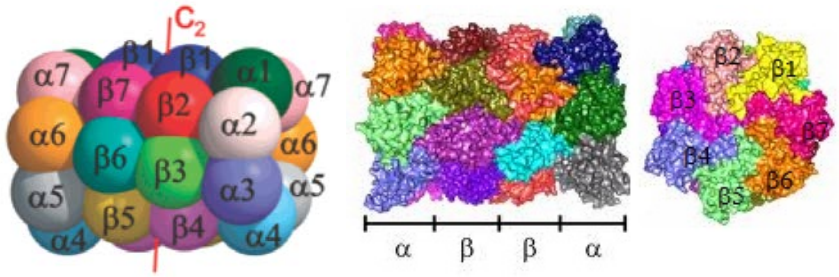

Figure 3.3. From left to right: topology of the 28 subunits of the 20S proteasome drawn as spheres, side view and front view of the enzyme by a space-filling visualization.

Interactions between sequence-specific contact surfaces of the various α- and β-type subunits (insertions and extensions) determine the unique locations of the individual subunits, and thus the overall assembly of the CP. For instance, the longest *C*-terminal extension, that of β2 (Pup1), embraces β3 (Pup3) subunit, and touches the next nearest neighbor, β4 (C11), contributing important *cis* contacts (within one β-ring). The most prominent *trans* contact

(between two β–rings) is mediated by β7 (Pre4). Its terminus inserts into a channel formed between the subunits β1 (Pre3) and β2 (Pup1) on the opposite ring.[6]

The overall structures and functions of the individual subunits are highly conserved among eukaryotic species, except for a specialized CP form that is associated with adaptive immune responses. Indeed, the yeast (*Saccharomyces Cerevisiae*) and mammalian (bovine) 20S proteasomes are characterized by the same highly ordered quaternary structures, as demonstrated by X-ray crystallography.[5] The distinguishing multiple peptidase activity of the eukaryotic 20S proteasomes is confined inside the inner cavity at distinct active sites located at the β-subunits. Moreover, proteolysis occurs within catalytic pockets of only three β–subunits (β1, β2, and β5), which harbour active threonine residues at their *N* termini and show *N*-terminal nucleophile (Ntn) hydrolase activity. It is worth noting that the proteasome is a threonine protease that does not fall into the known seryl, thiol, carboxyl and metalloprotease families. However, a common feature of most proteases, including proteasome, is the presence of a catalytic triad, namely three amino acids cooperatively interacting but just one cleaves the substrate by means of nucleophilic attack to the protein backbone.[5, 6] Indeed, the oxygen atom on the side chain of the *N*-terminal threonine ($Thr1O^{\gamma}$) is inherently nucleophilic but its nucleophilicity seems to be enhanced by surrounding amino acids of the catalytic triad. Two pairs of these three active sites face the interior of the cylinder since there are two beta rings. Furthermore, β1, β2, and β5 subunits recognize distinguishing side chains of different peptides, thus resulting in specific activity for each catalytic site, whereas the remaining β-subunits are inactive. In eukaryotic organisms the α-subunits are inactive as in archaebacterial proteasomes.[4]

As concerns substrate specificity, *in vitro* assays with chromogenic peptides revealed that proteasomal activities are restricted to only five distinct cleavage preferences: chymotrypsin-like (CL), trypsin-like (TL), peptidyl-glutamyl-peptide-hydrolizing-like (PGPHL, also called postacidic or caspase-like), branched chain amino acid-preferring (BrAAP), and small neutral amino acid-preferring activity (SNAAP).[4, 8] Among these catalytic activities, the first three are the most studied and are assigned to β5 (Pre2), β2 (Pup1), and β1 (Pre3) subunits, respectively. On the basis of several mutational investigations on the yeast CP and subsequent structural studies in complex with inhibitors bound to all active sites, the catalytic dynamics have been clarified.[4]

Generally, the major residue responsible for S1-specificity of each catalytic pocket (i.e., the pocket in a protease occupied by the substrate residue, called P1 residue, which immediately precedes the scissile amide bond) is located in position 45. In addition, adjacent subunits in the β-rings contribute to create the S1 pockets and are significant determinants for selectivity.

As aforesaid, PGPHL activity (protein cleavage after acidic residues) is mediated by the β1 subunit and structural studies demonstrated that its S1 pocket preferentially interacts with glutamate P1 residues of chromogenic substrates owing to the presence of Arg45 at the base of the same subunit. However, degradation experiments of yeast enolase have identified that this subunit has, besides its PGPHL-specificity, limited BrAAP activity.[4] Interestingly, crystallographic data of "calpain inhibitor I-CP" complex reveal that the hydrophobic norleucine side chain of the inhibitor projects toward the Arg45, thus providing an insight for the mechanism of this dual cleavage preference. Additional electron density nearby Arg45 was indeed interpreted as a bicarbonate anion, which is able to counterbalance its positive charge.[4]

In the β2 subunit, characterized by TL activity (hydrolysis at the *C*-terminal side of basic residues), a glycine residue is situated in the position 45. Consequently, the S1 pocket of subunit β2 is very spacious and therefore suitable for very large P1 residues; in fact, all basic-type amino acids (Lys, Arg, and His) are quite sterically demanding. In this case two facts are responsible for the TL specificity of this subunit: firstly, the presence of a glutamic acid residue (negatively charged) located in position 53 at the bottom of the S1 pocket, and secondly, the acidic side wall of this pocket deriving from by the neighboring subunit β3.[4, 8]

Finally, in addition to CL activity (protein cleavage after hydrophobic amino acid residues) BrAAP and SNAAP activities are ascribed to β5 subunit, as well. The chymotrypsin-like activity is explained by the apolar character of its S1 pocket with Met45 located on its base. However, the structural flexibility of this subunit around Met45 determines this multiple and distinguishing catalytic behavior. For example, in case of the "CP-lactacystin complex", the side chain of Met45 is oriented towards the isopropyl side chain of the inhibitor, thus filling the space of the S1 pocket; on the contrary, in the crystal structure of the "CP-calpain inhibitor I complex" the Met45 side chain is displaced by the bulky norleucine side chain of the inhibitor.[4, 8]

On the basis of the previous statements, X-ray crystallography generally helps to interpret the specificities of the active subunits but sometimes it also explains why they are

not rigidly observed. As aforementioned, it was found that S1 pocket of β1 subunit captures an anion (a bicarbonate) to balance the charge of the guanidino-group at its base when accomodates inhibitors with hydrofobic side chains. Such a variability in the character of the P1 sites, and the possibility for inhibitors or substrates to make additional contacts, add complexity to the prediction of their affinities to the enzyme. As a result of their broad specificity, proteasomes can hydrolyze substrates after almost every residue.

3.3. Experimental

3.3.1. Affinity tag strategy

The 20S proteasome conventional purification way,[6] based on subsequent chromatographic steps, is slower and more difficult than affinity tag method,[3] therefore we provided with SDL135 yeast strain, kindly supplied by Finley. This particular yeast strain is able to yield a tagged version of proteasome. The tag involved (TEV protease-cleavable protein A tag, hereinafter TEV-ProA) is located in the 20S core at β4 (Pre1) subunit. This module is inserted into the chromosomal yeast DNA by homologous recombination and allows capture of the protein of interest from the crude cell extract by one-step affinity purification. Protein A, indeed, binds tightly to the Fc fragment (i.e., crystallizable fragment) of the immunoglobulins of G type (IgG), allowing the purification of 20S proteasome on IgG resin. The proteasome can then be eluted from the resin by TEV protease cleavage (**Figure 3.4**).

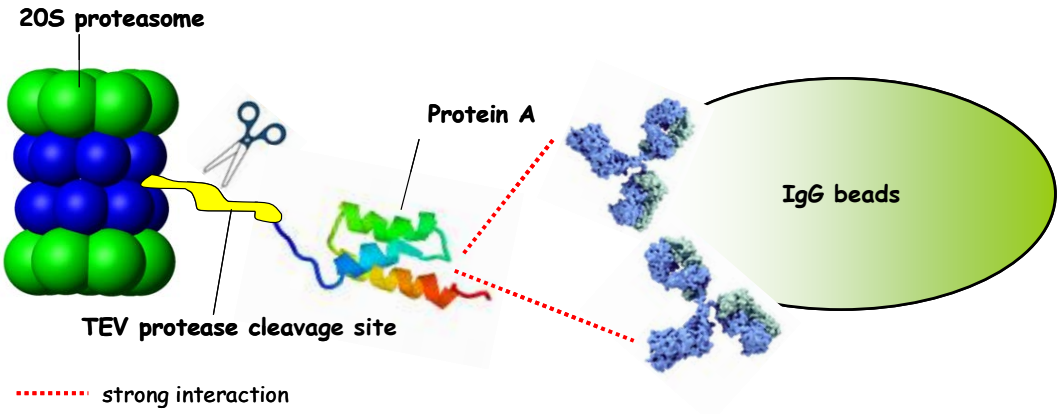

Figure 3.4. One step affinity purification by TEV protease cleavage.

The TEV protease recombinant protein has been produced in our laboratories in high yield in a stable mutant of *Escherichia Coli* (*vide infra*).

As regards the methodology adopted, after the progressive production of at least 12 L of yeast culture (for each attempt) in YPD-A (yeast extract, peptone, dextrose and adenine) medium till an OD_{600} value of ~ 5, the yeast pellet was collected by centrifugation and frozen at -80°C. Subsequently, yeast cells were thawed out overnight on ice, properly resuspended and lysed by means of a French Press at 2.69 kBar. The lysate was centrifuged and incubated with the previously described IgG resin. After resin washing, the 20S proteasome was cleaved from the ProA tag, bound to the IgG resin, by TEV protease. The enzyme was further purified by size exclusion chromatography (SEC).

After pooling and concentrating the proteasome fractions, the maintenance of the proteolytic activity has been tested by using a simple spectrophotometric method. The assay employs a specific 20S proteasome substrate, Suc-LLVY-AFC (i.e., *N*-Succinyl-Leu-Leu-Val-Tyr-7-amido-4-trifluoromethylcoumarin), which generates a highly fluorescent product (AFC) with an emission maximum at 505 nm upon cleavage by the chymotrypsin-like pocket of the active enzyme.

Finally, the pure 20S proteasome has been crystallized under different precipitating conditions. The crystal structures were solved by X-ray diffraction and subsequent data analysis. Data were collected at the id23eh1 line of ESRF synchrotron in Grenoble (France).

3.3.2. Materials

3.3.2.1. Chemicals, strains and labware used

EDTA (Janssen Chimica), magnesium acetate tetrahydrate, MES, MPD, TEMED for electrophoresis, Kanamycin, Tris-HCl (Fluka), IPTG, DTT (Inalco), DMSO, NaCl, sodium azide (Riedel-de Haën), yeast extract, tryptone, bacteriological agar Type A (Biokar diagnostics), APS, glycine and SDS for electrophoresis, EZBlue™ Gel Staining reagent (also called Blue Coomassie), acetic acid, D-(+)-glucose, adenine hemisulfate salt, Suc-LLVY-AFC peptide (Sigma-Aldrich), acrylamide/bis-acrylamide 40% solution, Tris base (AppliChem GmbH) and Low Molecular Weight Protein Standards 97.4-14.4 kDa (BioRad) were of high grade of pureness and used as purchased without any further purification.
Gel affinity resin (5 x 2 mL) with a minimum binding capacity of 2.0 mg of antibody (rabbit

IgG)/ mL of gel was supplied by MP Biochemicals whereas Vivaspin 500 and 15R hydrosart 30000 MWCO concentrators by Sartorius Stedim Biotech.

The SDL135 yeast strain (*Saccharomyces Cerevisiae*) was kindly supplied by Prof. Daniel Finley while the bacterium (*Escherichia Coli*) able to yield TEV protease was produced in-house.

3.3.2.2. Growth media composition

A. E. Coli (cells)

1. Luria-Bertani (LB)-agar solid medium (500 mL)
    - 2.5 g yeast extract
    - 5 g tryptone
    - 5 g NaCl
    - 7.5 g agar (1.5% w/v)
    - Kanamycin (1000X)
2. Luria-Bertani (LB) liquid medium (1 L):
    - 5 g yeast extract
    - 10 g tryptone
    - 10 g NaCl

B. Saccharomyces Cerevisiae (cells)

1. YPD-agar solid medium (500 mL):
    - 5 g yeast extract
    - 10 g peptone (tryptone)
    - 10 g dextrose (glucose)
    - 10 g agar (2% w/v)
2. YPD liquid medium (1 L) used for the inoculation culture (pH ~ 7):
    - 10 g yeast extract
    - 20 g peptone
    - 20 g dextrose

3.3.2.3. Buffers

A. E. Coli

1. *buffer A* (500 mL) pH 8: 30 mM Tris, 300 mM NaCl, 0.5 mM EDTA, 1 mM DTT

2. *buffer B* (250 mL) pH 8: 30 mM Tris, 300 mM NaCl, 500 mM imidazole, 0.5 mM EDTA,
1 mM DTT

B. <u>*Saccharomyces Cerevisiae*</u>

1. *Yeast lysis buffer* (1 L) pH 8.0: 50 mM Tris
2. *Washing buffer* (500 mL) pH 8.0: 50 mM Tris, 500 mM NaCl
3. *TEV protease buffer* (500 mL) pH 8.0: 50 mM Tris, 1 mM EDTA, 1 mM DTT
4. *Superdex buffer* (2 L) pH 7.5: 20 mM Tris,

3.3.3. Instrumentation

Yeast lysis was performed by two passes by means of a French Press (Constant Cell disruption system) at 2.5 kBar whereas *E. Coli* lysis at 1.35 kBar. Alternatively, *E. Coli* lysis was performed by a Sonic ruptor 400, International PBI.

Activity assays were carried out by Victor X4 Perkin Elmer 2030 Multilabel reader.

OD_{600} and A_{280} were recorded by a Varian Cary50 BioUV-Vis spectrophotometer.

Cultures and mixtures were centrifuged by two different multispeed refrigerated centrifuges:

- Avant J25 (rotor JA 9,100 and JA 25,50);
- ALC PK121R (rotor A-M10).

SDS-PAGE analyses were performed with a Consort EV243 Power Supply and SCIE-PLAS TV50 vertical electrophoresis units.

TEV protease purification was performed using a Ni^{2+}-affinity prepacked column (Ni-NTA column) (GE Healthcare) connected to an ÄKTA FPLC system.

SEC profiles for 20S proteasome were obtained using a Hiload 16/60 Superdex 200 prep grade gel filtration column (GE Healthcare) connected to an ÄKTA FPLC system. The column data are summarized in the following table.

Table 3.2. Main features for use of the Hiload 16/60 Superdex 200 prep grade column.

Property	Description
Matrix	Dextran covalently bound to highly cross-linked agarose
Dimensions	3.2 x 60 cm
pH stability	3-12(regular use); 1-14 (cleaning)
Temperature	+4 to +30°C (operating/storage)
Exclusion limit (globular proteins)	≈600,000 Da
Flow rate	0.3-1.6 mL/min
Pressure over column (maximum)	0.3 MPa
Mean particle size	34 μm
Optimal separation range (globular proteins)	10,000-600,000 Da

3.3.4. Protocols and methods

3.3.4.1. Production of N-His$_6$-tagged TEV protease

Since the chosen yeast strain (SDL135) yields proteasome with the TEV-ProA tag at the 20S core, TEV protease was produced in-house by using *E. Coli* cells transformed with the suitable plasmid (*N*-His$_6$-tagged TEV protease gene in a pET vector, kanamycin resistance). The selection of bacteria able to produce TEV protease was based on the resistance to the kanamycin antibiotic. In fact, only those bacteria containing the plasmid can produce the neomycin phosphotransferase II which is able to inactivate the antibiotic.

About 2 L of *E.Coli* culture were prepared and 2 mL of kanamycin (1000x) were added. The growth was carried out in a shaking incubator at 190 rpm at 29 °C until OD_{600} was approximately 0.7. Then the culture was induced by the addition of the activating agent IPTG (1 M stock, 0.5 mM as final concentration). The culture was incubated overnight at 16 °C under stirring at 190 rpm. Bacteria were harvested by centrifugation at 6500 rpm for 10 min at 4°C. The cell pellet was resuspended with 30 mL of buffer A. Lysis was achieved by lysozime action and sonication (alternatively, by use of a French Press). 430 μL of lysozyme were added (final concentration 1.34 mg/mL, about 90 μM) and the mixture obtained was incubated at 4°C under stirring for 30 min. After 15 sonication cycles for 30 seconds each, the culture was clarified by centrifugation for 25 min at 15000 rpm at 4 °C.

Subsequently, the Ni-NTA column was washed with a buffer containing 20 mM imidazole to

avoid unspecific binding by other proteins. The enzyme was purified by a 20 min gradient from 0 to 500 mM imidazole concentration (0-100% buffer B, flow 1 mL/min).

The amount of TEV protease was determined by measuring the absorbance at 280 nm of the protein solution against the elution buffer. The concentration can be calculated by the Lambert-Beer law using a specific extinction coefficient of 1.19 (a TEV solution of 1 mg/mL gives an A_{280} of 1.19; $\varepsilon \sim 32000\ M^{-1}\ cm^{-1}$).

The final solution was mixed with an equal volume of 50% glycerol solution and stored in 0.5 mL aliquots at – 80°C. The progress of both expression and purification was followed by SDS-PAGE. It is worth pointing out that DTT has been added in the buffers to restore enzyme activity lost by incidental oxidation since TEV is a cysteine protease. Moreover, DTT prevents dimers and oligomers formation by quantitatively reducing superficial disulfide bonds, thus maintaining monothiols in a reduced state.

3.3.4.2. Yeast growth

First, YPD liquid medium has been mixed with agar, a solidifying component for the solid media, autoclaved and poured into Petri dishes to solidify. Once received the SDL135 strain, yeast cells have been streaked on an agar plate and let to grow at 29 °C for two days. Other cells have been streaked on a second Petri dish by picking them from a freshly generated culture on solid medium. After this initial propagation phase in rich solid medium, the freshly prepared yeast cells have been inoculated in liquid medium (YPD) in the presence of adenine (YPDA medium). Generally, *Saccharomyces Cerevisiae* grows well at 30 °C in the presence of glucose as a carbon source and with good aeration by using baffled-bottom flasks. In order to increase aeration, the medium constituted no more than one-third of the total flask volume. The growth was carried out in a shaking incubator at 300 rpm at 29 °C. The density of the cells in the culture was determined spectrophotometrically by measuring its optical density at 600 nm (OD_{600}). When the OD_{600} value reached 4.5, eight Eppendorf tubes were frozen at –80 °C with a 1:1 yeast culture/glycerol volume ratio. After centrifugation of the remaining culture and decantation of the surnatant, the yeast cells were frozen at –80 °C. A new yeast culture was grown in YPD-agar solid medium by streaking a small amount of the content of one Eppendorf tube before freezing. This culture was then inoculated in YPDA medium and incubated at 29 °C for two days to an OD_{600} value of 4.1. Yeast cells were harvested by centrifugation at 7500 rpm for 15 min at 4°C. They were resuspended with the smallest amount of phosphate buffer (pH 7.3) and centrifuged again at 6500 rpm for 15 min at 4°C. After decantation, the obtained yeast pellets were frozen at –80 °C.

This whole procedure (streaking, inoculation in YPDA medium, growth to an OD_{600} value ranging 4 to 5, harvesting and storing) has been repeated several times till to obtain total at least about 130 g of *Saccharomyces Cerevisiae* cells (for each attempt). Besides, the wet weight (in grams) of yeast cells in the pellet was determined before freezing. This is approximately equivalent to the so-called packed cell volume (in mL), and for all subsequent steps it has been referred to as 1 volume.

3.3.4.3. IgG resin equilibration and regeneration

Since the acquired affinity gel was in 0.02 M sodium phosphate (pH 7.3), 140 mM sodium chloride, with 0.05% sodium azide and 10% glycerol (v/v), it was resuspended, washed with sterile milliQ water and recovered by centrifugation at 3000 rpm for 5 min at 4 °C. Other two washing-centrifuging cycles were repeated. Then, IgG beads were analogously washed many times with yeast lysis buffer. Therefore, the IgG resin was incubated at 4 °C overnight, under mild stirring (130 rpm) prior to yeast cells lysis.

After each use, the resin was regenerated by washing with 5 column volumes 0.5% glacial acetic acid (v/v) followed by 5 column volumes of yeast lysis buffer.

3.3.4.4. Extraction and purification of yeast 20S proteasome

In each attempt, yeast cells were let to thaw out overnight on ice (4°C room) and were then resuspended in a twofold volume of cold yeast lysis buffer. They were lysed by two passes by means of a French press at 2.5 kBar.

After each lysis step, pH value was monitored by universal indicator paper even if the yeast lysis buffer is designated to maintain the pH 7 during lysis as long as it is used in a 2:1 ratio with the cell pellet. The lysate has been centrifuged at 45000 g for 45 min and the clarified lysate was pooled and incubated for 2 h at 4°C with 6 mL IgG resin, equilibrated with yeast lysis buffer.

After incubation, the mixture was centrifuged for 8 min at 3200 rpm at 4 °C; the surnatants were decanted and pooled down to remove the unbound fractions. Subsequently, the resin was washed several times with washing buffer in order to remove regulatory particles from 20S core. The various washing fractions were stored at 4 °C. Then, the IgG beads were equilibrated with TEV protease buffer. The 20S proteasome was cleaved from the ProA tag bound to the IgG resin by the TEV protease.

The proteolysis *in vitro* occurred under the following conditions: the TEV protease (~ 50 nmol) was added to the 20S-ProA-IgG resin and the obtained mixture was incubated overnight at 4°C for about 15 h. The cleaved proteasome was eluted with yeast lysis buffer through the IgG resin column, which was repeatedly washed with yeast lysis buffer and subsequently regenerated.

The 20S proteasome solution was concentrated till to 1 mL by centrifugation at 4000 rpm at 4°C. The 20S proteasome was further purified using a Hiload 16/60 Superdex 200 size-exclusion chromatography column (total volume 120 mL, flow rate 1 mL/min, equilibrated in superdex buffer) in superdex buffer collecting fractions of 1 mL (**Table 3.2**).

After activity test, possible fractions ascribable to 26S/30S proteasomes were discarded whereas fractions related to the 20S proteasome were concentrated to a final volume ranging from 2 mL to 15 μL depending on the type of inhibition test to be performed subsequently.

The typical amount of purified 20S proteasome, estimated by absorption at 280 nm (ε = 704375 M^{-1} cm^{-1} [1]), was about 500 μg. It is worth noting that all preparative steps except SEC chromatography were carried out on ice or at 4°C. During all purification steps the 20S proteasome purity was assessed by SDS-PAGE.

3.3.4.5. Chymotrypsin-like activity assay

The proteasome activity assay is a relatively quick method to test the maintenance of its distinguishing enzymatic activity.

As previously mentioned, the assay is based on detection of the fluorophore 7-amido-4-trifluoromethylcoumarin (AFC) after cleavage from the labeled tetrapeptide Suc-LLVY-AFC (i.e., *N*-Succinyl-Leu-Leu-Val-Tyr-7-amido-4-trifluoromethylcoumarin, shown in **Figure 3.5**), which is a substrate specific for the chymotrypsin-like activity of the 20S proteasome.

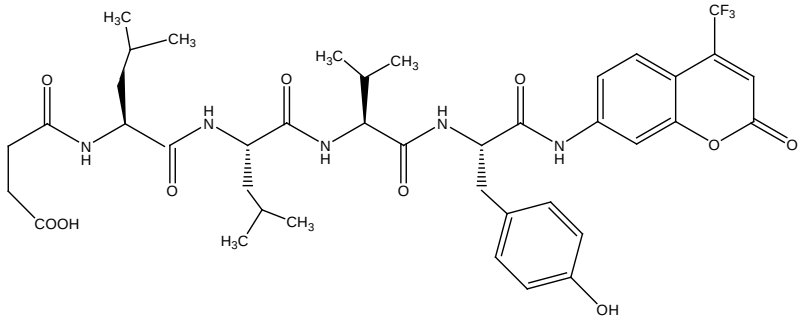

Figure 3.5. Chemical drawing of *N*-Succinyl-Leu-Leu-Val-Tyr-7-amido-4-trifluoromethylcoumarin, substrate for the chymotrypsin-like activity test.

[1] predicted value calculated by the sum of all constituent residues molar extinction coefficients at 280 nm from amino acid sequence data being Trp, Tyr and Phe the major contributors.

The peptide (10 mg) was reconstituted in DMSO (1.22 mL) at a final concentration of 10 mM. An *ad hoc* buffer (50 mM Tris, 0.04% (w/v) SDS, pH 8.2) was prepared to perform the activity tests. The choice of SDS percentage was not accidental but related to literature data. As a matter of fact, 20S proteasome activity is function of temperature, SDS concentration, and pH. In fact, the catalytic activity optimum is reached at about 0.05% SDS, pH 8 and 40 °C.[9]

Instead of directly checking 20S proteasome, chymotrypsin enzyme (1.44 μM) was used in order to check peptide quality and to set up the test. Fluorescence measurements were carried out at room temperature by means of a fluorometer equipped with a 420/535 nm filter set.

Afterwards, three different aliquots of 20S proteasome, purified for the first time, were added to three distinct wells containing the peptide substrate and the assay buffer up to 200 μL as final volume; after 20 seconds of mixing, the fluorescence kinetics was monitored for 80 min as shown in **Figure 3.6**.

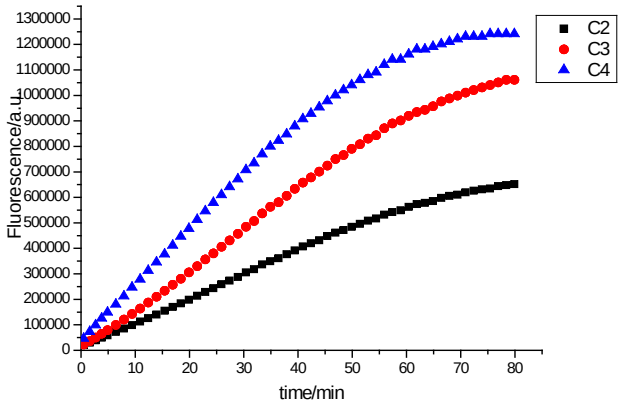

Figure 3.6. 20S proteasome activity assay obtained by recording fluorescence (λ_{exc}= 420 nm, λ_{em}=535 nm) in a 96-well plate.
C2 well composition: 173 μL buffer, 25 μL 20S proteasome, 2 μL fluorogenic peptide.
C3 well composition: 148 μL buffer, 50 μL 20S proteasome, 2 μL fluorogenic peptide.
C4 well composition: 123 μL buffer, 75 μL 20S proteasome, 2 μL fluorogenic peptide.

For the following purifications of the enzyme, the conditions related to the C2 well were exploited. A standard fluorogenic curve was not generated since the activity maintenance only had to be checked.

3.3.4.6. SDS-PAGE analysis

The following solutions were used as purchased:

1. acrylamide/bisacrylamide 40% (w/v) solution (mix ratio 37.5:1, T 30%, C 2.6%) ;
2. TEMED;
3. molecular weight standards (97,400÷14,400 or 170,000÷11,000 Da),

whereas the following aqueous solutions were prepared (using milliQ water):

A. resolving gel buffer (1.5 M Tris-HCl, pH 8.8);
B. stacking gel buffer (1 M Tris-HCl, pH 6.8);
C. 10% (w/v) SDS;
D. 10 % (w/v) APS;
E. running buffer 10X (0.25 M Tris, 1.92 M Glycine, 1% (w/v) SDS, pH 8.3);
F. SDS sample buffer 2X.

SDS-PAGE was performed using 8,6 x 6,8 cm discontinuous gels with running gels and stacking gels containing 12.5% and 7% of total acrylamide/*bis*-acrylamide, respectively. The composition of the prepared gels is reported in **Table 3.3**. Each gel was 1 mm thick and had 10 lanes.

Table 3.3. Experimental amounts used of reagents, solutions and buffers for the preparation of four gels.

	RESOLVING GEL	**STACKING GEL**
	Total acrylamide (mix ratio 37.5:1, C 2.6%)	
Substance	15%	7%
	Volumes	
Water	14.7 mL	13.3 mL
Acrylamide 40%	15 mL	3.5 mL
Tris Buffer	9.9 mL	2.9 mL
SDS 10% w/v	200 μL	180 μL
APS	104 μL	180 μL
TEMED	80 μL	6 μL
Approx. total volume	40 mL	20 mL

The specimens for the electrophoresis were prepared by mixing a definite amount of each sample with SDS sample buffer 2X (e.g. 50 μL+ 50 μL, respectively). Subsequently, samples were boiled for five minutes at 100°C and, hence, directly loaded in gel. Electrophoretic runs were performed in running buffer at 300 V and 45 mA for about 1 h.

After electrophoresis, the gels were stained following the protocol suggested by the Coomassie Blue supplier. The gels were placed into a clean container, rinsed with milliQ

water and boiled by a microwave oven for 2 min for three times. This removes the SDS in the gel that causes background staining. Successively, Coomassie Blue gel staining reagent was added, enough to completely cover the gel, which was boiled another time. After rinsing and destaining with 10% (v/v) acetic acid, the proteins are visualized as intense blue bands on a colourless background (**Figures 3.9, 3.10 and 3.11**).

3.3.4.7. X-ray diffraction data measurement

Crystals of the yeast 20S proteasome were grown by using the hanging-drop vapor diffusion method at 26°C. The estimated protein concentration used for crystallization trials was ~ 27 mg/mL in 20 mM Tris (pH 7.53), 1 mM EDTA, 1 mM NaN_3.

Crystals were obtained in drops containing 2 µL of protein and 1 µL of a precipitant solution composed of magnesium acetate, MES and MPD. The different conditions tested in eight wells are reported in the table below.

Table 3.4. Chemical composition of the eight wells used to crystallize 20S proteasome.

	1	2	3	4
A	**12%** MPD MES **0.1 M** MgAcetate **30mM** H_2O 375 µL	**14%** MPD MES **0.1 M** MgAcetate **30mM** H_2O 365 µL	**16%** MPD MES **0.1 M** MgAcetate **30mM** H_2O 355 µL	**18%** MPD MES **0.1 M** MgAcetate **30mM** H_2O 345 µL
B	**12%** MPD MES **0.1 M** MgAcetate **40mM** H_2O 375 µL	**14%** MPD MES **0.1 M** MgAcetate **40mM** H_2O 360 µL	**16%** MPD MES **0.1 M** MgAcetate **40mM** H_2O 350 µL	**18%** MPD MES **0.1 M** MgAcetate **40mM** H_2O 340 µL

Stock solutions used:
- MgAcetate tetrahydrate 1 M
- MES pH 6.5 1 M
- MPD pure (δ=0.921, MW=118.18)

A MPD gradient was tested across both the series A1-A4 and B1-B4. Moreover, Mg acetate concentration has been increased on passing from A to B group. The mixture was left equilibrating against 500 µL precipitant solution. Several crystals appeared within two days and grew to a final size of about 300 x 50 x 100 μm^3 **(Figure 3.7**).

X-Ray data were collected at the European Synchrotron Radiation Facility ESRF of Grenoble (France), beamline id23eh1. Before data collection, crystals were flash frozen in liquid nitrogen and measured at 100 K.

Figure 3.7. An example of 20S proteasome crystal properly mounted in a loop for X-Ray diffraction data acquisition.

The crystals diffract to a maximum resolution better than 2.7 Å. The crystals belong to monoclinic space group $P2_1$, according to the symmetry of the diffraction pattern and to the systematic absences. The unit cell dimensions are *a* = 135.7 Å, *b* = 301.4 Å and *c* = 144.9 Å, β = 113.2° . The unit cell contains two 20S proteasome oligomers, corresponding to a solvent content of about 47%.

3.4. Results and discussion

Before extracting 20S proteasome from yeast cells, it was necessary to produce TEV protease. This enzyme is able, indeed, to cleave the bond between the protein A tag and the β4 subunit of the 20S proteasome. The TEV protease was isolated by exploiting its *N*-His_6 tag which is able to replace a couple of water molecules among those coordinated to octahedral nickel(II) metal centers, bound to the resin of the Ni-NTA prepacked column. The enzyme elutes at about 18 mL at the beginning of %B gradient as shown in **Figure 3.8**. The various phases of recombinant protein espression and purification were followed by SDS-PAGE, as well (**Figure 3.9**).

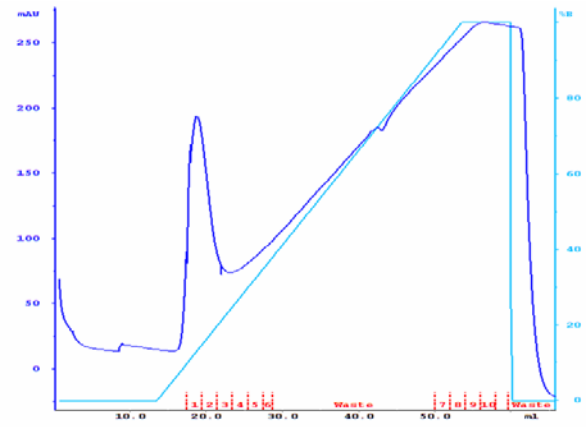

Figure 3.8. Ni-NTA affinity profiles obtained by a FPLC system.

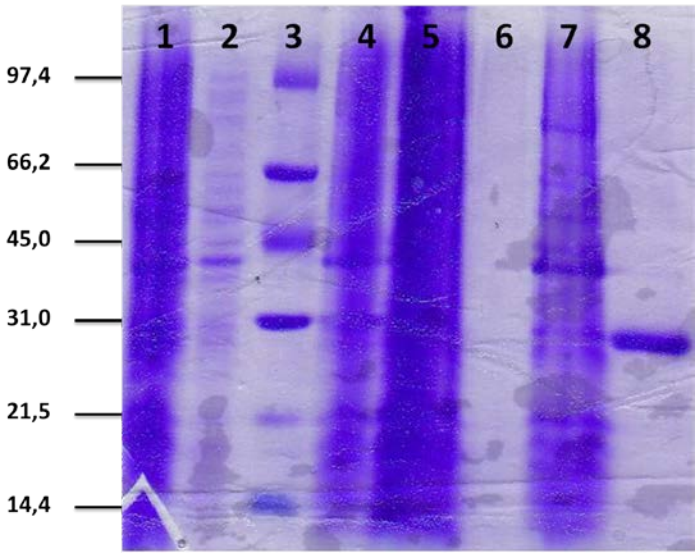

Figure 3.9. Electrophoretic pattern of TEV protease and of other samples studied during the production protocol.

Lane 1: *E.Coli* culture before IPTG induction
Lane 2: *E.Coli* culture induced by IPTG after incubation overnight
Lane 3: molecular weight standards (from the top to the bottom, 97.4, 66.2, 45.0, 31.0, 21.5, 14.4 kDa)
Lane 4: *E.Coli* cell pellet after protein espression
Lane 5: *E.Coli* surnatant after sonication
Lane 6: -
Lane 7: flow through fraction after passage through Ni-NTA column.
Lane 8: fraction 1 deriving from purification by means of Ni-NTA prepacked column.

The presence of a single band in lane 8 confirmed that the purified TEV protease was pure and in good agreement with the expected molecular weight (29 kDa). Lanes 1, 4, 5 and 7 are not diagnostic for the presence of TEV protease.

Following the TEV protease obtaining, yeast cell lysis and purification of the intracellular target 20S proteasome can thereby be performed. According to the SDS-PAGE analysis, the 20S proteasome obtained by affinity chromatography (lane I of **Figure 3.10**) was not pretty pure since some bands ascribable to the regulatory particles (19S proteasomes) are visible between 40 and 115 kDa or at higher MWs due to aggregation phenomena. Conversely, Lane II of **Figure 3.10** shows that 19S proteasomes are completely removed upon washing at high ionic strength since the visible bands set only between 40 and 17 kDa, in agreement with the MWs known for the subunits forming the CP core, ranging from about 16 to 35 kDa.

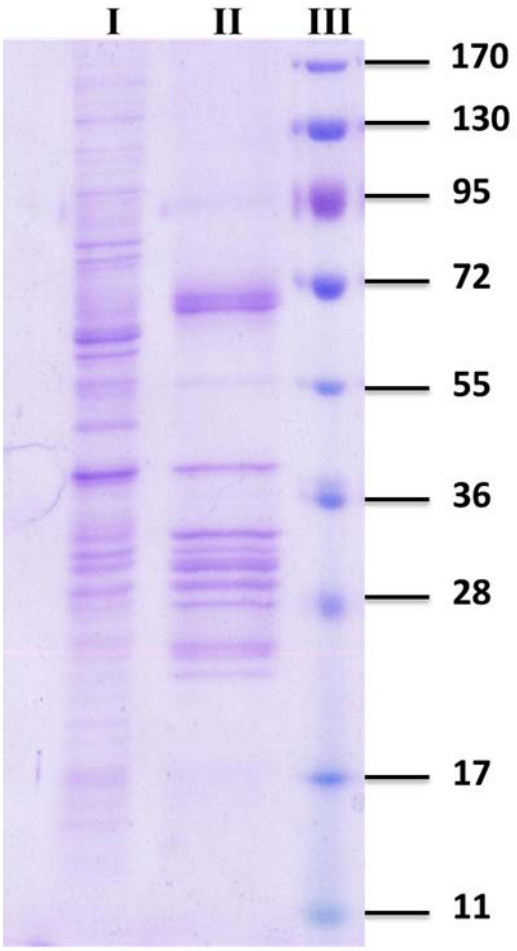

Figure 3.10. Electrophoretic pattern of 20S proteasome-containing samples (prior to incubation with TEV protease):
Lane I: pre-washing (IgG resin + 20S and 30S)
Lane II: after washing (IgG resin + 20S)
Lane III: molecular weight standards (kDa)

Afterwards, upon washing with NaCl buffer (Lane II and 2 of **Figures 3.10** and **3.11**, respectively), the proteasome was detached from the resin by TEV protease and then further purified by SEC chromatography (bands 3 and 4 in **Figures 3.11**; **Figure 3.12**). It is worth noting that the bands occurring at about 50-60 kDa (Lane II and 2 of **Figures 3.10** and **3.11**, respectively) are imputable to the resin degradation (immunoglobulin G heavy chains).

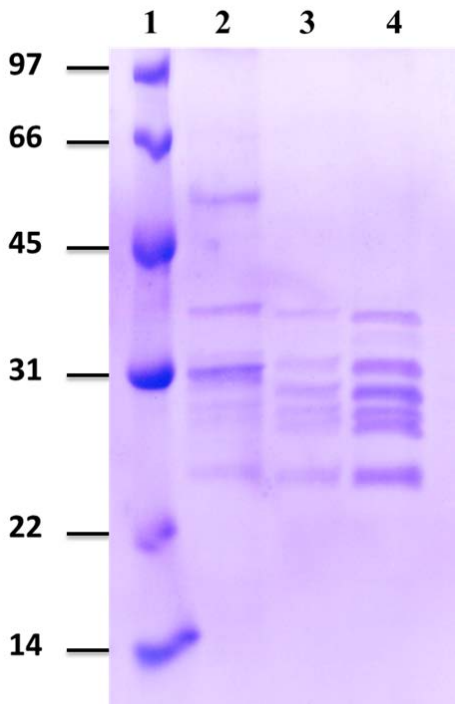

Figure 3.11. Electrophoretic pattern of 20S proteasome-containing samples:

Lane 1: molecular weight standards (kDa)
Lane 2: IgG resin after incubation with TEV
Lane 3: 20S+ TEV (diluted sample)
Lane 4: 20S + TEV (concentrated sample)

In each attempt, the maintenance of the proteolytic activity of the purified proteasome was tested by the CT-like activity assay described above. Possible 30S component fractions did not reveal fluorescence emission in activity trials because catalytic lumen is not accessible owing to the presence of regulatory particles (19S proteasome). Conversely, the fluorescence detected for the 20S proteasome fractions always rises with increasing of 20S proteasome concentration as shown in **Figure 3.6**, thus revealing an active CP core.

Once obtained the purified enzyme, some crystallization trials were undertaken resulting in the subsequent growth of several crystals within 48 h. Suitable crystals of the protein nicely diffracted to a maximum resolution of 2.7 Å. The yeast 20S proteasome structure solved by Groll *et al.*[6] was used as a template for molecular replacement and the obtained model was refined to a final R_{work} factor of 20.0% (R_{free} 24.6%). The final refined structure is shown in **Figure 3.13** and results in good agreement with literature data.[6]

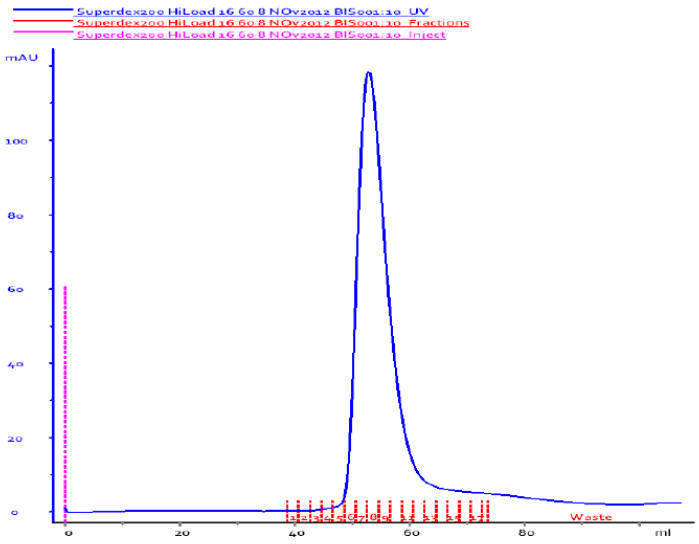

Figure 3.12. SEC profile (UV-Vis detector) obtained following the elution of the 20 proteasome in superdex buffer.

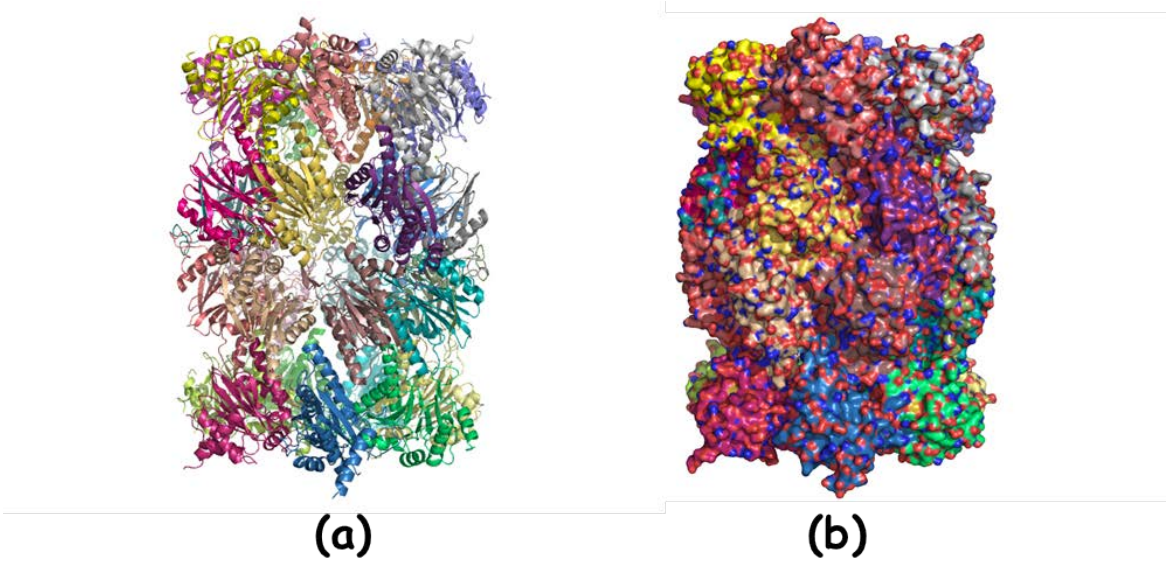

Figure 3.13. Ribbon backbone representation **(a)** and molecular surface visualized by space-filling representation (color code: blue for nitrogen atoms, red for oxygen atoms) **(b)** of the experimental structure of the 28 subunits defining the 20S proteasome.

Upon proteasome structure resolution, we tried many inhibition conditions using AuD8 (dissolved in DMSO) as a model compound. First, very low inhibitor/enzyme molar ratios had to be used compared to those considered at the Karmanos Cancer Institute (Detroit, U.S.A.) to determine IC_{50} values on the human purified proteasome (§ *Chapter 2*).

In fact, both crystal soaking (*diffusion of the inhibitor through the crystal)* and co-crystallization approach, carried out at a 50:1 inhibitor-20S proteasome molar ratio, turned out to be troublesome, thus leading to crystal packing damage. Even though such a ratio was decreased, the resulting crystals appeared injured. Thus, we took into account those strategies that result in enzyme inhibition under milder conditions.

It is known that sodium dodecyl sulfate (SDS), heating, polylysine or fatty acids can favor the enzyme channel opening, thus increasing the probability of inhibitor access to the 20S core.[10] As previously described, the catalytic activity optimum occurs at about 0.05% SDS (w/v), pH 8 and 40 °C.[9]

First, we considered co-incubation of 20S proteasome with AuD8 in the presence of SDS prior to attempting crystallization. Thus, in a trial the purified proteasome was incubated with the gold complex (previously dissolved in DMSO) at 4 °C for 15 h in a 8:1 inhibitor/enzyme molar ratio in the presence of SDS 0.04 % (w/v). It is worth pointing out that the SDS percentage was high enough to facilitate the access of AuD8 to the proteolytic chamber but lower than critical micelle concentration (0.24 % w/v).[11] After incubation, a chymotrypsin (CT)-like activity assay was carried out in order to compare the sample treated with AuD8 in the presence of SDS with the untreated one. **Figure 3.14** shows that all CT-like sites were seemingly inhibited after 15 h interaction whereas the enzyme not incubated with AuD8 was active. In fact, the fluorescence signal of the proteasome incubated with the complex sets at the level of background noise after subtracting the inherent fluorescence of the non-hydrolyzed substrate.

Before undertaking the crystallization trials, the same experiment was repeated using larger volumes and thereby a higher amount of protein. In this case, we observed 20S proteasome precipitation when adding SDS at 0.04% (w/v), resulting in the formation of a white suspension. Therefore, it is very likely that such macroscopic phenomenon could account for the trend observed in **Figure 3.14** (red trend), involving a tiny amount of the enzyme.

Consequently, we addressed our attention to a second approach to favor catalytic channel-opening, namely a temperature increase, always keeping the inhibitor/enzyme molar ratio quite low. It should be highlighted that proteins are usually handled at 4 or 0 °C.

AuD8 was incubated with the purified proteasome core in a 25:1 molar ratio, respectively, for 2 h at two different temperatures, 20 and 35°C, followed by the evaluation of the catalytic activity (**Figure 3.15**).

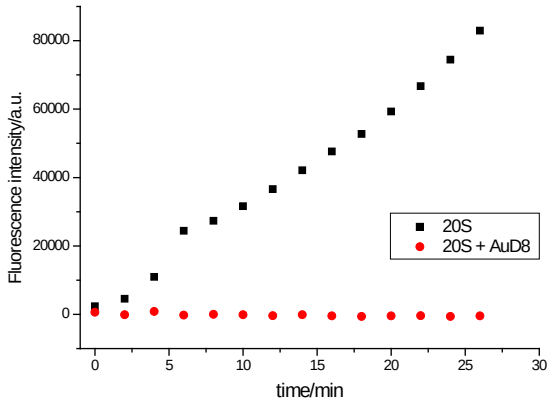

Figure 3.14. 20S proteasome activity assay obtained by recording fluorescence of the labeled tetrapeptide Suc-LLVY-AFC after hydrolysis in the chymotrypsin-like pocket of the enzyme (λ_{exc}= 420 nm, λ_{em}=535 nm, 96-well plate).
Well composition: 173 µL buffer (pH 8.2), 25 µL 20S proteasome (treated or not with AuD8), 2 µL fluorogenic peptide

The fluorescence signal recorded for the sample treated at 20 °C is more intense than that observed for the proteasome treated at 35 °C, pointing out that higher temperatures actually favor the access of our inhibitor in the catalytic channel. Additionally, as the final concentration in the wells of the control is half of that in the wells of the specimen incubated at 35 °C and they are characterized by a similar intensity trend, it seems that about 50% of CT-like pockets were inhibited after 2 h incubation with the gold compound. Thus, in the following attempt we increase both the incubation time (5 h) and the AuD8-enzyme molar ratio (50:1), resulting in the curves reported in **Figure 3.16**. Based on this complete inhibition of the enzyme, the mixture was concentrated up to about 20 mg/mL (V_{TOT} = 25 µL) in order to remove the gold complex present in excess (centrifugal concentrator MW cut-off = 30 kDa) before undertaking the crystallization trials.

We tried to obtain crystals by hanging-drop vapor diffusion method at 20 °C testing about 90 different crystallization conditions by means of an automatic nanodrop robot.

Since the crystallization conditions tested so far did not yield diffraction-quality crystals, the mechanism of inhibition of the enzyme by AuD8 has not been elucidated yet. However, some considerations deserve to be done. Like bortezomib (§ *Introduction*), AuD8 is an electrophilic species. Being coordination compounds[12], both types of inhibitors consist of an electrophilic trap, the semimetal element boron for the former and the metal center Au(III) for the latter. In its compounds, boron may form an extra reversible bond in order to complete the octet whereas the transition metal gold(III) forms four covalent bonds in a

square-planar geometry *via* an associative mechanism. Similar to boron in bortezomib, the metal center Au(III) could bind to the proteasomal active sites (*e.g.*, to a sulfur-containing amino acid), likely irreversibly, but it may also be involved in a redox process that would lead to the formation of gold(I)-containing species or metallic gold by oxidation of some residue of the multicatalytic protease such as the nucleophilic threonine.

On the basis of the results obtained, other attempts will likely be carried out in the future to elucidate this prominent biological interaction. In addition, since a lot of proteasome is required in each test and the yeast growth in flask is quite wearisome and not so fruitful, recently we started to grow yeast cells by means of a home-made fermentator, thus increasing the yeast pellet yields. Many parameters such as pO_2, culture pH, stirring intensity and temperature are currently under optimization. Once a high amount of *S. Cerevisiae* cells has been collected, new extraction, purification and crystallization attempts will be performed.

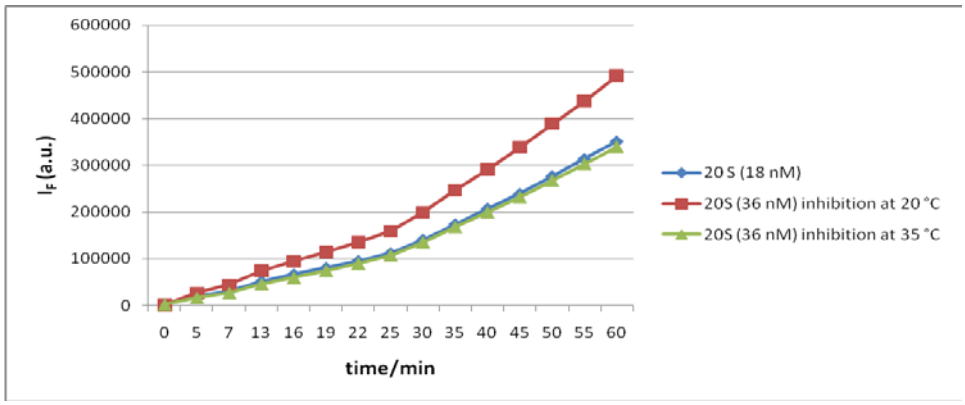

Figura 3.15. Catalytic activity evaluation after incubation of AuD8 for 2 h with 20S proteasome in a 25:1 molar ratio at 20 or 35 °C (λ_{exc}= 420 nm; λ_{em}= 535 nm).

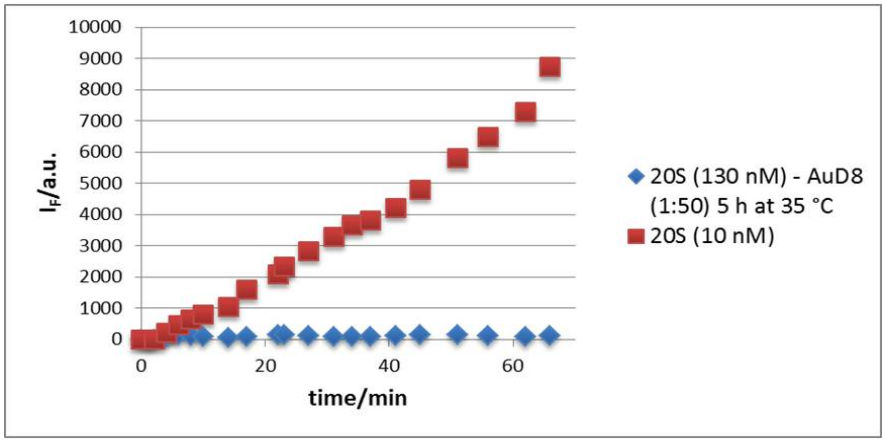

Figure 3.16 . Catalytic activity evaluation after incubation of AuD8 with 20S proteasome for 5 h in a 50:1 molar ratio at 35 °C (λ_{exc}= 420 nm; λ_{em}= 535 nm).

Chapter 3 References

(1) Groll, M.; Balskus, E. P.; Jacobsen, E. N. Structural Analysis of Spiro B-Lactone Proteasome Inhibitors. *J. Am. Chem. Soc.* **2008**, *130*, 14981-14983.

(2) Clerc, J.; Groll, M.; Illich, D. J.; Bachmann, A. S.; Huber, R.; Schellenberg, B.; Dudler, R.; Kaiser, M. Synthetic and Structural Studies on Syringolin A and B Reveal Critical Determinants of Selectivity and Potency of Proteasome Inhibition. *Proc. Natl. Acad. Sci. U. S. A.* **2009**, *106*, 6507-6512.

(3) Leggett, D. S.; Glickman, M. H.; Finley, D. Purification of Proteasomes, Proteasome Subcomplexes, and Proteasome-Associated Proteins from Budding Yeast. *Methods Mol. Biol.* **2005**, *301*, 57-70.

(4) Groll, M.; Huber, R. Inhibitors of the Eukaryotic 20S Proteasome Core Particle: A Structural Approach. *Biochim. Biophys. Acta Mol. Cell Res.* **2004**, *1695*, 33-44.

(5) Tanaka, K. The Proteasome: Overview of Structure and Functions. *Proc. Jpn. Acad. Ser. B Phys. Biol. Sci.* **2009**, *85*, 12-36.

(6) Groll, M.; Ditzel, L.; Löwe, J.; Stock, D.; Bochtler, M.; Bartunik, H. D.; Huber, R. Structure of 20S Proteasome from Yeast at 2.4 Å Resolution. *Nature* **1997**, *386*, 463-471.

(7) Milacic, V.; Dou, Q. P. The Tumor Proteasome as a Novel Target for Gold(III) Complexes: Implications for Breast Cancer Therapy. *Coord. Chem. Rev.* **2009**, *253*, 1649-1660.

(8) Groll, M.; Heinemeyer, W.; Jäger, S.; Ullrich, T.; Bochtler, M.; Wolf, D. H.; Huber, R. The Catalytic Sites of 20S Proteasomes and their Role in Subunit Maturation: A Mutational and Crystallographic Study. *Proc. Natl. Acad. Sci. U. S. A.* **1999**, *96*, 10976-10983.

(9) Ugai -i., S.; Tamura, T.; Tanahashi, N.; Takai, S.; Komi, N.; Ha Chung, C.; Tanaka, K.; Ichihara, A. Purification and Characterization of the 26S Proteasome Complex Catalyzing ATP-Dependent Breakdown of Ubiquitin-Ligated Proteins from Rat Liver. *J. Biochem.* **1993**, *113*, 754-768.

(10) Tanaka, K.; Yoshimura, T.; Ichihara, A. Role of Substrate in Reversible Activation of Proteasomes (Multi-Protease Complexes) by Sodium Dodecyl Sulfate. *J. Biochem.* **1989**, *106*, 495-500.

(11) Elworthy, P. H.; Mysels, K. J. The Surface Tension of Sodium Dodecylsulfate Solutions and the Phase Separation Model of Micelle Formation. *J. Colloid Interface Sci.* **1966**, *21*, 331-347.

(12) Dalla Via, L.; Nardon, C.; Fregona, D. Targeting the Ubiquitin-Proteasome Pathway with Inorganic Compounds to Fight Cancer: A Challenge for the Future. *Future Medicinal Chemistry* **2012**, *4*, 525-543.

Chapter 4. Preliminary studies of the interaction with the serum albumin

4.1. Bovine serum albumin as a good substitute of the human counterpart

In the context of pharmacokinetics of the model compound AuD8, used for investigating acute toxicity *in vivo* (§ *Chapter 5*), we focused on serum albumins as they are the main circulating proteins in the bloodstream (30–50 g/L human serum[1, 2]) with a molecular weight of 66.430 kDa[3] and, *per se*, a carrier for a number of endogenous and exogenous substances. Interestingly, human serum albumin (HSA) exhibits an average half-life of 19 days and is extremely resistant toward not neutral pH values (stable in the pH range 4÷9), high temperatures (heating at 60 °C for up to 10 h without deleterious effects) and organic solvents such as 40% ethanol.[4]

HSA plays several distinct functions and shows interesting binding properties.[5] In fact, it is the major protein responsible for the osmotic pressure of the blood and upon hydrolysis, its amino acids provide nutrition to peripheral tissues. Furthermore, HSA is the vehicle for long chain fatty acids, thus being essential for lipids metabolism. Regarding the binding properties, at endogenous level, HSA binds bilirubin, amino acids, steroid hormones, vitamins[2, 6] and, in the context of metal ions, calcium(II) and zinc(II) in a relatively nonspecific manner and copper(II) in a specific way. [2, 6]Serum albumin is also able to bind a large number of exogenous substances including therapeutic drugs such as benzodiazepines, penicillins, indole compounds and sulfonamides.[7]

Before the interaction studies, we carried out the protein sequence alignment of HSA (1E78.pdb) and the bovine analogue (BSA, 3V03.pdb), resulting in 76 % amino acid sequence identity, in agreement with literature data (**Figure 4.1**).[7]

Although HSA contains two extra amino acid residues at the *C*- terminus compared to BSA (583 total residues), both proteins are made up of two identical chains, A and B, in turn subdivided in three homologous evolutionarily related domains (I, II, III) (**Figure 4.2**). [2, 8] Furthermore, each chain, being predominantly in the α-helix form (74%, PDB 3V03) (**Figure**

4.3), contains 17 disulphide bonds and a free thiol group associated with the cysteine residue 34.[2, 9]

```
75.6% identity in 583 residues overlap; Score: 2441.0; Gap frequency: 0.2%

BSA,           1 DTHKSEIAHRFKDLGEEHFKGLVLIAFSQYLQQCPFDEHVKLVNELTEFAKTCVADESHA
HSA,           1 DAHKSEVAHRFKDLGEENFKALVLIAFAQYLQQCPFEDHVKLVNEVTEFAKTCVADESAE
                 * **** ********** ** ****** ********  ******* ************

BSA,          61 GCEKSLHTLFGDELCKVASLRETYGDMADCCEKQEPERNECFLSHKDDSPDLPKL-KPDP
HSA,          61 NCDKSLHTLFGDKLCTVATLRETYGEMADCCAKQEPERNECFLQHKDDNPNLPRLVRPEV
                  * ********* ** ** ****** ***** ********** **** * ** *  *

BSA,         120 NTLCDEFKADEKKFWGKYLYEIARRHPYFYAPELLYYANKYNGVFQECCQAEDKGACLLP
HSA,         121 DVMCTAFHDNEETFLKKYLYEIARRHPYFYAPELLFFAKRYKAAFTECCQAADKAACLLP
                    *  *   *  *  ******************  *  *   * ***** ** *****

BSA,         180 KIETMREKVLTSSARQRLRCASIQKFGERALKAWSVARLSQKFPKAEFVEVTKLVTDLTK
HSA,         181 KLDELRDEGKASSAKQRLKCASLQKFGERAFKAWAVARLSQRFPKAEFAEVSKLVTDLTK
                 *    *     *** *** *** ******* *** ****** ****** ** ********

BSA,         240 VHKECCHGDLLECADDRADLAKYICDNQDTISSKLKECCDKPLLEKSHCIAEVEKDAIPE
HSA,         241 VHTECCHGDLLECADDRADLAKYICENQDSISSKLKECCEKPLLEKSHCIAEVENDEMPA
                 ** ********************** *** ******** ************* *  *

BSA,         300 NLPPLTADFAEDKDVCKNYQEAKDAFLGSFLYEYSRRHPEYAVSVLLRLAKEYEATLEEC
HSA,         301 DLPSLAADFVESKDVCKNYAEAKDVFLGMFLYEYARRHPDYSVVLLLRLAKTYETTLEKC
                  ** * *** * ******* **** *** ***** **** * *  ****** ** *** *

BSA,         360 CAKDDPHACYSTVFDKLKHLVDEPQNLIKQNCDQFEKLGEYGFQNALIVRYTRKVPQVST
HSA,         361 CAAADPHECYAKVFDEFKPLVEEPQNLIKQNCELFEQLGEYKFQNALLVRYTKKVPQVST
                 **  *** **  ***  * ** **********  ** **** ***** **** *******

BSA,         420 PTLVEVSRSLGKVGTRCCTKPESERMPCTEDYLSLILNRLCVLHEKTPVSEKVTKCCTES
HSA,         421 PTLVEVSRNLGKVGSKCCKHPEAKRMPCAEDYLSVVLNQLCVLHEKTPVSDRVTKCCTES
                 ******** *****  **  **  **** *****  ** **********  ********

BSA,         480 LVNRRPCFSALTPDETYVPKAFDEKLFTFHADICTLPDTEKQIKKQTALVELLKHKPKAT
HSA,         481 LVNRRPCFSALEVDETYVPKEFNAETFTFHADICTLSEKERQIKKQTALVELVKHKPKAT
                 ***********  ******* *    **********   * *********** *******

BSA,         540 EEQLKTVMENFVAFVDKCCAADDKEACFAVEGPKLVVSTQTAL
HSA,         541 KEQLKAVMDDFAAFVEKCCKADDKETCFAEEGKKLVAASQAAL
                  **** **  * *** *** ***** *** ** ***   * **
```

Figure 4.1. Comparative sequence analysis of BSA and HSA performed by http://web.expasy.org/sim/ using sequence data deposited in the protein data bank. [http://www.rcsb.org]

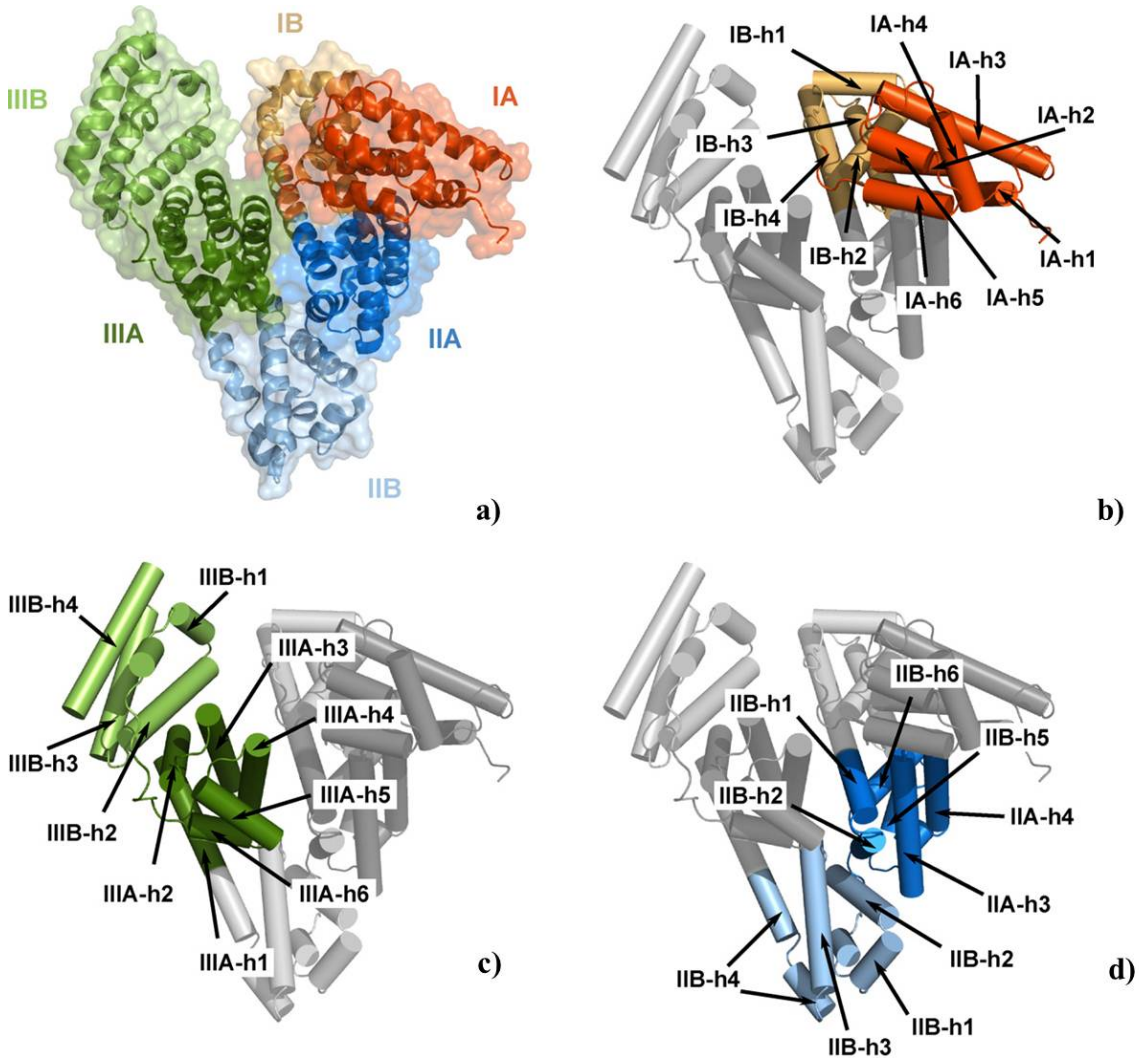

Figure 4.2. Domains and secondary structure elements of the chain A (likewise B) of BSA. Each domain is marked with a different color [orange for the domain I (IA-IB), light blue for the domain II (IIA-IIB) and green for the domain III (IIIA-IIIB)] **a),** and each subdomain is highlighted with a different shade, **b)**, **c)**, **d)**.

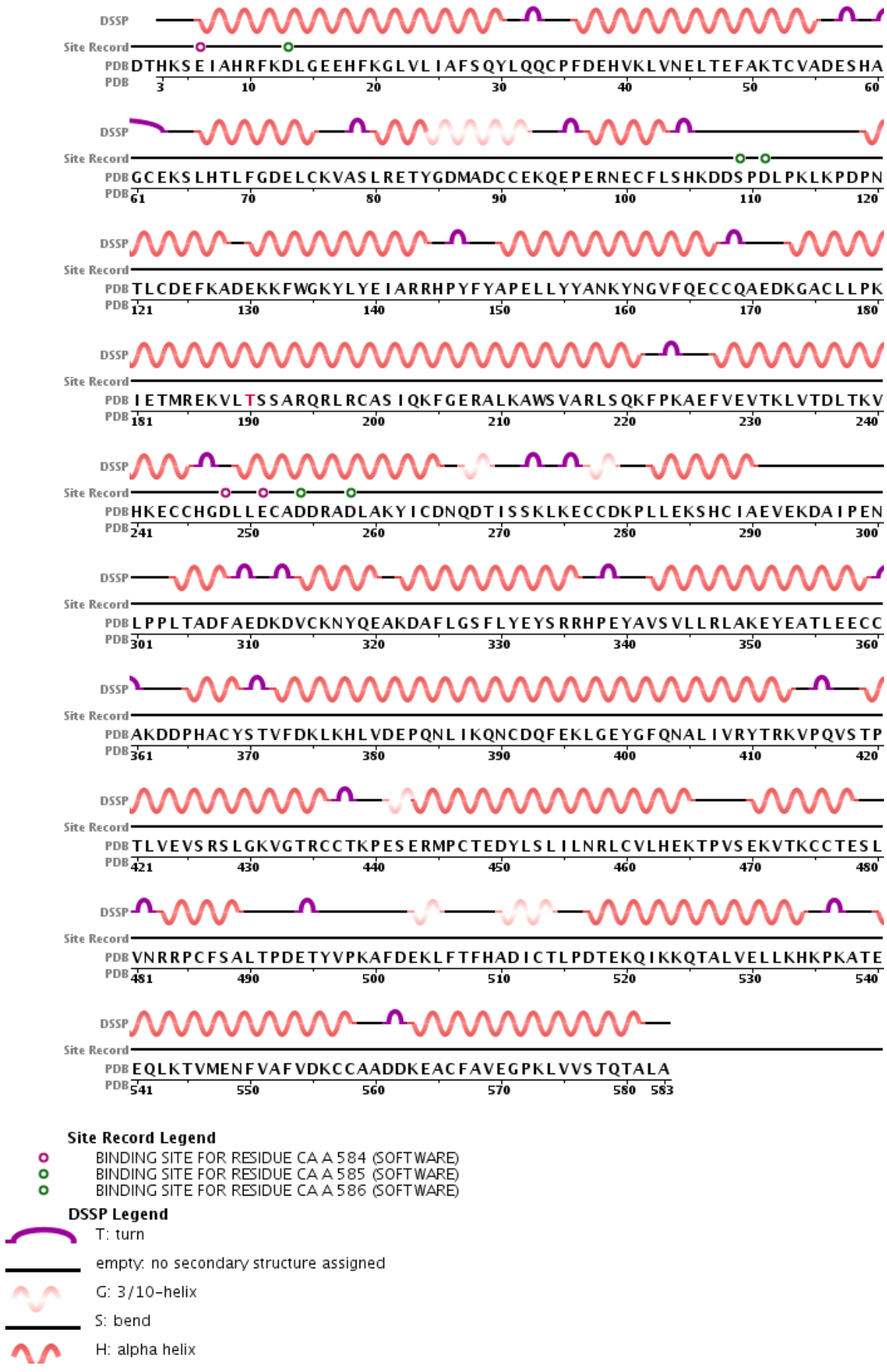

Figure 4.3. Amino acid sequence of BSA along with the showing of the α-helix content.

In addition of being more easily available, BSA contains two tryptophan residues per chain (therefore four for each dimer) instead of only one per chain as occurs in the human counterpart. Notably, in each albumin the common Trp (213b. *vs* 214h.) is buried in the protein core whereas the extra Trp (134) in BSA places on the surface (**Figure 4.4**), thus turning out a more sensitive structural probe.[10]

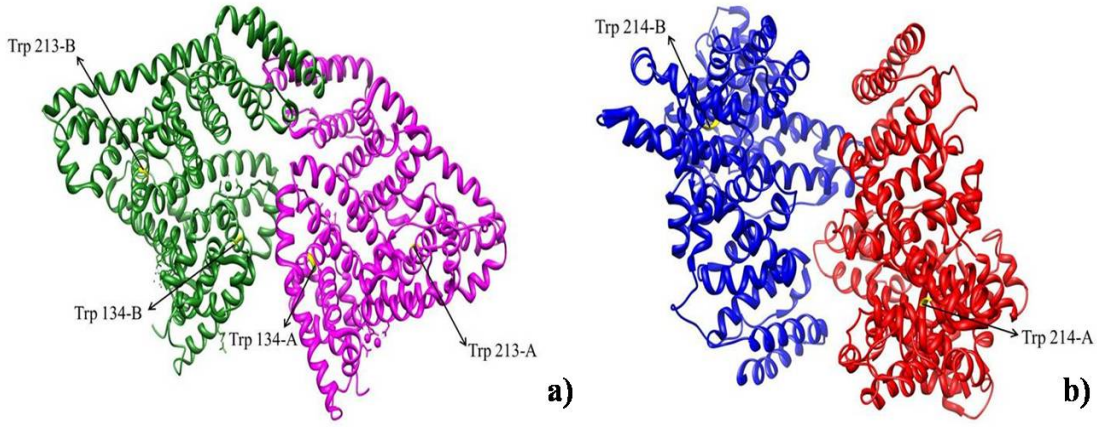

Figura 4.4. Ribbon backbone representation of the structure of BSA **(a)** and HSA **(b).**
The arrows indicate the tryptophane residues in each chain.

Based on the sequence homology between HSA and BSA, we carried out some kinetic studies to check whether an interaction takes place between AuD8 (dissolved in DMSO) and BSA at different molar ratios. Two different spectroscopic techniques were exploited, namely circular dichroism (CD) and fluorescence.

BSA concentration was kept fixed at either 1.5 μM or 15 μM whereas the added amount of AuD8 changed according to the following BSA-AuD8 molar ratios 5:1, 1:1, 1:5 and 1:10, thus elucidating a possible modification of the protein secondary structure (*via* CD) or evaluating changes in superficial or buried protein regions (*via* fluorescence quenching) upon interaction with the gold-based compound.

4.2. Circular dichroism

As previously mentioned, under physiological conditions, BSA is predominantly in the α-helix form (~74 %). The α-helix has an intense and typical CD spectrum (**Figure 4.5**). [11]The negative band at ~ 222 nm is has been ascribed to the π*←*n* transition of the peptide group. [12] The peptide π*←π transition gives rise to the other two bands, through exciton splitting[12, 13]: the negative band at ~208 nm (parallel exciton band) and the positive band at ~190 nm (perpendicular exciton band). However, the unordered component of the polypeptide backbone has to be considered, representing ~26 % of the whole structure. In aqueous solution, proteins in the unordered conformation have a distinguishing CD spectrum[14, 15] with a strong negative band near 197 nm (π*←π transition) and a weak band approximately at 220 nm (π*←*n* transition) (**Figure 4.5**).

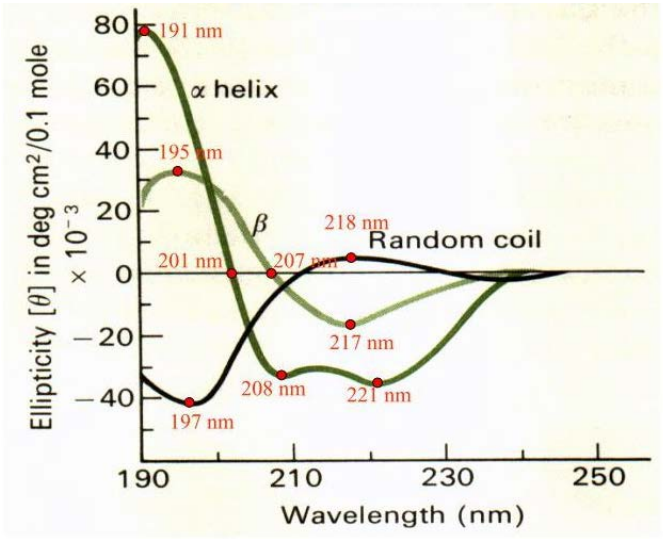

Figura 4.5. Typical dichroic spectra of the three most common protein secondary structures (α-helix, β-sheet and random coil, or better referred to as unordered conformation).

First, the region between 193 nm and 260 nm was taken into account since the above described dichroic bands attributable to the peptide chromophore occur in this range. The CD spectrum of the BSA protein (each black curve reported in **Figure 4.6**) is consistent with the known percentages of α-helix and unordered conformation (comparable intensities of the bands at 208 and 222 nm).

It should be noted that the hyperchromic shift of the curves related to the samples at around 195 nm is due to the presence of DMSO (<0.1% v/v). In fact, the same behavior occurs when only DMSO is added to BSA, observing a more intense band in that spectral region if compared to the BSA spectrum.

Initially, the overall behavior of BSA was observed over time (for 48 h) in order to check the stability of the protein and of the detection system (data not shown). Thus, the phenomena reported below are ascribable to the direct interaction of the albumin with the gold-based compound.

Regarding the 5:1 (BSA/AuD8) sample (**Figure 4.6a**), the CD curve, recorded straightaway after sample preparation, overlaps with the BSA curve while after 24 h, the spectrum is quite different, thus pointing out that a kind of interaction occurs. If we consider the equimolar situation (**Figure 4.6c**), a swinging behavior is detected over time likely due to a non-specific and reversible interaction. On the other hand, **Figure 4.6b** displays a dramatic change of the dichroic spectrum soon after the addition of the complex (in excess) to the protein. This phenomenon appears reinforced after 24 h interaction in terms of intensity, without changing the maxima wavelengths. This behavior could be attributed to an increasing amount of the metal compound bound to the protein.

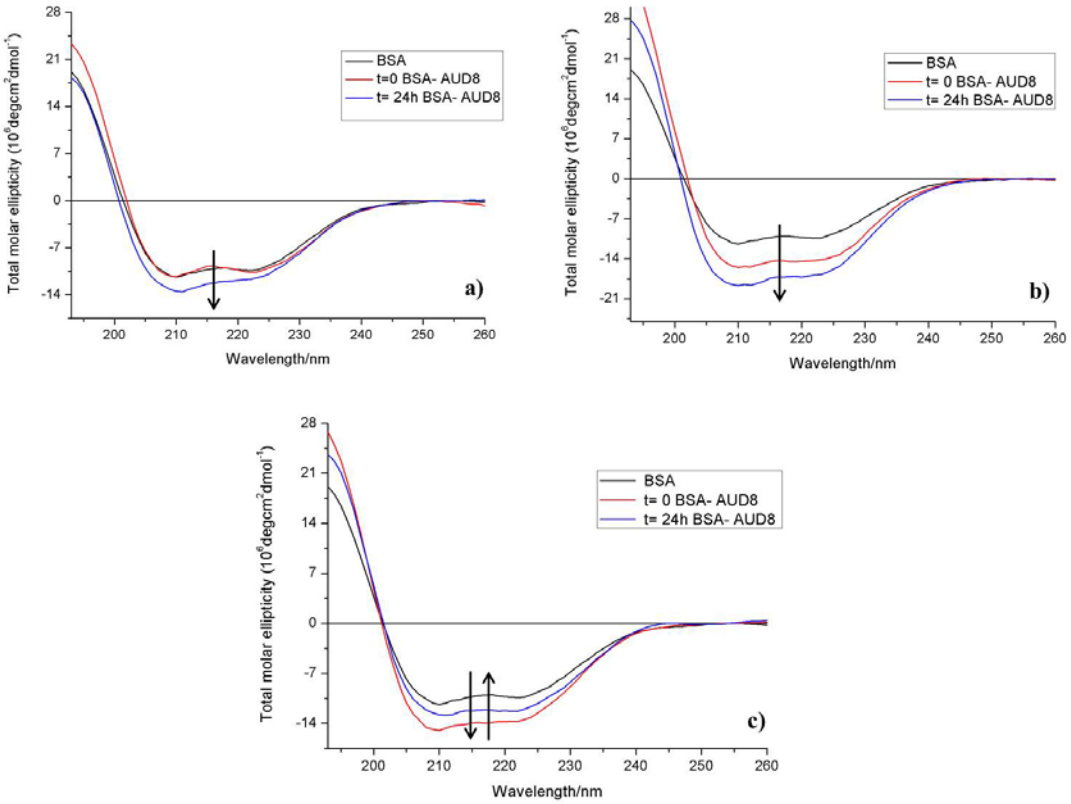

Figure 4.6. CD spectra recorded in the wavelength range 193 ÷260 nm at room temperature at the following BSA (1.5 µM) -AuD8 molar ratios: 5:1 **(a)**, 1:5 **(b)** and 1:1 **(c)**.

On the basis of these considerations, we focused on the BSA/AuD8 molar ratios 1:1 and 5:1 recording the kinetic trends for 24 h (**Figure 4.7**). In each condition, dichroic signal changes irregularly, from the intensity point of view, thus leading us to confirm that the intermolecular interaction between the serum albumin and the compound under examination is weak and

non-specific, likely due to van der Waals forces and/or transient hydrogen bonds occurring between the protein backbone and the dipeptide moiety of AuD8. Therefore, it seems that there is no high affinity binding site (on BSA) toward AuD8: the whole trend of the curves points out a reversible interaction. In fact, if the Au(III) center is directly involved in the coordination, likely irreversible, to some superficial amino acids, the spectrum features would be expected to change dramatically and irreversibly.[10] Furthermore, based on the hydrolysis process described later (§ *Chapter 5*), an interaction between negatively charged protein residues and the cationic gold(III)-aquo complex may occur. However, neither such Coulombic forces nor coordination phenomena probably take place in this case, as completely different over-time trends would be foreseen in terms of both intensity and CD maxima.

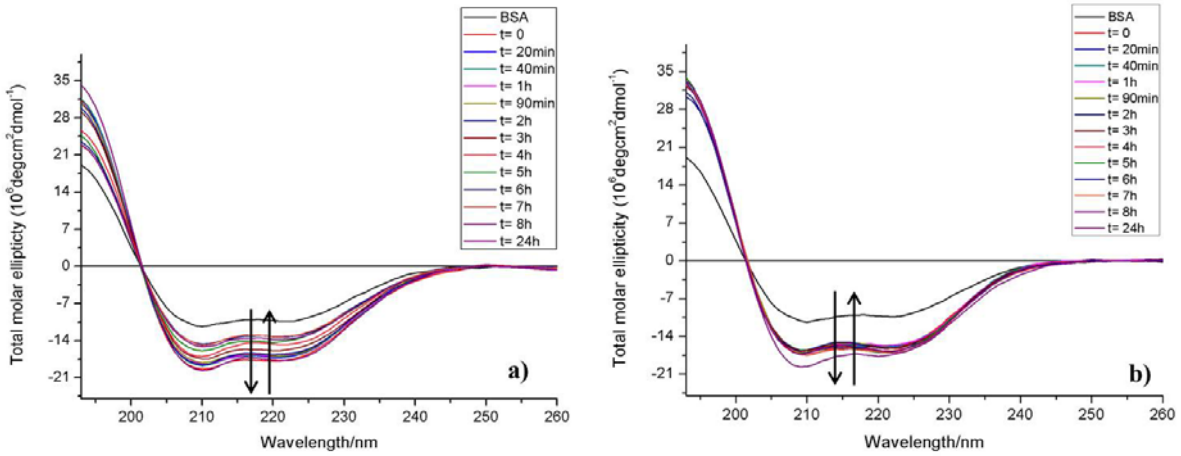

Figure 4.7. CD kinetic study in the wavelength range 193 ÷260 nm at room temperature involving the following BSA (1.5 μM) -AuD8 molar ratios: 5:1 **(a)**, and 1:1 **(b)**.

The kinetics has been repeated under equimolar conditions to confirm the swinging induction of α-helix. The α-helix expansion is reasonable since many peptide backbone regions are loops. It is likely that the presence of a tetrasubstituted amino acid in AuD8 (Aib) may favor the structural change from unordered conformation to α-helix.[16] Coordination phenomena occurring in the regions with unordered conformation may account for the increase of α-helical conformation as well.

If we consider the equation proposed by Chen and Yang to obtain approximate values of the fraction of helix [$f_\alpha = -([\theta]_{222,obs} + 2340) / (30300)$, where $[\theta]_{222,obs}$ stands for the observed 222-nm ellipticity, normalized respect to the numbers of amide bonds, in this case 582], about 90% of the BSA structure is in the α-helical conformation upon interaction with AuD8.[20]

Intriguingly, at a great excess of AuD8 (1:10 molar ratio), another trend of the curves is recorded over time (**Figure 4.8**). In fact, when comparing the collected spectra with the curves shown in **Figure 4.5**, it is possible to state that a structural change from α-helix to β-sheet or unordered conformations seems to occur at this BSA-compound molar ratio. In this context, some simulations are warranted to better define such a solution behavior.

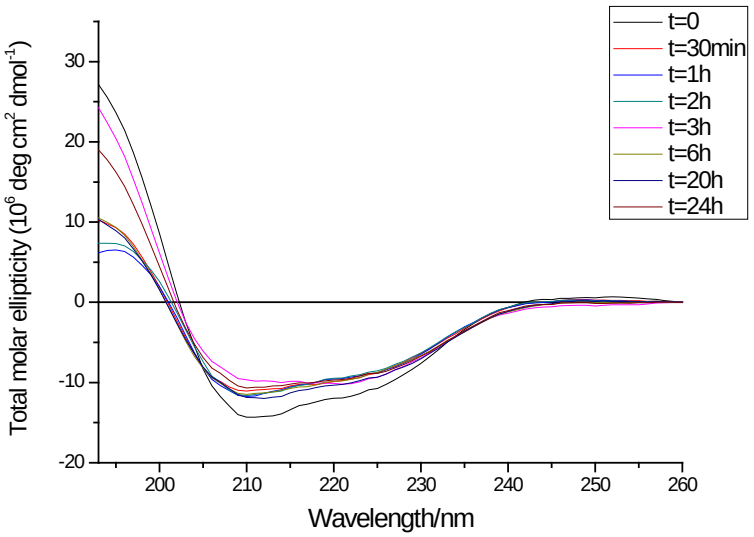

Figure 4.8. CD kinetic study in the wavelength range 193 ÷260 nm at room temperature at 1:10 BSA (1.5 μM) -AuD8 molar ratio.

Subsequently, we examined the CD wavelength range 250÷350 nm in order to check whether the interaction occurring between the metal-based compound and BSA involves the Au(III) center. In fact, in such UV region the transitions ascribable to the "metal core" (*i.e.*, *d-d* transitions and mainly the transitions of the chelating moiety -NCSS) are present (§ *Chapter 5*) and it is possible to exploit the absorption contributes of tryptophan, tyrosine and phenylalanine residues (band at about 270 nm) to check if AuD8 interacts in protein regions close to such aromatic amino acids. **Figure 4.9** shows the curve obtained under equimolar conditions at 15 μM after 24 h interaction. Notably, a small change is detected, thus supporting the hypothesis of a weak interaction which probably occurs nearby aromatic residues with no participation of the metal center. In the opposite case, Au(III) ion should pass from an almost symmetrical environment (slightly distorted square planar geometry according to the solved crystal structure) to a chiral condition, causing a pronounced spectral change in the considered wavelength range.

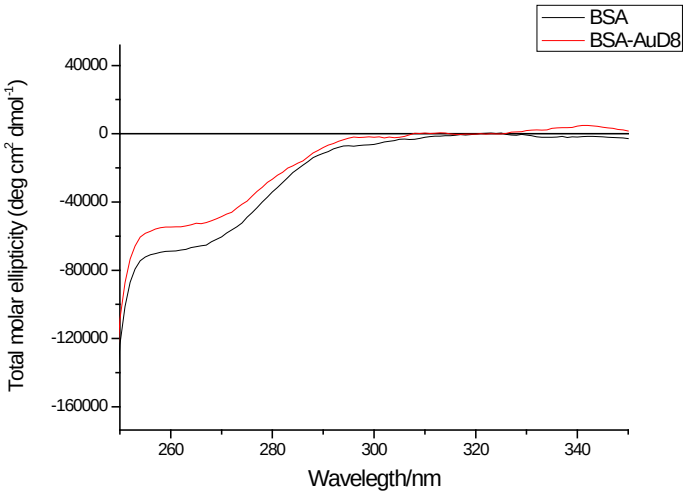

Figure 4.9. CD spectrum acquired in the wavelength range 250 ÷350 nm at room temperature after 24 h interaction between BSA (15 µM) and AuD8 at 1:1molar ratio.

4.3. Fluorescence

As mentioned above, BSA contains two tryptophan (Trp) residues per chain which are known to be excellent fluorogenic structural probes (**Figure 4.10**). Additionally, Trp is the only amino acid exhibiting a strong emission signal at room temperature. Since its lifetime and quantum yield are sensitive to the local environment[10], we exploited its fluorescence to monitor over time the interaction between the model compound and the chosen protein at different molar ratios.

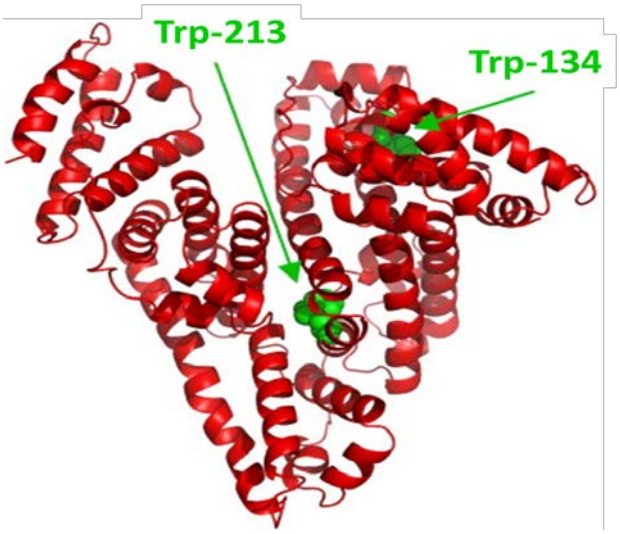

Figure 4.10. Structure of a chain of BSA visualized as a heart-shaped molecule. The two tryptophan residues are colored green (213: buried, 134: superficial).

In fact, the possible AuD8-induced conformational changes of the albumin may determine an increase or decrease in the rigidity/polarity of the Trp environment, which is then reflected on the detected fluorescence properties such as intensity and emission wavelength. On the other hand, similarly to water and oxygen, quenching by AuD8 may occur during the interaction as well. While surface Trp is easily accessible by AuD8, the buried counterpart requires the quencher to either have long-range effects or to penetrate into the tightly packed protein core.

First of all, we tested the fluorescence conditions usually employed in literature.[9, 17, 18] Thus, we first recorded an excitation spectrum exciting in the range 260÷310 nm with the emission wavelength fixed at 349 nm, thus identifying the excitation maximum at 288 nm. Subsequently, by excitation at 288 nm we confirmed that the emission maximum sets at 349 nm.

Two fluorescence kinetics were carried out at different BSA-AuD8 molar ratios (**Figure 4.11**) observing a gradual decrease in intensity over 24-h interaction. The phenomenon of quenching may account for this behavior due to the direct interaction of Trp134/213 with either the metal-based compound or a higher amount of endogenous quenchers such as water molecules and oxygen. In fact, each fluorophore may undergo a small structural change upon interaction (for example in an allosteric way) resulting in a different local environment at a molecular level, thereby justifying the decrease of the quantum yield.

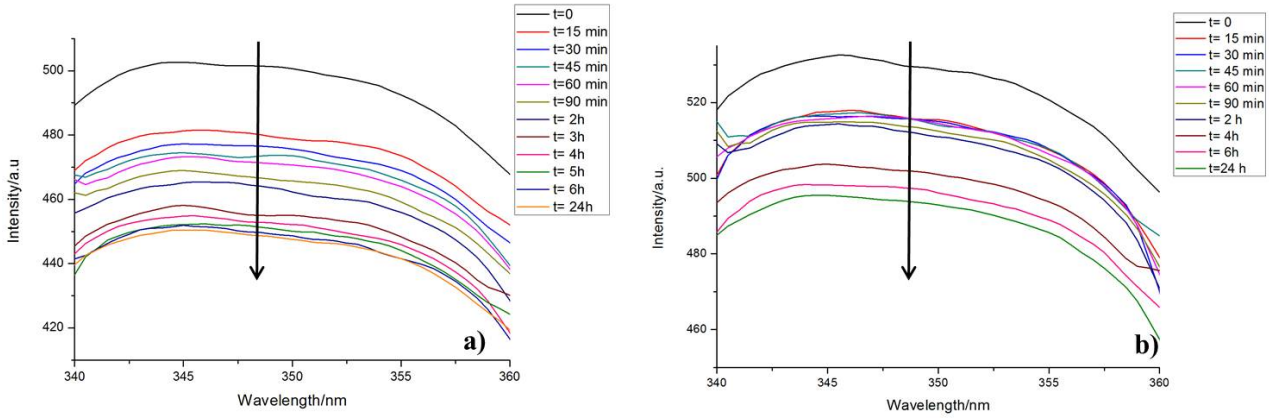

Figure 4.11. 24-h kinetic studies: fluorescence spectra in the 340 and 360 nm region, acquired at room temperature at different BSA (1.5 μM)-AuD8 molar ratios [1:1 **(a)** and 5:1 **(b)**].

In this context, in order to check whether the 24 h intensity lowering is actually due to the protein-AuD8 interaction, we acquired some fluorescence spectra with increasing of

compound equivalents, namely 1:1, 1:3 and 1:5 (**Figure 4.12**). Again, for any considered BSA-AuD8 ratio, an intensity decrease was recorded after 24 h interaction. Notably, an almost linear trend with a negative slop is observed with increasing of the AuD8 amount both at time 0 and after 24 h.

Thus, at both time 0 and after 24 h, increasing AuD8/BSA molar ratio, the number of intermolecular interactions occurring in the system becomes larger and Trp fluorescence progressively decreases.

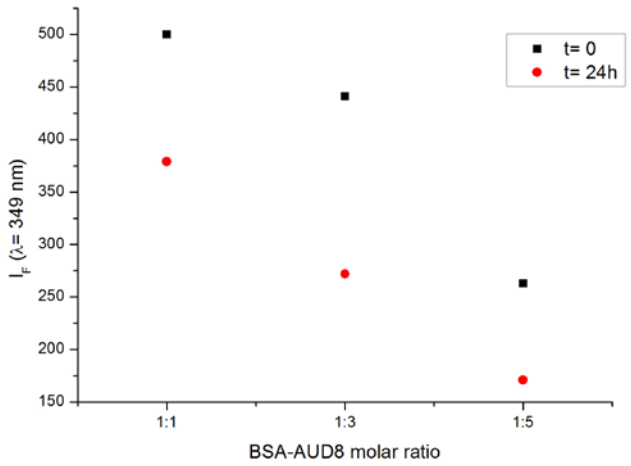

Figure 4.12. Fluorescence emissions at different protein-compound molar ratios both at time 0 and after 24 h interaction.

Finally, the fluorescence of a sample with the protein/AuD8 molar ratio 1:5 was monitored for 32 h (**Figure 4.13**) to better define the spectral modifications occurring upon interaction. A comparative analysis (i.e., the normalization of the curves) proves that the interaction under examination causes fluorescence changes only in terms of intensity, thus pointing out that AuD8 does not affect, directly or indirectly, the local environment polarity of the fluorophores. No wavelength shifts are indeed detected, neither for the fully exposed Trp, emitting at 349 nm, nor for the buried Trp, whose emission appears as a shoulder at about 320 nm.[21] Furthermore, about 50% of the fluorescence intensity is lost upon interaction.

To better explain this scenario, some studies are ongoing in order to distinguish between collisional and static quenching.

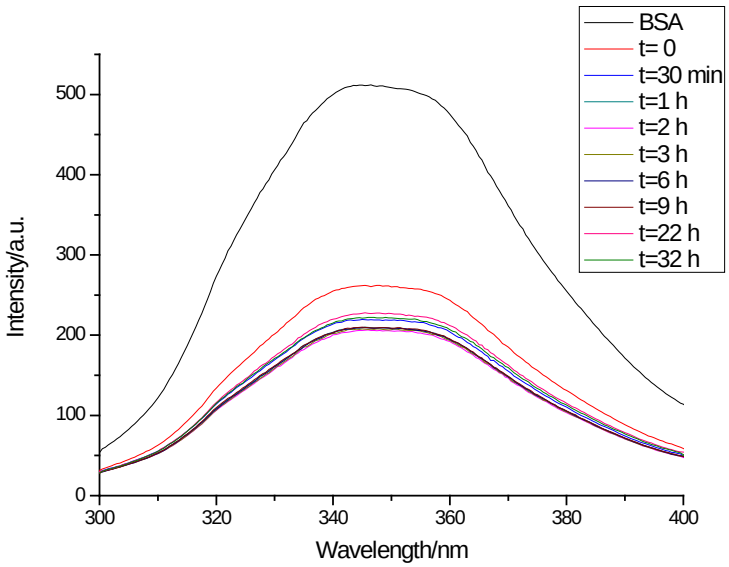

Figure 4.13. 32-h kinetic studies: fluorescence spectra acquired at room temperature at 1:5 BSA (1.5 μM)-AuD8 molar ratio.

In conclusion, in this work we have used quite high AuD8-BSA molar ratios (up to 10) in order to distinguish the type of interaction. On the contrary, under physiological conditions, the AuD8-BSA molar ratio would be very low and AuD8 could be feebly and non-specifically bound to albumin. In fact, following endovenous administration the abundant serum albumin should be able to sequester and, in light of the results herein reported, weakly interact with the gold compound, thus being an optimal vehicle for AuD8 systemic distribution *in vivo*. Additionally, based on the EPR effect in malignancies (§ *Chapter 6*) the passive tumor targeting may take place as well.[4, 19]

Chapter 4 references

1) Sakai, H.; Miyagawa, N.; Horinouchi, H.; Takeoka, S.; Takaori, M.; Tsuchida, E.; Kobayashi, K. Intravenous Infusion of Hb-Vesicles (Artificial Oxygen Carriers) After Repetitive Blood Exchange with a Series of Plasma Expanders (Water-Soluble Biopolymers) in a Rat Model. *Polym. Adv. Technol.* **2011**, *22*, 1216-1222.

(2) Sugio, S.; Kashima, A.; Mochizuki, S.; Noda, M.; Kobayashi, K. Crystal Structure of Human Serum Albumin at 2.5 Å Resolution. *Protein Eng.* **1999**, *12*, 439-446.

(3) Hirayama, K.; Akashi, S.; Furuya, M.; Fukuhara, K. Rapid Confirmation and Revision of the Primary Structure of Bovine Serum Albumin by ESIMS and Frit-FAB LC/MS.

Biochem. Biophys. Res. Commun. **1990**, *173*, 639-646.

(4) Kratz, F. Albumin as a Drug Carrier: Design of Prodrugs, Drug Conjugates and Nanoparticles. *J. Controlled Release* **2008**, *132*, 171-183.

(5) Peters Jr., T. Serum Albumin. *Advances in Protein Chemistry* **1985**, *37*, 161-245.

(6) He, X. M.; Carter, D. C. Atomic Structure and Chemistry of Human Serum Albumin. *Nature* **1992**, *358*, 209-215.

(7) Majorek, K. A.; Porebski, P. J.; Dayal, A.; Zimmerman, M. D.; Jablonska, K.; Stewart, A. J.; Chruszcz, M.; Minor, W. Structural and Immunologic Characterization of Bovine, Horse, and Rabbit Serum Albumins. *Mol. Immunol.* **2012**, *52*, 174-182.

(8) Punith, R.; Seetharamappa, J. Spectral Characterization of the Binding and Conformational Changes of Serum Albumins upon Interaction with an Anticancer Drug, Anastrozole. *Spectrochimica Acta - Part A: Molecular and Biomolecular Spectroscopy* **2012**, *92*, 37-41.

(9) Hamdani, S.; Joly, D.; Carpentier, R.; Tajmir-Riahi, H. A. The Effect of Methylamine on the Solution Structures of Human and Bovine Serum Albumins. *J. Mol. Struct.* **2009**, *936*, 80-86.

(10) McCaul, C. P.; Ludescher, R. D. Room Temperature Phosphorescence from Tryptophan and Halogenated Tryptophan Analogs in Amorphous Sucrose. *Photochem. Photobiol.* **1999**, *70*, 166-171.

(11) Holzwarth, G.; Doty, P. The Ultraviolet Circular Dichroism of Polypeptides. *J. Am. Chem. Soc.* **1965**, *87*, 218-228.

(12) Woody, R. W.; Tinoco Jr., I. Optical Rotation of Oriented Helices. III. Calculation of the Rotatory Dispersion and Circular Dichroism of the Alpha- and 310-Helix. *J. Chem. Phys.* **1967**, *46*, 4927-4945.

(13) Tinoco Jr., I.; Woody, R. W.; Bradley, D. F. Absorption and Rotation of Light by Helical Polymers: The Effect of Chain Length. *J. Chem. Phys.* **1963**, *38*, 1317-1325.

(14) Greenfield, N.; Fasman, G. D. Computed Circular Dichroism Spectra for the Evaluation of Protein Conformation. *Biochemistry* **1969**, *8*, 4108-4116.

(15) Curtis Johnson Jr., W.; Tinoco Jr., I. Circular Dichroism of Polypeptide Solutions in the Vacuum Ultraviolet [33]. *J. Am. Chem. Soc.* **1972**, *94*, 4389-4390.

(16) Gobbo, M.; Biondi, L.; Filira, F.; Formaggio, F.; Crisma, M.; Rocchi, R.; Toniolo, C.; Broxterman, Q. B.; Kamphuis, J. Helix Induction Potential of N-Terminal A-Methyl, A-Amino Acids. *Lett. Peptide Sci.* **1998**, *5*, 105-107.

(17) Sivakumar, R.; Naveenraj, S.; Anandan, S. Interactions of Serum Albumins with Antitumor Agent Benzo [a] Phenazine - A Spectroscopic Study. *J Lumin* **2011**, *131*, 2195-2201.

(18) Zhou, B.; Qi, Z. -.; Xiao, Q.; Dong, J. -.; Zhang, Y. -.; Liu, Y. Interaction of Loratadine with Serum Albumins Studied by Fluorescence Quenching Method. *J. Biochem.*

Biophys. Methods **2007**, *70*, 743-747.

(19) Maeda, H.; Bharate, G. Y.; Daruwalla, J. Polymeric Drugs for Efficient Tumor-Targeted Drug Delivery Based on EPR-Effect. *European Journal of Pharmaceutics and Biopharmaceutics* **2009**, *71*, 409-419.

(20) Y.-H. Chen, J. T. Yang, *Biochem. Biophys. Res. Commun*., **1971**, 44, 1285-1291.

(21) Lakowicz, *J.R. Principles of Fluorescence Spectroscopy* (3rd Ed.); Springer, 2006.

Chapter 5. Solution stability studies preclusive to the acute toxicity tests in vivo

In prospect to carry out studies of acute toxicity in mice, the proper vehicle to administer as a control and to use as solvent for the test compound (AuD8) had to be defined. Two administration ways were taken into account, intravenous (i.v) and oral ones. Once defined the suitable medium for the i.v. route, i.e. DMSO-EtOH-RL 50:10:40% v/v where RL stands for Ringer Lactate (Eurospital®), a kinetic study was performed by UV-Vis spectrophotometry. In order to better clarify the spectral features, several media were considered such as the reference solvent DMSO, ethanol, water, sodium chloride solution (also called saline solution), RL and phosphate buffered saline (abbreviated as PBS). Under every condition, several electronic spectra were recorded over time to elucidate the reactivity of AuD8.

Concerning the oral administration route, a sunflower-seed oil (Collina d'oro®), was used as a vehicle. Thus, we investigated the AuD8 stability after stirring in this medium for 3 h by far FT-IR and ^{1}H-NMR spectroscopies.

5.1. Stability studies under different medium conditions

5.1.1. Stability studies in DMSO

As mentioned above, some electronic spectra of AuD8 were acquired in DMSO (190-600 nm) over 48 h (**Figure 5.1**) at 25 °C at a concentration of 100 μM and the main features have been collected in **Table 5.1**. It is worth highlighting that the Au(III) complex is well soluble in DMSO where it proved by ^{1}H-NMR to be stable over 48 h (data not shown). Furthermore, this solvent was used to dissolve the compound prior to treating tumor cells (< 0.5% v/v).[1,15] Thus, DMSO has been considered as a reference medium for the spectrophotometric studies described in this chapter.

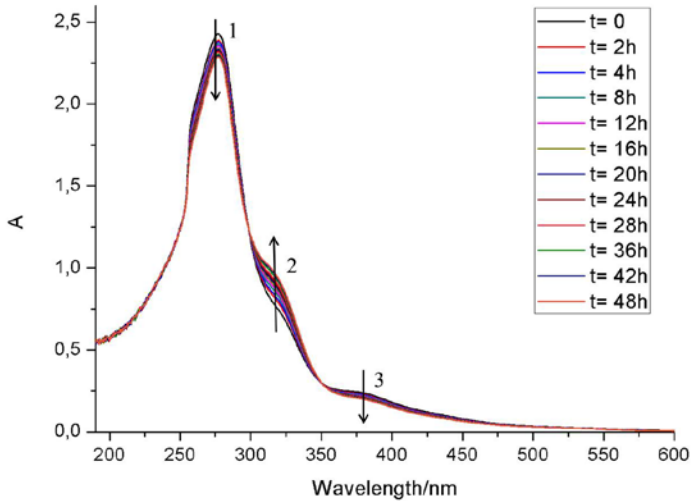

Figure 5.1. AUD8 UV-Vis spectra recorded in DMSO over 48 hours at 25°C.

Table 5.1. Main absorption bands in the UV-VIS electronic spectra acquired in different media.

Solvent	λ_{max}/nm (logε^{*})		
	Band 1	**Band 2**	**Band 3**
DMSO [(a) #]	277.3 (4.39)	315.3 (4.00)	375.7 (3.39)
EtOH [(a)]	267.5 (4.31)	312.5 (3.97)	390.9 (3.14)
Water [(b)]	272.2 (4.09)	313.4 (4.05)	394.4 (2.48)
Saline solution [(b)]	263.7 (4.21)	311.0 (3.83)	384.8 (2.82)
RL [(b)]	272.1 (4.19)	313.4 (4.16)	398.1 (2.85)
PBS [(b)]	271.9 (4.12)	313.0 (4.08)	396.6 (3.16)
DMSO-EtOH-RL [(b)] 50:10:40%	274.3 (4.18)	315.9 (4.11)	405.5 (3.05)

* evaluated at time 0.
(a) performed at 25 °C.
(b) performed at 37 °C.
when performed at 37 °C, the bands set at 277.3, 316.7 and 391.4 nm.

Band 1 and band 2 display very large molar extinction coefficients (ε) and have been ascribed in the literature to intraligand π*←π transitions mainly located in the -NCS and -CSS moieties, respectively.[2, 3] Moreover, an intraligand π*←*n* transition, where *n* is the in-plane non-bonding sulfur orbital, should be recorded at around 340 nm.[4] However, this band is not observed owing to the overlap with the more intense adjacent bands.

Only in this medium a shoulder at 257 nm is visible. Owing to the quite high oxidizing power of Au(III), such transition has been ascribed to an electron transfer of the type $u \leftarrow g$ from a 4p orbital (σ symmetry) of the bromide ligands to the lowest unfilled 5d orbital.[5] The same type of transition has been attributed to the weak band 3, its lower intensity being explained by a decreased overlap between the 5d metal orbital and the involved 4p orbital (in this case with a π symmetry).[5] However, some investigators have ascribed band 3 to an intramolecular M → L charge transfer involving the M *nd* orbitals and the dithiocarbamato π* system.[6, 7] In this regard, it can be of some interest to stress that recent DFT calculations carried out in the framework of the zeroth order regular approximation (ZORA) scalar relativistic approach on a series of square planar Pt(II) (isoelectronic with Au(III)) dithiocarbamato complexes have pointed out that the LUMO is not a Pt(II) 5$d_{x^2-y^2}$-based AO (**Figure 5.2**) rather a S-based MO. In this type of covalent complexes, both σ and π contributions should be taken into account since the relative position of the 5d-based MOs is the result of a subtle balance between σ and π M–L interaction. To better define nature, energy and localization of AuD8 transitions, time dependent DFT calculations are going to be run.[16]

In light of these considerations and the observed extinction coefficient (~2400), although the slightly distorted square-planar geometry, the probability that actual $d \leftarrow d$ transitions (spin allowed but symmetry forbidden[17]) take place is very low. Anyway, if they occur, their contribution to the observed band in terms of intensity may be considered negligible. However, for practicality reasons, in the following sections the band 3 will be discussed as if it is due to solely $d \leftarrow d$ transitions.

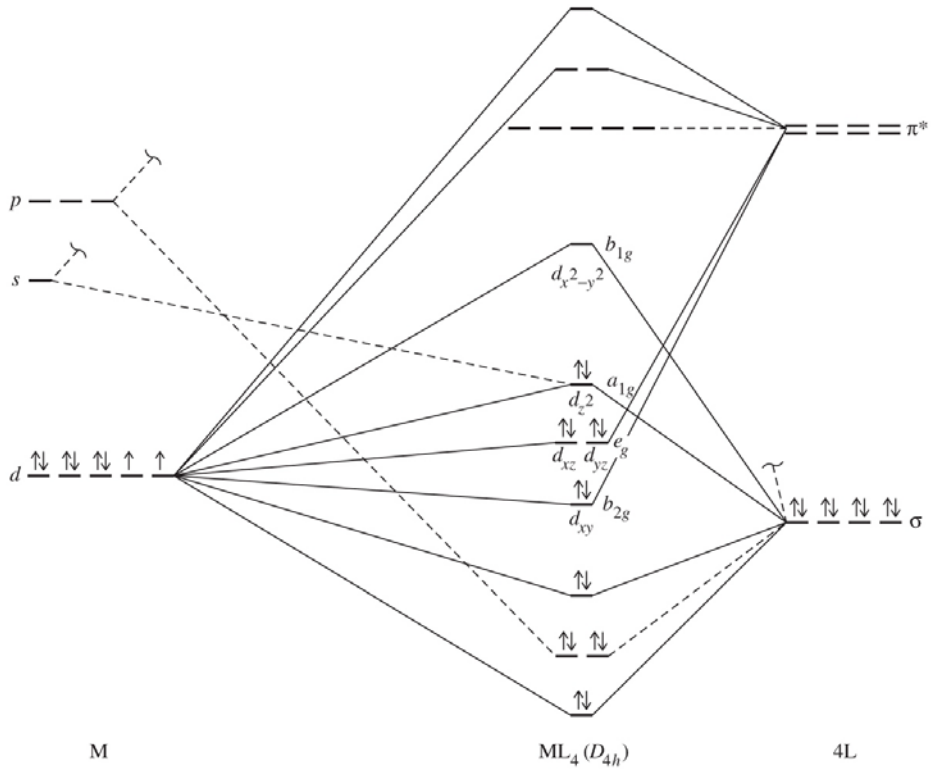

Figure 5.2. Qualitative energy splitting of the *5d* orbitals in a square-planar geometry.

Overall, the maxima wavelengths do not change, thus confirming that the compound is stable throughout 48-h acquisition. Nevertheless, bands 1 and 3 show a progressive absorbance lowering while band 2 intensity increases over time. It is likely that a hydrolysis reaction takes place to a small extent owing to the presence of water in the used DMSO, being not perfectly anhydrous.[8, 9,18] On the other hand, a coordination process involving DMSO molecules might occur as well.

Since the i.v. vehicle contains also ethanol, we checked the AuD8 stability in this alcohol as well (spectrum not shown). Table 5.1 reports the observed band maxima. It is worth highlighting that on passing from ethanol ($\varepsilon = 24.30$, 25 °C) to water ($\varepsilon = 78.54$, 25 °C)[19], a red shift is detected for the $\pi^* \leftarrow \pi$ transitions, namely bands 1 and 2, due to the greater stabilization of π^* orbitals compared to π orbitals in a more polar solvent.[20]

5.1.2. Stability studies in water

The evolution with time has been followed by UV-Vis spectrophotometry in deionized water for 48 h at 37 °C under stirring (**Figure 5.3**), the compound AuD8 being previously dissolved in DMSO (final concentration 100 μM, 6.6% v/v content of DMSO). **Table 5.1** reports only the absorptions recorded at the time 0.

The positions of the bands 1, 2 and 3 does not substantially change but their intensities slightly increase within the first 15, 45 and 50 minutes, due to the immediate hydrolysis of the gold(III)-halogen bonds giving rise to the corresponding aquo complex (positively charged) which is more water soluble and likely characterized by a higher molar extinction coefficient.[8] Then, the conversion to the hydroxo derivative (neutral) can be associated with the subsequent absorbance decrease and formation of precipitate.

In this medium, a new band immediately rises at 546 nm (but its intensity decreases after about 1 h) and is ascribable to the formation of gold nanoparticles, thus pointing out that a metal-ligand dissociation process takes place in water. It is likely that the free dithiocarbamato ligands may act as cappants thereby stabilizing the surface of these nanoclusters and preventing their aggregation. Moreover, the bromide ligands and the free dithiocarbamate may act as *in situ* reductants, thus favoring the $Au^{III} \rightarrow Au^{0}$ conversion. According to the surface plasmon resonance theory[21,22,23], the obtained quantum dots are estimated to be about 20 nm wide.

In comparison with the electronic spectrum acquired in DMSO, in water the bands show a different pattern. In fact, the band 2 is now well distinguishable, both bands 1 and 2 (attributed to intramolecular intraligand transitions $\pi^{*} \leftarrow \pi$ located in the –NCS and –CSS moieties, respectively) displaying a blue-shift on moving from DMSO to water with an ε now comparable. Furthermore, the *d-d* band is detected at higher wavelengths (394 nm) and this red shift is probably caused by a stabilization of the $d_{x^2-y^2}$ orbital (or alternatively the S-based LUMO, see § *5.1.1*) in water due to the high dielectric constant of this solvent. In fact, the band 3 sets at shorter wavelengths when organic solvents with lower dielectric constant (*i.e.*, DMSO and ethanol) are used.

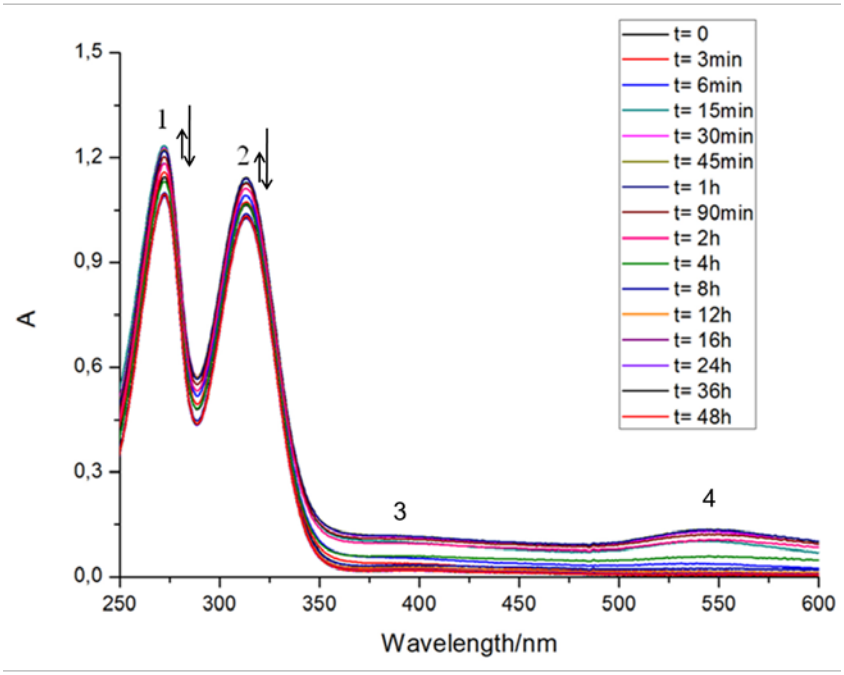

Figure 5.3. AUD8 UV-Vis spectra recorded in water over 48 hours at 37 °C.

5.1.3. Stability studies in saline solution

Regarding the band 3, likewise organic solvents, the same blue-shifted behavior, in comparison with water, occurs also in the investigated saline solution (**Figure 5.4**), in agreement with literature data related to aqueous solutions containing strong electrolytes.[10] In particular, we studied the stability of AuD8 in a solution of sodium chloride in water (0.9% w/v) because it is commonly employed in intravenous infusions of drugs into patients. Also in this case, AuD8 was beforehand dissolved in DMSO and subsequently diluted with saline solution (6.3% v/v content of DMSO) to yield the final concentration of 100 μM. Then, UV-Vis spectra were recorded (230÷600 nm) over 24 h at 37 °C under stirring. **Table 5.1** collects the main features of the spectrum recorded at time 0, the bands showing similar over-time trends to those obtained with DMSO. However, in saline solution the band 2 is not overlapped to band 1 as takes place in DMSO. Furthermore, the initial extinction coefficients are lower than those detected in DMSO. On the whole, the maximum position of the bands is essentially unchanged over time, pointing out that the gold center remains in the +3 oxidation state due to the stabilization effects played by the chelating dithiocarbamato ligand. [8, 11]

The change in spectral intensity has been ascribed again to the progressive hydrolysis of gold(III)-bound bromide ions, leading to the hydroxo complex and/or the water-soluble

aquo one. In order to better define this species, a greater amount of compound was dissolved in saline solution and let to stir at 37 °C for 24 h at the final concentration of 100 μM, thus resulting in the formation of a yellow precipitate. After centrifugation, the solid was washed twice with ethanol and once with *n*-pentane and finally dried *in vacuo* in the presence of P_2O_5. Then, a far FT-IR spectrum was acquired and it is reported in **Figure 5.5**. It should be noted that dithiocarbamato moiety is not affected by the medium as the corresponding diagnostic bands appear unchanged (ν_s(SCS) at around 545 cm^{-1}; $\nu_{a/s}$(SAuS) at around 411 and 380 cm^{-1}, respectively). On the contrary, as expected, the Au-Br vibrational modes disappear in the 220÷250 cm^{-1} region, thus supporting the hypothesis of hydrolysis of the complex. Additionally, new bands set in the spectral range 315÷350 cm^{-1} and they are have been ascribed to Au-OH stretching. In fact, the compound $Au(OH)_3$, available in laboratory, shows bands in the same spectral region.

The gold(III) center is quite acidic and therefore lowers the pK_a of coordinate water molecules, thus accounting for the formation of the hydroxo derivative [dtcAu$(OH)_2$], in agreement with literature data.[8,9,18] Moreover, after centrifugation the liquid phase was stored and the final pH was measured to be 4.55, so confirming the formation of a species containing coordinated hydroxo groups.

Regarding the spectral intensities, a hyperchromic effect is immediately observed for the band 2 whereas a hypochromic effect and a slight bathochromic shift are detected for the band 1 (from 270 to 272 nm) associated with the progressive hydrolysis and hydroxo complex precipitation. It should be noted that the band at around 380 nm immediately increases over time and changes the shape. However, after about 4 hours its absorbance decreases. Such a behavior in this spectral region may be explained considering the contribution of the metal-to-ligand charge-transfer transition when hydroxo groups are bound to gold(III) center.[12]

Remarkably, from a comparative analysis of the spectra recorded in water and in saline solution, it seems that the formation of the hydroxo complex occurs to a greater extent in the presence of salt, thus pointing out that sodium chloride plays a key role in the reaction. Owing to the high concentration of chloride anions (155 mM), we hypothesized a Br/Cl ligand exchange (as bromide ion is a good leaving group) along with a release of the second bromide ion, being replaced by a water molecule. Upon water coordination, its protons are quite acidic and such a character is enhanced by a possible interaction with the chloride ligand, thus leading to the leaving of HCl and formation of a [SS=Au(OH)H_2O] complex (following the entrance of a second water molecule). This species likely evolves toward the

final compound [SS=Au(OH)$_2$]. In fact, as already mentioned, the final pH of the liquid phase was acidic.

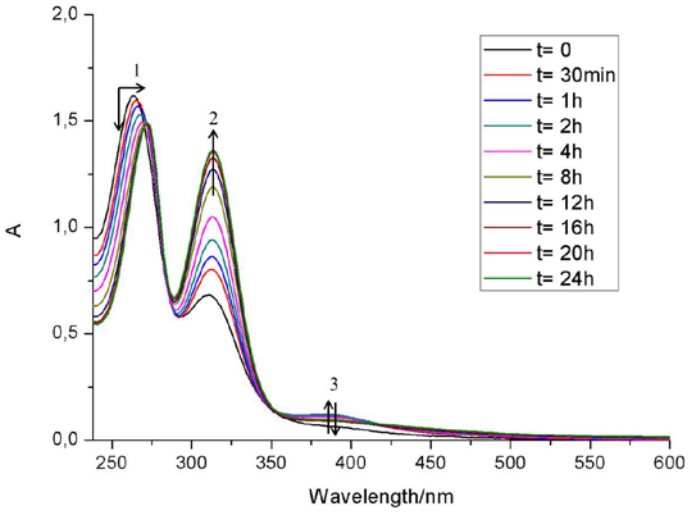

Figure 5.4. AuD8 UV-Vis spectra recorded in saline solution over 24 hours at 37 °C.

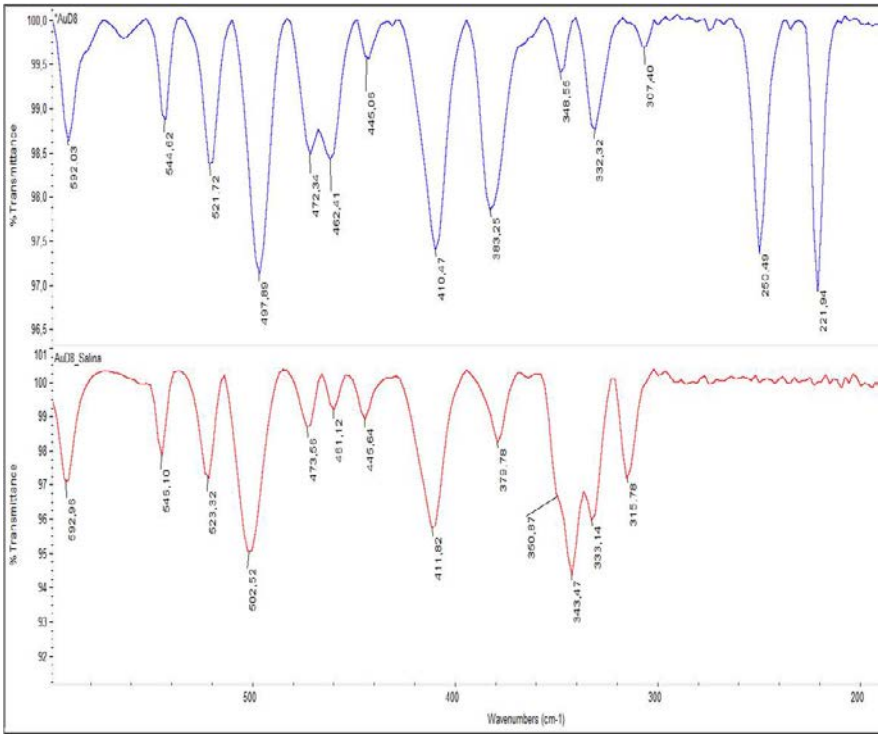

Figure 5.5. Far FT-IR spectra recorded for the complex AuD8 (upper panel) and AuD8 after 24 h in saline solution (lower panel).

5.1.4. Stability studies in Ringer Lactate

As previously described, besides DMSO and ethanol, the vehicle defined for the i.v. administration comprises also Lactated Ringer's solution (hereinafter RL) at 40% v/v. RL is a sterile water solution that is isotonic with blood and used for intravenous administration. RL contains NaCl (205 mM), lactic acid (58 mM), NaOH (59 mM), $CaCl_2$ (5 mM), and KCl (11 mM) with a pH value of 6.75. RL is generally used to replace fluid lost by the body in different injuries including severe burns, trauma, significant blood loss, dehydration and surgery. Another common use is the treatment of renal failure in small animals, where the solution is administered subcutaneously instead of the i.v. way.

The chemical behavior of AuD8 was tested in this medium for 24 hours at 37 °C under stirring (**Figure 5.6**). Similarly to the foregoing cases, the compound was dissolved in DMSO beforehand the addition to RL (6.6% v/v DMSO content), yielding a final concentration of 100 µM.

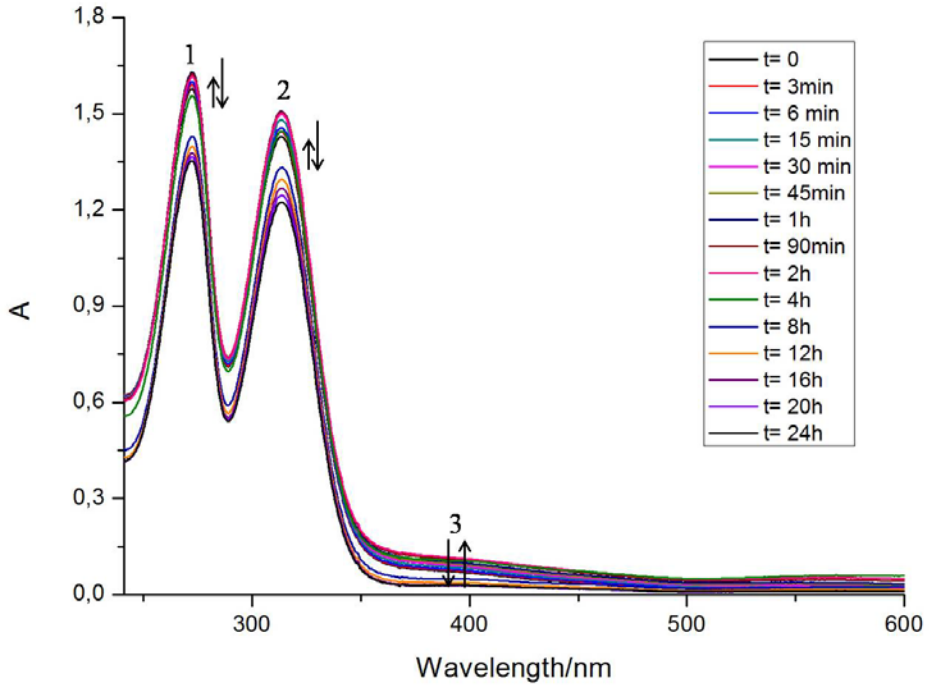

Figura 5.6. AuD8 UV-Vis spectra recorded in Ringer Lactate over 24 hours at 37 °C.

Table 5.1 collects the main features of the spectrum recorded at time 0, including the λ_{max} values which are essentially unchanged over time.

In light of the previous considerations, the gold center remains in the +3 oxidation state and the modification in spectral intensity is again ascribed to the progressive hydrolysis of gold(III)-bound bromide ions, leading to the aquo and/or hydroxo complexes.[13, 14,18]

The overall behavior is similar to those observed in water, except for a more protracted absorbance increase (120 mins for bands 1 and 2, instead of 15 and 45 mins, respectively).
In this solvent the *d-d* transition sets at 398 nm whereas it occurs at 385 nm in saline solution. Based on the composition of both media, such shift may be explained considering the presence of lactate ($CH_3CH(OH)COO^-$) in RL, which might coordinate to the gold center due to its potentially metal-chelating character.

5.1.5. Stability study in phosphate buffered saline (PBS)

Compared to saline solution (138 mM NaCl), PBS contains also KCl (2.7 mM) and the pH is buffered at 7.4 (at 25 °C) with phosphate (0.01 M). PBS (buffer often used in *in vitro* experiments) was used to simulate the physiological conditions when administering AuD8 *in vivo*.

Similar to the previous studies, AuD8 was predissolved in DMSO and then diluted with PBS to the final concentration of 100 μM (5.2% v/v DMSO content). Electronic spectra were subsequently recorded (240-600 nm) over 24 h (**Figure 5.7**) at 37 °C under stirring. **Table 5.1** shows the absorptions in the spectrum recorded at time 0.
Band 2 shows a comparable ε with band 1, as occurred in water. Intriguingly, the absorption spectrum shows a dramatic change soon after the addition of the complex to the physiological medium. The position of the bands does not basically change, but their intensities strongly lower over time, due to the possible hydrolysis of the Au(III)-Br bonds, followed by the precipitation of a light yellow water-insoluble compound at a final pH of 8.58 wherein the species PO_4^{3-} is present. ($pK_{a,1}$= 2.12; $pK_{a,2}$ = 7.21; $pK_{a,3}$= 12.67)[19]. So far, the obtained precipitate has been partially characterized by its far FT-IR spectrum (**Figure 5.8**) showing absorptions at around 350÷370 cm^{-1}, consistent with the coordination of phosphates[24], which replace hydroxo groups (upon hydrolysis) or the original bromide ligands. Intriguingly, if this species is kept in PBS for other 24 h, it turns into brownish, thus leading us to hypothesize a subsequent reduction of the complex to yield Au(I)- or Au^0-containing derivatives.

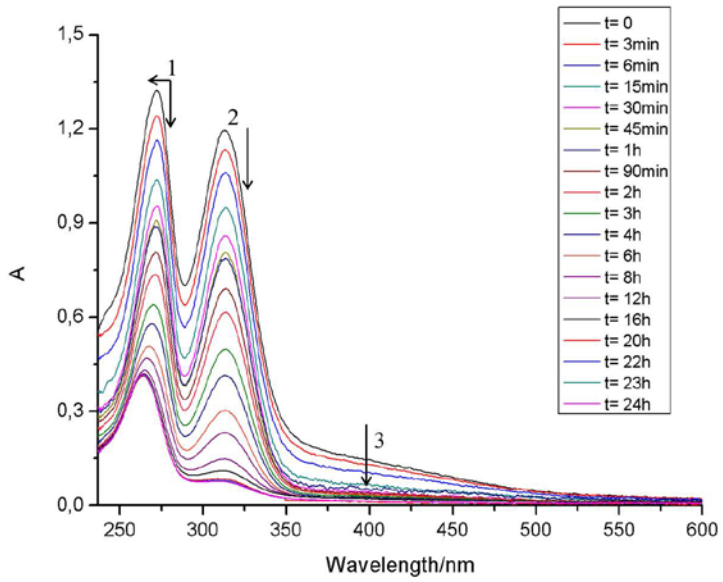

Figure 5.7. AuD8 UV-Vis spectra recorded in PBS over 24 hours at 37 °C.

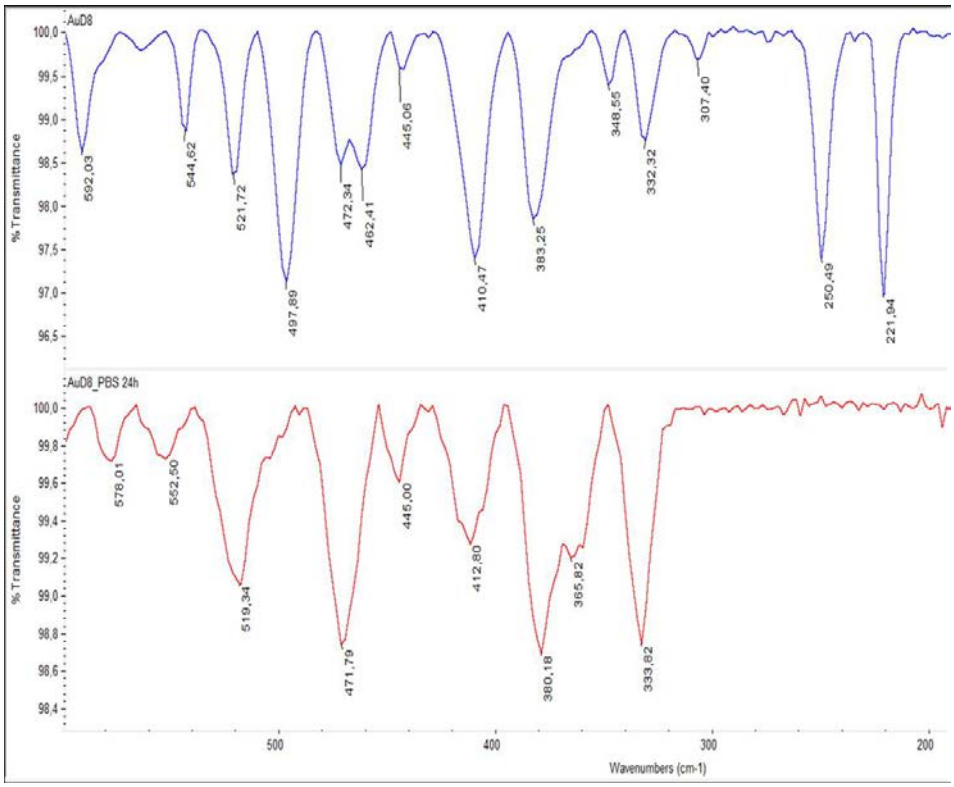

Figure 5.8. Far FT-IR spectra recorded for the complex AuD8 (upper panel) and AuD8 after 24 h in PSB (lower panel).

5.1.6. Stability study in the complete vehicle chosen for acute toxicity in mice (intravenous administration route)

Concerning sample formulation for the i.v. administration way, several attempts were carried out in order to find out the better vehicle in terms of aqueous medium percentage (as high as possible) and DMSO amount which is necessary to properly dissolve the quite hydrophobic complex AuD8. Thus, the selected medium was DMSO-EtOH-Ringer Lactate (Eurospital®) 50:10:40% v/v. It is worth noting that ethanol was used to decrease the relative amount of DMSO but the alcoholic percentage could not be higher than 10% in order to prevent compound precipitation, thus ruling out the possibility of the onset of severe physiological phenomena such as embolism in the subsequent tests *in vivo*.

In this spectrophotometric study, a calculated amount of AuD8 was predissolved in DMSO and subsequently diluted with ethanol. Then, RL was added according to the volume ratios previously reported to yield the final concentration of 100 μM. UV-Vis spectra were immediately acquired under stirring in the wavelength range 253 ÷ 600 nm over 24 h (**Figure 5.9**) at 37 °C. In the **Table 5.1** are reported the main features of the spectrum recorded at time 0.

In this mixed medium, bands 1 and 2 show an increase of the intensities within the first 60 minutes, followed by a progressive lowering of the whole spectrum over the next 23 hours along with the formation of a yellow precipitate. Again, the high metal oxidation state +3 is kept because there is no wavelength change during the investigated time. Based on the previous results related to the other solvents, the observed behavior can be ascribed to the immediate hydrolysis of AuD8 resulting in the substitution of the halogen ions with water molecules. Then, the deprotonation of the Au(III)-aquo complex likely may lead to the hydroxo counterpart which is insoluble in this mixture of solvents. In order to confirm this hypothesis, a larger amount of complex was dissolved in the mixture under examination (DMSO-EtOH-RL) and let to stir at 37 °C for 24 h at the final concentration of 100 μM, thus resulting in the formation of a yellow/light brown precipitate. After centrifugation, the solid was washed twice with ethanol and once with *n*-pentane and finally dried *in vacuo* in the presence of P_2O_5. Then, a far FT-IR spectrum was acquired and it is reported in **Figure 5.10**. As expected, the Au-Br vibrational modes disappear in the 220÷250 cm^{-1} region, thus supporting the hypothesis of hydrolysis of the complex. Additionally, new absorptions are visible in the spectral range 350÷370 cm^{-1} and they are ascribed to Au-OH stretching[24], also based on the spectrum recorded for the compound $Au(OH)_3$. Furthermore, it is possible that

the lactate ion coordinates the gold(III) center, being the former a chelating ligand and the latter a border-line metal ion (between hard and soft character).

Following the prominent initial hydrolysis of part of the sample, the overall profile of the spectrum resembles that obtained in pure DMSO, thus suggesting that the remaining AuD8 molecules are mainly solvated by the organic solvents (*i.e.*, DMSO and ethanol, total 60% v/v). Furthermore, if we consider the final curves in this kinetics (Figure 5.9) the absorbance change recorded every 4 h is progressively smaller, pointing out that the hydrolysis process occurs more slowly.

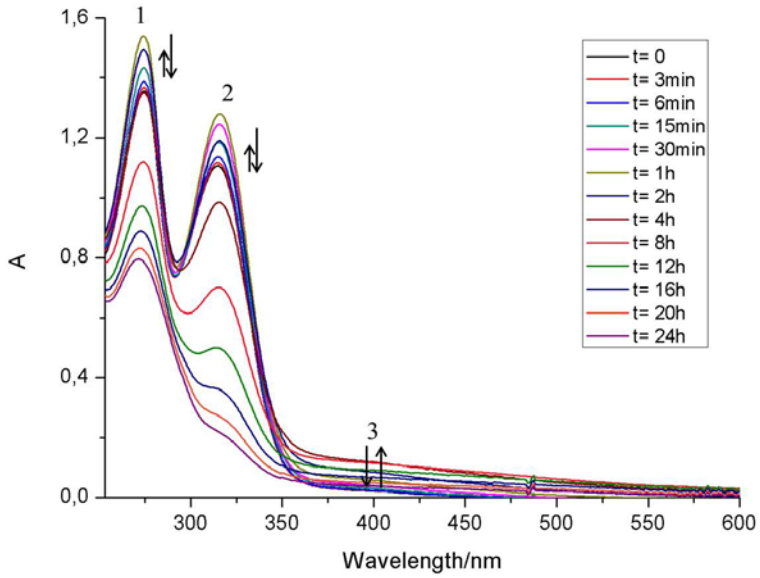

Figure 5.9. AUD8 UV-Vis spectra recorded in DMSO-EtOH- Ringer Lactate (50:10:40% v/v) over 24 hours at 37 °C.

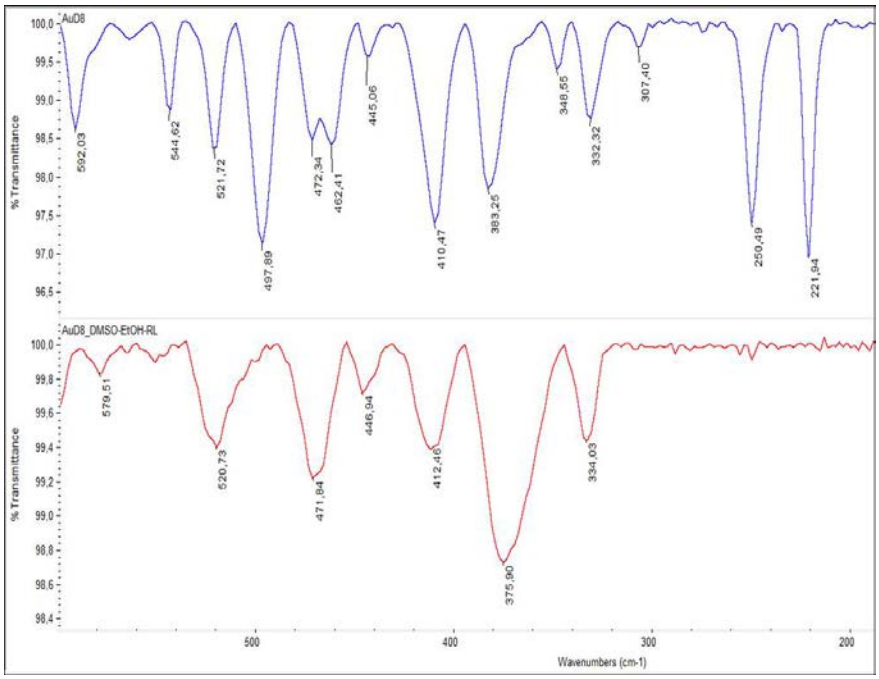

Figura 5.10. Far FT-IR spectra recorded for the complex AuD8 (upper panel) and AuD8 after 24 h in DMSO-EtOH-RL (50:10:40% v/v), lower panel.

5.1.7. Stability study in the vehicle chosen for acute toxicity in mice (oral administration route)

In this test, 8.8 mg of AuD8 were grinded and then suspended with 2 mL of sunflower-seed oil (Collina d'oro®). The orange-brown suspension was stirred for 3 h at 37 °C and then centrifuged. The solid was washed twice with water and once with *n*-pentane and finally dried *in vacuo* overnight in the presence of P_2O_5. Subsequently, the solid was characterized by elemental analysis, NMR and FT-IR spectroscopies.

Figure 5.11 reports the NMR spectrum acquired in deuterated acetone and the resonances of the isolated solid are unchanged compared to AuD8 whose signals are highlighted by arrows. The elemental analysis also confirms that the complex is stable in this vehicle and shows a higher carbon percentage (calc: 21.76; found: 28.66) due to the presence of oil in agreement with the NMR signals recorded at higher fields. IR spectra (near and far) confirm the stability in this medium used to orally treat mice. For instance, the **Figure 5.12** shows that the diagnostic bands (around 545, 411 and 380, 220÷250 cm^{-1} attributed to the vibrational modes ν_s(SCS), $\nu_{a/s}$(SAuS) and $\nu_{a/s}$(BrAuBr), respectively) in the Far-IR region remain intact following 3 h interaction with the vehicle.

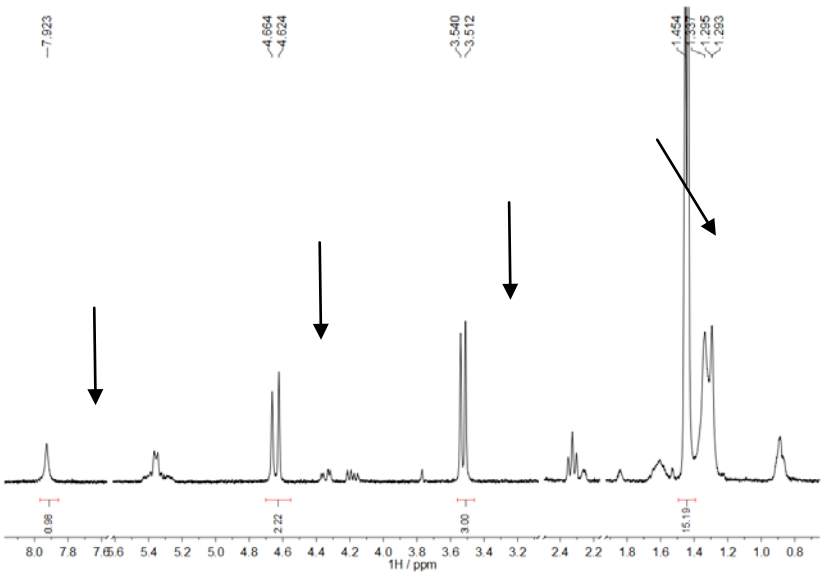

Figure 5.11. ^{1}H-NMR spectrum (acetone-D6, 300 MHz) of AuD8 after 3 h in sunflower-seed oil.

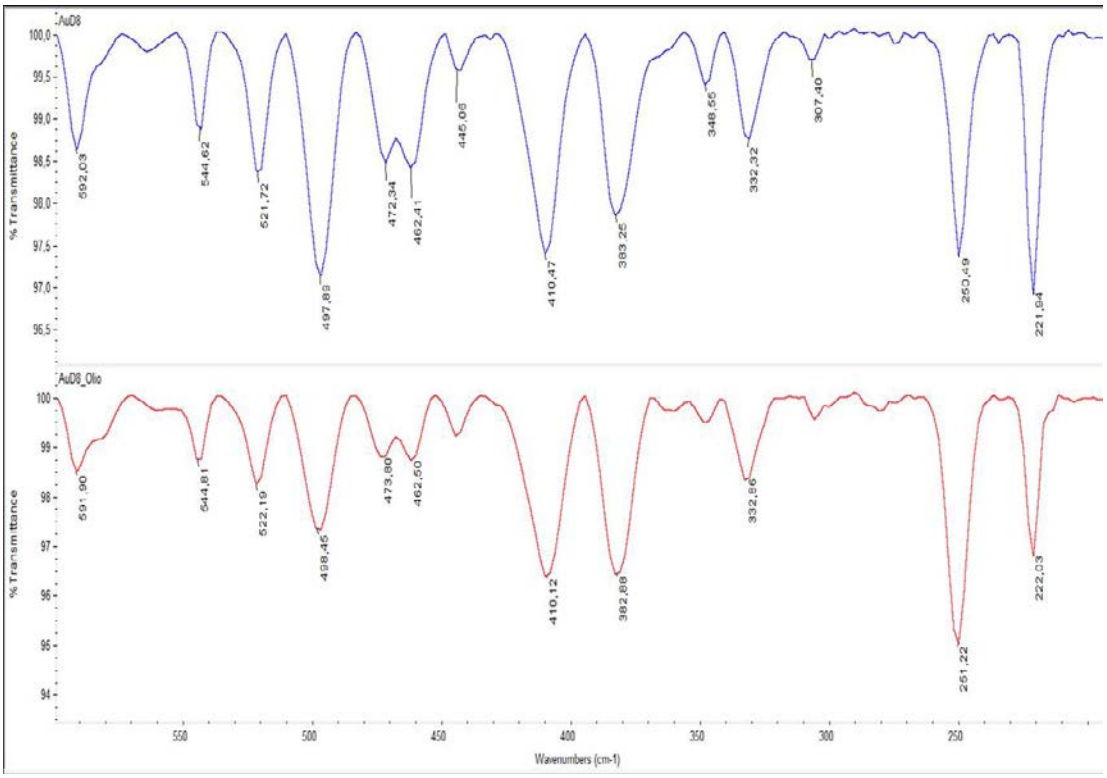

Figure 5.12. Far FT-IR spectra recorded for the complex AuD8 (upper panel) and AuD8 after 3 h In sunflower-seed oil (lower panel).

5.2. Investigation of AuD8 acute toxicity in mice

To further confirm the good chemotherapeutic index of our gold(III)-based compounds (§ *Chapter 2*), we performed an investigation of acute toxicity of AuD8, chosen as a model compound. We used healthy mice and we worked following the Good Laboratory Practice (GLP) regulations at the *Barbara Ann Karmanos Cancer Institute*, Department of Oncology, School of Medicine, Wayne State University, Detroit, U.S.A. in collaboration with Prof. Q. Ping Dou.

The CD-1® (outbreed, albino background) mouse was the selected species because it is accepted by many regulatory authorities and there is a lot of literature data on this strain.

Intravenous (i.v.) and oral (by gavage) administrations of a single dose to female and male mice, at three different dosages, were selected as these ways present a reduced barrier to absorption and are a typical way used in humans. In addition, such administration routes give a measure of the toxicity more stringent than the subcutaneous route previously used for other *in vivo* assays.

Being AuD8 a metal complex (additionally, insoluble in water), both administration vehicles were carefully defined on the basis of stability studies carried out in different media by various analytical techniques as reported in the previous sections of this chapter.

5.2.1. Experimental

Mice were supplied by Charles River (Ann Arbor, MI, U.S.A.) and they were 6 weeks old at the start of study. The animals were acclimated to laboratory conditions for 1 week prior to dose administration. Each animal has been identified through toe clipping and suspended into wire-mesh cages with controlled atmosphere [temperature (21.0 ÷ 23.0 °C), humidity (21 ÷ 47.4%) and light (12 hours light/dark cycle)]. Standard diet for rodents has been used, and filtered and sterilized water was provided *ad libitum.*

AuD8 was administered by intravenous and oral way, both in male and female mice. Each group of mice, divided by route of administration, was divided into three dose levels in turn:

- **Intravenous route** (40 mice of which 20 females and 20 males):
  I. Ctrl group (vehicle) composed of 5 females and 5 males.
  II. Dose 1 (**5 mg/kg**) composed of 5 females and 5 males.
  III. Dose 2 (**10 mg/kg**) composed of 5 females and 5 males.

IV. Dose 3 (**15 mg/kg**) composed of 5 females and 5 males.

- **Oral route** (40 mice of which 20 females and 20 males):

V. Ctrl group (vehicle) composed of 5 females and 5 males.

VI. Dose 1 (**15 mg/kg**) composed of 5 females and 5 males.

VII. Dose 2 (**30 mg/kg**) composed of 5 females and 5 males.

VIII. Dose 3 (**60 mg/kg**) composed of 5 females and 5 males.

Concerning sample formulation, for the i.v. administration way (**Table 5.2**)**,** a calculated amount of AuD8 was dissolved in DMSO and subsequently diluted with ethanol and Ringer Lactate (hereinafter RL, Eurospital®) to yield the required final concentration (Vehicle: DMSO-EtOH-RL 50:10:40% v/v). Each i.v. treated animal was injected at the tail vein with an exact volume of 100 μL. This volume contained the amount of specimen as described in **Table 5.2**.

The samples for the oral administration way were prepared by grinding a defined amount of AuD8 followed by its mixing with sunflower-seed oil (Collina d'oro®), thus obtaining a fine suspension at the proper dose (**Table 5.3**). With respect to this second group, the animals were treated by gavage with an exact volume of 500 μL. This volume contained the proper amount of AuD8 reported in Table 5.3. It is worth noting that it was necessary to administer the exact dose directly on the gastric organ or lower oesophagus through feeding needles (gavage). Entry was obtained through the mouth without anaesthesia using hand restraint and a feeding needle with a ball tip. Such a system avoids any trauma to the oral cavity and prevents introduction of the needle and therefore of AuD8 into the trachea.

Table 5.2. Data collected for the group (40 mice) treated *via* the intravenous (i.v.) route at the tail vein.

ACUTE TOXICITY TEST (Intravenous way)							
Weeks							
	1	**2**	**Animals (5 females & 5 males)**	**Dose (mg/mouse)**	**Volume (μL/mouse)**	**Dose (mg/subgroup)***	**Total V(mL)***
Controls	**Vehicle**	**Sacrifice**	**10 5♀+ 5♂**	**0,0**	**100**	**0.0**	**1.1♀+ 1.1 ♂**
Group 1a	**treatment 5 mg/kg AUD8**	**Sacrifice**	**10 5♀+ 5♂**	**0.14♀ + 0.17♂**	**100**	**1.5♀ + 1.9♂**	**1.1♀ + 1.1♂**
Group 1b	**treatment 10 mg/kg AUD8**	**Sacrifice**	**10 5♀+ 5♂**	**0.27 ♀+ 0.35♂**	**100**	**3.0 ♀+ 3.9♂**	**1.1 ♀+ 1.1♂**
Group 1c	**treatment 15 mg/kg AUD8**	**Sacrifice**	**10 5♀+ 5♂**	**0.41 ♀+ 0.53♂**	**100**	**4.5 ♀+ 5.8♂**	**1.1 ♀+ 1.1♂**
Total			**40**				

* On the basis of the dead volume of the injection system and the loss due to the filtration after dissolution, in order to have enough volume to inject, a greater amount of test material was prepared (considering 11 mice instead of 5). Each mouse was injected with exact 100 μL.

TABLE 5.3. Data collected for the group (40 mice) orally treated by gavage.

ACUTE TOXICITY TEST (oral way)							
	Weeks						
	1	2	Animals (5 females & 5 males)	Dose (mg/mouse)	Volume (µL/mouse)	Dose (mg/subgroup)*	Total V (mL) including dead volume*
Controls	Vehicle	Sacrifice	10 5♀+ 5♂	0	500	0.0	3♀+ 3 ♂
Group 2a	treatment 15 mg/kg AUD8	Sacrifice	10 5♀+ 5♂	0.44♀ + 0.56♂	500	2.6♀ + 3.4♂	3♀ + 3 ♂
Group 2b	treatment 30 mg/kg AUD8	Sacrifice	10 5♀+ 5♂	0.87 ♀+ 1.11♂	500	5.2 ♀+ 6.7♂	3 ♀+ 3 ♂
Group 2c	treatment 60 mg/kg AUD8	Sacrifice	10 5♀+ 5♂	1.74 ♀+ 2.22 ♂	500	10.4 ♀+ 13.3 ♂	3 ♀+ 3 ♂
Total			40				

* On the basis of the dead volume of the injection system, in order to have enough volume to inject, a greater amount of test material was prepared (considering 6 mice instead of 5). Each mouse was injected with exact 500 µL.

Animals have been examined for signs of reaction to treatment (possible clinical signs and mortality) on dosing, 1, 4 and 8 hours post-dose on day 0, 24 hours after dosing on day 1, then daily (morning) thereafter for 14 days. Weight of each animal was evaluated prior to injection, the following day, after 7 and 14 days when sacrificing by carbon dioxide asphyxiation. Then, the major organ systems of the cranial, thoracic and abdominal cavities have been examined for all animals and stored in neutral buffered formalin (10%) for future histopathologic evaluations. Necropsy evaluation was scheduled only in the case of evident alteration due to the toxicity of the studied molecule.

5.2.2. Results and discussion

No dead animal neither signs of toxicity have been observed during the study for all the treated animals. There were no clear clinical findings on all survivors as well.

The control group and the AuD8-treated groups did not show any clinical symptoms after single oral treatment or single i.v. treatment. Likewise, the control group and the AuD8-treated groups did not display clinical symptoms throughout the post-treatment period as well, except some i.v. treated males that appeared catatonic and with reduced mobility for few minutes just after the injection.

It is worth highlighting that no changes have been observed in body weights for any mouse during the study and there were no significant differences between groups (**Figure 5.13**).

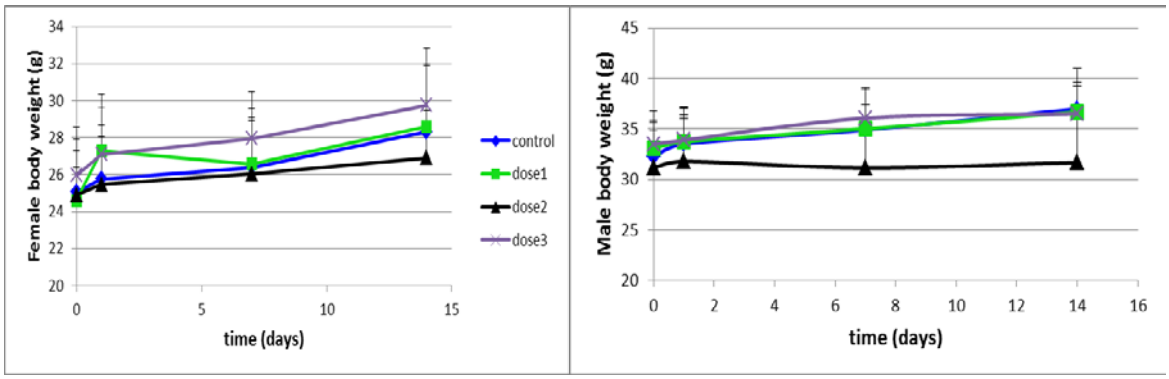

Figure 5.13. Female and male body weights during the post-injection period for the i.v. treated group (reported as an example).

With respect to necropsy**,** no gross anatomic findings and/or alterations in the main organs and/or tissues have been observed. In the orally treated groups, the organ weights were absolutely normal for all the animals whereas in the i.v. treated groups, the organ weights were almost normal for all the animals except for some of them which showed (with respect to controls):

- a significative decrease (evaluated with t Student) in spleen and adrenals weight (male animals treated at 5 and 10 mg/kg, **Figure 5.14**);
- a significative difference (evaluated with t Student) for spleen and ovaries weights (female group treated at 10 mg/kg, **Figure 5.15**).

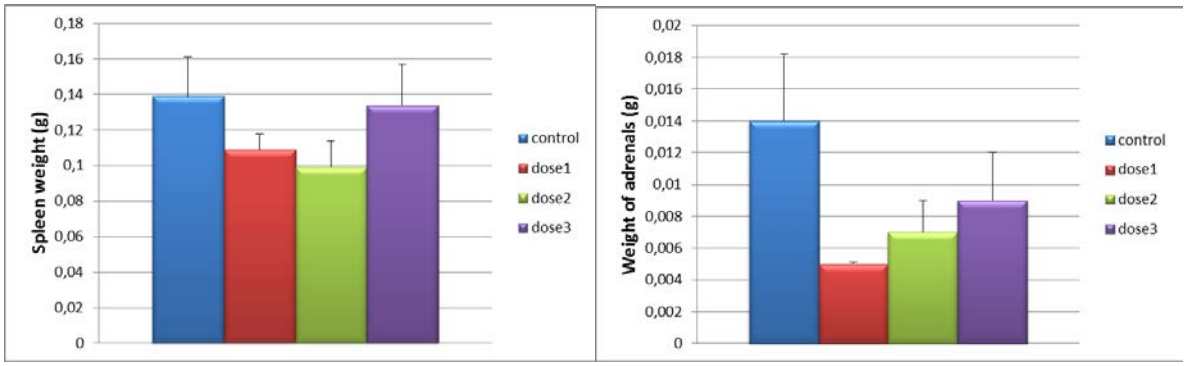

Figure 5.14. Spleen and adrenals weights (after 14-day post-treatment period) of male mice i.v. treated at the tail vein.

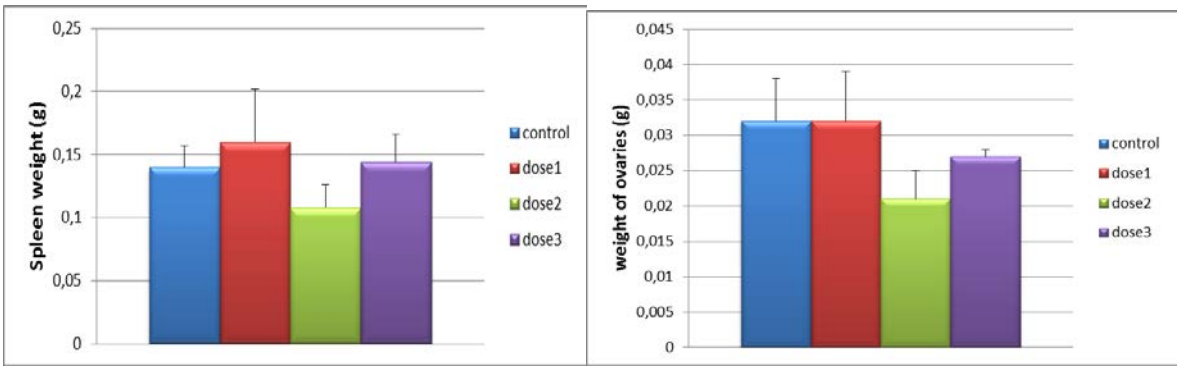

Figure 5.15. Spleen and ovaries weights (after 14-day post-treatment period) of female mice i.v. treated at the tail vein.

Overall, after a 14-day post-treatment observation, the median lethal dose (LD_{50}) of AuD8 was not reached, allowing to state to be higher than 15 mg/kg body weight when administered intravenously or 60 mg/kg body weight when administered orally (both males and females).

It is known that oncological patients are i.v. treated with cisplatin (reference drug) usually every 21 days at 75-80 mg/m^2. This dose for a 70-kg person corresponds to a treatment of about 2 mg/kg body weight. Thus, the data herein recorded and representative of a safety dose as high as at least 15 mg/kg and 60 mg/kg for i.v. and orally treated mice, respectively, are very encouraging. Besides, it has to be underlined that the chemotherapy with AuD8 on nude mice was performed at 1 (§ *Chapter 2*) or 2 mg/kg.[15,25]

Chapter 5 references

(1) Negom Kouodom, M.; Ronconi, L.; Celegato, M.; Nardon, C.; Marchiò, L.; Dou, Q. P.; Aldinucci, D.; Formaggio, F.; Fregona, D. Toward the Selective Delivery of Chemotherapeutics into Tumor Cells by Targeting Peptide Transporters: Tailored Gold-Based Anticancer Peptidomimetics. *J. Med. Chem.* **2012**, *55*, 2212-2226.

(2) Criado, J. J.; Lopez-Arias, J. A.; Macias, B.; Fernandez-Lago, L. R.; Salas, J. M. Au(III) Complexes of Tris-Dithiocarbamate Derivatives of A-Amino Acids: Spectroscopic Studies, Thermal Behaviour and Antibacterial Activity. *Inorg. Chim. Acta* **1992**, *193*, 229-235.

(3) Forghieri, F.; Preti, C.; Tassi, L.; Tosi, G. Preparation, Properties and Reactivity of Gold Complexes with some Heterocyclic Dithiocarbamates as Ligands. *Polyhedron* **1988**, *7*, 1231-1237.

(4) Lee, A. W. M.; Chan, W. H.; Ho, M. F. Ultraviolet Spectrophotometric Determination of Amino Acids by Formation of Dithiocarbamates. *Anal. Chim. Acta* **1991**, *246*, 443-445.

(5) Gangopadhayay, A. K.; Chakravorty, A. Charge Transfer Spectra of some Gold (III) Complexes. *J. Chem. Phys.* **1961**, *35*, 2206-2209.

(6) Franchini, G. C.; Giusti, A.; Preti, C.; Tassi, L.; Zannini, P. Coordinating Ability of Methylpiperidine Dithiocarbamates Towards Platinum Group Metals. *Polyhedron* **1985**, *4*, 1553-1558.

(7) Hadjikostas, C. C.; Katsoulos, G. A.; Shakhatreh, S. K. Synthesis and Spectral Studies of some New Palladium(II) and Platinum(II) Dithiocarbimato Complexes. Reactions of Bases with the Corresponding N-Alkyldithiocarbamates. *Inorg. Chim. Acta* **1987**, *133*, 129-132.

(8) Messori, L.; Abbate, F.; Marcon, G.; Orioli, P.; Fontani, M.; Mini, E.; Mazzei, T.; Carotti, S.; O'Connell, T.; Zanello, P. Gold(III) Complexes as Potential Antitumor Agents: Solution Chemistry and Cytotoxic Properties of some Selected Gold(III) Compounds. *J. Med. Chem.* **2000**, *43*, 3541-3548.

(9) Marcon, G.; Carotti, S.; Coronnello, M.; Messori, L.; Mini, E.; Orioli, P.; Mazzei, T.; Cinellu, M. A.; Minghetti, G. Gold(III) Complexes with Bipyridyl Ligands: Solution Chemistry, Cytotoxicity, and DNA Binding Properties. *J. Med. Chem.* **2002**, *45*, 1672-1677.

(10) STOGRYB A EQUATIONS FOR CALCULATING THE DIELECTRIC CONSTANT OF SALINE WATER. *IEEE Trans. Microwave Theory Tech.* **1971**, *MTT-19*, 733-736.

(11) Ronconi, L.; Fregona, D. The Midas Touch in Cancer Chemotherapy: From Platinum- to Gold-Dithiocarbamato Complexes. *Dalton Transactions* **2009**, 10670-10680.

(12) Calamai, P.; Guerri, A.; Messori, L.; Orioli, P.; Paolo Speroni, G. Structure and DNA Binding Properties of the Gold(III) Complex [AuCl2(Esal)]. *Inorg. Chim. Acta* **1999**, *285*, 309-312.

(13) Messori, L.; Abbate, F.; Marcon, G.; Orioli, P.; Fontani, M.; Mini, E.; Mazzei, T.; Carotti, S.; O'Connell, T.; Zanello, P. Gold(III) Complexes as Potential Antitumor Agents: Solution Chemistry and Cytotoxic Properties of some Selected Gold(III) Compounds. *J. Med. Chem.* **2000**, *43*, 3541-3548.

(14) Sakai, H.; Miyagawa, N.; Horinouchi, H.; Takeoka, S.; Takaori, M.; Tsuchida, E.; Kobayashi, K. Intravenous Infusion of Hb-Vesicles (Artificial Oxygen Carriers) After Repetitive Blood Exchange with a Series of Plasma Expanders (Water-Soluble Biopolymers) in a Rat Model. *Polym. Adv. Technol.* **2011**, *22*, 1216-1222.

(15) C. Nardon, S. M. Schmitt, H. Yang, J. Zuo, D. Fregona, and Q. P. Dou, "The cutting-edge Au(III)-peptidomimetics may revolutionize the anticancer therapy: preclinical studies against human breast neoplasia", under submission.

(16) M. Casarin, personal communication.

(17) A. B. P. Lever, *Inorganic Electronic Spectroscopy*, Elsevier, Amsterdam, 1984.

(18) G. Mestroni, E. Alessio, G. Sava, S. Pacor, M. Coluccia, A. Boccarelli, *Met.-Based Drugs*, **1994**, 1, 43.

(19) *Handbook of Chemistry and Physics*, 64th ed., CRC Press, 1983-1984

(20) Skoog, D.A.; Leary, J.J. *Chimica analitica strumentale*, Edises, 1995.

(21) G. Mie, *Ann. Phys.*, **1908**, 25, 377.

(22) U. Schubert, N. Husing, *Synthesis of Inorganic Materials*, Wiley-VCH, 2005.

(23) B.V. Enustun, J. Turchevich, Coagulation of Colloidal gold, *JACS*, **1963**, 85(21), 3317-3328.

(24) K. Nakamoto, *Infrared and Raman Spectra of inorganic and Coordination compound*, 4th Ed, John Wiley & sons , 1986.

(25) M. Celegato, C. Nardon, D. Fregona, M. Mongiat, L. Ronconi, C. Borghese, V. Canzonieri, N. Casagrande, A. Colombatti, D. Aldinucci, "Antitumor activity of gold(III) dithiocarbamato-peptide in prostate cancer cells and xenografts", under submission.

Part II
Targeting the CCK8 receptor

Chapter 6. Targeted therapy in cancer treatment

It is recognized that the use of targeted drugs results in better patient outcomes in many types of cancer. The ideal target should be one which is not expressed in normal cells. However, as far as we know, such a target has not been discovered yet.

Within the site-specific anticancer chemotherapy, drug targeting may be achieved by passive or active targeting, the first taking advantage of the peculiar pathophysiological features of the tumor tissues, the second exploiting well-defined biomolecules. In the first case, it has to bear in mind, as mentioned in the introduction chapter of this thesis, that the tumor vasculature is very different from normal counterpart, being structurally irregular. In fact, the vessels are leaky thus enabling diapedesis (extravasation) of drugs within the tumor interstitium. A dysfunctional lymphatic drainage is associated with this phenomenon, resulting in enhanced fluid retention and therefore increased accumulation of high molecular weight species including proteins and drug-loaded nanoparticles (*e.g.*, micelles, liposomes, dendrimers, nanotubes and quantum dots). The ideal size of these systems to pass through the gap junction between endothelial cells of the leaky and defective architecture ranges from 100 to 600 nm. This property of macromolecular species to accumulate in tumor tissue much more than in normal one could be exploited to raise the retention of anticancer drugs in cancerous cell vasculature and it is referred to as the enhanced permeability and retention effect (EPR). [1-3]

In the second case, namely with respect to the active targeting, molecular aspects associated with the tumor microenvironment (§ *Chapter 1*) have to be taken into account. It is worth pointing out that there are two subcategories within this therapeutic approach, that is the cellularly targeted therapy and the molecularly targeted therapy. The former exploits receptors, antigens or proteins up-regulated on the cell surface upon malignant transformation whereas the latter is addressed to specific molecules in the tumor cytoplasm, including enzymes, transporters and nucleic acids, involved in the cell progression and tumor growth, thus leading to effects on selected biochemical pathways.

In the present work, we focused on the active targeting with the first strategy, *viz*. the receptor-mediated approach, thus selectively allowing the delivery of our complexes into

pathological cells and minimizing the damage to healthy ones. In particular, the ligands and antibodies used in receptor- and antigen-mediated strategies, respectively, should have high affinity for their overexpressed cell surface targets.

In the *Introduction*, FDA-approved monoclonal antibodies (mAbs) were briefly described since they are able to recognize specific overexpressed antigens or receptors (biomarkers) involved in the efficient tumor growth and proliferation, such as the prostate specific membrane antigen (PSMA) and the human epidermal receptor-2 (Her2). Interestingly, similarly to Her-2, the EGF (epidermal growth factor) receptor belongs to the family of receptor tyrosine kinases and is highly expressed (100-fold greater than normal cells) in a variety of human cancers such as prostate, lung and breast.[2, 4]

A recent strategy is based on the aptamers which are DNA or RNA oligonucleotides able to selectively bind to antigens. Compared to mAbs, these biomolecules are cheaper and more easily synthetized. A study on pegylated docetaxel-loaded nanoparticles showed that they able to recognize the extradomain of PSMA thanks to the surface-decoration with *ad hoc* RNA aptamers.[2]

Other researchers have exploited transferrin (Tf), the protein carrier of Fe^{3+}, in targeted strategies. In fact, its receptors (TfR) are up-regulated (2-10 fold) on the surface of various malignant cells.[5] The TfR can be targeted by direct interaction with conjugates of its ligand transferrin or by mAbs specific for the TFR.[1, 2] These studies showed higher efficiency of Tf-bound drug-loaded delivery systems compared to the unconjugated counterpart (*e.g.*, paclitaxel and doxorubin). [1, 2]

Remarkably, cancer cells have proved to express also different glycans compared with normal ones. Thus, new molecular recognition processes may involve lectin-carbohydrate interactions. These glycoprotein-based systems turned out to be promising both *in vitro* and *in vivo*, improving oral bioavailability as well.[1]

As mentioned in the *Introduction*, the vascular endothelial growth factor receptor (VEGFR) is considered so far the most prominent inducer of tumor angiogenesis since the up-regulation and binding of its ligand (VEGF) triggers its activation and thereby a signaling cascade. In fact, several oncogenes and local hypoxia are known to cause the overexpression of VEGF, resulting in the up-regulation of both VEGFR-1 and -2 in tumor endothelial cells.[6] Many examples are reported in literature targeting VEGFR and allowed successful reduction of vessel density in tumors. For instance, the mAb Bevacizumab is a angiogenesis inhibitor approved for treating colorectal cancer in 2004.[1]

Another studied strategy relies on the use of peptides containing the sequence Arg-Gly-Asp (RGD) since they display high affinity toward cell adhesion systems such as αvβ3 integrin (a heterodimeric transmembrane receptor), preferentially expressed on the angiogenic endothelium in malignant or diseased tissues.[7] For instance, the peptide RGD-4C proved able to deliver doxorubicin to tumor neovasculature, thus showing higher anticancer activity against human breast xenografts in mice.[8]

In addition to the receptors of growth factors such as VEGFR and EGF, other peptide receptors are highly expressed in some tumor cells, including those related to hormones (*e.g.*, LHRH that is luteinizing hormone-releasing hormone), the somatostatine peptide, the vasoactive intestinal peptide and the gastrine-related peptide (bombesin)[9, 10]. Furthermore, for diagnostic and therapeutic applications peptides are becoming an alternative to other targeting moieties, including the previously described mAbs and aptamers, because of their small size, higher stability to degradation if properly designed, easier preparation and lower immunogenicity.[9, 10] Based on these considerations, we focused our attention on the family of cholecystokinin (CCK) peptides whose receptors are normally present on the cell surface but are up-regulated after malignant transformation (*Chapter 7*).

Chapter 7. CCK8 receptor-mediated targeted delivery

7.1. Design of Au(III)-CCK8 derivatives

In the previous chapter, we described different strategies aimed at obtaining new potential drugs able to target neoplastic tissues while letting unharmed those normal. In this context, we focused our attention on the family of cholecystokinin (CCK) peptides whose receptors are normally present on the cell surface but come to be up-regulated after malignant transformation.

CCK was first identified in the gastrointestinal tract in late 1950s[11] and initially characterized as a peptide made up of 33 amino acid residues. It is now known that CCK exists in many biologically active molecular forms which derive from a single 115-amino-acid precursor (proCCK). The major forms of CCK range from 4 to 58 residues in length, namely CCK-58, CCK-39, CCK-33, CCK-22, CCK-8 (sulfated and unsulfated), CCK7, CCK5 and CCK-4 (or G-4), CCK-8 being the predominant species.[11] The process, yielding active peptides of variable length, keeps the same five terminal amino acids at their *C*-terminus. Interestingly, these fragments are implicated in various regulatory functions; for instance, they can act as neurotransmitters in the brain and in the regulation of various functions of the gastrointestinal tract (primarily at the level of the stomach, pancreas, and gallbladder).[26] In addition, they can work as physiological growth factors in most parts of the gastrointestinal tract [12] and also as stimulatory growth factors in several neoplasms, such as colon, brain and gastric cancers.[27,28]

Two different receptor types, called CCK1-R and CCK2-R receptors, recognize CCK and mediate its action.[13] These receptors are localized in the cell membrane, belong to the G-protein coupled receptor superfamily and show physiologic distribution in several different tissues. In particular, CCK1-R and CCK2-R are located predominantly in the gastrointestinal tract and in the central nervous system, respectively. Overexpression of both of these receptor subtypes has been demonstrated in some human tumors.[14] The CCK1-R has been found to be overexpressed in a number of pancreatic adenocarcinomas and, to a smaller

extent, in gastroenteropancreatic (GEP) neuroendocrine) tumors (38%), in meningiomas (30%) and some neuroblastomas (19%). The CCK2-R has been found to be up-regulated in a large percentage of medullary thyroid cancers (92%) and in astrocytomas (62%)[15], in tumors of neuroendocrine origin such as small cell lung cancers (57%) and GEP tumors including insulinoma.[16] It has also been found in stromal ovarian cancers (100%), which are rather rare. [15, 17-19]

Among the several biologically active forms of CCK, the octapeptide amide CCK8 (i.e., CCK26-33) can bind both receptor subtypes, although the sulfated form of CCK8 (with a sulfate moiety on Tyr27 side chain) is 1000-fold more active than the non-sulfated CCK8 in binding type 1 CCK receptor. Hence, non-sulfated CCK8 displays higher affinity toward CCK2-R.

A detailed characterization of the interaction between CCK8 and its receptors is crucial for the development of CCK8 derivatives bearing chelating agents able to coordinate, with high stability, metals for applications in cancer diagnosis or therapy. Remarkably, the structural characterization of the biomolecular complex of CCK8 with the 47-residue *N*-terminal extra-cellular arm of CCK1-R has been achieved by high-resolution NMR and computation refinement. [20, 21] The NMR structure of the complex suggests that the *C*-terminus of CCK8 binds to CCK1 receptor (*N*-terminal end). In particular, intermolecular NOEs (Nuclear Overhauser Enhancement) clearly showed Tyr27 and Met28 of CCK8 in close contact with Trp39 of the receptor within the complex (**Figure 7.1**). Based on this structural evidence, as discussed above, the recognition sequence corresponds to the last five amino acids at the *C*-terminal end. Thus, any modification on the CCK8 *N*-terminal end should not affect receptor binding for both subtypes since the terminal amino group points toward the extra-cellular space. On the contrary, changes in the sequence at the *C*-terminus would lead to a dramatic reduction of the biological effects.[22]

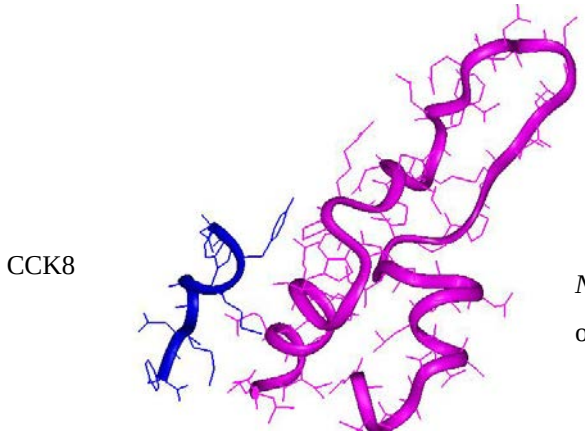

Figure 7.1. Interaction between the CCK8 peptide and CCK1-R *N*-terminal fragment (47 residues).

Upon binding (K_D ~20 nM), CCK8 is internalized into the cell through receptor-mediated endocytosis, thus leading to a cascade of biological events. [23]

Concerning the sequence, we replaced two methionines with two norleucine (Nle) (conservative replacement)[24], thus leading to the amino acid sequence H-Sar[25]-Asp[26]-Tyr[27]-Nle[28] -Gly[29]-Trp[30]-Nle[31]-Asp[32]-Phe[33]-NH_2 (with the numbering according to CCK33) with the *C*-terminus amidated as in the natural peptide. This replacement takes into account that Met and Nle are characterized by a similar steric hindrance and does not cause a decreased activity.[14, 24] Secondly, Met is a sulfur-containing amino acid which could interfere when performing the reaction with Au(III). In fact, besides the possibility of undesired coordination to the metal center, a redox process might occur resulting in the reduction of the noble metal oxidation state due to the Met susceptibility to oxidant agents.[24] Based on the former considerations, our sequence should target chiefly the receptor CCK2. Furthermore, because the above-listed tumors expressing CCK1 receptors usually also express a large amount of somatostatin receptors, which lead to the use of well-established drugs such as ^{90}Y-labeled DOTATOC, the development of CCK1-targeting chemotherapeutics is not a primary necessity.[16]

In the present work, a sarcosine residue has been added as a spacer between the chelating sulfur-based moiety, subsequently introduced, and the biologically active region. Such a residue was chosen as *N*-terminal end to resemble our previous complexes (*Part I*).
The nonapeptide synthesis was carried out in solid-phase under standard conditions using the Fmoc strategy. It is worthwhile to note that during the synthesis both Asp and Tyr were protected with *tert*-butoxy (O*t*Bu) protecting groups at the side chains whereas the residue

Trp was protected with a Boc group (*tert*-butoxycarbonyl). This was to prevent coordination by carboxylate groups or nitrogen on the Trp residue. The cleavage from the resin occurred under conditions that leave most standard side-chain protecting groups intact.

It should be specified that it has been difficult to find out the more proper conditions for the coordination of the Au(III) center. In fact, the first attempts resulted in a non-specific coordination of the Au(III) metal center, occurring on the peptide backbone instead of the intended *N*-terminus sarcosine.[29]

Additionally, some preliminary stability studies of the bond gold-sulfur were carried out under acidic and basic conditions prior to choosing the protecting groups of the CCK8 peptide (Boc and O*t*Bu). In each case, a small Au(III) dithiocarbamato complex was used as a model compound.

7.2 Experimental

7.2.1. Stability studies under basic conditions

These studies were carried out under the typical conditions used to remove the Fmoc protecting group from the *N*-terminus end of amino acids: 20% (v/v) piperidine in DMF. The model compound was AuL10 (**Figura 7.2**), previously synthesized and characterized.[25]

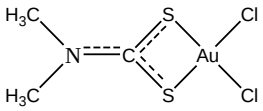

Figura 7.2. Structure of the compound AuL10.

Procedure

3 mL of 20% v/v piperidine in DMF were used to dissolve AuL10 (10.8 mg, 27.8 μmol), obtaining an orange muddy mixture which turned into yellowish-green with time. The mixture was let to stir for 30 min at room temperature. After centrifugation, a light green solid was isolated, washed several times with *n*-pentane and finally dried under vacuo in the presence of P_2O_5.

The color change and the insolubility in DMSO and DMF (wherein AuL10 dissolves) have been ascribed to the formation of a new gold-based complex as a consequence of the unstability of the Au-S bonds in these conditions. The undertaken analyses (FT-IR and elemental analysis: C, 12.29; H, 1.99; N, 4.36; S, 19.40%.) confirmed this hypothesis. In fact, the disappearance of the Au-Cl stretchings at 355 and 342 cm^{-1} (**Table 7.1**) was associated with the formation of a previously synthetized and studied dinuclear Au(I) complex, depicted in **Figure 7.3**.[25,30]

Table 7.1. Selected (the most diagnostic bands) IR frequencies (cm^{-1}).

Compound	$\tilde{\nu}$ (N-CSS)	$\tilde{\nu}$ (SCS)		$\tilde{\nu}$ (SAuS)		$\tilde{\nu}$ (ClAuCl)	
		asim	sim	asim	sim	asim	sim
AuL10 reagent	1576	1049	551	409	382	355	342
AuL10 piperidine-treated	1501	1050	568	391		-	-
Au(I) species	1499	1052	569	391		-	-

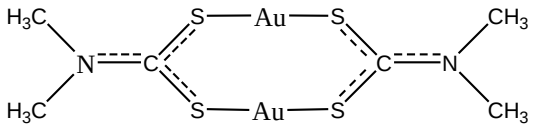

Figura 7.3. Structure of the Au(I) dithiocarbamato derivative ($C_6H_{12}Au_2N_2S_4$, MW. = 634.37; elemental analysis %: (calculated) found C (11.36) 12.80, H (1.91) 2.01, N (4.42) 4.13, S (20.22) 19.48).

The comparison of the diagnostic IR bands (**Table 7.1**) confirms that the reduction Au(III)→Au(I) takes place in basic environment, leading to the formation of a dimeric complex.

7.2.2. Stability studies under acidic conditions

These studies were carried out under the typical conditions used to remove the *Boc* and O*t*Bu protecting groups from amino and carboxylic groups, respectively: 50% TFA – 50% DCM (v/v).

The model compound was AuL12 (**Figura 7.4**), previously synthesized and characterized.[25] AuL12 is a derivative of the *N*-methylglycine, functionalized as an ethyl ester. The choice was not accidental since we aimed to test the lability of the Au-S bond along with the possibility of the ester hydrolysis.

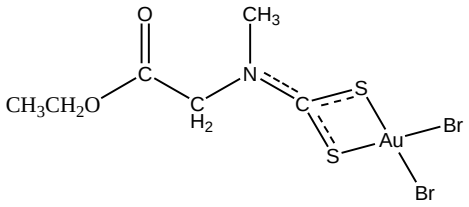

Figura 7.4. Structure of the compound AuL12 ($C_6H_{10}AuBr_2NO_2S_2$, MW. = 549.06; elemental analysis %: (calculated) found C (13.13) 13.24, H (1.84) 1.79, N (2.55) 2.48, S (11.68) 11.69).

Procedure

To a solution of AuL12 (10.1 mg, 18.4 μmol) in DCM (2.5 mL), 2.5 mL of TFA were added under vigorous stirring at room temperature. The solution, initially yellow and transparent, became slightly muddy after a few minutes. The test was stopped after 3 h and the most of solvent was removed by a flux of N_2, the product being precipitated with diethyl ether. Following centrifugation, the isolated orange solid was dried *in vacuum* in the presence of P_2O_5.

In light of the elemental analyses (C, 13.40; H, 1.80; N, 2.37; S, 11.70%), the NMR and IR spectra obtained before and after the acidic treatment (**Tables 7.2** and **7.3**), it was possible to state that the dithiocarbamato moiety (S-Au(III)-S) is not affected by strong acids.

Table 7.2. ^{1}H-NMR, (300 MHz) chemical shifts [δ] in acetone-D_6.

Compound	CH_3 (t)	CH_2O (q)	CH_3N (s)	CH_2N (s)
AuL12 reagent	1.28	4.28	3.56/3.61[a]	4.77/4.80[a]
AuL12 treated	1.27	4.27	3.56/3.60[a]	4.77/4.79[a]

[a] Two forms in solution. Symbols for multiplicities of signals: (s) = singlet, (t) = triplet, (q) = quartet.

Table 7.3. Selected (the most diagnostic bands) IR frequencies (cm^{-1}).

Compound	$\tilde{\nu}$ (N-CSS)	$\tilde{\nu}$ (C=O)	$\tilde{\nu}$ (C-O)	$\tilde{\nu}$ (SCS)		$\tilde{\nu}$ (SAuS)		$\tilde{\nu}$ (BrAuBr)	
				asim	sim	asim	sim	asim	sim
AuL12 reagent	1560	1739	1224	1001	575	416	382	251	228
AuL12 TFA-treated	1561	1737	1217	1000	574	422	384	249	229

7.2.3. Synthesis of the nonapeptide Sar-CCK8

The Sar-CCK8 peptide was obtained by solid phase peptide synthesis (SPPS), under standard conditions using the Fmoc strategy. NovaSyn® TG Sieber resin (0.69 mmol/g, 0.15 mmol, 217 mg) was used as a polymeric support as it is ideal for the Fmoc-SPPS of partially protected peptide amide fragments. DMF was used as a solvent.

The peptide chain was elongated by sequential Fmoc-AA-OH coupling and Fmoc deprotection. Fmoc deprotection was carried out by 30% solution of piperidine in DMF after the coupling of each amino acidic residue. All couplings were performed twice for 1 hour, by using an excess of 4 equivalents for the single amino acid derivative. The α-amino acids were *in situ* activated by the standard HOBt/PyBop/DIPEA procedure. Sarcosine was introduced as the last residue at the *N*-terminus. Then, a small-scale cleavage from the resin was performed in order to check the peptide quality (Fmoc-Sar-CCK8 peptide, deprotected on the side chains). Purity and identity were assessed by LC-MS analysis (C18-Phenomenex column). The elution was carried out with H_2O/0.1% TFA (A) and CH_3CN/0.1% TFA (B) from 20–80% over 20 min at a flow rate of 0.8 mL min^{-1}.

Subsequently, the Fmoc protecting group was removed from sarcosine prior to carrying out the cleavage on the whole resin. In particular, the fully side chain-protected peptide was cleaved from resin by treating the resin for 2 min with 2.5 mL of a solution 1% TFA in DCM. This procedure was repeated 13 times to avoid side chain-protecting groups cleavage. In fact, filtrates, which contained crude product, were collected into a flask containing 10% pyridine in methanol, and evaporate under reduced pressure at 5% of the volume. The product was precipitated at 0°C by adding water. An ESI-MS analysis was performed in chloroform/methanol (50:50% v/v) (**Figure 7.5**).

Final yield: 80%.

$C_{73}H_{104}F_3N_{11}O_{18}$ (MW. 1480.66) Elemental analysis %: (calculated) found C (59.22) 59.31, H (7.08) 7.12, N (10.41) 10.35.

Slightly soluble in ether, ethanol, water, acetone; insoluble in *n*-pentane and *n*-esane.

^{1}H NMR (DMSO-D6, 300 MHz), δ/ppm: 8.29-7.3 [many singlets, 10H, amide NH], 7.53 [s, 1H, H-NCOOtBu Trp], 6.94-6.44 [m, 13H, aromatic protons], 4.26-3.81 [many multiplets, 9H, αCH/αCH$_2$ + 2H αCH$_2$ Sar], 2.7-2.0 [m, 13H, βCH$_2$ + NCH$_3$ Sar], 1.22-0.86 [three distinct singlets, 48H, O*t*Bu + (CH$_2$)$_3$ of Nle], 0.44 [s, 6H, -CH$_3$ of Nle]

MS, [M]$^+$ calculated (found): 1366.77 (1366.8).

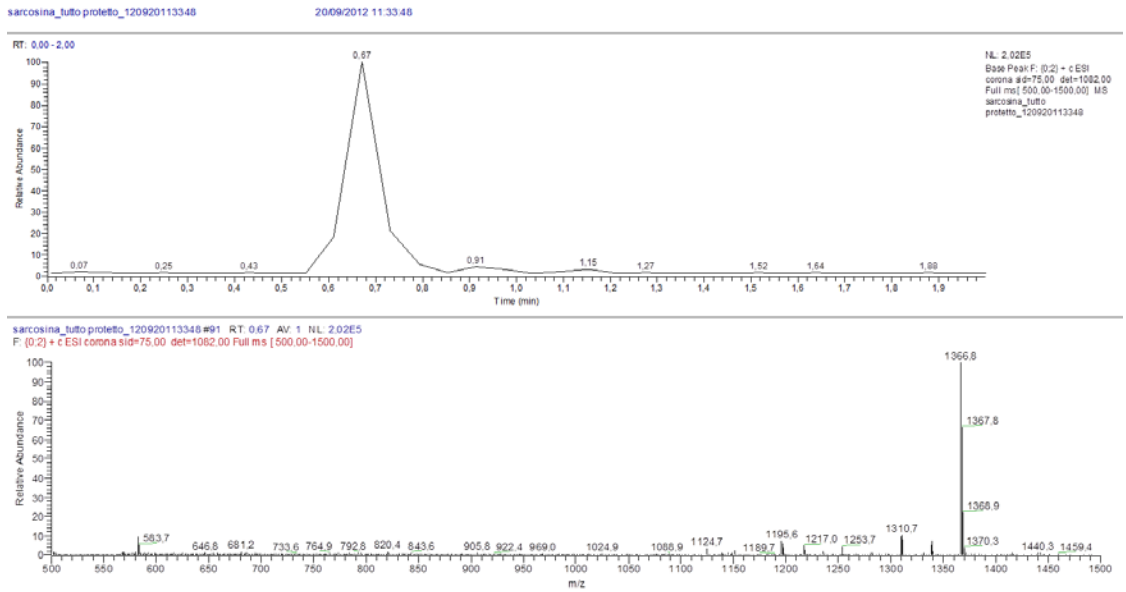

Figure 7.5. Total ionic current and ESI-Ms profile of the peptide Sar-CCK8 (fully side-chain protected).

7.2.4. Synthesis of the complex AuSarCCK8 (fully side-chain protected)

1 eq. (35.3 mg) of the protected peptide SarCCK8 was suspended in ethanol along with KOH (1 eq.). After a few minutes, CS_2 (1 eq.) was added and the mixture was stirred for 1h. Then, the ligand suspension was added to a water solution of $KAuBr_4 \cdot 2H_2O$ (1 eq.), leading to the formation of a dark orange suspension. After 48h, the mother liquor was removed and the solid washed with water and *n*-pentane. Prior to characterization, the orange product was dried in a dessicator in the presence of P_4O_{10}. Since the foreseen resonances were not easily detectable in the ^{1}H-NMR spectrum due to its crowded appearance for the presence of by-products, the solid was washed with acetone and diethyl ether and turned into yellow. Upon

drying again *in vacuo*, the corresponding ^{1}H-NMR spectrum and UV-Vis spectrum were recorded in DMSO-D6 and chloroform/methanol (50-50% v/v), respectively (**Figure 7.6 and 7.7**).

$C_{72}H_{102}AuBr_2N_{11}O_{16}S_2$ (MW. 1798.55) Elemental analysis %: (calculated) found C (48.08) 49.95, H (5.72) 5.78, N (8.57) 8.62, S (3.57) 3.49.

Slightly soluble in ether, ethanol, water, acetone; insoluble in *n*-pentane and *n*-esane.

^{1}H NMR (DMSO-D6, 300 MHz), δ/ppm: 8.17-7.67 [many singlets, 10H, amide NH], 7.52 [s, 1H, H-NCOOtBu Trp], 7.30-6.81 [m, 13H, aromatic protons], 4.62-4.18 [m, 9H, αCH + 2H NCH_2 Sar], 3.67-3.56 [m, 5H, NCH_3 Sar + αCH_2 Gly], 3.12-2.27 [m, 10H, βCH_2], 1.61-1.245 [three distinct singlets, 48H, O*t*Bu + $(CH_2)_3$ of Nle], 0.82 [s, 6H, -CH_3 of Nle].

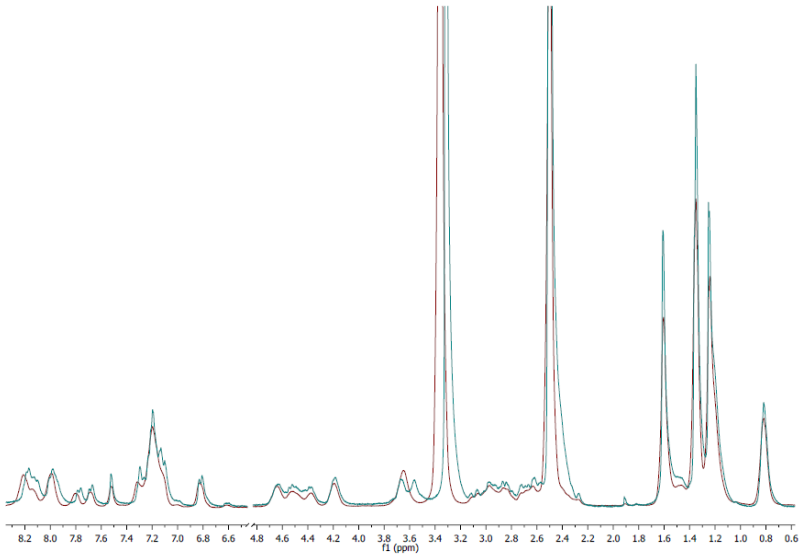

Figure 7.6 ^{1}H-NMR spectrum (300 MHz, DMSO-D6) of the AuSarCCK8 complex (free peptide in purple, gold-compound in blue).

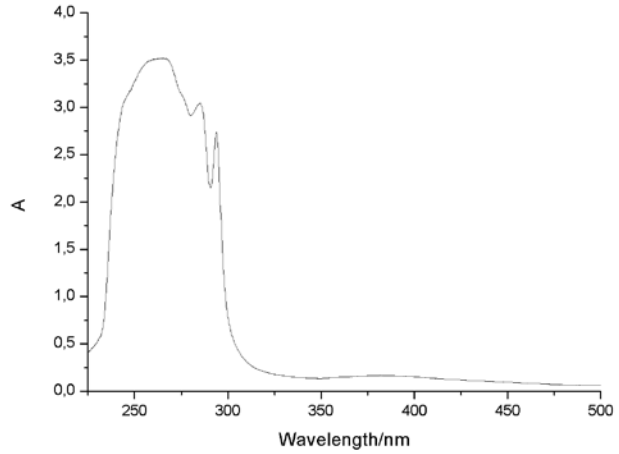

Figure 7.7. UV-Vis spectrum of the complex AuSarCCK8 acquired at room temperature in chloroform/methanol (50-50% v/v).

7.2.5. Discussion

Preliminary analyses (elemental, 1D-NMR and UV-Vis) show that the synthesis of the intended complex was successful. In fact, the foreseen changes in the NMR signals are visible in the region 4.5-3.5 ppm. In light of our previous compounds, these signals are attributed to the $-NCH_3$ and $-NCH_2$ protons of the formed dithiocarbamato group (**Figure 7.8**), being the remaining resonances substantially unaffected by the coordination to the metal center.

A new band rises in the electronic spectrum at 382.9 nm (log ε= 2.60) which has been ascribed to the d←d transitions within the metal core. The other diagnostic bands (intraligand $\pi^*\leftarrow\pi$ transitions mainly located in the -NCS and -CSS moieties) are overlapped with those related to the Trp, Phe and Tyr amino acid residues.

Further characterizations are ongoing (2D-NMR including HMBC-NMR, FT-IR, ESI-MS). The subsequent step will be the deprotection of the side chains under acidic conditions wherein the bonds Au-S proved stable in previous stability studies. Once obtained the fully deprotected form of the complex, preliminary *in vitro* studies aimed at comparing the cytotoxic activity on CCK8 receptor-overexpressing tumor cell lines and CCK8R-negative cell lines (control) are planned.

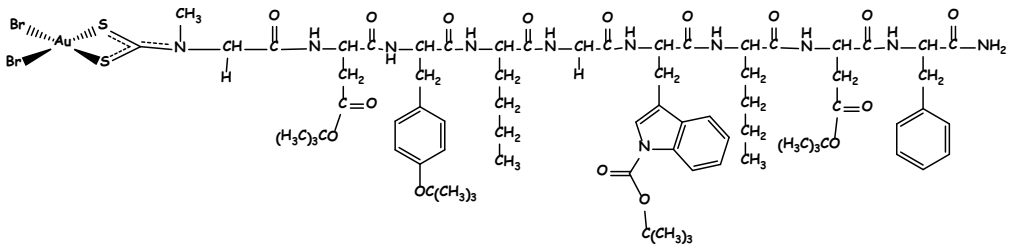

Figure 7.8. Structure of the complex AuSarCCK8 (fully side-chain protected).

Part II references

(1) Mohanty, C.; Das, M.; Kanwar, J. R.; Sahoo, S. K. Receptor Mediated Tumor Targeting: An Emerging Approach for Cancer Therapy. *Current Drug Delivery* **2011**, *8*, 45-58.

(2) Arias, J. L. Drug Targeting Strategies in Cancer Treatment: An Overview. *Mini-Reviews in Medicinal Chemistry* **2011**, *11*, 1-17.

(3) Maeda, H.; Bharate, G. Y.; Daruwalla, J. Polymeric Drugs for Efficient Tumor-Targeted Drug Delivery Based on EPR-Effect. *European Journal of Pharmaceutics and Biopharmaceutics* **2009**, *71*, 409-419.

(4) Salomon, D. S.; Brandt, R.; Ciardiello, F.; Normanno, N. Epidermal Growth Factor-Related Peptides and their Receptors in Human Malignancies. *Crit. Rev. Oncol.* **1995**, *19*, 183-232.

(5) Anabousi, S.; Bakowsky, U.; Schneider, M.; Huwer, H.; Lehr, C. -.; Ehrhardt, C. In Vitro Assessment of Transferrin-Conjugated Liposomes as Drug Delivery Systems for Inhalation Therapy of Lung Cancer. *European Journal of Pharmaceutical Sciences* **2006**, *29*, 367-374.

(6) Shweiki, D.; Itin, A.; Soffer, D.; Keshet, E. Vascular Endothelial Growth Factor Induced by Hypoxia may Mediate Hypoxia-Initiated Angiogenesis. *Nature* **1992**, *359*, 843-845.

(7) Brooks, P. C.; Montgomery, A. M. P.; Rosenfeld, M.; Reisfeld, R. A.; Hu, T.; Klier, G.; Cheresh, D. A. Integrin A(V)B 3 Antagonists Promote Tumor Regression by Inducing Apoptosis of Angiogenic Blood Vessels. *Cell* **1994**, *79*, 1157-1164.

(8) Arap, W.; Pasqualini, R.; Ruoslahti, E. Cancer Treatment by Targeted Drug Delivery to Tumor Vasculature in a Mouse Model. *Science* **1998**, *279*, 377-380.

(9) Lu, Y.; Yang, J.; Sega, E. Issues Related to Targeted Delivery of Proteins and Peptides. *AAPS Journal* **2006**, *8*, E466-E478.

(10) Das, M.; Mohanty, C.; Sahoo, S. K. Ligand-Based Targeted Therapy for Cancer Tissue. *Expert Opinion on Drug Delivery* **2009**, *6*, 285-304.

(11) Wang, H.; Wong, P. T. -.; Spiess, J.; Zhu, Y. Z. Cholecystokinin-2 (CCK2) Receptor-Mediated Anxiety-Like Behaviors in Rats. *Neurosci. Biobehav. Rev.* **2005**, *29*, 1361-1373.

(12) Hakanson, R.; Sundler, F. Trophic Effects of Gastrin. *Scandinavian Journal of Gastroenterology, Supplement* **1991**, *26*, 130-136.

(13) Wank, S. A.; Pisegna, J. R.; De Weerth, A. Brain and Gastrointestinal Cholecystokinin Receptor Family: Structure and Functional Expression. *Proc. Natl. Acad. Sci. U. S. A.* **1992**, *89*, 8691-8695.

(14) Reubi, J. C.; Schaer, J. -.; Waser, B. Cholecystokinin (CCK)-A and CCK-B/Gastrin Receptors in Human Tumors. *Cancer Res.* **1997**, *57*, 1377-1386.

(15) Reubi, J. C. Peptide Receptors as Molecular Targets for Cancer Diagnosis and Therapy. *Endocr. Rev.* **2003**, *24*, 389-427.

(16) Reubi, J. C.; Waser, B. Concomitant Expression of several Peptide Receptors in Neuroendocrine Tumours: Molecular Basis for in Vivo Multireceptor Tumour Targeting. *European Journal of Nuclear Medicine and Molecular Imaging* **2003**, *30*, 781-793.

(17) Reubi, J. C.; Waser, B. Unexpected High Incidence of Cholecystokinin-B/Gastrin Receptors in Human Medullary Thyroid Carcinomas. *International Journal of Cancer* **1996**, *67*, 644-647.

(18) Reubi, J. C.; Schaer, J. -.; Waser, B. Cholecystokinin (CCK)-A and CCK-B/Gastrin Receptors in Human Tumors. *Cancer Res.* **1997**, *57*, 1377-1386.

(19) Imdahl, A.; Mantamadiotis, T.; Eggstein, S.; Farthmann, E. H.; Baldwin, G. S. Expression of Gastrin, Gastrin/CCK-B and Gastrin/CCK-C Receptors in Human Colorectal Carcinomas. *J. Cancer Res. Clin. Oncol.* **1995**, *121*, 661-666.

(20) Pellegrini, M.; Mierke, D. F. Molecular Complex of Cholecystokinin-8 and N-Terminus of the Cholecystokinin A Receptor by NMR Spectroscopy. *Biochemistry (N. Y.)* **1999**, *38*, 14775-14783.

(21) Giragossian, C.; Mierke, D. F. Intermolecular Interactions between Cholecystokinin-8 and the Third Extracellular Loop of the Cholecystokinin A Receptor. *Biochemistry* **2001**, *40*, 3804-3809.

(22) Wank, S. A. G Protein-Coupled Receptors in Gastrointestinal Physiology I. CCK Receptors: An Exemplary Family. *American Journal of Physiology - Gastrointestinal and Liver Physiology* **1998**, *274*, G607-G613.

(23) Roettger, B. F.; Rentsch, R. U.; Pinon, D.; Holicky, E.; Hadac, E.; Larkin, J. M.; Miller, L. J. Dual Pathways of Internalization of the Cholecystokinin Receptor. *J. Cell Biol.* **1995**, *128*, 1029-1041.

(24) Gilles, A. -.; Marliere, P.; Rose, T.; Sarfati, R.; Longin, R.; Meier, A.; Fermandjian, S.; Monnot, M.; Cohen, G. N.; Barzu, O. Conservative Replacement of Methionine by Norleucine in Escherichia Coli Adenylate Kinase. *J. Biol. Chem.* **1988**, *263*, 8204-8209.

(25) Ronconi, L.; Giovagnini, L.; Marzano, C.; Bettìo, F.; Graziani, R.; Pilloni, G.; Fregona, D. Gold Dithiocarbamate Derivatives as Potential Antineoplastic Agents: Design, Spectroscopic Properties, and in Vitro Antitumor Activity. *Inorg. Chem.* **2005**, *44*, 1867-1881.

(26) Walsh,J.H.; Gastrin. In: Walsh, J.H. and Dockray, G.J. (eds.), Gut Peptides: Biochemistry and Physiology, 1994, 75.

(27) Smith, J.P. and Solomon, T.E. *Gastroenterology*, **1988**, *95*, 1541.

(28) Renfeld, J.F. and van Solinge, W.W. *Adv.Cancer.Res*. **1994**, *63*, 295.

(29) B.D. Glisic; U. Rychlewska; M. Djuran, Reactions and structural characterization of Au(III) complexes with amino acids, peptides and proteins, *Dalton Trans*., **2012**, 41, 6887

(30) Akerstrom S., *Ark. Kemi*, 1959, *14*, 387-401

Part III
Versatile building blocks in click chemistry to generate new targeted anticancer agents

Chapter 8. The Huisgen 1,3-dipolar cycloaddition

In addition to coordinate the Au(III) metal center to a receptor peptide (§ *Part II*), we also addressed our attention on a versatile and powerful synthetic strategy, namely "click chemistry". Click reactions generate substances joining small units (selective toward each other) together by heteroatom bonds (typically, C-X-C) quickly, reliably and in quantitative yield. Inspired by the nature, which generates substances using small modular units, in 2001 the Nobel Laureate K. Barry Sharpless introduced such chemical paradigm and listed other stringent criteria to set a reaction within the click chemistry context[1]:

- ✓ the reaction must occur under simple and mild conditions involving readily available reagents and materials and must be modular, stereospecific and generally applicable because orthogonal to conventional methods;
- ✓ simple product isolation
- ✓ non-hazardous by-products and removable by non-chromatographic methods
- ✓ no solvent or use of water.

Another remarkable feature of click reactions is their high thermodynamic driving force, usually higher than 20 kcal mol^{-1}.[1] Among click approaches, there are the following connecting reactions: i) epoxide ring-opening, ii) formation of hydrazone or Schiff base adducts, iii) alkylation of free thiols or amines, iv) disulfide bond formation and v) olefin metathesis.[1, 2]

However, most of the mentioned strategies share some drawbacks. For example, the involved reactive groups on the building blocks, being either electrophiles or nucleophiles, may react in undesired ways with other molecules present in the system (*i.e.*, proteins and enzymes if the reaction occurs in biological systems).[26] Intriguingly, an alternative is offered by the "cream of the crop" of the click strategies, that is the Huisgen 1,3-dipolar cycloaddition reaction of azides and alkynes, thus yielding 1,2,3-triazoles as linking moieties (**Figure 8.1**).

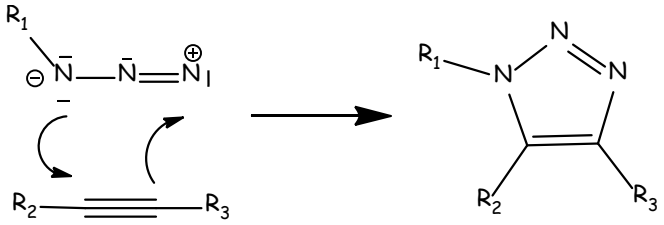

Figure 8.1. The Huisgen 1,3-dipolar cycloaddition of azides and acetylenes to give 1,2,3-triazoles**.**

This synthetic approach is very attractive due to its high chemoselectivity and regiospecificity.[3] In fact, azide groups are not reactive toward a large variety of other functional groups. Therefore, exergonic click reactions take place only when good dipolarophiles, such as acetylenes, are favorably oriented with respect to the azide. Among the resonance structures reported in **Figure 8.2**, three of them are characterized by a separation of charge.

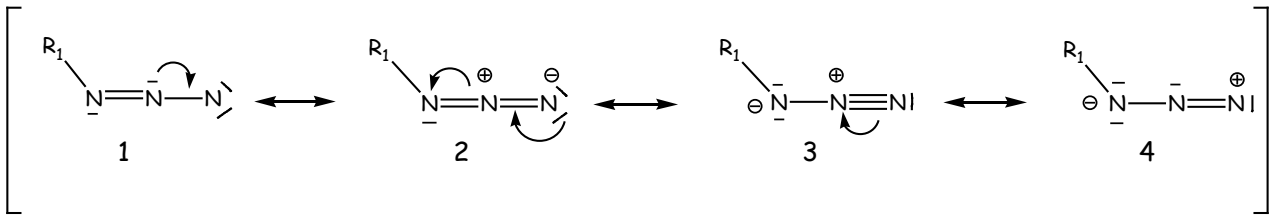

Figure 8.2. Resonance structures of organic azides.

The dipolar structures of type 3 and 4 can account for the easy decomposition into the corresponding nitrene and molecular nitrogen as well as the reactivity as a 1,3-dipole, respectively. Notably, the azide group is extraordinary stable toward oxygen, water and most of organic synthesis conditions (however, safety precautions should be taken into account when dealing with azides, *vide infra*) [4] and, thus, it seems to be the only three-atom dipole which is almost devoid of side reactions. On the other hand, alkynes are generally unreactive toward functional groups present in other molecules or biomolecules as well. Indeed, the azide-based click chemistry has been widely exploited to selectively modify virus particles[5], cells[6], proteins[7,8], and enzymes[9,10]. In addition, hydrolytical and thermal stabilities[3] of the cycloaddition product (Figure 8.1) make this reaction particularly appealing for us for the functionalization of a large variety of receptor peptides with transition metal complexes to be used as targeted bullets toward cancer cells, thus sparing normal ones.

According to the **Figure 8.3**, the triazole-forming reaction may require high temperatures and, usually results in a mixture of the 1,4 and 1,5 regioisomers.[11, 12]

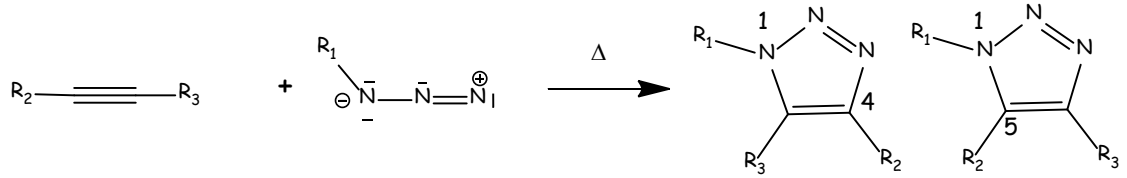

Figure 8.3. The cycloaddition of terminal alkynes and azides generates two possible regioisomers (1,4,5-trisubstituted 1,2,3-triazoles), namely, if considering for instance the substituent R_2, the 1,4 and 1,5-disubstituted derivatives.

However, Sharpless and coworkers found that the Cu(I)-catalyzed cycloaddition of terminal alkynes and azides proceeds efficiently and regiospecifically in aqueous media at room temperature to generate only 1,4-disubstituted 1,2,3-triazoles.[3, 13, 14] Copper(I) salts (e.g., CuI, CuCl, CuOTf $\cdot C_6H_6$, CuBr-dimethyl sulfide complex)[15, 16]can be used but under these conditions, one equivalent of a nitrogen base and acetonitrile as co-solvent are required. Furthermore, formation of undesired by-products such as diacetylenes, bis-triazoles, and 5-hydroxytriazoles, was often observed.[13] Interestingly, better indexes of product purity and yields are usually obtained by *in situ* reduction of Cu(II) salts. Furthermore, the reaction results less expensive and the product purer than adding directly Cu(I) salts. Such a reduction is commonly carried out by addition of ascorbic acid and/or sodium ascorbate. Regarding the catalytic mechanism, there is general agreement on the formation of copper(I) acetylide as initial step and no reaction is observed with internal alkynes. Density functional theory calculations offer evidence for a stepwise cycloaddition instead of a concerted [2+3] reaction.[17]

Chapter 9.
Synthesis and development of a versatile gold(III)-based building block

The Huisgen 1,3-dipolar cycloaddition has been described in *Chapter 8* and, owing to its unprecedented level of reliability, scope, and selectivity to create covalent bonds between different building blocks, more and more investigators exploit this recent synthetic process. Several studies are ongoing to achieve better mechanistic understanding of the reactivity features.[13]

To date, organic chemists have learned to safely work with azides despite the widespread "azidophobia". However, in the inorganic field, investigators should take major precautions when handling organic azides and transition metals. Because of concerns about the safety, we spent some time to define proper non-hazardous reaction conditions. In fact, heavy-metal azides are used in explosive technology in which they work as detonators.[18] Thus, in order to attempt to make optimum use of the still untapped potential of azides in the bioinorganic chemistry context, we paid much attention to prevent heat, shock and intense radiation as well as handling the reagents and products with metallic objects.

We planned to link different receptor peptides with gold(III) metal ion exploiting the azide technology. In this regard, based on the aforementioned considerations (§ *Chapter 8*), we decided to "click" together our building blocks in the absence of the catalyst Cu(I) (**Figure 9.1**) as its *in situ* formation would require reducing conditions. In fact, a redox process may occur in the presence of Au(III), resulting in the formation of the more stable species Au(I) and Au^0. Huisgen 1,3-dipolar cycloadditions carried out in water without copper(I) have been reported although they are not so numerous.[26,27] H. L. Qin *et al*. studied the "click" among different types of azides and alkynes and found that in most cases the yields can be raised with increasing the reaction temperature or by protracting the reaction time. Remarkably, they also reported that higher reaction temperatures favor the formation of the 1,4-disubstituted triazole regioisomer.[27]

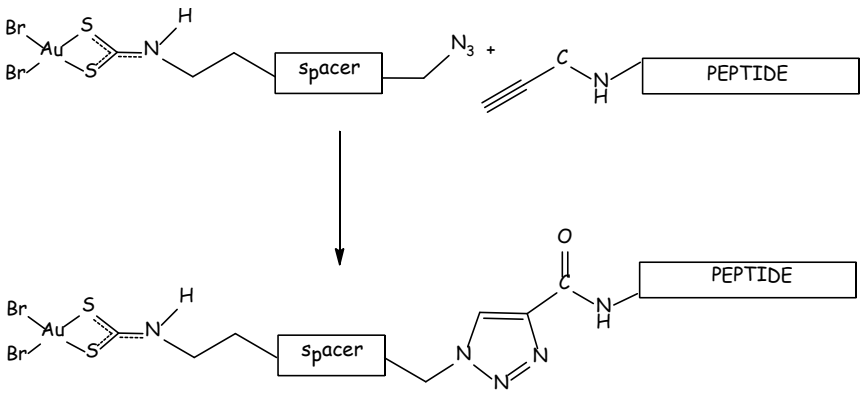

Figure 9.1. Building blocks involved in our designed click reaction: the Au(III) dithiocarbamato complex of an azido-spacer-amine (ASA) and the receptor peptide functionalized with an alkyne group.

Before performing the click reaction we focused on the synthesis of the Au(III) dithiocarbamato complex derived from the organic azide. Regarding the used reagents, azidoaurates of the alkali metals are known to be very unstable, leading to heavy explosions[19,28] and CS_2 is reported to vigorously react with azides.[18] Therefore, we started the synthetic sequence of new anticancer agents under extreme caution. Several reaction conditions were tried but only three of them are herein described.

9.1. Experimental

The first two synthetic routes involved the use of a base in order to favor the ligand formation. It is known that the ligand anionic form is more stable than the dithiocarbamic acid owing to the electronic delocalization in the -CSS moiety. Moreover, the dithiocarbamato salt is more efficient in coordinating to the metal center, generally resulting in higher yields. KOH and NaOEt were used in the first and second attempt, respectively.

9.1.1. Synthesis of the Au(III) azide-dithiocarbamato complex (AuCAD) under basic conditions (KOH)

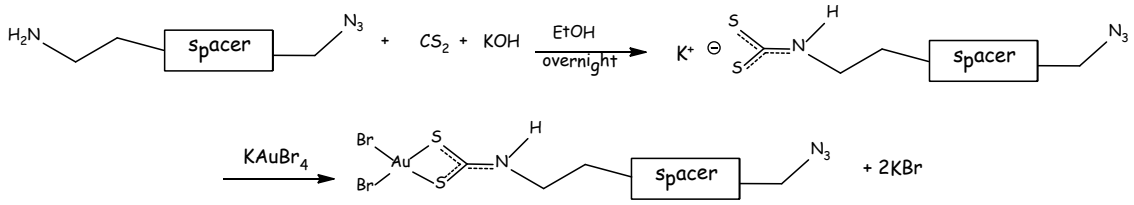

Figure 9.2. Reaction scheme for the synthesis of the gold(III)-based azide derivative using KOH.

The dithiocarbamato ligand was synthesized in ethanol by adding CS_2 (4 eq.) and the organic azide (226.8 μmol, azido-spacer-amine, hereinafter ASA) to a ethanol solution of KOH (1 eq.) with a presumed final pH of 13. After stirring for 30 min, the pH value lowered to about 7 and the mixture became suddenly cloudy and a white precipitate appeared. The ligand mixture was then added to a solution of $KAuBr_4 \cdot 2H_2O$ in ethanol (1 eq.), thus leading to the immediate precipitation of a brown solid that was filtered off and washed several times with water. However, the precipitate was quite gluey therefore it was treated with ethyl acetate to improve the consistency. The final solid was dried over P_4O_{10}.

Yield: 10%

9.1.2. Synthesis of the Au(III) azide-dithiocarbamato complex (AuCAD) under basic conditions (NaOEt)

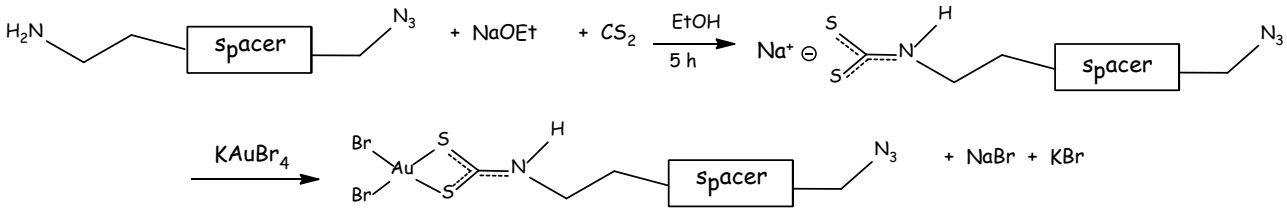

Figure 9.3. Reaction scheme for the synthesis of the gold(III)-based azide derivative using NaOEt.

Similarly to the strategy adopted in the previous attempt, ASA (164.6 μmol) was slowly added to an ethanol solution of NaOEt (1 eq.), the final pH being about 11. Then, CS_2 (10 μL, 1 eq.) was added to the solution. The mixture was slowly added under stirring to an ethanol solution of dihydrate $K[AuBr_4]$ (97.4 mg, 1 eq.), leading to the formation of a dark orange solid. Then, it was washed with ethanol and dried *in vacuo*.

Yield: 18%

9.1.3. Synthesis of the Au(III) azide-dithiocarbamato complex (AuCAD) via template reaction

A water solution of ASA (101.4 μmol) and CS_2 (1 eq.) was treated with a solution of $KAuBr_4 \cdot 2H_2O$ in water (1 eq.), leading to the almost immediate formation of a yellow suspension, which then turned into orange (**Figure 9.4**). During the addition of the last aliquots, the solid changed color into brown. After 5-min stirring, the crude product was separated by centrifugation obtaining a reddish-brown oil. Subsequently, it was washed with *n*-pentane before drying overnight in a desiccator.

Yield: 25 %.

9.1.4. AuCAD characterization

MW. 650.16. Elemental analysis %: (calculated) found C (16.63) 17.20, H (2.64) 2.71, N (8.62) 8.98, S (9.86) 10.15.

Soluble in acetone, ethanol, ethylacetate, acetonitrile, DMSO and toluene; slightly soluble in acetic acid and benzene; insoluble in water, *n*-pentane and *n* -esane.

IR (KBr): 3199/3084 [ν(N-H)], 2926-2863 [$\nu_{a/s}$(-CH_2-)], 2108 [$\nu_a(RN_3)$], 1563 [ν (N-CSS)], 1462/1454 [δ(-CH_2-)], 1280 [$\nu_s(RN_3)$], 1033 [ν_a(SCS)], 552 [ν_s(SCS)] cm^{-1}.

^{1}H NMR (acetone, 300 MHz), δ/ppm: 4.62 and 4.36 [t, 1H, NH-CSS], 3.92 [m, 2H, CH_2-(NHCSS)], 3.88 [m, 2H, -CH_2- (b)], 3.42 [t, 2H, CH_2-N_3].

MS, $[M]^+$ calculated (found): 850.10 (850.0980).*

* cationic species with two dithiocarbamato ligands

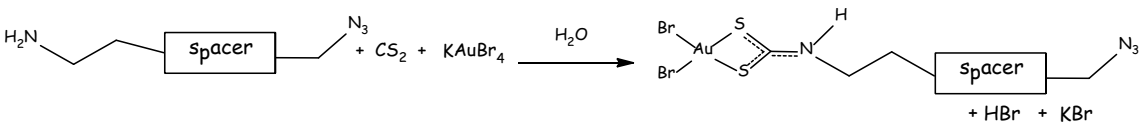

Figure 9.4. Synthesis strategy of the gold(III)-based azide derivative AuCAD by a template reaction.

9.2. Discussion

With respect to the last attempt, although the isolated oil was gluey, the subsequent desiccation *in vacuo* allowed us to obtain the product as a powder. Even if the pureness of the final product is satisfying, the yield of the reaction is very low thereby some endeavors will be done to increase it.

Regarding the AuCAD characterization, first of all, it is worth noting that the coordination did not affected the azido group, thus keeping its out-of-phase stretching (vs) at 2108 cm^{-1} and the in-phase counterpart at 1280 cm^{-1}. Following the formation of the complex, the IR spectrum becomes more crowded and the most diagnostic bands, ascribable to the ν (N-CSS), ν_a(SCS) and ν_s(SCS), set at 1563, 1033 and 552 cm^{-1}, respectively.[20,21] Furthermore, concerning the ν (N-H) two weak combination bands are present at 3199 and 3084 cm^{-1}. The occurrence of two N-H stretching frequencies may be explained with the presence of two forms related to the in plane/out of plane position of the NH group and/or isomers in agreement with NMR data. Interestingly, the ASA spectrum (pure liquid) shows two medium bands of approximately equal intensity at 3369 and 3300 cm^{-1} due to asymmetric and symmetric -NH_2 stretchings overlapped to the water stretching.[29] In addition, a shoulder at 3184 cm^{-1} has been attributed to the first overtone of NH_2 scissoring enhanced by Fermi resonance interaction with the NH_2 symmetric stretching. [29]

Concerning the azide organic backbone in the AuCAD spectrum, the pattern occurring in the region 2926÷2863 cm^{-1} is ascribable to asymmetric and symmetric stretching vibrations of the -CH_2- groups. The bands at 1462 and 1454 cm^{-1} are due to the -CH_2 scissoring.[29]

With respect to the ESI-MS characterization, the base peak visible at 850 Da was ascribed to a gold(III) cation bearing two negatively charged chelating ligands, thus resulting in a species with a net charge of +1. The formation of a 1:2 species was indeed already observed for other compounds previously studied in our reaserch group.

Regarding the NMR spectrum (**Figure 9.6**), on passing from the free organic azide to the gold complex a downfield shift was detected, the major being observed for H_a and H_b atoms (**Figure 9.5**) which are closer to the chelating moiety. In particular, the H_a resonance moves from 3.4 ppm to 3.9 ppm while the multiplet of the latter shifts from 3.7 ppm to 3.9 ppm. It is worth highlighting that upon coordination the -NH group signal places at about 4.5

ppm whereas in the ligand precursor the NH_2 group resonance sets at 2.85 ppm. The remaining hydrogen atoms are only slightly affected by the coordination.

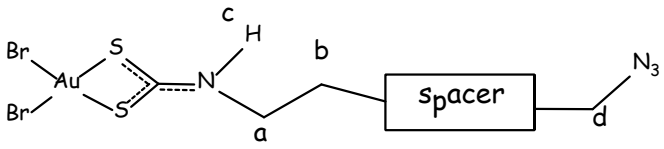

Figure 9.5. Chemical drawing and proton labels of the dithiocarbamato complex Au(III)-azide, AuCAD.

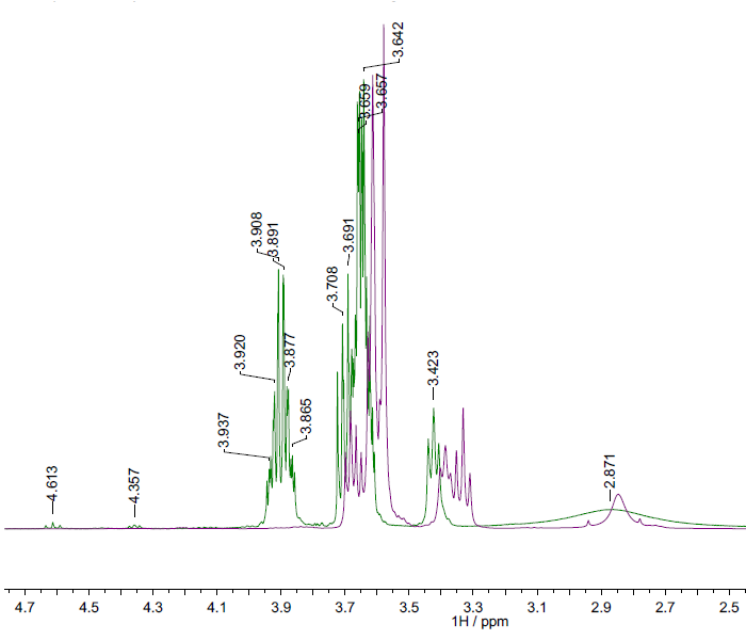

Figure 9.6. ^{1}H-NMR spectrum of AuCAD (green) and the free azide (violet) in acetone-D6 (300 MHz).

Similar to the first- and second-generation compounds,[22-24] two distinct signals (triplet of H_c) appear at 4.61 and 4.36 ppm. We trace this phenomenon back to the presence of two isomers whose nature has not been identified yet or of two forms related to the possible orientation of the proton H_c with respect to the coordination plane. Furthermore, these triplets show very low intensity likely due to the occurrence of intra/inter-molecular hydrogen bonds or with water molecules whose resonance is very broad. Since the H_c proton could have a very low value of pK_a, an exchange between protium and deuterium may account for this behavior as well.

Finally, an electronic spectrum of AuCAD was acquired in ethanol at 308 μM in the wavelength range 225÷500 nm. **Table 9.1** collects the data recorded for both the free azide (50 μM in ethanol) and AuCAD.

With respect to the gold-azide complex, the shoulder I has not been undoubtedly ascribed in the literature to a particular electronic transition and it is still the subject of debate:

sometimes it has been assigned either to an intraligand π*←π transition located in the -NCSS moiety[25] or to intraligand *p*←*d* transitions between levels originated by sulfur atoms[30-31], and it has even been not ascribed in most cases.[32] Band II and band III show very large molar extinction coefficients (ε) and correspond to intraligand π*←π transitions mainly located in the -NCS and -CSS moieties, respectively. Compared to our previous derivatives, containing the dithiocarbamato-sarcosine moiety, some slight spectral differences appear, thus suggesting that the nature of the substituent bound to the nitrogen atom is significant (–H for AuCAD and -CH_3 in the case of AuL12 and AuD8). In fact, the former band shows an ipsochromic shift and a slightly lower ε compared to our previous studied compounds. Likewise, band III displays a blue-shift as well, even if greater than the one evaluated for the band II. The band at 382.3 nm (band IV) is also affected by the *N*-substituent type. This weak band has been attributed to *d*←*d* transitions within the metal orbitals (spin allowed but symmetry forbidden) and its position and intensity are clearly indicative of a square-planar coordination of the metal.[31]

At 320.8 nm a low intensity band is detected and assigned to an intraligand π*←*n* transition where *n* is the in-plane non-bonding sulfur orbital.[33]

Table 9.1. UV-Vis absorption bands of the free azide, AuCAD and two model gold-based compounds.

Compound	λ_{max} /nm (log ε)				
	Band I	**Band II**	**Band III**	**Band IV**	**Band V**
Azide [(a)]	259.1 (4.45)	266.0 (4.53)	273.6 (4.59)	281.7 (4.58)	298.4 (4.40)
AuCAD1[(a)]	236.3 (3.85)	254.8 (4.04)	285.6 (4.00)	382.3 (2.98)	/
AuL12 [(b)]	236.2 (3.99)	261.3 (4.47)	310.4 (4.02)	415.2 (3.18)	/
AuD8 [(a)]	228.0 (3.89)	267.5 (4.31)	312.5 (3.97)	390.9 (3.14)	/

[(a)] performed in ethanol;
[(b)] performed in methanol.

In order to study the stability of this new compound, some electronic spectra were recorded in ethanol over 72 h at 25°C (**Figure 9.7**). Overall, the maxima wavelengths did not change, thus pointing out that the compound was stable throughout 70-h acquisition. The over-time absorbance decrease was ascribed to the partial precipitation of the complex.

A kinetic study was carried out also in acetonitrile highlighting the stability of the compound over 3 days.

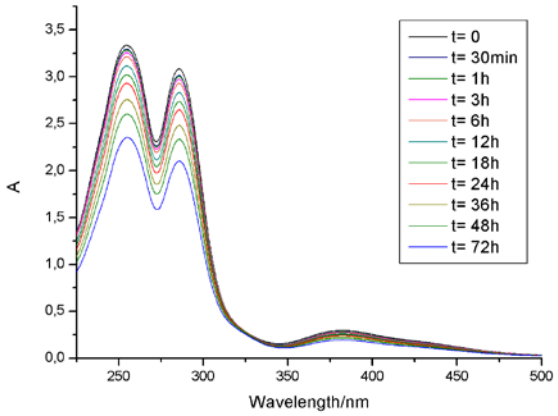

Figure 9.7. UV-Vis kinetics performed in ethanol at 25 °C over 72 h.

9.3. "Click" reaction using a model tetrapeptide

9.3.1. Prop-GDYK synthesis

After the design and the initial development of the versatile gold(III)-based building block AuCAD, we tested its chemical stability with increasing temperature in acetonitrile wherein it is well solubilized. Since the compound was shown to reduce to metallic gold at temperatures higher than 50 °C, required to favor the click reaction with the alkyne moiety, the click reaction was attempted several times at room temperature.

A tetrapeptide was synthetized to be used as a model in preliminary "click" tests. In fact, the chosen sequence Gly-Asp-Tyr-Lys (GDYK) contained basically most of the types of amino acids, namely a neutral, an acidic, an aromatic and a basic residue, respectively.

Regarding the synthesis, the peptide GDYK functionalized with propiolic acid to yield an alkyne group at the *N*-terminus, was synthesized by using standard solid-phase 9-fluorenylmethoxycarbonyl (Fmoc) procedure and a Syro I MultiSynThec GmbH (Wullener, Germany) automatic synthesizer. The Rink amide MBHA resin (loading 0.7 mmol/g) was used as the solid-phase support, and syntheses were performed on a scale of 200 μmol. Fmoc-protected amino acids (4 eq. with respect to resin loading) were coupled according to the known PyBop/HOBt/DIPEA method: Fmoc-amino acid (1 equiv), PyBOP (1 equiv), HOBt (0.5 mM in DMF, 1 equiv), and DIPEA (1.0 mm in DMF, 2 equiv). The Fmoc protecting groups were removed with 30% v/v piperidine in DMF. All couplings were performed twice for 1 h. Propiolic acid (HC≡C-COOH, 4 eq.) was coupled once for 1 h with

4 equivalents of PyBop/HOBt as activating agents and 8 equivalents of DIPEA. The final compound (Prop-GDYK) was fully deprotected and cleaved from the resin for two hours with TFA with 2.5% (v/v) water and triisopropylsylane (2.0%), as scavengers, at room temperature, and then precipitated with ice-cold ethyl ether, filtered, dissolved in water, and lyophilized.

The crude peptide was purified by RP-HPLC using a Phenomenex C18 column eluted with H_2O/0.1% TFA (A) and CH_3CN/0.1% TFA (B) from 1-50% over 30 min at a flow rate of 20 mL min^{-1}. Purity and identity were assessed by LC-MS using a C18 column and eluting with H_2O/0.1% TFA (A) and CH_3CN/0.1% TFA (B) from 20–80% over 10 min at a flow rate of 0.8 mL min^{-1}.

Final Yield: 90%.

9.3.2. Prop-GDYK characterization

$C_{26}H_{32}F_3N_5O_{11}$ (MW. 647.55) Elemental analysis %: (calculated) found C (48.22) 48.29, H (4.98) 4.83, N (10.82) 10.54.

MS, $[M]^+$ calculated (found): 534.22 (534.23).

9.3.3. Click reaction

After many attempts, the "click" proved successful when AuCAD (3.71 μmol, dissolved in acetonitrile) was let to react under stirring at room temperature for 30 h hours with Prop-GDYK (1 eq., previously dissolved in buffer HEPES (10 mM, pH 7.4)-CH_3CN 50-50% v/v) in a 1:1 molar ratio.

The crude compound was purified by RP-HPLC using a C18 column eluted with H_2O/0.1% TFA (A) and CH_3CN/0.1% TFA (B) from 20–80% over 20 min at a flow rate of 20 mL min^{-1}. Purity and identity were assessed by LC-MS eluting with H_2O/0.1% TFA (A) and CH_3CN/0.1% TFA (B) from 20–80% over 10 min at a flow rate of 0.8 mL min^{-1}.

The obtained HPLC profile is visible in **Figure 9.9** and the peak at 16.40 min has been ascribed to the intended product (**Figure 9.10**) as it elutes midway between the peak of AuCAD (22.03 min) and the reagent Prop-GDYK (7 min). The HPLC chromatogram shows the presence of not reacted AuCAD at 22 min and an impurity at 19 min. The ESI-MS analysis of the species eluted at 16.40 min displays a peak at 1136 Da, in agreement with the

species reported in Figure 9.10. Furthermore, the band at 357 nm in the electronic spectrum has been attributed to the 1,2,3-triazole ring formed during the coupling reaction.

Other characterizations will be carried out shortly. Afterwards AuCAD will be conjugated to various targeting peptides and the derivative preliminary tested *in vitro*.

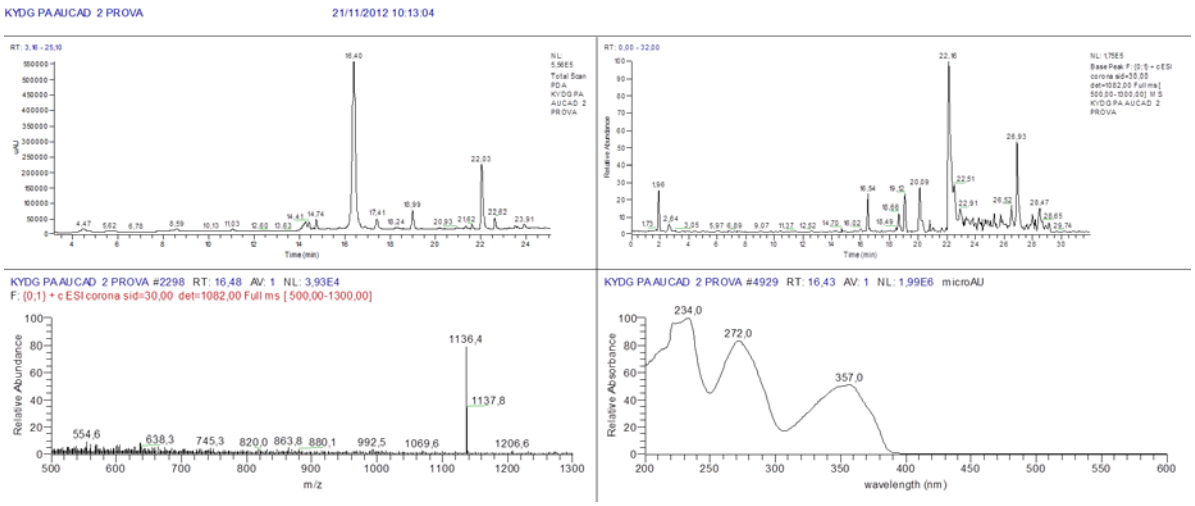

Figure 9.9. First row: HPLC profile (left) and total ionic current (right);
second row: ESI-MS spectrum of the species eluting at 16.40 min in the HPLC profile (left) and its UV-Vis profile (right).

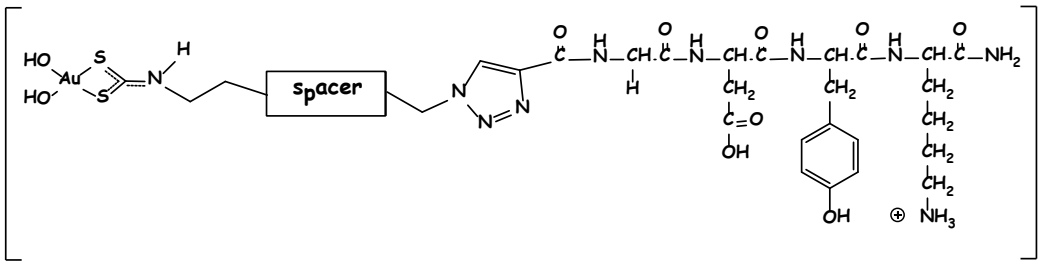

Figure 9.10. Structure of the obtained complex AuCAD-spacer-GDYK-NH_2 in the hydrolyzed form.

Part III references

(1) Kolb, H. C.; Finn, M. G.; Sharpless, K. B. Click Chemistry: Diverse Chemical Function from a Few Good Reactions. *Angewandte Chemie - International Edition* **2001**, *40*, 2004-2021.

(2) Melillo, D. G.; Shinkai, I.; Liu, T.; Ryan, K.; Sletzinger, M. A Practical Synthesis of (±)-Thienamycin. *Tetrahedron Lett.* **1980**, *21*, 2783-2786.

(3) Cavalli, S.; Tipton, A. R.; Overhand, M.; Kros, A. The Chemical Modification of Liposome Surfaces Via a Copper-Mediated [3 + 2] Azide-Alkyne Cycloaddition Monitored by a Colorimetric Assay. *Chemical Communications* **2006**, 3193-3195.

(4) Wieser-Jeunesse, C.; Matt, D.; De Cian, A. Directed Positioning of Organometallic Fragments Inside a Calix[4]Arene Cavity. *Angewandte Chemie - International Edition* **1998**, *37*, 2861-2864.

(5) Wang, Q.; Chan, T. R.; Hilgraf, R.; Fokin, V. V.; Sharpless, K. B.; Finn, M. G. Bioconjugation by Copper(I)-Catalyzed Azide-Alkyne [3 + 2] Cycloaddition. *J. Am. Chem. Soc.* **2003**, *125*, 3192-3193.

(6) Link, A. J.; Vink, M. K. S.; Tirrell, D. A. Presentation and Detection of Azide Functionality in Bacterial Cell Surface Proteins. *J. Am. Chem. Soc.* **2004**, *126*, 10598-10602.

(7) Deiters, A.; Cropp, T. A.; Mukherji, M.; Chin, J. W.; Anderson, J. C.; Schultz, P. G. Adding Amino Acids with Novel Reactivity to the Genetic Code of Saccharomyces Cerevisiae. *J. Am. Chem. Soc.* **2003**, *125*, 11782-11783.

(8) Deiters, A.; Cropp, T. A.; Summerer, D.; Mukherji, M.; Schultz, P. G. Site-Specific PEGylation of Proteins Containing Unnatural Amino Acids. *Bioorganic and Medicinal Chemistry Letters* **2004**, *14*, 5743-5745.

(9) Speers, A. E.; Adam, G. C.; Cravatt, B. F. Activity-Based Protein Profiling in Vivo using a Copper(I)-Catalyzed Azide-Alkyne [3 + 2] Cycloaddition. *J. Am. Chem. Soc.* **2003**, *125*, 4686-4687.

(10) Speers, A. E.; Cravatt, B. F. Profiling Enzyme Activities in Vivo using Click Chemistry Methods. *Chemistry and Biology* **2004**, *11*, 535-546.

(11) Rondelez, Y.; Rager, M. -.; Duprat, A.; Reinaud, O. Calix[6]Arene-Based Cuprous "Funnel Complexes": A Mimic for the Substrate Access Channel to Metalloenzyme Active Sites. *J. Am. Chem. Soc.* **2002**, *124*, 1334-1340.

(12) Gibson, V. C.; Redshaw, C.; Clegg, W.; Elsegood, M. R. J. Novel Metal Imido Calixarene Complexes. *Journal of the Chemical Society, Chemical Communications* **1995**, 2371-2372.

(13) Rostovtsev, V. V.; Green, L. G.; Fokin, V. V.; Sharpless, K. B. A Stepwise Huisgen Cycloaddition Process: Copper(I)-Catalyzed Regioselective "Ligation" of Azides and Terminal Alkynes. *Angewandte Chemie - International Edition* **2002**, *41*, 2596-2599.

(14) Hassane, F. S.; Frisch, B.; Schuber, F. Targeted Liposomes: Convenient Coupling of Ligands to Preformed Vesicles using "Click Chemistry". *Bioconjug. Chem.* **2006**, *17*, 849-854.

(15) Tornøe, C. W.; Christensen, C.; Meldal, M. Peptidotriazoles on Solid Phase: [1,2,3]-Triazoles by Regiospecific Copper(I)-Catalyzed 1,3-Dipolar Cycloadditions of Terminal Alkynes to Azides. *J. Org. Chem.* **2002**, *67*, 3057-3064.

(16) Rostovtsev, V. V.; Green, L. G.; Fokin, V. V.; Sharpless, K. B. A Stepwise Huisgen Cycloaddition Process: Copper(I)-Catalyzed Regioselective "Ligation" of Azides and Terminal Alkynes. *Angewandte Chemie - International Edition* **2002**, *41*, 2596-2599.

(17) Reetz, M. T.; Waldvogel, S. R. B-Cyclodextrin-Modified Diphosphanes as Ligands for Supramolecular Rhodium Catalysts. *Angewandte Chemie (International Edition in English)* **1997**, *36*, 865-867.

(18) Bräse, S.; Gil, C.; Knepper, K.; Zimmermann, V. Organic Azides: An Exploding Diversity of a Unique Class of Compounds. *Angewandte Chemie - International Edition* **2005**, *44*, 5188-5240.

(19) Afyon, S.; Höhn, P.; Armbrüster, M.; Baranov, A.; Wagner, F. R.; Somer, M.; Kniep, R. Azidoaurates of the Alkali Metals. *Zeitschrift fur Anorganische und Allgemeine Chemie* **2006**, *632*, 1671-1680.

(20) Herlinger, A. W.; Wenhold, S. L.; Long II, T. V. Infrared Spectra of Amino Acids and their Metal Complexes. II. Geometrical Isomerism in Bis(Amino Acidato) Copper (II) Complexes. *J. Am. Chem. Soc.* **1970**, *92*, 6474-6481.

(21) Bonati, F.; Ugo, R. Organotin(IV) N,N-Disubstituted Dithiocarbamates. *J. Organomet. Chem.* **1967**, *10*, 257-268.

(22) Negom Kouodom, M.; Ronconi, L.; Celegato, M.; Nardon, C.; Marchiò, L.; Dou, Q. P.; Aldinucci, D.; Formaggio, F.; Fregona, D. Toward the Selective Delivery of Chemotherapeutics into Tumor Cells by Targeting Peptide Transporters: Tailored Gold-Based Anticancer Peptidomimetics. *J. Med. Chem.* **2012**, *55*, 2212-2226.

(23) Ronconi, L.; MacCato, C.; Barreca, D.; Saini, R.; Zancato, M.; Fregona, D. Gold(III) Dithiocarbamate Derivatives of N-Methylglycine: An Experimental and Theoretical Investigation. *Polyhedron* **2005**, *24*, 521-531.

(24) Ronconi, L.; Giovagnini, L.; Marzano, C.; Bettìo, F.; Graziani, R.; Pilloni, G.; Fregona, D. Gold Dithiocarbamate Derivatives as Potential Antineoplastic Agents: Design, Spectroscopic Properties, and in Vitro Antitumor Activity. *Inorg. Chem.* **2005**, *44*, 1867-1881.

(25) Hadjikostas, C. C.; Katsoulos, G. A.; Shakhatreh, S. K. Synthesis and Spectral Studies of some New Palladium(II) and Platinum(II) Dithiocarbimato Complexes. Reactions of Bases with the Corresponding N-Alkyldithiocarbamates. *Inorg. Chim. Acta* **1987**, *133*, 129-132.

(26) Lewis, W. G.; Green, L. G.; Grynszpan, F.; Radić, Z.; Carlier, P. R.; Taylor, P.; Finn, M. G.; Sharpless, K. B. Click Chemistry in Situ: Acetylcholinesterase as a Reaction Vessel for the Selective Assembly of a Femtomolar Inhibitor from an Array of Building Blocks. *Angewandte Chemie - International Edition* **2002**, *41*, 1053-1057.

(27) Wang, Z. -.; Qin, H. -. Regioselective Synthesis of 1,2,3-Triazole Derivatives Via 1,3-Dipolar Cycloaddition Reactions in Water. *Chemical Communications* **2003**, *9*, 2450-2451.

(28) Evans B.L.; *Proc. R.Soc.Lond.A.*, **1958**, 246, 199-203.

(29) Silverstein R.M., Webster F.X. and Kiemle D. J., *Spectrometric Identification of Organic Compounds*, 7th edition, John Wiley & Sons, 2005.

(30) H.Ito, J. Fujita, K. Saito, *Bull. Chem. Soc. Japan*, **1967**, 40, 2584.

(31) A. B. P. Lever, *Inorganic Electronic Spectroscopy*, Elsevier, Amsterdam, 1984.

(32) G. C. Pellicani, W. D. D. Malavasi, *J. Inorg. Nucl. Chem.*, **1975**, 37, 477.

(33) A. W. M. Lee, W. H. Chan, M. F. Ho, *Anal. Chim. Acta*, **1991**, 443.

Section 2
Cu(II) dithiocarbamato derivatives

Chapter 10. The endogenous transition metal Copper

10.1. Copper and its chemistry

Copper is the 29th element in the periodic table and belongs, along with silver and gold, to the 11th group of transition metals, its electronic configuration being [Ar]3d^{10}4s^{1} .
Copper is widespread in nature as metal and its major ore is chalcopyrite ($CuFeS_2$). Copper is traditionally extracted from chalcopyrite by oxidative roasting in a limited air supply to give Cu_2S and FeO; the latter is removed by combination with silica to form a dross, and Cu_2S is converted to Cu^0 by the subsequent reaction.

$$Cu_2S + O_2 \rightarrow 2Cu + SO_2$$

The obtained metal is purified by electrolysis.
In the last years, different methods were developed in order to avoid SO_2 emission; among them, there is bacterial leaching in which natural occurring bacteria called *Acidithiobacillus thiooxidans* oxidize sulfide to sulfate ion; then metal is recovered by elettrodeposition from sulfate solution.[1, 2]
In its elemental form, copper is a soft and ductile reddish metal with high thermal and electrical conductivities. It is the least reactive of the first row transition metals; in fact, it is attacked by non-oxidizing acids only in the presence of air, or with hot concentrated sulfuric acid producing Cu(II) sulfate. It reacts with nitric acid at any concentration. Copper also dissolves in ammonia aqueous solution yielding the ammoniacal complex and reacts at high temperature with O_2 and halides leading to Cu(II) oxide and its dihalides respectively.[2]

The chemistry of copper, especially in solution, is mainly represented by the oxidation state +2, however copper presents other important oxidation states like Cu(III) and primarily Cu(I), whereas Cu(IV) is very rare.

Copper is the only first row metal to exhibit a quite stable +1 oxidation state, however, such an oxidation state is unstable in aqueous solution with respect to the metal and the Cu(II) oxidation state, due to the corresponding redox potentials:

$$Cu^+ + e^- \rightleftharpoons Cu \qquad E^0 = 0.52\ V$$

$$Cu^{2+} + e^- \rightleftharpoons Cu^+ \qquad E^0 = 0.15\ V$$

Therefore, Cu(I) ions usually undergo disproportionation reactions in aqueous medium. Nevertheless, this oxidation state can be stabilized by the formation of insoluble compounds (e.g., CuCl or CuCN) or some complexes like $[Cu(CN_4)]^{3-}$.[2] Cuprous compounds share a d^{10} electronic configuration therefore are diamagnetic as well as colorless unless a charge transfer transition occur. Moreover, there is no crystal field stabilization so the structure of cuprous complex can be very different according to the involved ligands. The tetrahedral coordination is the most common, but linear and trigonal planar geometries, with a coordination number of two and three respectively, are known as well. Owing to its soft character, Cu(I) prefers ligands with soft donor atoms such as sulfur or phosphorus, while nitrogen becomes a good donor atom as its lone pair is involved in an aromatic system.

The oxidation state +2 is certainly typical for most copper compounds including a large number of salts and plenty of complexes with well-defined aqueous chemistry. The major feature of copper(II) is its d^9 electronic configuration. Such configuration makes its coordination geometry subject to Jahn Teller distortion if the metal center is placed in a cubic geometry.[1] Copper(II) can adopt different geometries and coordination numbers, 6 (characterized by octahedral geometry with the predicted tetragonal distortion) and 4 (distorted tetrahedral or square planar geometry) being the most common. Coordination number of five is often observed as well.

The great variety of available coordination geometries for Cu(II) complexes allows a huge assortment in coordinating ligands and donor atoms. Furthermore its border line soft/hard Lewis acid character promotes coordination with ligands having different donor atoms, although the preferred remains nitrogen.[2]

Copper(III) has not been studied a lot as rare until recently except for the high temperature superconductor $YBa_2Cu_3O_{7-x}$. However, there is now an increased evidence of Cu(III) complexes containing ligands capable of stabilize this oxidation state: periodates, fluorides, as well as dithiocarbamates, phosphine, arsine and glycine.[3] With a d^8 electronic configuration, Copper(III) complexes have mostly a coordination number of four and adopt a square planar structure.

Copper(IV) is very rare. It exists in the red Cs_2CuF_6 which is made by fluorinating $CsCuCl_3$ at 520 K. The $[CuF_6]^{2-}$ ion, with a d^7 electronic configuration, is low spin and possesses a Jahn–Teller distorted octahedral structure.[2]

10.2. Biochemistry of Copper

Copper, being an endogenous species, presents interesting biochemical properties. It is found in all living organisms and, in particular, is the third most abundant transition metal ion in human body[3a,3b]. Due to its easy switching from Cu(I) to Cu(II) and *vice versa* under physiological conditions, copper is found in many metalloproteins and enzymes in the form of Cu(I), Cu(II) and Cu(III) ions as well.[4] As expected, copper enzymes are involved mostly in redox processes such as electron transfer reactions (azurin, plastocyanin, laccase)[4] and oxygenation reactions (tyrosinase, ascorbate oxidase) . Copper is present in some crucial enzymes as cytochrome oxidase and Zn,Cu super-oxide dismutase involved in mitochondrial respiration and in antioxidative pathways, respectively.[5] A copper-based oxygen transporter also exists, namely hemocyanin, which carries oxygen in the hemolymph of most mollusks and some arthropods. [5, 6]

Copper-based enzymes have been classified into three different categories on the basis of the coordination geometry of the copper center and the nature of its ligands.[3a] Ceruloplasmine and azurine belong to the 1st type and are characterized by one copper center in a distorted tetrahedral environment with two histidine and a cystein as ligands (the fourth ligand is changeable). Superoxide dismutase belongs to the 2nd type with one copper center in a square planar coordination, while hemocyanin contains a 3rd type center with two copper(I) ions each bounded to three histidine.

Likewise many other essential metals, copper becomes toxic when its concentration raises above physiological levels. Imbalance in copper homeostasis can indeed lead to peculiar disorders including Menkes disease which is caused by copper deficiency, and its counterpart, that is Wilson disease, due to copper overload.[6] For all these reasons, copper trafficking and homeostasis has been extensively studied. Although recently the identification of many details of these processes has been achieved, unanswered questions remain.[12]

A recent adult human dietary recommendation for copper is set at (1.5 ÷ 3) mg Cu/d, based on copper requirements estimated in the range of (1.2 ÷ 2.0) mg Cu/d. [13] Absorption takes place mainly in the stomach and in the small intestine. Then the liver regulates its delivery into the bloodstream.

There are two important proteins responsible for delivery of copper throughout the organism. Ceruloplasmin is the main vector in the serum carrying about 70% total copper to the tissues followed by albumin (12–18%).[7] The first systematic studies on copper uptake by

eukaryotic cells were performed on the yeast *Saccharomices Cerevisiae.*[8] Two proteins, yCTR1 and yCTR3, were identified to mediate copper uptake, and constitute the first members of a widely conserved family of high affinity copper transporters. In fact, these transporters were found in plants and mammals as well. These proteins contain many copper-coordinating residues such as histidine, cysteine, and methionine. Human copper transporters (hCTR1) contain three transmembrane helices arranged in such a way to form a central pore.[9] Intriguingly, copper is delivered to the extracellular histidine-rich *N*-terminal domain of hCTR1 where it is driven into the pore; then, it passes through the pore and exits at the inner surface. Radioactive ^{64}Cu uptake assays[10] have provided insight into the kinetics of copper transport and binding affinity. Furthermore, ^{64}Cu transport turned out to be an energy-independent process, stimulated by extracellular acidic pH and high K^+ concentrations. Notably, it is generally believed that the permeating form of copper is Cu(I). In fact, competitive studies using others metal ions show copper transport inhibition when Ag^+ is added, whereas no inhibition is observed by the addition of divalent cations such as Zn^{2+}, Mn^{2+}, Cd^{2+}.

Once copper is transported into the cytosol by hCtr1, different chaperones shuttle copper to their corresponding enzymes (i.e. Atx1 shuttles copper to the ATPases, CCS, namely copper chaperone for SOD1, to superoxide dismutase). However the copper loading mechanism of these chaperones has not been elucidated yet. Interestingly excess of copper in the cell is removed by chelation by the protein metallothioneins which plays an important role in scavenging free copper.[3b,14]

Chapter 10 references

(1) F. Cotton and G. Wilkinson, Advanced inorganic chemistry, Interscience Publisher, 1972.

(2) C. E. Houscroft and S. A. G, Inorganic Chemistry, Pearson education limited, 2008.

(3) M. D. W and O. G. D, "Copper (III) complexes and their reactions," in *Properties of Copper*, 1981. 3a. M. Rosette and E. Roat-Malone, bioinorganic chemistry: a short course, Wiley Interscience, 2002; 3b. I. Bertini, H. B. Gray, S. J. Lippard and J. S. Valentine, Bioinorganic chemistry, University Science Book, 1994.

(4) Dennison, C. Investigating the Structure and Function of Cupredoxins. *Coord. Chem. Rev.* **2005**, *249*, 3025-3054.

(5) Linder, M. C.; Goode, C. A.; Editors Biochemistry of Copper. [in: Biochem. Elem., 1991; 10]. **1991**, 525.

(6) Bull, P. C.; Cox, D. W. Wilson Disease and Menkes Disease: New Handles on Heavy-Metal Transport. *Trends Genet.* **1994**, *10*, 246-252.

(7) Linder, M. C.; Hazegh-Azam, M. Copper Biochemistry and Molecular Biology. *Am. J. Clin. Nutr.* **1996**, *63*, 797S-811S.

(8) Dancis, A.; Yuan, D. S.; Haile, D.; Askwith, C.; Eide, D.; Moehle, C.; Kaplan, J.; Klausner, R. D. Molecular Characterization of a Copper Transport Protein in S. Cerevisiae: An Unexpected Role for Copper in Iron Transport. *Cell* **1994**, *76*, 393-402.

(9) Aller, S. G.; Unger, V. M. Projection Structure of the Human Copper Transporter CTR1 at 6-Å Resolution Reveals a Compact Trimer with a Novel Channel-Like Architecture. *Proc. Natl. Acad. Sci. U. S. A.* **2006**, *103*, 3627-3632.

(10) Puig, S.; Lee, J.; Lau, M.; Thiele, D. J. Biochemical and Genetic Analyses of Yeast and Human High Affinity Copper Transporters Suggest a Conserved Mechanism for Copper Uptake. *J. Biol. Chem.* **2002**, *277*, 26021-26030.

(11) Lee, J.; Peña, M. M. O.; Nose, Y.; Thiele, D. J. Biochemical Characterization of the Human Copper Transporter Ctr1. *J. Biol. Chem.* **2002**, *277*, 4380-4387.

(12) E. Maryon, S. Molloy, A. Zimnicka and J. H. Kaplan, "biometals," vol. 20, 2007

(13) N. R. Council, *Recommended dietary allowance 10th ed*, National Academic Press, 1989

(14) J. Mawani and C. Orwig, "Esentials metals related metabolic disorders," in *Medicinial bioinorganic chemistry*, Wiley VCH, 2011

Chapter 11. Targeting cancerous cells by exploitation of their enhanced copper uptake: newly synthesized Cu(II) potential therapeutics

11.1. Copper and Cancer

As previously stated, imbalance of copper normal homeostasis is known in several human genetic disorders such as Menkes disease[1], Wilson disease[2] and Occipital Horn syndrome (OHS). In particular, Wilson disease is related to copper accumulation in the liver and the brain of affected patients and is usually treated with the administration of copper chelators like D-penicilamine or trientine. Moreover, copper has also been reported to play a major role in the pathogenesis of neurodegenerative diseases, including amyotrophic lateral sclerosis (ALS), Alzheimer Disease, and the prion-mediated encephalopathies.[3] Remarkably, a close relationship seems to exist between copper and cancer as well. In fact, in 1980, it was proposed that copper plays an important role in angiogenesis.[4]

which is the process that generates new blood vessels from the existing vascular bed. Among the transition metals, only copper was found to be a co-factor required for several angiogenic mediators including the vascular endothelial growth factor (VEGF)[5], basic fibroblast growth factor (bFGF) [6], interleukin-1 (IL-1) and IL-8[7]. Furthermore, it was found that copper increases the affinity of angiogenin, a potent angiogenic molecule, toward endothelial receptors.[8] The rise of copper levels has been shown to elicit the proliferation and the integrin-mediated migration of endothelial cells as well.[9]

Other studies showed that copper metabolism is deeply altered in neoplastic development in human cancer and in tumor-bearing animals[10, 11], and that serum copper levels are related with tumor incidence and weight, malignant progression, and recurrence in a variety of human cancers including Hodgkin's lymphoma, leukemia and cancer of the breast, cervix, liver, and lung[12-15] as well as brain tumors.[16]

Within the chemotherapy context, the first exploited strategy was the *in situ* reaction of chelators (*e.g.*, trientin, *D*-penicilamine, tetrathiomolybdate)[17, 18] used as prodrugs, with the pro-angiogenic copper, thus converting the tumor cell copper to a selective anti-cancer weapon. In this field, D. Chen *et al.* reported that Disulfiram (dimer of diethyldithiocarbamato, $C_{10}H_{20}N_2S_4$) significantly inhibited tumor growth *in vivo* (74%) after 30 days of treatment (mice bearing MDA-MB-231 breast cancer xenografts) by selectively inhibiting tumor proteasome and thus inducing apoptosis.[17] The activity of these prodrugs is related not only to their ability to remove copper (antiangiogenic effects) but primarily to the cytotoxic properties of the active complexes spontaneously formed *in situ* between such organic ligands and the copper ion. Thus, the most recent strategy has been involving copper chemotherapeutics which could exploit the enhanced copper uptake in tumor cells. Several families of copper complexes have been synthesized and tested as anticancer agents including coordination compounds with *N*-, *P*- and *S*-donor ligands such as thiosemicarbazone.[19-21]
In 2008, some Cu(II) dithiocarbamates were synthesized in our research group using as ligands *N,N*-dimethyl dithiocarbamate, pyrrolidine dithiocarbamate and dithiocarbamates of a series of sarcosine ester derivatives (§ *Introduction*).[22] All of them were found to be quite effective as cytotoxic agents in preliminary *in vitro* studies with very low IC_{50} values when tested on cell lines also resistant to the reference drug cisplatin.[23] Based on these encouraging data, we aimed to design new simple copper(II) dithiocarbamato complexes in order to acquire the know-how necessary to develop novel receptor compounds that are more difficult to synthesize because of the presence of various functional groups in the receptor-targeted moiety, which may either react with the transition metal by redox processes or coordinate the Cu(II) ion. Thus, in this work four low-molecular weight compounds have been synthesized and widely characterized. In particular, two different classes of compounds were taken into account, thus comparing them in their chemical and biological properties.

The first category involved dithiocarbamates of secondary amines containing heteroatoms, aimed at raising the poor water solubility of our compounds, thus preventing the use of DMSO as a vehicle for biological tests. Two amines with correlated structures were selected (*i.e.*, methylethanolamine and diethanolamine) and the resulting complexes are reported in **Figure 11.1**, showing a 2:1 ligand-to-metal stoichiometry.

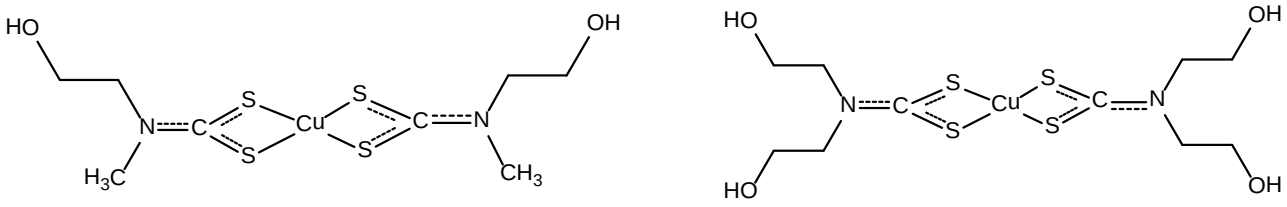

CuC2 **CuC5**

Figure 11.1. CuC2, copper bis[*N*,*N*-(2-hydroxyethyl)methyldithiocarbamate]; CuC5, copper bis[*N*,*N*-bis(2-hydroxyethyl)dithiocarbamate].

The second class of compounds (**Figure 11.2**) was designed to closely resemble the chemical features of our gold(III) derivatives and ultimately of cisplatin, $[PtCl_2(NH_3)_2]$. In this case, there is only a dithiocarbamato ligand which contains a methyl group bound to one sulfur atom, thus being neutral, contrary to the previous compounds that comprise anionic ligands. Accordingly, such a small structural change in the ligand causes an outstanding modification of the coordination sphere around the metal center. In fact, only one dithiocarbamato ligand coordinates the copper ion in an asymmetrical bidentate way, while the other two coordination sites are available for two chloride ions or other anionic ligands depending on the employed copper salt. Therefore, the designed complexes are, to some extent, similar to cisplatin as hydrolysis can easily take place on the two chloride ions, the dithiocarbamato moiety acting as a carrier toward tumor cells.

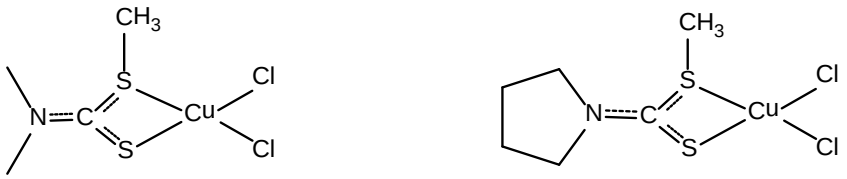

CuC6 **CuC12**

Figure 11.2. CuC6, copper(II) dichloro(*S*-methyl,dimethyldithiocarbamate); CuC12, copper (II) dichloro(*S*-methyl,1-pyrrolidinedithiocarbamate).

After the synthesis and the wide chemical characterization of the reported compounds, the last step of this work has been the biological evaluation of all compounds on the HeLa tumor cell line. In this regard, preliminary anticancer activity tests have been performed in collaboration with the Dept. of Pharm. Sciences, University of Padua.

11.2. Characterization techniques for copper (II) dithiocarbamates

Different techniques for the characterization of metal complexes are available and, in our case, they can be related either to the dithiocarbamato moiety or to the Cu(II) center. However, we focused on some techniques that can give us information on both the organic ligand and the inorganic moiety of our complexes. In the following part, it will be described how some of these techniques are applied to the analysis of our compounds.

11.2.1. FT-IR and FT-Far IR Characterization

IR and Far IR measurements are among the most significant techniques for the characterization of metal dithiocarbamates and a detailed discussion of the resulting spectra is required.

Concerning the dithiocarbamato moiety, three main regions of the IR spectrum are of interest. Firstly, the (1450-1580) cm^{-1} region is associated with the ν(N-CSS) vibration. The appearance of a band in that region indicates a carbon-nitrogen bond order intermediate between a single bond (ν ≈1250÷1350 cm^{-1}) and a double bond (ν ≈1640÷1690 cm^{-1}).[24] Three possible resonance structures are reported by Chatt *et al.* [25] (**Figure 11.3**), characterized by a strong delocalization of electrons in the dithiocarbamato moiety. Among them, structure III is very important because its contribution is responsible for the multiple bond character of the N-CSS bond.

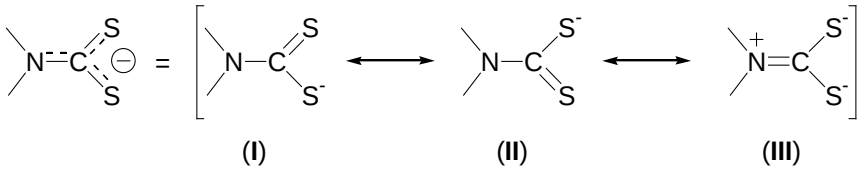

Figure 11.3. Resonant formulae of the dithiocarbamato moiety -$NCSS^-$.

On passing from the free dithiocarbamate to the corresponding complex, the band associated with the N-CSS stretching is shifted to higher energies due to an increased carbon-nitrogen double bond character and, consequently, a greater contribution of the structure III.[26-28] The softer is the metal center, the stronger is its bonding with the dithiocarbamato ligand; in fact, dithiocarbamates have a soft Lewis base character due to the presence of sulfur donor atoms. Notably, a stronger metal-ligand bond determines indirectly a higher frequency for the N-CSS stretching.[29]

The second important region is found in the (940-1060) cm^{-1} range where the ν(C-S) modes are foreseen. From the analysis of this IR region, we can discern the bonding type of the dithiocarbamato ligands in their complexes by the Bonati-Ugo method.[30] The bands attributed to the –CSS moiety are usually coupled to other vibrations and are very sensitive to the local environment, but they are also useful to distinguish between mono- and bidentate coordination.[31]

The presence of only one band in the investigated region, commonly ascribed to the ν_a(SCS) mode, is assumed to indicate a completely symmetric bond of the dithiocarbamato ligand, thus highlighting a bidentate coordination.[32] Conversely, a split band indicates an asymmetrically-bonded bidentate ligand or a monodentate ligand. These different binding modes are shown in **Figure 11.4**.

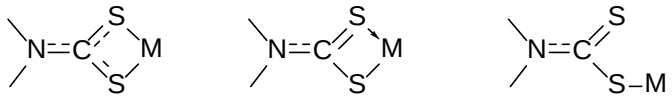

Figure 11.4. Different ways of metal-sulfur binding in dithiocarbamato complexes: symmetrical bidentate (a), asymmetrical bidentate (b) and monodentate (c).

A typical band for both the complexes and the free dithiocarbamato precursors takes place in the range (420-630) cm^{-1} and is ascribed to the ν_s(SCS).

Finally, metal-sulfur stretching modes can be observed in the range (250-420) cm^{-1} at wavenumbers increasing with the oxidation state of the metal. It is possible to detect, in the same range, also the metal-halide stretching modes.[50]

11.2.2. UV-Vis Characterization

Copper(II) dithiocarbamates can be analyzed by UV-Vis spectrophotometry since the features of both the dithiocarbamato moiety and the metal centre give rise to peculiar absorptions.

Normally, a large variety of stereochemistries are observed for Cu(II) complexes and, interestingly, Jahn-Teller effect rules out regular O_h and T_d symmetries in favor of distorted geometries, unless sterically demanding and rigid ligands are present. A careful analysis of the UV-Vis spectra can play a key role in the geometry determination for such complexes, especially when X-ray crystallographic data are not available.

Moreover, the Cu(II) centre has a d^9 electronic configuration that allows the use of the positive hole formalism reducing the issue of defining its electronic levels essentially to a one-electron problem, thus easily foreseeing the absorption bands of its complexes. The splitting energies of d orbitals in ligands field for some common coordination geometries, are shown in **Figure 11.5**.

The positive hole formalism considers the hole excitation instead of the electron one. As a result, electronic transitions are readily obtained, for any geometry, simply reversing the energetic order of orbitals. Thus, while for octahedral and tetrahedral stereochemistries only one transition is possible ($T_{2g} \leftarrow E_{2g}$ and $E_2 \leftarrow T_2$, respectively) for the other geometries we can foresee three different d-d transitions.

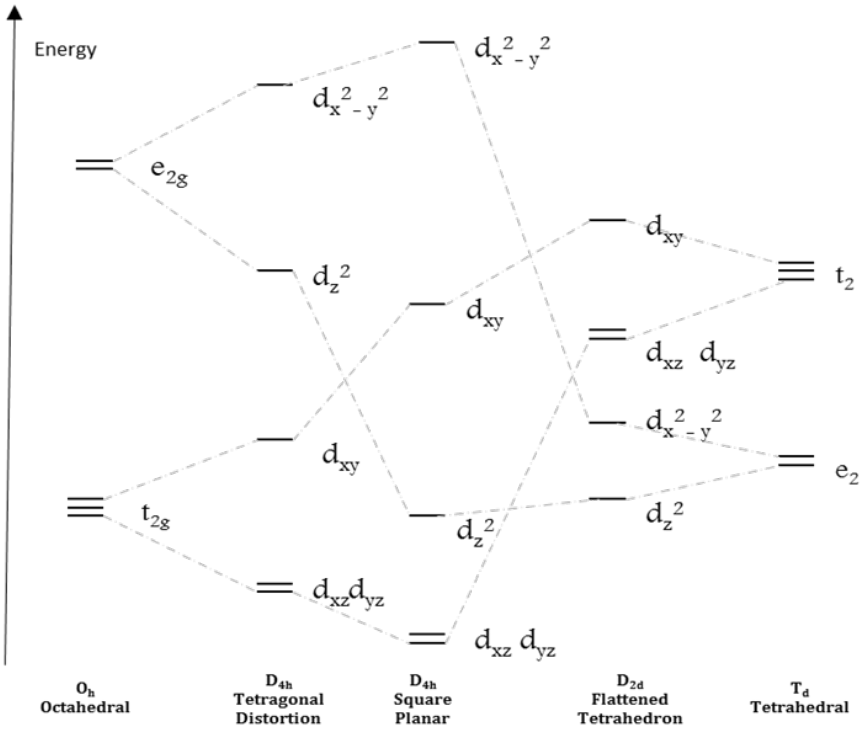

Figure 11.5. Splitting of the energy levels related to the d orbitals for the most common coordination geometries.

With respect to Cu(II) dithiocarbamates, their electronic spectra have been related to their coordination geometries by *Choi et al*. using bis(di-isopropyldithiocarbamato) copper (II) as a model compound.[33]

Starting from an ideal D_{2h} geometry for the metal center, that allows the SCS angle to be less of 90° (small ligand bite) on the plane, as well as the presence of two axial ligands, it is possible to calculate this energy level sequence $d_{xy} > d_{z^2} > d_{x^2-y^2} > d_{xz,\ yz}$. Among the three expected electronic transitions, $d_{z^2} \leftarrow d_{xy}$ appear at lower energies (around 625 nm), while the

transitions $d_{x^2-y^2} \leftarrow d_{xy}$ and $d_{xz,\,yz} \leftarrow d_{xy}$ are overlapped, thus leading to a broad band at higher energies (around 435 nm). A schematic representation of the discussed transitions is shown in **Figure 11.6**

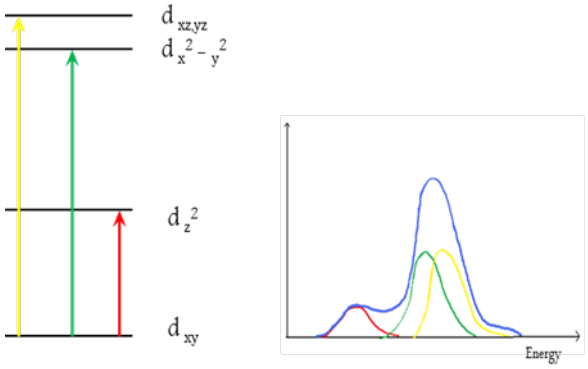

Figure 11.6. Schematic representations of electronic transitions for a D_{2h} symmetry using the positive hole formalism.

For the band intensities, it is worth noting that, for a D_{2h} symmetry, Laporte rule is valid. Therefore, d-d transitions are actually forbidden and characterized by very low intensities. Nevertheless, the broad band related to the transitions $d_{x^2-y^2} \leftarrow d_{xy}$ and $d_{xz,yz} \leftarrow d_{xy}$ seems to be too high in intensity, especially if compared to $d_{z^2} \leftarrow d_{xy}$ transition, leading *Choi et al.*[33] to hypothesize that some kind of geometrical distortion of the D_{2h} geometry may occur. In particular, they suppose that copper atom could lift up from the σ_h plane, thus generating a C_{2v} distortion which make the transition $d_{xz,\,yz} \leftarrow d_{xy}$ more allowed and, therefore, a more intense band is observed (**Figure 11.7**).

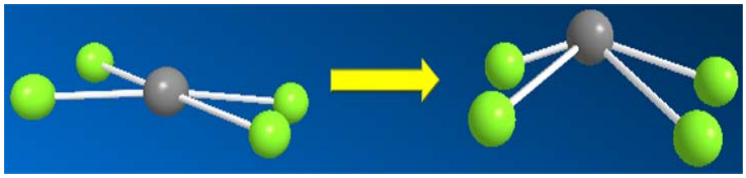

Figure 11.7. Schematic representation of C_{2v} distortion.

The dithiocarbamato moiety can be informative as well, with two strong bands at around 287 and 270 nm for copper (II) dithiocarbamates[22], that can be attributed to the intramolecular intraligand transitions $\pi^* \leftarrow \pi$ located in the S-C-S and the N-C-S moieties, respectively.[34, 35]. A band of much lower intensity is sometimes visible at around 360 nm (for copper dithiocarbamates) and it is assigned to $\pi^* \leftarrow n$ transitions in sulfur atoms.[36]

11.2.3. NMR Characterization

Nuclear Magnetic Resonance is an useful technique to gain insight into the organic moiety of metal complexes. Nevertheless, in the case of paramagnetic copper(II), the metal exerts a great influence on the spectrum shape.

Cu(II) is a paramagnetic center with S=1/2, being characterized by a d^9 electronic configuration. The magnetic moment for copper(II) compounds can be calculated by the "only spin" expression $\mu = 2\sqrt{S(S+1)}$, which better correlates with experimental data than the complete expression or the Van Vleck's one. The resulting magnetic moment is $\sqrt{3}\ \mu_B$.[51] It is known that attempts to acquire an NMR spectrum of a paramagnetic sample often lead to discouraging results. In fact, the coupling of the magnetic moment of unpaired electrons with that of the observed nucleus results in a fast nuclear relaxation (broad lines). Furthermore, this coupling generates an additional term in the nuclear shielding formal expression, thus dominating the overall shift.[37]

Despite these considerations, ^{1}H-NMR analysis for the synthesized complexes has been performed, sometimes obtaining spectra with very broad peaks. Moreover, for those complexes, whose ^{1}H-NMR spectrum was simpler, ^{13}C-NMR spectrum was recorded as well. Indeed, this spectrum is very important for confirming the identity of the synthesized molecules, owing to the presence of a characteristic peak related to dithiocarbamato carbon in the range (185-220) ppm.[38]

11.2.4. ESI-MS Characterization

ElectroSpray Ionization is the MS technique most widely applied for inorganic and metallorganic compounds for which gaseous phase ionization methods are obviously not available. However, regarding copper complexes in general and dithiocarbamates in particular, some elucidations are necessary.

First of all, it is worth noting that reduction processes can be observed for various metal ions, especially in positive ion mode. This process is favored for easily reducible metal ions such as Cu(II) and Fe(III).[52] For this reason, Cu(I)-containing species are often detected in ESI-MS spectra of Cu(II) salts and in some complexes as well.[39] Several possible mechanisms have been proposed in order to explain this process, being a charge transfer the most accredited one. According to this hypothesis, a charge transfer could take place in the gas phase

between the solvent and the metal complex, thus leading to the reduction of the latter. Giannelli *et al*. verified the validity of this hypothesis in the case of their *N*-donor Cu(II) complexes.[39]

If we consider more in detail the copper dithiocarbamato complexes, a further consideration has to be done. ESI-MS analysis of the complex $[Cu(DEDT)_2]$ leads to the molecular ion $[Cu(III)(DEDT)_2]^+$ as a base peak, due to an electrochemical oxidation of the original species in the experimental conditions.[40] A partial explanation of this phenomenon can be found in the electron rich nature of the DTC ligands. In fact, it is known that these ligands are generally able to stabilize metal centers in high oxidation states, such as Cu(III).

11.3. Experimental

11.3.1. Synthesis of the complexes $[Cu\{S_2CNR(CH_2CH_2OH)\}_2]$ (CuC2 and CuC5)

*11.3.1.1. Synthesis of $[Cu\{S_2CNCH_3(CH_2CH_2OH)\}_2]$ (**CuC2**)*

To a suspension of NaOH in methanol, CS_2 and methylethanolamine were added in an equimolar ratio measuring a pH value between 8 and 9. The reaction mixture was stirred for an hour at room temperature and the pH lowered to 7. Thus, the solution was added dropwise to a methanol solution of copper chloride that turned immediately into a dark colour. After 2 hours of stirring a brown solid was observed in suspension and was isolated and washed with water and diethyl ether. The product was then dried in a desiccator in the presence of P_4O_{10}, the final yield being 63%.

Anal. calcd. (found) for $C_8H_{16}CuN_2S_4O_2$ (MW=364.06): C, 26.39 (26.56); H, 4.43 (4.30); N, 7.69 (7.66); S, 35.23 (36.33);

Soluble in DMSO, methanol and acetone, slightly soluble in water and diethyl ether, acetonitrile and chloroform

*11.3.1.2. Synthesis of [Cu{$S_2CN(CH_2CH_2OH)_2$}$_2$] (**CuC5**)*

To a solution of diethanolamine in diethyl ether, stirred at room temperature, CS_2 was added in equimolar ratio. After few minutes copper (II) acetate was also added to the reaction mixture that immediately turned into light yellow with a dark precipitate formation. After 2 hours a black product was isolated by centrifugation and washed with diethyl ether. The black residue was then re-cristallyzed from methanol giving a final yield of 60%.

Anal. calcd. (found) for $C_{10}H_{20}CuN_2S_4O_4$ (MW=424.11): C, 28.32 (28.64); H, 4.75 (4.80); N, 6.60 (6.48); S, 30.24 (29.48);

Soluble in DMSO, methanol and acetone, slightly soluble in water, diethyl ether and acetonitrile, insoluble in chloroform.

11.3.2. Synthesis of methylated dithiocarbamato copper (II) complexes (CuC6 and CuC12)

Prior to the synthesis of the second group of complexes, the preparation of their methylated ligands was performed.

11.3.2.1. Synthesis of DMDTM

The synthesis of DMTM ligand was carried out according to a modified literature method.[41, 42] DMDT sodium salt was dissolved in a 3:2 v/v ethanol:water solution under heating (up to 50°C); then the reaction mixture was allowed to very slowly reach room temperature thus avoiding precipitation of the dissolved salt. CH_3I was then added to the solution. After 1 h a white product was precipitated by addition of water to the reaction mixture; it was then isolated and washed with cold water. The product was then dried *in vacuo* with P_4O_{10}. Subsequently, further product was obtained by spontaneous precipitation from mother liquor stored in freezer giving a final yield of 85%.

Anal. Calcd. (found) for $C_4H_9NS_2$ (MW=135.26) C 35.32 (35.48), H 6.71 (6.52), N 10.36 (9.93), S 47.42 (47.81)%

Soluble in methanol, acetone, DMSO, acetonitrile, diethyl ether and chloroform, insoluble in water.

11.3.2.2. Synthesis of PyDTM

PyDTM ligand was synthesized following a published procedure.[43]

An ethanol solution of methyl iodide was dropwise added under stirring at room temperature to an aqueous solution of PyDT ammonium salt in an equimolar amount. After 1 h, a white crystalline precipitate was spin dried and washed several times with an ethanol-water 1:1 (v/v) solution. The resulting product was dried in a desiccator in the presence of P_4O_{10}. Final yield: 96%.

Anal. Calcd. (found) for $C_6H_{11}CuCl_2NS_2$ (MW=161.29): C 44.68 (44.24), H 6.88 (6.83), N 8.68 (8.70), S 39.76 (39.92)%

Soluble in methanol, acetone, DMSO, acetonitrile, diethyl ether and chloroform, insoluble in water.

*11.3.2.3. Synthesis of [Cu(DMDTM)Cl_2] (**CuC6**)*

Copper (II) chloride was first dissolved in the minimal amount of methanol, then diethyl ether was added. The ligand, previously dissolved in diethyl ether was dropwise added in an equimolar amount. The reaction mixture was let stirring in the dark for 4 hours. After that, a reddish brown precipitate was centrifuged, washed with cold ether and finally dried in a desiccator with P_4O_{10}. Final yield: 78.0%

Anal. Calcd. (found) for $C_4H_9CuCl_2NS_2$ (MW=269.71): C 17.81 (17.98), H 3.36 (3.28), N 5.19 (5.09), S 23.78 (24.41)%

Soluble in DMSO and acetone, methanol and acetonitrile, insoluble in diethylether and chloroform; slowly decomposes to reagents in water.

*11.3.2.4. Synthesis of [Cu(PyDTM)Cl_2] (**CuC12**)*

The synthesis was performed as reported in the previous paragraph. After 4 hours a dark brown precipitate was isolated by means of a centrifuge, washed with water and cold ether and finally dried *in vacuo* in the presence of P_4O_{10}. Final Yield: 55.8%

Anal. Calcd. (found) for $C_6H_{11}CuCl_2NS_2$ (MW=295.74): C 24.35 (24.71), H 3.70 (3.64), N 4.74 (4.62), S 21.69 (22.90)%

Soluble in DMSO, methanol and acetonitrile, slightly soluble in acetone, insoluble in water and chloroform.

11.4. Results and discussion

$[Cu\{S_2CNR(CH_2CH_2OH)\}_2]$: CuC2 and CuC5

While the complex CuC5 has been widely studied, the complex CuC2 has been only recently synthesized, together with CuC5, to test their biological properties as antibacterial and antifungal agents.[44]

In the present work, different routes of synthesis (with respect to those reported before) were investigated for these complexes, in order to improve the yield, to make reaction easier, and to improve the consistency, thus making these compounds available for biological testing as anticancer agents. Then, for each compound, we selected the product deriving from the reaction strategy able to yield the best elemental analysis, IR/NMR data and physical state (solid instead of gluey).

First strategy

In the first attempt, the synthesis of the two complexes was performed in diethyl ether, using copper(II) chloride as copper precursor and exploiting a one-pot reaction. The reaction scheme for complex CuC5 is presented below as an example.

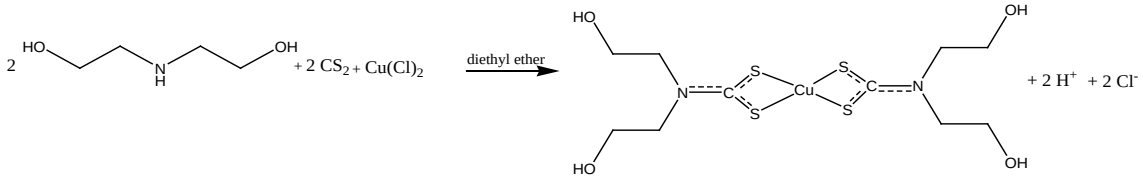

Figure 11.8. First strategy: reaction scheme for the complex CuC5.

Both the dark products appeared oily and sticky, certainly unsuitable for biological tests, as well as its IR characterization and elemental analysis. However, ESI-MS analysis, performed in methanol with 1% formic acid, confirmed the product identity in both cases. **Figures 11.9** and **11.10** report on ESI-MS spectra for the complexes CuC2 and CuC5, respectively.

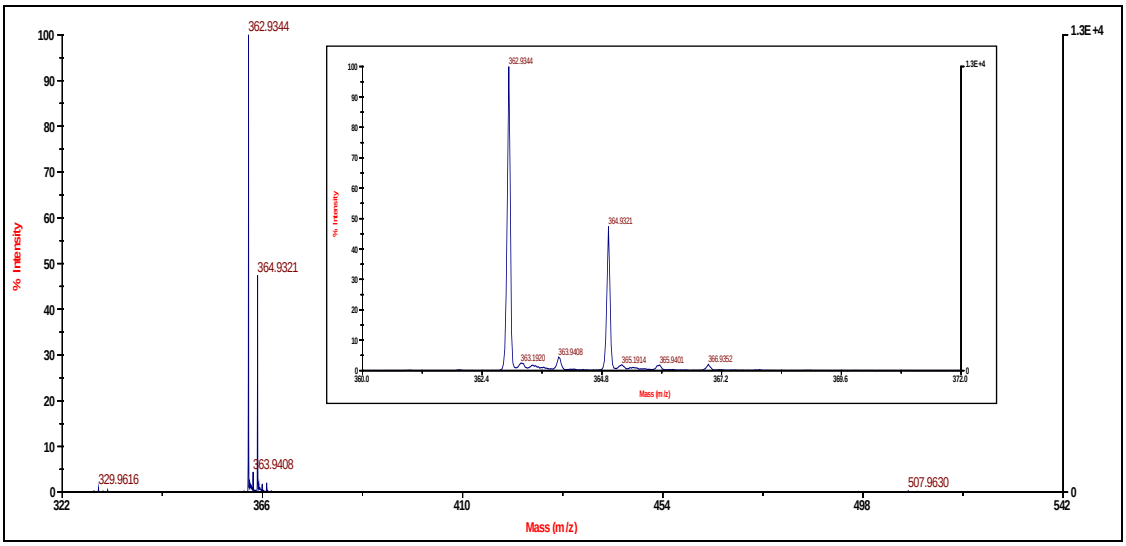

Figure 11.9. ESI-MS spectrum for complex CuC2 and its magnification in the right panel.

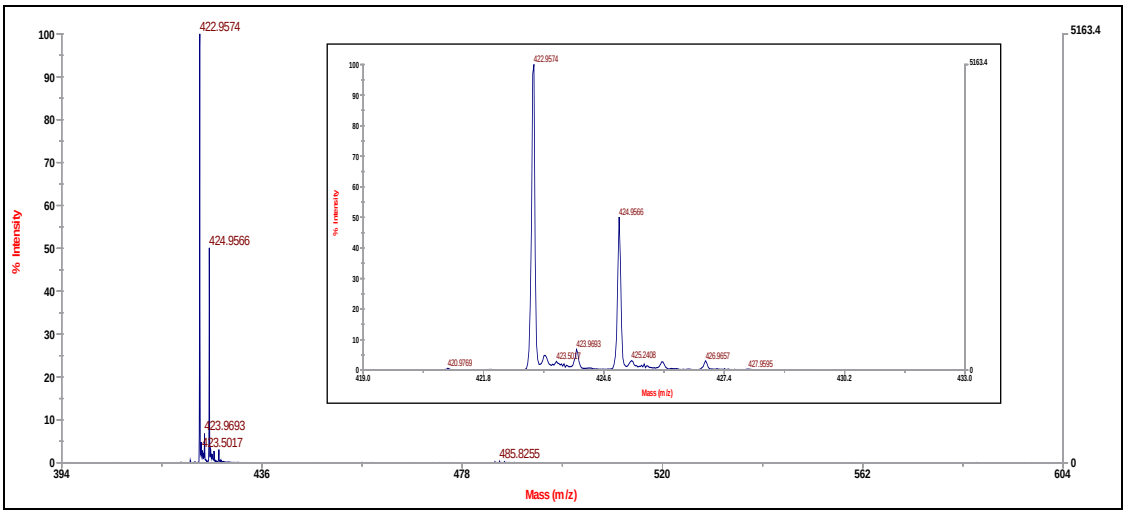

Figure 11.10. ESI-MS spectrum for complex CuC5 and its magnification in the right panel

For both spectra the base peak is represented by the molecular ion $[Cu(III)(DTC)_2]^+$, whose conversion to Cu(III) takes place in the capillary as explained above in section 1.4. The isotopic pattern (^{63}Cu : ^{65}Cu) of these peaks is in agreement with their relative natural abundance 69.2 % : 31.8%.[51]

Second strategy

In the second route, we changed solvent and reaction conditions: methanol was used as solvent and the reaction was performed in two steps. At first, dithiocarbamato sodium salt was synthesized then the ligand solution was added to a copper chloride solution in methanol leading to the complex formation. Reaction scheme is reported below for complex CuC2 as an example.

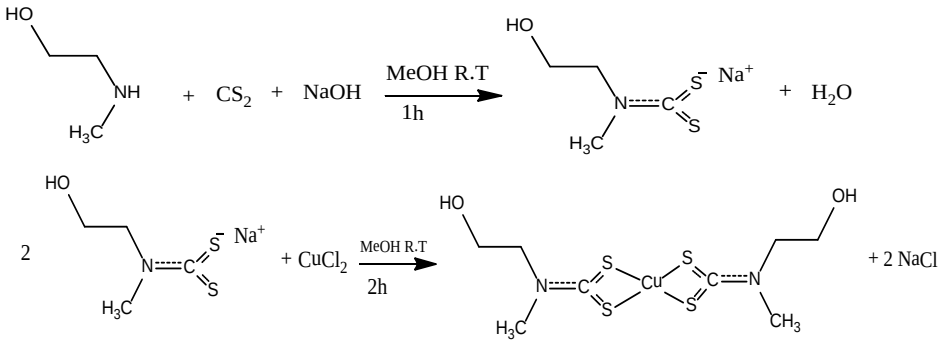

Figure 11.11. Second strategy: reaction scheme for the complex CuC2**.**

If compared to the first strategy, where we obtained oily products, the second way of synthesis allowed us to obtain solid compounds. Elemental analyses and ESI-MS spectra were performed on the two complexes leading to the following results.

Anal. calcd. (found) for complex **CuC2**: $C_8H_{16}CuN_2S_4O_2$ (MW=364.06): C, 26.39 (26.56); H, 4.43 (4.30); N, 7.69 (7.66); S, 35.23 (36.33);

ESI-MS spectrum for complex **CuC2**: base peak at 362.93 m/z with isotopic peak at 364.92 m/z, attributed to the M^+ molecular ion $[Cu(III)\{NCS_2CH_3(CH_2CH_2OH)\}_2]^+$.

Anal. calcd. (found) for complex **CuC5**: $C_{10}H_{20}CuN_2S_4O_4$ (MW=424.11): C, 28.32 (26.15); H, 4.75 (4.27); N, 6.60 (5.52); S, 30.24 (31.46);

ESI-MS spectrum for complex **CuC5**: base peak at 422.96 m/z with isotopic peak at 424.96 m/z, attributed to the M^+ molecular ion $[Cu(III)\{NCS_2(CH_2CH_2OH)\}_2]^+$. Other peaks are visible (yet not identified).

Although the elemental analysis and the mass spectrum of complex CuC5 point out the presence of impurities in the crude product, a dark green crystalline compound precipitated from its mother liquors.

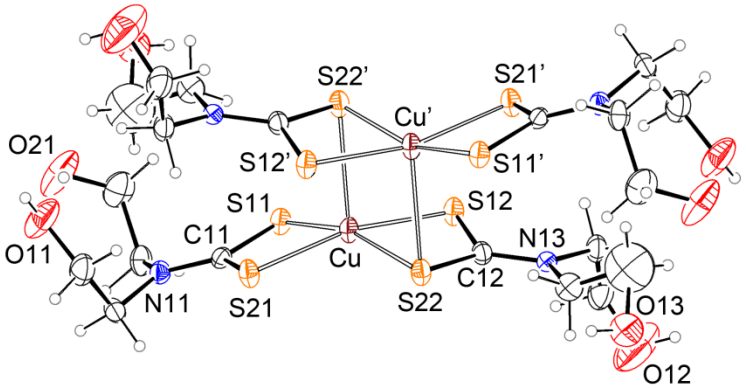

Figure 11.12. Molecular structure of complex CuC5 with thermal ellipsoids at the 30% probability level.

The resolved structure (**Figure 11.12**) is dinuclear, and lies on an inversion center. Each metal adopts a square pyramidal geometry by virtue of two *S,S*- bidentate dithiocarbamato ligands that define the basal plane, and, at a longer distance, by the coordination of one sulfur atom, S(22), of a symmetry related molecule. The peripheral OH groups do not take part into the metal coordination but are involved in an extensive net of hydrogen bonds that define the crystal packing. The long metal-metal separation of 3.461(1) Å rules out any metallophilic interaction[45, 46] for this compound (*see Appendix*). The obtained structure confirmed the proposed stoichiometry. Notably, the elemental analyses of the obtained crystal are in perfected agreement with the calculated values.[47]

Anal. calcd. (found) for the crystal of complex CuC5: $C_{10}H_{20}CuN_2S_4O_4$ (MW=424.11): C, 28.32 (28.56); H, 4.75 (4.77); N, 6.60 (6.40); S, 30.24 (30.67).

Third strategy

In this attempt, the working conditions adopted in the first strategy were maintained unchanged except for copper(II) chloride, being replaced by copper(II) acetate, as reported by De Lima *et al.*.[44] The reaction scheme is shown below for the complex CuC2 as an example.

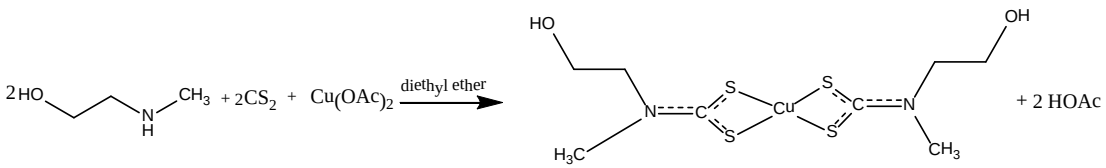

Figure 11.13. Third strategy: reaction scheme for complex CuC2.

Both the products have been recrystallized from methanol obtaining dark solids. The elemental analyses and ESI-MS data of the resulting compounds are presented below.

Anal. calcd. (found) for complex **CuC2**: $C_8H_{16}CuN_2S_4O_2$ (MW=364.06): C, 26.39 (24.84); H, 4.43 (4.00); N, 7.69 (6.94); S, 35.23 (32.54);
ESI-MS spectrum for complex **CuC2**: base peak at 362.93 m/z with isotopic peak at 364.92 m/z, attributed to the M^+ molecular ion $[Cu(III)\{NCS_2CH_3(CH_2CH_2OH)\}_2]^+$. Other peaks are visible (yet not identified).

Anal. calcd. (found) for complex **CuC5**: $C_{10}H_{20}CuN_2S_4O_4$ (MW=424.11): C, 28.32 (28.64); H, 4.75 (4.80); N, 6.60 (6.48); S, 30.24 (29.48);
ESI-MS spectrum for complex **CuC5**: base peak at 422.96 m/z with isotopic peak at 424.96 m/z, attributed to the M^+ molecular ion $[Cu(III)\{NCS_2(CH_2CH_2OH)\}_2]^+$.

For further in-depth characterization, all complexes obtained from the second and third synthetical routes were characterized by IR and Far-IR spectroscopies, as well as by UV-VIS spectrophotometry (in DMSO). ^{1}H-NMR spectra have been registered for these complexes as well, but resulted awfully influenced by the Cu(II) paramagnetism showing very broad signals.
We discuss below the data regarding the complex CuC2 and complex CuC5, obtained by the second strategy and the third one, respectively, on the basis of the best elemental analysis and IR data. Such two compounds were lastly used for biological testing.

FT-IR Characterization

The most diagnostic bands for the two complexes are presented in **Table 11.1** along with the corresponding assignments.

Table 11.1. Selected IR frequencies.

IR active mode	ν(O-H)	ν(C-H)	ν(N-CSS)	ν_a(SCS)	ν_s(SCS)	ν(S-Cu-S)
CuC2	3427 br[(a)]	2930-2912 w	1509 s	983 m	566 w	362 s
CuC5	3258 br[(a)]	2930-2910 w	1487 s	988 m	554 w	336 s

s = strong; w = weak; m = medium, br = broad; a/s = asymmetric/symmetric stretching vibrations.
[(a)] involved in hydrogen bonds

The spectra for the two complexes are quite similar (**Figure 11.14**). Both present a symmetrical bidentate binding mode for dithiocarbamato ligands as pointed out by the presence of only one band in the ν_a(SCS) region (*see section 11.2.1*).

It is worth noting that the signals related to S-Cu-S stretching and to the the ν(N-CSS) are detected at higher frequencies for complex CuC2 than for CuC5. These findings allow to suppose a stronger metal-ligand bonding for complex CuC2 with respect to complex CuC5. Both complexes are characterized by the presence of hydrogen bonds that shift the ν(O-H) towards lower frequencies.

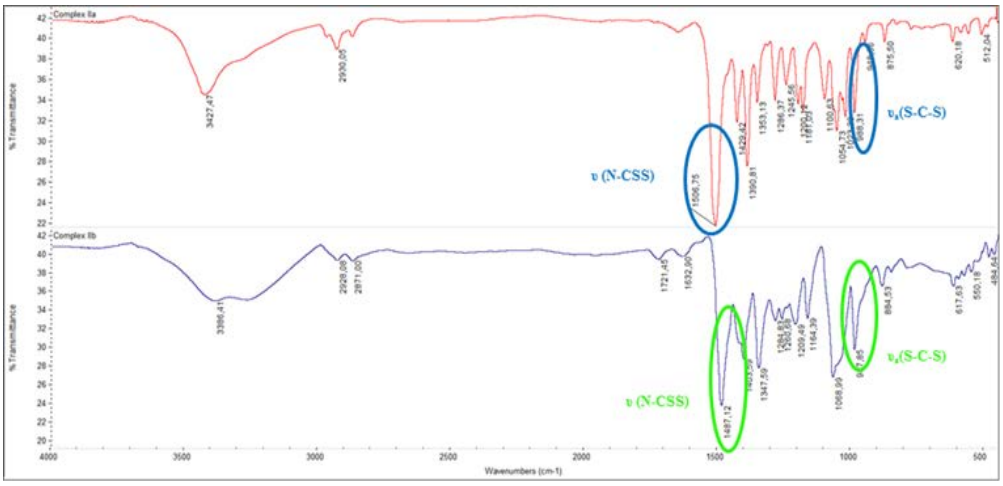

Figure 11.14. FT-IR spectra of complexes CuC2 (upper panel) and CuC5 (lower panel).

UV-VIS Characterization

Electronic spectra have been acquired for both the complexes in DMSO at the concentration of 25 µM. The band absorption of the most diagnostic bands are reported in **Table 11.2**.

Table 11.2. Absorption bands and corresponding molar extinction coefficients in the UV-Vis spectra.

	λ_{max}/nm (logε)		
compound	**$\pi^* \leftarrow \pi$ (N-C-S)**	**$\pi^* \leftarrow \pi$ (S-C-S)**	***d-d* transitions**
CuC2	272.5 (4.80)	282.7[(a)] (4.76)	435.3 (4.01)
CuC5	274.7 (4.45)	286.7[(a)] (4.32)	440.3 (4.01)

[(a)] shoulder.

The two spectra appear very similar to each other with a few nanometers shift in maxima position, with the compound CuC2 showing higher energy for every transition and, in general, higher molar extinction coefficient as well. Both the intraligand and d-d absorptions are in agreement with literature data.[22]

Intriguingly, in the range 400÷500 nm a broad band was observed with an ε value of about 10000 cm^{-1} M^{-1}. The presence of a charge transfer transition in addition to the previously discussed d-d transitions ($d_{x^2-y^2} \leftarrow d_{xy}$ and $d_{xz,\ yz} \leftarrow d_{xy}$) may account for this high

absorptivity.[33]At present, the paucity of literature data does not enable us to clearly identify the type of transition, namely ligand to metal (LMCT) or metal to ligand charge transfer (MLCT). However, on one side, the electron-rich nature of the metal and, on the other side, the capability of the dithiocarbamato ligands to stabilize high oxidation states, prompted us to hypothesize that the observed transition is a MLCT.

Methylated dithiocarbamato ligands

The synthesis of the methylated ligands has been carried out following procedures developed in our research group. High methylation yields are obtained when the starting dithiocarbamic salt is easily isolable or available, thus limiting the choice of possible ligands for this reaction. Two different ligands were chosen, namely PyDT and DMDT, in order to compare the biological activity of the resulting methylated complexes with that of their bis-chelated counterparts.[22] The reaction scheme is reported here for PyDT as an example.

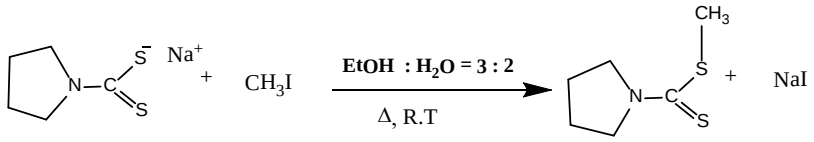

Figure 11.15. Reaction scheme for PyDTM.

^{1}H-NMR Characterization

We performed a ^{1}H-NMR spectrum on the precipitated white product, checking the presence of a new signal related to the methyl group. The ^{1}H-NMR signals for the two ligands are reported below.

DMDTM ^{1}H-NMR, δ(ppm): 2.54 (s, 3H, S-CH_3); 3.35, 3.46 (s , 6H, CH_3-N-CH_3)

Notably, two distinct signals were recorded for the two *N*-methyl groups, due to their different magnetic environments caused by the presence of the -SCH_3 group and the partial character of double bond that rules out the free rotation around the N-CSS bond. The upfield signal is attributed to the *N*-methyl group closer to the *S*-methyl moiety, whose electronic cloud slightly shields these CH_3N- protons.[48]

PyDTM ^{1}H-NMR, δ(ppm): 1.91, 2.02 (m, 4H, CH_2-CH_2); 2.55 (s, 3H, S-CH_3); 3.61, 3.77 (tr, 4H, CH_2-N-CH_2)

In this case two different signals were recorded not only for the two *N*-methylene groups, but also for the ring protons. For the above described reasons, the multiplet and triplet placed at higher fields are attributed to the -CH_2 and N-CH_2 closer to the SCH_3 group, respectively.[42]

FT-IR Characterization

The major bands for the two methylated ligands are reported in the table below.

Table 11.3. Selected IR frequencies.

IR Active modes	ν(C-H)	ν(N-CSS)	ν_a(S=C-S)	ν_s(S=C-S)
DMDTM	2913 m	1506 s, br	977, 948 s	568 m
PyDTM	2969-2867 w	1461, 1440 s, br	1004, 944	578 m

s = strong; w = weak; m = medium; br = broad; a/s = asymmetric/symmetric stretching vibrations.

Unlike the IR spectra of the previous complexes CuC2 and CuC5, the spectra here studied appear very crowded in the regions of interest, therefore very difficult to be interpreted. This behavior is ascribable to the presence of the –SCH_3 group which lowers the symmetry of the ligands. Thus, the bands owing to ν(N-CSS) are always broad and sometimes split, whereas two or three distinct bands are recordable in the region of S=C-S stretching making impossible a correct attribution. Based on these considerations, the spectra of this type of ligand have to be considered as a simple finger print of the molecule, rather than being used to better characterize the final products.

UV-VIS Characterization

UV-Vis spectra have been acquired for the two ligands in DMSO at 50 μM concentration. The main absorption bands are presented below.

Table 11.4. Absorption bands and corresponding molar extinction coefficients in the UV-Vis spectrum.

compound	λ_{max}/nm (logε)	
	$\pi^* \leftarrow \pi$ (N-C-S)	$\pi^* \leftarrow \pi$ (S-C-S)
DMDTM	255.8 (3.88)	276.0 (4.05)
PyDTM	255.3 (3.87)	275.7 (4.05)

The spectra of DMDTM and PyDTM result very similar to each other, in terms of both the energy of the transitions and the extinction molar coefficient.

Methyl-dithiocarbamato copper(II) complexes

Copper complexes with methyl-dithiocarbamato ligands have never been synthesized before. Nevertheless, platinum(II), palladium(II), gold(III) and ruthenium(III) complexes with this type of ligands were previously studied in our research group in order to evaluate their biological activity as anticancer agents.[42, 48] Therefore, in the present work, the complexation reaction was performed by a procedure similar to that exploited for the synthesis of Pt(II) and Pd(II) *S*-methylated dithiocarbamates.[49]

Concerning the palladium derivatives, it was found that these complexes were heat- and photo-sensitive, thus resulting in the progressive elimination of CH_3Cl and the subsequent polymerization of the complex, resulting in either [PdCl(DTC)(DTCM)] or $[PdCl(DTC)]_n$ species.[43, 49] Thus, we decided to carry out the complexation step in the dark.

The previously used synthetic strategy, which involved diethyl ether as a solvent, has been slightly modified in order to increase the purity of the products. In fact, the poor solubility of copper(II) chloride in this solvent led to the presence of $CuCl_2$ in the isolated solid. Therefore, we preferred to first dissolve copper(II) salt in the minimal amount of methanol and, then, we added diethyl ether. This choice gives rise to lower yields (being the products quite soluble in methanol), but the purity of the resulting complexes was really improved.

The reaction scheme is reported below for PyDTM complex as an example.

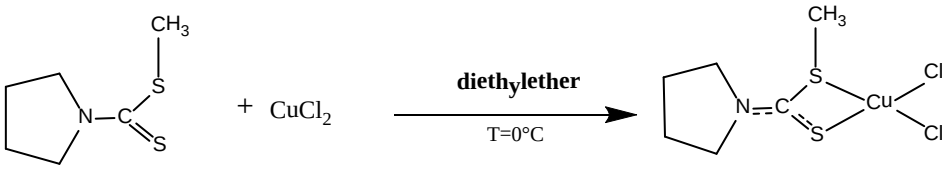

Figure 11.16. Reaction scheme for the complex CuC12.

The obtained complexes were characterized by means of medium-IR and far-IR as well as by UV-VIS spectrophotometry in DMSO and ^{1}H-NMR, ^{13}C-NMR spectroscopy in DMSO-D6.

^{1}H-NMR Characterization

For the two complexes, ^{1}H-NMR spectra have been recorded and the resulting signals are reported below.

CuC6 ^{1}H-NMR, δ(ppm): 2.51 (s, 3H, S-CH_3); 3.33, 3.44 (s , 6H, CH_3-N-CH_3)

CuC12 ^{1}H-NMR, δ(ppm): 1.90, 2.00 (m, 4H, CH_2-CH_2); 2.53 (s, 3H, S-CH_3); 3.59, 3.75 (tr, 4H, CH_2-N-CH_2)

Interestingly, the chemical shifts obtained for such complexes are almost identical to those recorded for their related ligands. Therefore, for this class of compounds, the paramagnetic nature of Cu(II) center does not seem to influence at all the magnetic environment of the involved ligand. This behavior may be caused by the lower strength of the Cu-S bond in these complexes.

Based on what discussed above for the ligands, for each split resonance, we can attribute the upfield signal to the methyl/methylenic group closer to S-CH_3, whose electrons shield, to some extent, the nearest protons.

A ^{1}H^{1}H-NOESY spectrum for the complex CuC12 has been recorded to better assign the observed signals (**Figure 11.17**). In fact, this bidimensional spectrum could highlight a spatial relation between the *S*-methyl group and a specific *N*-alkyl group.

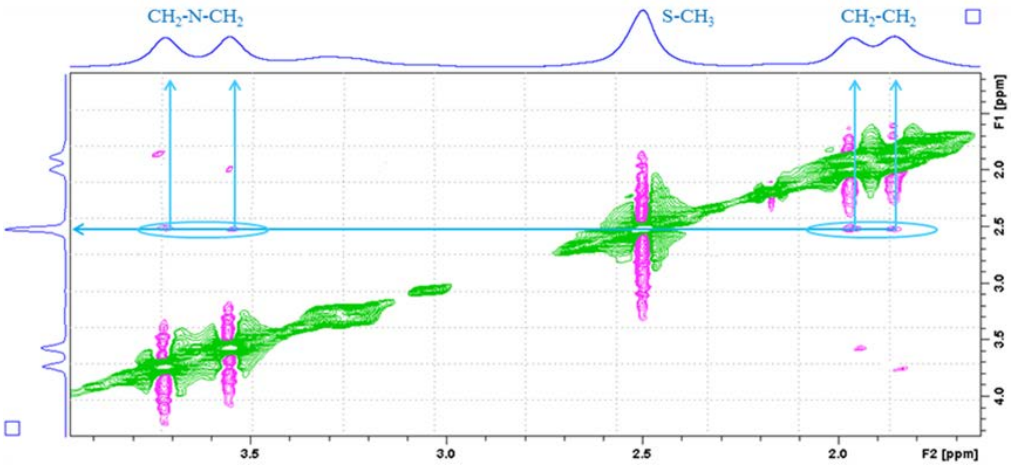

Figure 11.17. NOESY spectrum of complex CuC12 (400 MHz, DMSO-d_6). Interesting correlation peaks are highlighted in light blue.

Intriguingly, the NOESY spectrum showed weak correlation signals of the *S*-methyl group with all the methylenes. Moreover, for each group of signals the intensities of the two correlation peaks are quite identical, preventing us from understanding which methylene group stand on the same side of the S-CH_3. Surprisingly, the stronger correlation signals are recorded for the -CH_2-CH_2- moiety rather than for the CH_2-N-CH_2 protons which should be, in principle, closer to the S-CH_3. This phenomenon can be explained assuming that, in the complex, the 5-member ring is folded in such a way that the -CH_2-CH_2- protons become spatially closer to the S-CH_3 group.

^{13}C-NMR Characterization

^{13}C-NMR spectra have been acquired for these complexes in order to verify the presence of S-CH_3 group with its characteristic upfield chemical shift.[49] The resulting signals are reported below.

CuC6 ^{13}C-NMR, δ(ppm): 18.9 (S-**C**H3); 44.0, 40.0 (CH3-N-**C**H3); 195.2 (S-C-S)

CuC12 ^{13}C -NMR, δ(ppm): 18.4 (S-**C**H3); 23.3, 25.1 (CH2-CH2); 54.4, 49.9 (CH2-N-CH2); 191.4 (S-C-S)

In both spectra, the resonance peaks ascribed to S-**C**H_3 are at around 19 ppm, while the S-C-S dithiocarbamic carbons are visible at very low fields.

X-Ray Characterization

Single crystals were obtained from mother liquors of the two complexes CuC6 and CuC12 and their structure have been solved by means of X-Ray diffraction. The obtained structures are reported below (**Figures 11.18** and **11.19**) and the calculated and found analyses for the crude complex CuC6 are reported for comparison as well. A summary of the X-ray crystallographic data is shown in appendix.

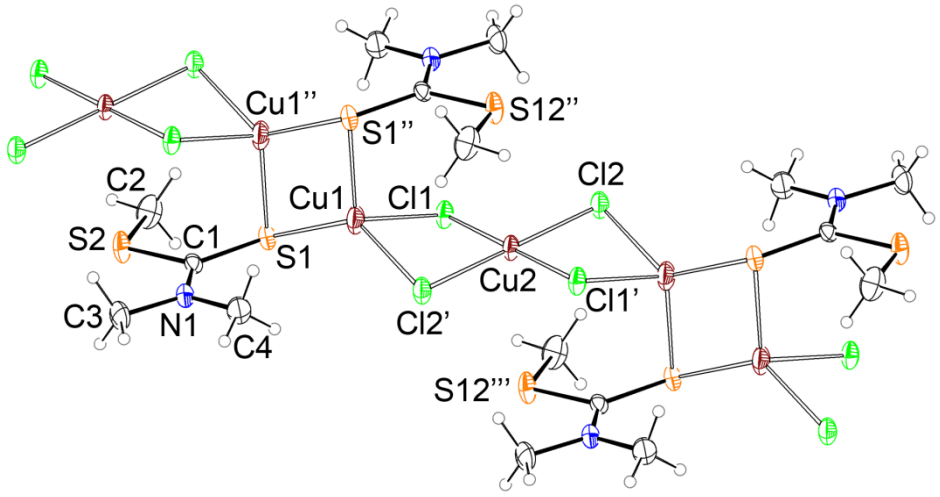

Figure 11.18. Portion of the molecular chain of brown crystals precipitated in the mother liquors of complex CuC6,
with thermal ellipsoids at the 30% probability level.
Calculated elemental analysis for $[Cu(I)_2Cu(II)Cl_4(C_4H_9NS_2)_2]$: C, 15.94; H, 3.01; N, 4.65 ; S, 21.27%

Anal. Calculated (found) for the crude complex **CuC6** ($C_4H_9CuCl_2NS_2$): C 17.81 (17.98), H 3.36 (3.28), N 5.19 (5.09), S 23.78 (24.41)%

The structure shown in **Figure 11.18** is polynuclear and the molecular assembly forms a chain that runs along the *c* crystallographic axis. In the crystal both Cu(I) and Cu(II) oxidation states are present, namely Cu(1) and Cu(2), respectively. Accordingly, the geometry of Cu(1) is distorted tetrahedral, whereas that of Cu(2) is square planar. Cu(1) is surrounded by two sulfur atoms of two symmetry related ligands and by two bridging chloride anions. At variance, Cu(2) is surrounded by four chloride anions, and the very long distance of 3.229(2) Å between Cu(2) and two thioether sulfur atoms, S(2), suggest that the Cu(2) coordination is in fact square planar and not distorted octahedral. Since Cu(2) lies on an inversion center whereas Cu(1) is on a general position, the number of metals in the +1 oxidation state is double than those in the +2 state. On the base of the short Cu(1)-Cu(1) separation (2.595(1) Å), significantly shorter than the Cu(1)-Cu(2) one, a certain degree of metal-metal interaction is expected to occur between these two atoms (*see Appendix*).

Concerning the calculated crystal elemental analysis, it is evident that the solved crystal structure cannot be ascribed to the compound CuC6. In fact, the elemental analysis values found for the isolated product are in perfect agreement with theoretical values for complex CuC6, whereas the calculated values for the crystal are quite different from those found for the crude product.

We hypothesized that the obtained crystal may derive from the degradation of complex CuC6, in which partial reduction of Cu(II) to Cu(I) has occurred, or it could be the thermodynamic favored product.

On the contrary, after the isolation of the powdered compound CuC12, we obtained some colorless crystals from its mother solution. Its X-ray analysis clearly showed that it corresponds to unreacted ligand PyDTM (**Figure 11.19**). The molecule presents a significant electron delocalization in the fragment that comprises the thioamido function, N(1)-C(1)-S(1), as inferred by the bond distances and bond angles (*see Appendix*). In fact, the C(1)-N(1) distance is approximately 0.2 Å shorter than the N(1)-C bond distances within the penta-atomic ring. In addition, the C(1)-S(1) bond distance is significantly shorter (1.745(2) Å) than the C(1)-S(2) one (1.791(2) Å). This latter distance is more close to the value of the C(2)-S(2) distance, which is typical for a C-S single bond.

Interestingly, the *S*-methyl group places on the same side with respect to thiocarbonyl moiety, the same occurring in the solved structures shown in Figure 6.18. As deduced by the $^{1}H^{1}H$-NOESY NMR spectrum, it is likely that the S-CH_3 group changes its side upon

coordination to Cu(II) since we observed its correlation cross peaks with all the -CH_2- of the 5-member ring, thus pointing out a spatial distance lower than 4.5 Å.[53]

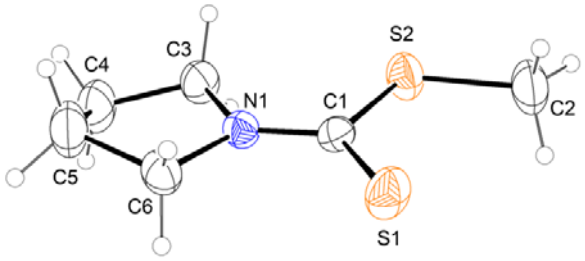

Figure 11.19. Molecular structure of white crystals precipitated in the mother liquors of complex CuC12, with thermal ellipsoids at the 30% probability level.

IR Characterization

The major bands for the two complexes are reported in **Table 11.5** with their respective attributions.

Table 11.5. Selected IR frequencies.

IR active modes	ν(N-CSS)	ν_a(S=C-S)	ν_s(S=C-S)	ν(S-Cu-S)	ν(Cu-Cl)
CuC6	1530 br	974 m, 941 s	557 w	301s	249
CuC12	1516 m, 1483 s, 1432 m	995 w, 971w 934 s, 907m	582 w	300 m/328 w	280 s

s = strong; w = weak; m = medium; br = broad; a/s = asymmetric/symmetric stretching vibrations.

Similar to the corresponding ligands, the IR spectra of these complexes are complicated and crowded with bands, because of the marked asymmetry of the ligands. The asymmetric binding mode of the ligand is confirmed by the presence of several bands ascribable to the ν_a(S=C-S) in the involved region. Remarkably, the signals related to the N-CSS stretching in the complexes are shifted to higher frequencies than in the ligands due to metal coordination.

Concerning the Far IR spectra, the major bands are identified through a comparison with the absorptions of the corresponding ligands. In fact, the newly arisen signals must be related to Cu-S or Cu-Cl vibrational modes. For the complex CuC12, two signals may be ascribed to S-Cu-S stretching, owing to the asimmetry of the ligand whereas for complex CuC6 only a very broad band can be assigned to that vibrational mode. Considering the Cu-Cl stretching, a dissimilar bond length in both complexes may account for the difference in the wavenumbers, according to literature.[54] Finally, a band attributed to Cl-Cu-Cl bending is

recognizable in all the spectra (at 187 cm^{-1} for complex CuC6 and 200 for complex CuC12).[54] Notably, such a band results particularly strong for complex CuC6 likely due to the lower rigidity of this compound.

The acquired spectra are presented in the figures below. The Far-IR spectrum of each complex is reported together with that of the corresponding ligand, for comparison purpose.

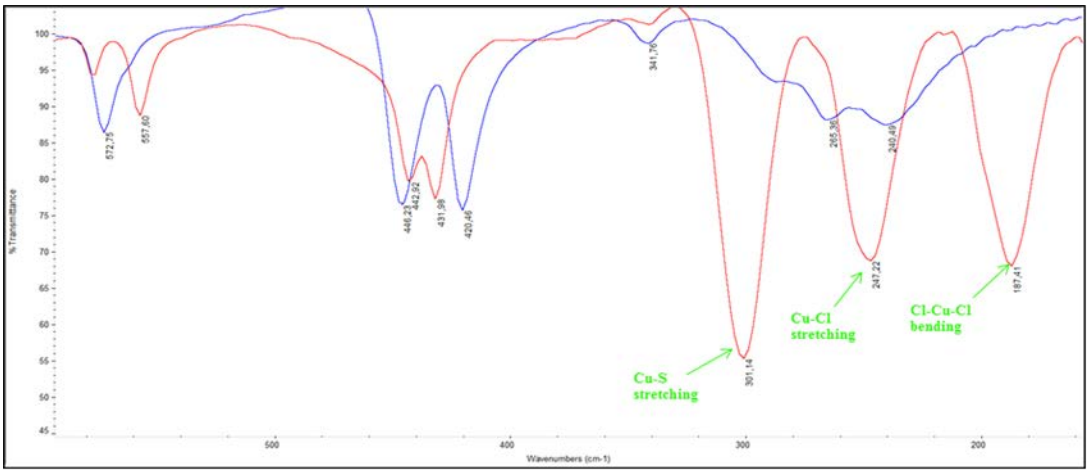

Figure 11.20. FT-Far IR spectrum of complex CuC6 (red) and DMDTM (blue). The highlighted signals are those involving metal-ligand vibrations.

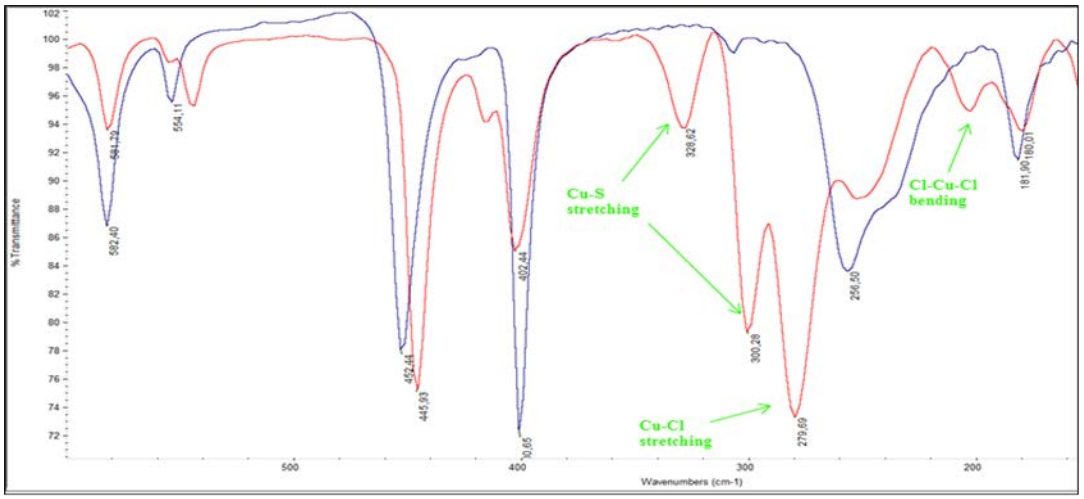

Figure 11.21. FT-Far IR spectrum of complex CuC12 (red) and PyDTM (blue). The highlighted signals are those involving metal-ligand vibrations.

UV-VIS Characterization

UV-Vis spectra have been acquired for these complexes in DMSO at 50 µM concentration. The main absorption bands are reported in the Table below.

Table 11.6. Absorption bands and related molar absorptivities in the UV-Vis spectrum.

compound	λ_{max}/nm (log ε)		
	$\pi^* \leftarrow \pi$ (S-C-S)	$\pi^* \leftarrow \pi$ (N-C-S)	d-d transitions
CuC6	255.5/4.09	276.7/4.26	-

CuC12	256.6/3.85	274.0/4.00	403.1/2.82

The $\pi^* \leftarrow \pi$ transitions for both complexes occur with no significant shifts compared to the spectra of their ligands. The d-d transitions are detectable only for complex CuC12, thus pointing out a greater distortion of the C_s symmetry for this complex. Conversely, a square planar symmetry may be assumed for the complexes CuC6, as stated by Laporte rule. Accordingly, *d-d* transitions are very weak and hence difficult to be identified. Similar to what observed for gold(III)-based compounds, a little shoulder occurs at about 321.2 nm for all complexes and can be attributed to an intraligand $\pi^* \leftarrow n$ transition, where *n* stands for the in-plane non-bonding sulfur orbitals.[35]

ESI-MS Characterization

ESI-MS analyses have been carried out for both complexes whose data are reported below. ESI-MS spectrum of complex CuC6 is shown in **Figure 11.22** as an example.

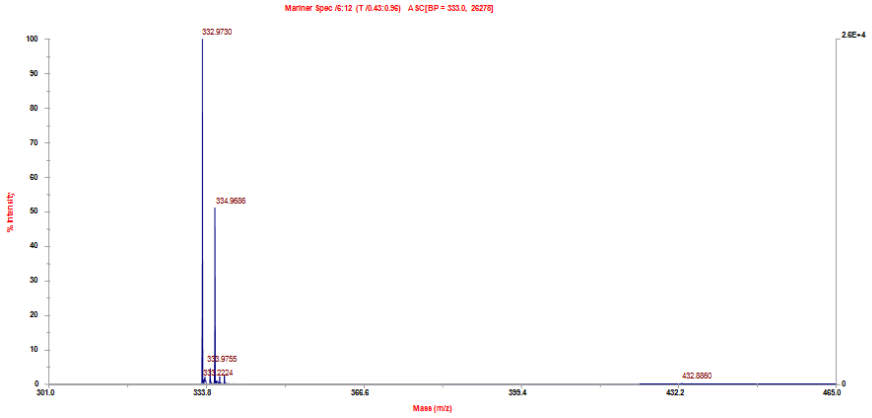

Figure 11.22. ESI-MS spectrum of complex CuC6 in methanol with 1% of formic acid.

The spectrum presents a base peak at 332.97 m/z with the corresponding isotopic peak at 334.96 m/z, attributed to the species $[Cu(I)\{DMDTM\}_2]^+$, Likewise, the ESI-MS spectrum of the complex CuC12 shows the base peak at 385.00 m/z ($[Cu(I)\{PyDTM\}_2]^+$), with the typical isotopic pattern. Other fragmentation peaks are insignificant in intensity.

It should be noted that for each spectrum the base peak is represented by the ion $[Cu(I)(DTCM)_2]^+$ in which the original Cu(II) center is reduced to Cu(I) and another DTCM ligand replaced the chlorides ions. Hence, for these derivatives the peculiar copper(II) tendency to reduce in the ESI-MS experimental conditions[52] overcomes the dithiocarbamate capability of stabilizing high oxidation states. Compared to the first class of herein studied

compounds, this behavior can be traced back to either the methylation of the chelating ligand or to the presence of the two chloride ions.

Biological evaluation

The synthesized copper(II) complexes were tested to investigate their ability to induce cell death in human tumor cell lines. Preliminary studies were carried out using human uterus cervix cancer cells (HeLa cell line). In order to examine the growth-inhibitory effects of tested compounds, cells were incubated for 24 h and 72 h at different concentrations of copper complexes. Three of the investigated complexes induced considerable cell death and the results are reported as IC_{50} values in **Table 11.7**. The other complex has shown a IC_{50} value higher than 20 μM and is not reported in the table.

Table 11.7. Antiproliferative activity of CuC2, CuC5 and CuC12 complexes. IC_{50} data are calculated as average value of at least three experiments ± S.D.

Compound	IC_{50} values (μM)	
	24 h	72 h
CuC2	0.33 ± 0.03	0.7 ± 0.2
CuC5	3.5 ± 0.6	5 ± 1
CuC12	1.9 ± 0.9	1.5 ± 0.7
cisPt	7 ± 5	1.5 ± 0.6

It is worth noting that the evaluated IC_{50} values are comparable or lower than that obtained for the reference drug after 72 h incubation. Interestingly, the latter shows an IC_{50} value at least two fold higher compared to our compounds after 24h incubation, thus leading us to hypothesize a different mechanism of action for our complexes. Interestingly, IC_{50} values of CuC2 and CuC5 increase with incubation time, contrary to CuC12 and cisplatin. Furthermore, the substitution of an ethanolic chain (CuC5) with a methyl group (CuC2) determined a significant improvement in the antiproliferative activity. Hence, it may be inferred that a greater hydrophilicity is a limiting factor to the biological activity of our copper compounds.

HeLa cells were treated also with the ligand PyDTM alone in order to confirm that the proliferation-inhibitory effect of CuC12 is due to the coordination at the metal center. No anticancer activity was observed when treating with the ligand at concentrations comparable with those used for CuC12. In fact, PyDTM showed an IC_{50} value of about 40 μM after 72 h treatment. The same experiments performed with DMDTM resulted in a complete inactivity of the ligand.

Regarding the second class of compounds (CuC6 and CuC12), similarly to cisplatin, we designed two hydrolysable groups since, from the bioinorganic chemistry point of view, labile sites at the metal center usually result necessary for prodrugs to trigger their

antiproliferative action. Unexpectedly, complexes with two dithiocarbamato ligands (first category, namely CuC2 and CuC5) proved to be active as well, despite the presence of more stable bonds (*i.e.*, Cu-S), thus leading us to hypothesize a metabolic activation in the cell environment. An *in situ* change in the chemical structure of the parent compound could account for the observed biological activity.

UV-Vis kinetic studies in culture medium

Stability studies on the biologically active complexes (**Figure 11.23**) have been carried out in culture medium to gain insight into the behavior of these compounds in a physiological-like milieu.

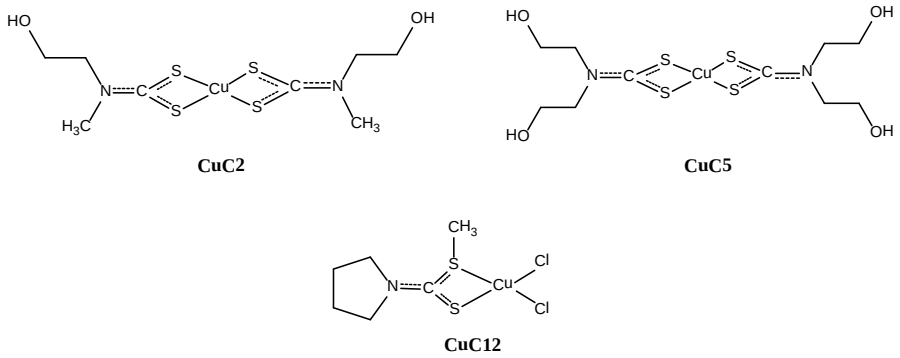

Figure 11.23. Biologically active complexes.

In this regard, the UV-Vis spectra have been acquired at 37 °C over 24 h in order to better simulate the physiological environment. For comparison purpose, data of the kinetic experiments in DMSO (used as a reference solvent) are presented as well. Moreover, data were collected also in saline solution, since it represents a middle way between the reference solvent and the culture medium.

Before recording any electronic spectrum in aqueous medium, each sample was freshly prepared by predissolution of the compound in the minimal amount of DMSO, followed by proper dilution with saline solution or culture medium to yield the required concentration.

The spectra of the complexes CuC5 and CuC12 in the three different media are shown in **Figure 11.24.** Complex CuC5 was chosen as a model for both complex CuC2 and CuC5, being their spectra and their behavior with time nearly identical, owing to their similarity.

In the tables below we report, for each compound, the absorption bands of UV-Vis spectra in the three media at time 0 and after 24 h.

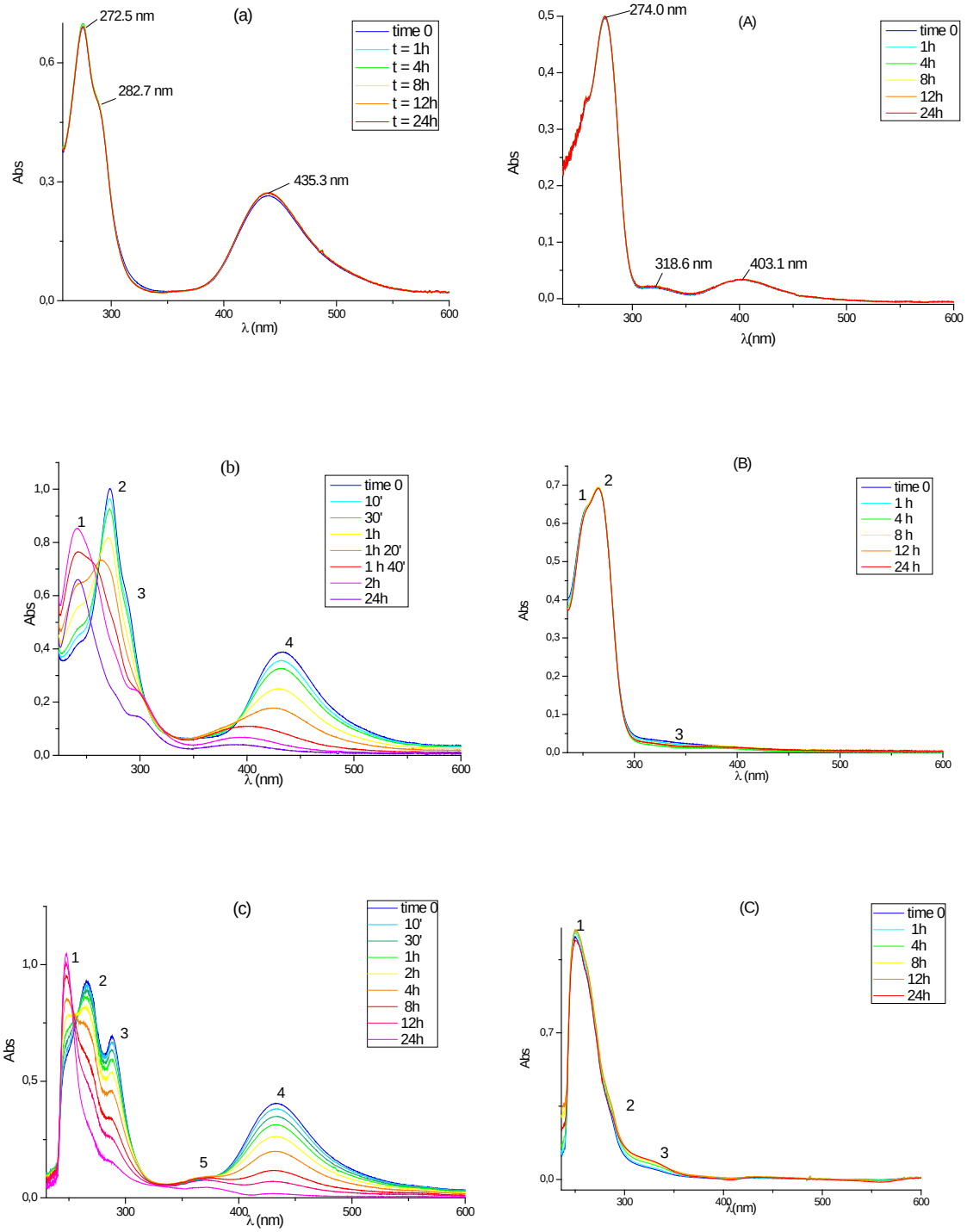

Figure 11.24. UV-Vis kinetic studies of complex CuC5 (left panel) and complex CuC12 (right panel), carried out in DMSO (a, 25 μM; A, 50 μM), Saline solution 50 μM (b, B), in Culture Medium 100μM (c, C).

Table 11.8. Selected UV-Vis bands in DMSO.

Complex	DMSO λ_{max} /nm (log ε)					
	t = 0 h			t = 24 h		
	$\pi^* \leftarrow \pi$ (N-C-S)	$\pi^* \leftarrow \pi$ (S-C-S)	d-d transitions	$\pi^* \leftarrow \pi$ (S-C-S)	$\pi^* \leftarrow \pi$ (N-C-S)	d-d transitions
CuC2	272.5 (4.80)	282.7[(a)] (4.76)	435.3 (4.01)	273.0 (4.76)	281.5[(a)] (4.72)	434.2 (3.95)
CuC5	274.7 (4.45)	286.7[(a)] (4.32)	440.3 (4.01)	274.8 (4.44)	286.8 (4.31)	439.7 (4.04)
CuC12[(b)]	256.6 (3.85)	274.0 (4.00)	403.1 (2.82)	256.6 (3.85)	274.0 (4.00)	403.1 (2.82)

[(a)] shoulder; [(b)] complex CuC12 shows also a shoulder of little intensity at about 318 nm ascribed to π*←n transitions.

Table 11.9. Selected UV-Vis bands in saline solution.

Complex	Saline solution λ_{max} /nm (log ε)							
	t = 0 h				t = 24 h			
	1	**2**	**3**	**4**	**1**	**2**	**3**	**4**
CuC2	240.3[(a)] (4.08)	267.8 (4.49)	282.7 (4.26)	430.8 (4.08)	244.1 (4.22)	259.8 (4.24)	295.2 (3.61)	395.9 (3.47)
CuC5	243.5[(a)] (4.01)	272.2 (4.40)	286.9 (4.19)	433.8 (3.99)	241.3 (4.22)	276.3[(a)] (3.76)	296.6 (3.57)	394.1 (3.00)
CuC12	252.1 (4.10)	264.8 (4.14)	326.3[(a)] (2.79)		252.3 (4.10)	264.8 (4.14)	326.3[(a)] (2.66)	

[(a)] shoulder.

Table 11.10. Selected UV-Vis bands in cell culture medium.

Complex	Culture medium λ_{max} /nm (log ε)								
	t = 0 h				t = 24 h				
	1	**2**	**3**	**4**	**1**	**2**	**3**	**4**	**5**
CuC2	247.3[(a)] (3.70)	263.7 (3.85)	287. (3.67)	432.5 (3.46)	246.6 (3.87)	265.7[(a)] (3.37)	288.7 (3.18)	432.3 (2.52)	369.9[(a)] (2.72)
CuC5	246.5[(a)] (3.78)	266.8 (3.97)	288.4 (3.84)	432.3 (3.61)	247.6 (4.02)	267.7[(a)] (3.48)	286.9 (3.19)	432.2 (2.27)	368.2 (2.65)
CuC12	250.2 (4.06)	285.5[(a)] (3.53)	330.5[(a)] (2.68)		249.9 (4.06)	285.5[(a)] (3.53)	330.5[(a)] (2.93)		-

[(a)] shoulder.

Complex CuC12 proved to be quite stable in the three different media, being band maxima and molar extinction coefficients very similar throughout 24 hours. The shoulder at about 318 nm showed a red shift under physiological conditions (saline solution and culture medium), with respect to the spectrum in DMSO. Moreover, on passing from the reference solvent to the aqueous solutions, the d-d band at 430 nm disappeared. Bands 1 and 2 in saline solution are ascribable to $\pi^* \leftarrow \pi$ transitions located in N-CSS and S-C-S moiety, respectively and show a blue shift with respect to the spectrum in DMSO. Concerning the culture medium, the spectra show a broad band at around 250 nm, that changes intensity over time. This band could be assigned to both N-CSS and S-C-S $\pi^* \leftarrow \pi$ transitions. Band 3 also changes its intensity during 24 hours and may be ascribed to $\pi^* \leftarrow n$ transition in sulfur atoms. Overall the spectra of complex CuC12 show little interaction with culture medium.

The bischelate complexes CuC2 and CuC5, resulted stable in DMSO, instead they show a dramatic evolution with time (in the maxima and in the intensities) both in saline solution and in culture medium. In the case of saline solution, this change is completed within few hours, after which the absorbance slowly decreases with no further modification of band maxima, thus pointing out the formation of new species which progressively precipitate. This behavior in aqueous medium is likely due to the presence of the hydroxyl groups. In fact, similar bischelate complexes as for example $[Cu(DMDT)_2]$, proved to be stable in culture medium (data not shown).

Based on these considerations, the instability of both the complexes in the two aqueous media may account for the experimental observations, namely the IC_{50} values of such complexes are greater after 72 h incubation than after 24 h. Therefore, we hypothesized that the new species is less active than the parent compounds or not active at all. To test this hypothesis, we set up an *ad hoc* experiment. We placed the two complexes (dissolved in culture medium) in the incubator at 37 °C for 24 hours under controlled atmosphere prior to treating tumor cells. Then, we observed more viable cells compared to treating soon after sample preparation, thus highlighting that the parent compound is not a prodrug and the second species displays lower antiproliferative activity. Furthermore, CuC2 and CuC5 triggered cell death quite fast as detached cells were observed after a few hours of treatment. Characterization of the newly formed species is ongoing and will allow us to fully assign the new bands.

11.3.6. Appendix

A summary of X-ray crystallographic data is presented in the table below.

	CuC5	**M.L. CuC6**	**PyDTM**
Empirical formula	$C_{10}H_{20}CuN_2O_4S$	$C_8H_{18}Cl_4Cu_3N_2S$	$C_6H_{11}NS_2$
Formula weight	424.06	602.90	161.28
Colour, habit	Green, block	Black, block	Colorless, plate
Crystal size, mm	0.22x0.18x0.13	0.18x0.11x0.09	0.44x0.40x0.07
Crystal system	Triclinic	Triclinic	Monoclinic
Space group	*P*-1	*P*-1	$P2_1/n$
a, Å	7.855(3)	7.874(1)	9.481(2)
b, Å	9.765(4)	8.105(1)	8.204(1)
c, Å	11.954(4)	8.782(1)	11.875(2)
α, deg.	83.081(6)	71.549(2)	90
β, deg.	81.566(6)	86.489(2)	109.792(2)
γ, deg.	69.696(5)	64.881(2)	90
V, $Å^3$	848.3(6)	479.6(1)	869.1(3)
Z	2	1	4
T, K	293(2)	293(2)	293(2)
ρ (calc), Mg/m^3	1.660	2.087	1.233
μ, mm^{-1}	1.793	4.279	0.534
θ range, deg.	1.73 to 26.63	2.45 to 26.72	2.39 to 25.49
No.of reflns / unique	10285 / 3551	5843 / 2028	3848 / 1564
GooF	1.089	1.001	1.040
*R*1	0.0647	0.0391	0.0426
*wR*2	0.1922	0.0806	0.1132

ML CuC6/ CuC12 = crystal precipitated from mother liquors of complex CuC6/ CuC12

$R1 = \Sigma||F_O|-|F_C||/\Sigma|F_O|$, $wR2 = [\Sigma[w(F_O^2-F_C^2)^2]/\Sigma[w(F_O^2)^2]]^{½}$, $w = 1/[\sigma^2(F_O^2) + (aP)^2 + bP]$, where $P = [\max(F_O^2,0) + 2F_C^2]/3$

Selected bond lengths (Å) and angles (°) for the obtained crystal structures are presented in the subsequent table [’ = -x; -y; -z, ¥ = 1-x; 1-y; 2-z, ¥¥ = 1-x; 1-y; 1-z, § = 1-x; -y; 1-z, §§ = -x; 1-y; 1-z].

CuC5			
Cu-S(11)	2.316(2)	S(12)-Cu-S(22)	76.57(5)
Cu-(S21)	2.310(2)	S(11)-Cu-S(12)	102.07(6)
Cu-S(12)	2.325(2)	S(21)-Cu-S(22)	100.21(5)
Cu-S(22)	2.337(2)	S(21)-Cu-S(22)’	98.87(6)
Cu-S(22)’	2.773(2)	S(11)-Cu-S(22)’	102.80(6)
Cu-Cu’	3.461(1)	S(12)-Cu-S(22)’	94.69(6)
S(11)-Cu-S(21)	76.69(5)	S(22)-Cu-S(22)’	95.17(5)
M.L. CuC6			
Cu(1)-S(1)	2.271(1)	S(1)-Cu(1)-S(1)¥¥	113.47(4)
Cu(1)-S(1)¥¥	2.452(1)	S(1)-Cu(1)-Cl(1)	103.01(5)
Cu(1)-Cl(1)	2.417(1)	S(1)-Cu(1)-Cl(2)¥	132.15(6)
Cu(1)-Cl(2)¥	2.324(2)	Cl(1)-Cu(1)-S(1)¥¥	110.55(5)
Cu(2)-Cl(1)	2.278(1)	Cl(1)-Cu(1)-Cl(2)¥	85.92(5)
Cu(2)-Cl(2)	2.297(2)	S(1)’’-Cu(1)Cl(2)¥	106.49(5)
Cu(1)-Cu(1)¥¥	2.595(1)	Cl(1)-Cu(2)-Cl(2)	90.14(4)
Cu(1)-Cu(2)	3.230(1)	Cl(1)-Cu(2)-Cl(2)¥	89.86(4)
CuC12			
Cu(1)-S(11)	2.312(1)	S(12)§-Cu(1)-Cl(3)	119.70(3)
Cu(1)-Cl(1)	2.4142(8)	S(11)-Cu(1)-Cl(3)	115.13(3)
Cu(1)-Cl(3)	2.4333(9)	Cl(1)-Cu(1)-Cl(3)	83.82(3)
Cu(1)-S(12)§	2.2964(9)	S(12)§-Cu(1)-Cl(1)	113.95(3)
Cu(2)-Cl(1)	2.2568(8)	Cl(1)-Cu(2)-Cl(3)	91.39(3)
Cu(2)-Cl(2)	2.3239(8)	Cl(1)-Cu(2)-Cl(2)	91.53(3)
Cu(2)-Cl(2)§§	2.2954(8)	Cl(2)§-Cu(2)-Cl(2)	83.84(3)
Cu(2)-Cl(3)	2.2678(8)	Cl(1)-Cu(2)-O(12)	93.26(5)
Cu(2)-O(12)	2.417(2)	Cl(3)-Cu(2)-O(12)	93.32(5)
Cu(1)-Cu(2)	3.3466(6)	Cl(2)§§-Cu(2)-O(12)	94.85(5)
Cu(2)-Cu(2)§§	3.4372(6)	Cl(2)-Cu(2)-O(12)	93.82(5)
		Cl(3)-Cu(2)-Cl(2)§§	92.23(3)
S(12)§-Cu(1)-S(11)	108.76(3)	S(11)-Cu(1)-Cl(1)	113.71(3)
PyDTM			
C(1)-S(1)	1.745(2)	S(1)-C(1)-S(2)	125.0(1)
C(1)-S(2)	1.791(2)	C(1)-S(2)-C(2)	101.6(1)
C(1)-N(1)	1.331(3)	S(1)-C(1)-N(1)	124.6(2)
S(2)-C(2)	1.821(2)	S(2)-C(1)-N(1)	110.4(2)

Chapter 11 references

(1) Bertini, I.; Rosato, A. Menkes Disease. *Cell Mol. Life Sci.* **2008**, *65*, 89-91.

(2) Shyamal, D. K.; Ray, K. Wilson's Disease: An Update. *Nat. Clin. Pract. Neurol.* **2006**, *2*, 482-493.

(3) Gaggelli, E.; Kozlowski, H.; Valensin, D.; Valensin, G. Copper Homeostasis and Neurodegenerative Disorders (Alzheimer's, Prion, and Parkinson's Diseases and Amyotrophic Lateral Sclerosis). *Chem. Rev.* **2006**, *106*, 1995-2044.

(4) McAuslan, B. R.; Reilly, W. Endothelial Cell Phagokinesis in Response to Specific Metal Ions. *Exp. Cell Res.* **1980**, *130*, 147-157.

(5) Sen, C. K.; Khanna, S.; Venojarvi, M.; Trikha, P.; Christopher Ellison, E.; Hunt, T. K.; Roy, S. Copper-Induced Vascular Endothelial Growth Factor Expression and Wound Healing. *Am. J. Physiol. Heart Circ. Physiol.* **2002**, *282*, H1821-H1827.

(6) Nasulewicz, A.; Mazur, A.; Opolski, A. Role of Copper in Tumour Angiogenesis - Clinical Implications. *J. Trace Elem. Med. Biol.* **2004**, *18*, 1-8.

(7) Moriguchi, M.; Nakajima, T.; Kimura, H.; Watanabe, T.; Takashima, H.; Mitsumoto, Y.; Katagishi, T.; Okanoue, T.; Kagawa, K. The Copper Chelator Trientine has an Antiangiogenic Effect Against Hepatocellular Carcinoma, Possibly through Inhibition of Interleukin-8 Production. *Int. J. Cancer* **2002**, *102*, 445-452.

(8) Soncin, F.; Guitton, J. -.; Cartwright, T.; Badet, J. Interaction of Human Angiogenin with Copper Modulates Angiogenin Binding to Endothelial Cells. *Biochem. Biophys. Res. Commun.* **1997**, *236*, 604-610.

(9) Hu, G. -. Copper Stimulates Proliferation of Human Endothelial Cells Under Culture. *J. Cell. Biochem.* **1998**, *69*, 326-335.

(10) Linder, M. C.; Hazegh-Azam, M. Copper Biochemistry and Molecular Biology. *Am. J. Clin. Nutr.* **1996**, *63*, 797S-811S.

(11) Apelgot, S.; Coppey, J.; Fromentin, A.; Guille, E.; Poupon, M. F.; Roussel, A. Altered Distribution of Copper (64Cu) in Tumor-Bearing Mice and Rats. *Anticancer Res.* **1986**, *6*, 159-164.

(12) Coates, R. J.; Weiss, N. S.; Daling, J. R.; Rettmer, R. L.; Warnick, G. R. Cancer Risk in Relation to Serum Copper Levels. *Cancer Res.* **1989**, *49*, 4353-4356.

(13) Gupta, S. K.; Shukla, V. K.; Vaidya, M. P.; Roy, S. K.; Gupta, S. Serum Trace Elements and Cu/Zn Ratio in Breast Cancer Patients. *J. Surg. Oncol.* **1991**, *46*, 178-181.

(14) Gupta, S. K.; Shukla, V. K.; Vaidya, M. P.; Roy, S. K.; Gupta, S. Serum and Tissue Trace Elements in Colorectal Cancer. *J. Surg. Oncol.* **1993**, *52*, 172-175.

(15) Diez, M.; Cerdan, F. J.; Arroyo, M.; Balibrea, J. L. Use of the Copper/Zinc Ratio in the Diagnosis of Lung Cancer. *Cancer* **1989**, *63*, 726-730.

(16) Yoshida, D.; Ikeda, Y.; Nakazawa, S. Quantitative Analysis of Copper, Zinc and Copper/Zinc Ratio in Selected Human Brain Tumors. *J. NEURO-ONCOL.* **1993**, *16*, 109-115.

(17) Chen, D.; Cui, Q. C.; Yang, H.; Dou, Q. P. Disulfiram, a Clinically used Anti-Alcoholism Drug and Copper-Binding Agent, Induces Apoptotic Cell Death in Breast Cancer Cultures and Xenografts Via Inhibition of the Proteasome Activity. *Cancer Res.* **2006**, *66*, 10425-10433.

(18) Daniel, K. G.; Chen, D.; Orlu, S.; Cui, Q. C.; Miller, F. R.; Dou, Q. P. Clioquinol and Pyrrolidine Dithiocarbamate Complex with Copper to Form Proteasome Inhibitors and Apoptosis Inducers in Human Breast Cancer Cells. *Breast Cancer Res.* **2005**, *7*, R897-R908.

(19) Sigman, D. S.; Graham, D. R.; D'Aurora, V.; Stern, A. M. Oxygen-Dependent Cleavage of DNA by the 1,10-Phenanthroline-Cuprous Complex. Inhibition of E. Coli DNA Polymerase I. *J. Biol. Chem.* **1979**, *254*, 12269-12272.

(20) Tamura, H.; Imai, H.; Kuwahara, J.; Sugiura, Y. A New Antitumor Complex: Bis(Acetato)Bis(Imidazole)Copper(II). *J. Am. Chem. Soc.* **1987**, *109*, 6870-6871.

(21) Berners-Price, S. J.; Sadler, P. J. Phosphines and Metal Phosphine Complexes: Relationship of Chemistry to Anticancer and Other Biological Activity. *Struct. Bonding (Berlin)* **1988**, *70*, 27-102.

(22) Giovagnini, L.; Sitran, S.; Montopoli, M.; Caparrotta, L.; Corsini, M.; Rosani, C.; Zanello, P.; Dou, Q. P.; Fregona, D. Chemical and Biological Profiles of Novel Copper(II) Complexes Containing S-Donor Ligands for the Treatment of Cancer. *Inorg. Chem.* **2008**, *47*, 6336-6343.

(23) Márta, E.; Ronconi, L.; Nardon, C.; Fregona, D. Noble Metal-Dithiocarbamates Precious Allies in the Fight Against Cancer. *Mini-Reviews in Medicinal Chemistry* **2012**, *12*, 1216-1229.

(24) Herlinger, A. W.; Wenhold, S. L.; Long II, T. V. Infrared Spectra of Amino Acids and their Metal Complexes. II. Geometrical Isomerism in Bis(Amino Acidato) Copper (II) Complexes. *J. Am. Chem. Soc.* **1970**, *92*, 6474-6481.

(25) Chatt, J.; Duncanson, L. A.; Venanzi, L. M. Dithiocarbamates, Infrared Spectra and Structure. *Suom. Kemistil. B* **1956**, *29B*, 75-84.

(26) Brown, D. A.; Glass, W. K.; Burke, M. A. The General use of i.R. Spectral Criteria in Discussions of the Bonding and Structure of Metal Dithiocarbamates. *Spectrochim. Acta Part A Mol. Spectrosc.* **1976**, *32*, 145-147.

(27) Castillo, M.; Criado, J. J.; Macias, B.; Vaquero, M. V. Chemistry of Dithiocarbamate Derivatives of Amino Acids. I. Study of some Dithiocarbamate Derivatives of Linear A-Amino Acids and their Nickel(II) Complexes. *Inorg. Chim. Acta* **1986**, *124*, 127-132.

(28) Ito, H.; Fujita, J.; Saito, K. Absorption Spectra and Circular Dichroisms of Metal Complexes. I. Platinum(II)-, Palladium(II)- and Gold(III)- Complexes Containing Optically Active Diamines. *Bull. Chem. Soc. Jap.* **1967**, *40*, 2584-2591.

(29) Ronconi, L.; Giovagnini, L.; Marzano, C.; Bettìo, F.; Graziani, R.; Pilloni, G.; Fregona, D. Gold Dithiocarbamate Derivatives as Potential Antineoplastic Agents: Design, Spectroscopic Properties, and in Vitro Antitumor Activity. *Inorg. Chem.* **2005**, *44*, 1867-1881.

(30) Bonati, F.; Ugo, R. Organotin(IV) N,N-Disubstituted Dithiocarbamates. *J. Organomet. Chem.* **1967**, *10*, 257-268.

(31) Kellner, R.; Nikolov, G.; Trendafilova, N. Detecting the Bonding Type of Dithiocarbamate Ligands in their Complexes as Inferred from the Asymmetric Thiocarbonyl Mode. *Inorg. Chim. Acta* **1984**, *84*, 233-239.

(32) Srivastava, T. N.; Kumar, V. Some Triorganotin(IV) Dithiocarbamates. *J. Organomet. Chem.* **1976**, *107*, 55-61.

(33) Choi, S. -.; Menzel, E. R.; Wasson, J. R. Electronic Spectra of Copper(II) Dithiocarbamates. *Journal of Inorganic and Nuclear Chemistry* **1977**, *39*, 417-422.

(34) Faraglia, G.; Sitran, S.; Montagner, D. Pyrrolidine Dithiocarbamates of Pd(II). *Inorg. Chim. Acta* **2005**, *358*, 971-980.

(35) Lee, A. W. M.; Chan, W. H.; Ho, M. F. Ultraviolet Spectrophotometric Determination of Amino Acids by Formation of Dithiocarbamates. *Anal. Chim. Acta* **1991**, *246*, 443-445.

(36) Janssen, M. J. Physical Properties of Organic Thiones. I. Electronic Absorption Spectra of Nitrogen-Containing Thione Compounds. *Recl. Trav. Chim. Pays-Bas Belg.* **1960**, *79*, 454-463.

(37) Rastrelli, F.; Bagno, A. Predicting the NMR Spectra of Paramagnetic Molecules by DFT: Application to Organic Free Radicals and Transition-Metal Complexes. *Chem. --Eur. J.* **2009**, *15*, 7990-8004, S7990/1-S7990/25.

(38) Van Gaal, H. L. M.; Diesveld, J. W.; Pijpers, F. W.; Van Der Linden, J. G. M. 13C NMR Spectra of Dithiocarbamates. Chemical Shifts, Carbon-Nitrogen Stretching Vibration Frequencies, and Π Bonding in the NCS2 Fragment. *Inorg. Chem.* **1979**, *18*, 3251-3260.

(39) Gianelli, L.; Amendola, V.; Fabbrizzi, L.; Pallavicini, P.; Mellerio, G. G. Investigation of Reduction of Cu(II) Complexes in Positive-Ion Mode Electrospray Mass Spectrometry. *Rapid Commun. Mass Spectrom.* **2001**, *15*, 2347-2353.

(40) Schoener, D. F.; Olsen, M. A.; Cummings, P. G.; Basic, C. Electrospray Ionization of Neutral Metal Dithiocarbamate Complexes using in-Source Oxidation. *J. Mass Spectrom.* **1999**, *34*, 1069-1078.

(41) Ainley, A. D.; Davies, W. H.; Gudgeon, H.; Harland, J. C.; Sexton, W. A. The Constitution of the so-Called Carbothialdines and the Preparation of some Homologous Compounds. *Journal of the Chemical Society (Resumed)* **1944**, 147-152.

(42) Giovagnini, L.; Mancinetti, E.; Ronconi, L.; Sitran, S.; Marchiò, L.; Castagliuolo, I.; Brun, P.; Trevisan, A.; Fregona, D. Preliminary Chemico-Biological Studies on Ru(III) Compounds with S-Methyl Pyrrolidine/Dimethyl Dithiocarbamate. *J. Inorg. Biochem.* **2009**, *103*, 774-782.

(43) Faraglia, G.; Sitran, S.; Montagner, D. Pyrrolidine Dithiocarbamates of Pd(II). *Inorg. Chim. Acta* **2005**, *358*, 971-980.

(44) De Lima, G. M.; Menezes, D. C.; Cavalcanti, C. A.; Dos Santos, J. A. F.; Ferreira, I. P.; Paniago, E. B.; Wardell, J. L.; Wardell, S. M. S. V.; Krambrock, K.; Mendes, I. C.; Beraldo, H. Synthesis, Characterisation and Biological Aspects of Copper(II) Dithiocarbamate Complexes, [Cu{S 2CNR(CH 2CH 2OH)} 2], (R = Me, Et, Pr and CH 2CH 2OH). *J. Mol. Struct.* **2011**, *988*, 1-8.

(45) Pyykkö, P. Strong Closed-Shell Interactions in Inorganic Chemistry. *Chem. Rev.* **1997**, *97*, 597-636.

(46) Sculfort, S.; Braunstein, P. Intramolecular D 10-D 10 Interactions in Heterometallic Clusters of the Transition Metals. *Chem. Soc. Rev.* **2011**, *40*, 2741-2760.

(47) Radha, A.; Seshasayee, M.; Radha, K.; Aravamudan, G.; Subramanyam, C. Structure of Bis[N,N-Bis(2-Hydroxyethyl)Dithiocarbamato]Copper(II), [Cu(C5H10NO2S2)2]. *Acta Crystallogr. , Sect. C: Cryst. Struct. Commun.* **1985**, *C41*, 1166-1169.

(48) Ronconi, L.; Giovagnini, L.; Marzano, C.; Bettìo, F.; Graziani, R.; Pilloni, G.; Fregona, D. Gold Dithiocarbamate Derivatives as Potential Antineoplastic Agents: Design, Spectroscopic Properties, and in Vitro Antitumor Activity. *Inorg. Chem.* **2005**, *44*, 1867-1881.

(49) Faraglia, G.; Fregona, D.; Sitran, S.; Giovagnini, L.; Marzano, C.; Baccichetti, F.; Casellato, U.; Graziani, R. Platinum(II) and Palladium(II) Complexes with Dithiocarbamates and Amines: Synthesis, Characterization and Cell Assay. *J. Inorg. Biochem.* **2001**, *83*, 31-40.

(50) K. Nakamoto, *Infrared and Raman Spectra of inorganic and Coordination compound*, 4th Ed, John Wiley & sons, 1986.

(51) C. E. G. Houscroft and A. Sharp, *Inorganic Chemistry*, 3rd Ed. Pearson education limited, 2008.

(52) W. Henderson and J. S. MCIndoe, *Mass Spectrometry of Inorganic, Coordination and Organometallic Compounds*, John Wiley and Sons, 2005.

(53) R. M. Silverstein, F. X. Webster and D. J. Kiemle, Spectrometric Identification of Organic Compounds, 7th edition, John Wiley & Sons, 2005.

(54) P. Drozdzewski and E. Kordon, *Spectrochimica Acta Part A* , **2000**, 56, 1299-1304.

Final remarks

In the field of anticancer chemotherapy, the research has been increasingly addressing its endeavors to the development of novel therapies that should enhance the therapeutic efficacy of drugs while reducing their side-toxicity. To date, within the targeted therapy, thanks to a deeper understanding of the biologic basis of cancer, two strategies are pursued, namely the cellularly targeted therapy and the molecularly targeted therapy.

In this work, we have focused on the first approach in order to selectively deliver our complexes into cancerous cells and minimize the damage to healthy ones. First, we identified some membrane receptors and transporters up-regulated in some human cancers. Second, we designed new coordination compounds with the related cell-specific ligands as targeting moieties for a site-specific delivery, leading to three distinct classes of Au(III)-based compounds.

Among the peptidomimetics, based on preliminary cell-line screens, we selected the complexes AuD6 and AuD8, which differ only in the substituents at the α–carbon atom at the *C*-terminus, for further pharmacological testing. Several advanced preclinical studies were performed taking into account those required to enter phase I clinical trials. In particular, the acute toxicity on animal models and the anticancer activity (both *in vitro* and *in vivo*) were investigated. Experimental evidences allow us to assess that the median lethal dose (LD_{50}) of AuD8 is higher than 15 mg/kg or 60 mg/kg body weight when administered intravenously or orally, respectively (both males and females). These data are very encouraging as the chemotherapy with AuD8 on nude mice was performed at 1 or 2 mg/kg body weight (s.c.). Overall, mice appeared healthy and very active, and did not display signs of fatigue, weight loss or anorexia when treated with AuD6 or AuD8. Remarkably, both complexes overcame the known cisplatin resistance in MDA-MB-231 cells, finding out the proteasome as an intracellular target. Based on this result, the elucidation of the mechanism of inhibition of such protease at the atomic level was pursued by X-ray crystallography. Thus, regarding the steps of yeast cell growth, protein extraction and purification, a protocol has been progressively defined. The pure proteasome was successfully crystallized and analyzed by X-Ray diffraction, turning out a maximum resolution of 2.7 Å. Conversely, the crystallization of the enzyme along with the inhibitor AuD8 was attempted plenty of times, without yielding diffraction quality crystals so far.

In this work another biomolecule has been considered, that is the serum albumin, finding out that AuD8 weakly interacts with it.

In light of the remarkable biological results collected in this work, further pharmacological studies are warranted including investigation in metabolic cages of the chronic toxicity in animals (monitoring biochemical markers both in urine and blood after multiple administrations) and some pharmacokinetic aspects such as adsorption, distribution, metabolism and clearance. Intriguingly, some transcriptomic studies are ongoing to comprehensively characterize tumor response to our drug (AuD8 as a model). As described in the introduction, neoplastic cells display different patterns of gene expression compared to normal ones. Thus, by collecting transcriptomes (small percentage of the genetic code that is transcribed into RNA molecules) and comparing them by data-driven algorithms before and after treatment with AuD8, it will possible to get a global view of the resulting changes in the intracellular networks upon drug perturbation. In other words, this investigation should yield a deep mechanistic understanding of what biochemical pathways, crosstalks and feedbacks are affected by our compound, considering the treatment as an exogenous stimulus. Preliminary data have shown that AuD8 triggers cell death very quickly by a non-cisplatin-like mechanism of action (with no DNA involvement). Additionally, some studies will be carried out to check whether our compounds actually cross the cell membrane by internalization mechanisms mediated by the transporters PEPT using ^{14}C-peptides.

The second type of herein-considered gold-based anticancer agents exploited the CCK8 peptide targeting the cholecystokinin receptors. While designing the peptide sequence, particular attention was paid on the possible side-chain protecting groups. Hence, two tests were carried out to mimic the harsh conditions typically requested to remove the protecting groups, resulting in the stability of the Au-S bond only under acidic conditions. Hence, CCK8 was synthesized according to the Sheppard's strategy, using amino acid residues with *t*Bu-type-protecting groups, and then widely characterized. The corresponding gold-based complex was synthetized and its complete characterization is ongoing. The biological activity will be tested *in vitro* on CCK8 receptor-positive and -negative human cancer cell lines.

The careful initial design of the gold-containing building block and the mild conditions adopted in the "click" reaction proved to be successful in yielding the molecule Au^{III}-spacer-model tetrapeptide. An international patent application is going to be filed with respect to this versatile synthesis approach. Based on the general applicability of this strategy, we have been identifying other membrane receptors up-regulated in some human

malignancies to be used as suitable targets for cancer-specific drug delivery. Then, new coordination compounds will be designed with these receptor-related ligands, resulting in the third generation of our dithiocarbamato complexes, which will be biologically studied to test their anticancer activity and their selectivity.

Concerning the new copper complexes, the results discussed above will be useful in the future when designing and synthetizing copper-containing receptor compounds. In fact, copper complexes targeting up-regulated receptors are more difficult to obtain than the gold-based counterparts owing to the borderline Lewis acid character of the Cu(II) metal center. The syntheses of Cu(II) peptidomimetics and the CCK8 derivative will be pursued. Likewise, the click strategy will be attempted as well. Additional biological studies will be carried out, both *in vitro* and *in vivo,* on the herein-reported complexes CuC2, CuC5, Cuc6 and CuC12.

Acknowledgements

"Ma chi te l'ha fatto fare??!!??".... ecco, questa è una voce che ho sentito spesso dentro di me in questi 3 anni di Dottorato.. 3 anni lunghi dal punto di vista dei numerosi sacrifici psico-fisici fatti ma brevi, brevissimi per i tempi della ricerca. Allora chi me l'ha fatto fare di non aver mai un minuto per me? la risposta è semplice: la PASSIONE per la Ricerca contro il cancro. Sento da anni e sento tuttora che questa è la mia vocazione. Sento che questo è il campo in cui posso dare al massimo il mio contributo scientifico. Ma in questo percorso non sono stata sola: numerose persone mi hanno accompagnata e sostenuta a 360°. Poiché la tesi è già piuttosto lunga cerco di essere breve almeno in questa parte o almeno ci provo...

Innanzitutto Grazie Prof.!! – soltanto così ho sempre chiamato il mio supervisore Prof. Dolores Fregona – semplicemente grazie per essere così diversa dagli altri... ed avermi aperto gli occhi numerose volte sulle questioni più disparate. Grazie anche per aver sempre creduto in me proponendomi di svolgere esperimenti biologici piuttosto delicati e il cui risultato ha per noi un valore immenso. Grazie per il suo appoggio e la sua comprensione dimostratimi tutte le volte (vi assicuro tante!!) in cui le cose non andavano per il verso giusto.

Per restare in tema biologico, ringrazio il Prof. Q.P. Dou per avermi accolta nel suo gruppo di ricerca americano ed avermi dato grande libertà a livello sperimentale così da esprimere le mie idee e applicarle con "gli occhi del chimico". Grazie a tutti gli amici che a Detroit ho conosciuto e hanno reso quei 6 mesi oltreoceano indimenticabili: Sara, Daniela, Jian, Taskeen, Min, George, Rahul, Rany, Carol, Di e Cindy. In questo contesto approfitto per ringraziare anche la Fondazione "Ing. Aldo Gini" che ha sostenuto finanziariamente il mio periodo di ricerca negli U.S.A. e i direttori della Scuola di Dottorato in ordine cronologico Prof. Maurizio Casarin e Prof. Antonino Polimeno per il loro appoggio.

In questi 3 anni mi sono anche cimentata nel campo della cristallografia di proteine e se questo è stato possibile è grazie al Prof. Giuseppe Zanotti (Dip. Scienze Biomediche, Università di Padova). Grazie per il suo interesse nel mio progetto di ricerca e il suo entusiasmo. Un profondo

ringraziamento va alla Dr. Laura Cendron che mi ha sempre seguito con grande passione e disponibilità dall'espressione delle proteine alla loro estrazione, dalla purificazione alla fase di cristallizzazione. Un grazie anche a tutto il gruppo: Sara, Marco, Sandra, Lorenza, Munan, Marco, Ilenia e Paola.

Un altro grazie immenso va al Prof. Fernando Formaggio per la sua infinita disponibilità e per avermi permesso di entrare nel suo gruppo per quanto concerne la sintesi dei peptidi riportati in questa tesi.

Un profondo grazie per la collaborazione ai Prof. D. Carbonera, V. Di Noto, G. Morelli, L. Dalla Via e ai Dr. B. Biondi, M. De Zotti, D. Dalzoppo, A. Accardo, L. Marchiò, L. Toschi, L. Calore, R. Schiesari, I. Menegazzo ed I. Montagner.

Sempre a livello accademico, non posso scordarmi dei miei compagni di avventura di questi 3 anni e del loro aiuto a 360 °: grazie Edoardo, Gloria, Giulia, Federico (ti ho stressato parecchio con la storia degli IR bassi...) ed Arianna. Un grazie di cuore va anche ai "miei" laureandi, alcuni ora già laureati, che mi hanno affiancato, soffrendo insieme per gli ostacoli da superare ma anche gioendo dei piccoli passi fatti in avanti nelle ricerche: Stefano Genesin, Mauro Paolini, Naike Casagrande, Irene Simonato, Ilaria Tezza, Elia Santinon, Cinzia Imberti, Valeria Crosetta, Claudia Bonfio e Leonardo Brustolin. Con tutti voi è nata anche una bella amicizia che spero duri nel tempo!! Più recente è invece l'amicizia con la "new entry" Simone Scintilla... grazie anche a te per il tuo supporto morale, sempre prezioso.

Publications and communications during the PhD studies

CONFERENCE PROCEEDINGS

1. **C. Nardon**, D. Fregona, "Design and development of new metal-based biosensors for the early detection of cancer antigens in oncology", *Proc. From Molecular Structure to Systems Biology-Convegno Nazionale della Divisione di Chimica dei Sistemi Biologici* - S. Vito di Cadore (BL) (Italy), 2010, P-XXII.
2. **C. Nardon**, D. Fregona, "New lanthanide-based biosensors for the early detection of cancer antigens", *Proc. XXXVIII Congresso Nazionale di Chimica Inorganica* - Trieste (Italy), 2010, OC 5.
3. L. Ronconi, G. Boscutti, E. M. Nagy, **C. Nardon**, A. Jirillo, D. Fregona, "From cisplatin to world-shattering gold(III) anticancer agents", *Proc. 1st International Michelangelo Conference: promises and challenges in developing new drugs in oncology*, Fondazione Cariplo, Milano (Italy), 30/6-1/7/2011.
4. G. Boscutti, **C. Nardon**, L. Ronconi, A. Trevisan, F. Formaggio, Q. P. Dou, L. Dalla Via, D. Fregona, "Gold-based peptidomimetics for a targeted anticancer therapy", *Proc. Pharmacobiometallics*, San Benedetto del Tronto, (Italy) 28-30/10/2011.
5. **C. Nardon**, Q. P. Dou, D. Fregona, "In vitro and in vivo anticancer activity of recently patented gold-based peptidomimetics targeting peptide transporters", *Proc. 12th Eurasia Conference on Chemical Sciences*, Dassia, Corfu, Greece, 16-21 April 2012, S2-OP7.
6. **C. Nardon**, L. Ronconi, G. Boscutti, M. Paolini, F. Formaggio and D. Fregona, "Biological studies on Au(III) peptidomimetics about to enter phase I clinical trials", *Proc. 12th Workshop on PharmacoBioMetallics –BIOMET12*, Padova (Italy), 26-28 October 2012-OC11.
7. A. Accardo, **C. Nardon**, G. Boscutti, D. Tesauro, I. Saccone, D. Fregona and G. Morelli, "Selective delivery of chemotherapeutics into tumor cells by use of targeting peptides", *Proc. 12th Workshop on PharmacoBioMetallics –BIOMET12*, Padova (Italy), 26-28 October 2012-OC5.
8. A. Adami, L. Dalla Via, C. Imberti, **C. Nardon**, L. Marchiò, V. Di Noto, and D. Fregona, "A new strategy in chemotherapy: preliminary studies on Cu(II) complexes aimed at exploiting the enhanced copper uptake in malignancies", *Proc. 12th Workshop on PharmacoBioMetallics* – BIOMET12, Padova (Italy), 26-28 October 2012-OC6.

ORAL COMMUNICATIONS

- ✓ *XXXVIII Congresso Nazionale di Chimica Inorganica*, Trieste, 13-16 September 2010
- ✓ *12th Eurasia, International Conference on Chemical Sciences*, Dassia, Corfu, Greece, 16-21 April 2012 (presentation winning an **IUPAC AWARD**)
- ✓ *12th Workshop on PharmacoBioMetallics –BIOMET12*, Padova (Italy), 26-28 October 2012 (Best oral presentation)

PEER-REVIEWED PAPERS

1. E. M. Nagy, **C. Nardon**, L. Giovagnini, L. Marchiò, A. Trevisan and D. Fregona. "Promising Anticancer Mono- and Dinuclear Ruthenium(III) Dithiocarbamato Complexes: Systematic Solution Studies". *Dalton Transactions*, 2011, 40, 11885-11895.

2. M. N. Kouodom, L. Ronconi, M. Celegato, **C. Nardon**, L. Marchiò, Q. P. Dou, D. Aldinucci, F. Formaggio, D. Fregona. "Toward the selective delivery of chemotherapeutics into tumor cells by targeting peptide transporters: tailored gold-based anticancer peptidomimetics". *Journal of Medicinal Chemistry*, 2012, 55, 2212-2226.

3. L. Dalla Via , **C. Nardon**, D. Fregona. "Targeting the proteasome-ubiquitin pathway with inorganic compounds to fight cancer: a challenge for the future". Special issue "Targeted oncology" in *Future Medicinal Chemistry,* 2012, 4 (4), 525-543.

4. E. M. Nagy, L. Ronconi, **C. Nardon**, D. Fregona. "Noble metal-dithiocarbamates precious allies in the fight against cancer", *Mini-Reviews in Medicinal Chemistry,* 2012, 12(12),1216-1229.

5. J. Zuo, C. Bi, Y. Fan, D. Buac, **C. Nardon**, K.G. Daniel, Q.P. Dou. "Cellular and Computational Studies of Proteasome Inhibition and Apoptosis Induction in Human Cancer Cells by Amino Acid Schiff Base-Copper Complexes. *Journal of Inorganic Biochemistry,* 2013, 118, 83-93.

6. L. Ronconi, **C. Nardon**, G. Boscutti, D. Fregona, "Perspective gold(III)-dithiocarbamato anticancer therapeutics: learning from the past, moving to the future", as a chapter in the volume of the e-book series *Advances in Anti-Cancer Agents in Medicinal Chemistry.*

7. **C. Nardon**, S. M. Schmitt, H. Yang, J. Zuo, D. Fregona, and Q. P. Dou, "The cutting-edge Au(III)-peptidomimetics may revolutionize the anticancer therapy: preclinical studies against human breast neoplasia", under submission.

8. M. Celegato, D. Fregona, **C. Nardon**, M. Mongiat, L. Ronconi, C. Borghese, V. Canzonieri, N. Casagrande, A. Colombatti, D. Aldinucci, "Antitumor activity of gold(III) dithiocarbamato-peptide in prostate cancer cells and xenografts", under submission.

9. **C. Nardon**, M. Favaro, S. Sitran, and D. Fregona. "Synthesis, characterization and preliminary in solution luminescence studies of Pr(III) and Sm(III) dithiocarbamato complexes", under submission.